DOI: 10.31577/ahs-2023-0024.01.0001

ACTA HYDROLOGICA SLOVACA

Volume 24, No. 1, 2023, 3 – 8

The influence of land use change on transport of water and energy in ecosystem and climate change

Viliam NOVÁK*

Increasing population led to the increasing demand to food, raw materials, water and energy, followed by the increasing intensification of land use, and increasing industrial and agricultural production. This led to fossil fuels combustion and related carbon dioxide emissions, to building of structures impermeable to water as industrial infrastructure, transport facilities and dwelling structures, which basically change land properties, structure of water and energy fluxes of biosphere, and to climate change of the Earth. The aim of this paper is to quantify the influence of modified evaporating surfaces by land use changes on water and energy fluxes in modified ecosystems. The influence of land use changes on energy fluxes in the boundary layer of atmosphere is compared to the influence of carbon dioxide concentration increase. It was demonstrated that the contribution of land use changes can be more significant than the influence of carbon dioxide emissions on atmosphere boundary layer temperature.

KEY WORDS: ecosystem, land use changes, carbon dioxide emission, global warming, climate change

Introduction

Natural reasons of climate change

Climate of the Earth was changed continuously. In the past, the climate changed mostly by natural, or non-anthropogenic reasons. The ice age ended approximately ten thousand years ago; medieval warm period (9–13 century) was followed by the so called „little ice age“ (14–19 century). Those climate changes were relatively slow. It is not known exactly, what was the reason of such changes, but it was a mixture of natural reasons, like Milankovich cycles (Milankovich, 1930), volcanic activity (Kirchner et al., 1999), or collision of the Earth with extraterrestrial body. Actually observed climate changes are predominantly due to human activity, because in the last centuries there were not observed significant changes of solar activity, nor changes of our planetary system orbits. Therefore, actually observed climate changes are mostly due to anthropogenic reasons (Balek, 2006; Nemešová, 2007; Kutílek and Nielsen, 2010; Novák, 2021; Kučera, 2021).

Anthropogenic reasons of climate change

Scientific literature devoted to climate change and their reasons is prioritizing the influence of carbon dioxide concentration increase (and other so called „greenhouse gases“) in an atmosphere and its contribution to the long wave radiation to the boundary layer of atmosphere, which is increasing its temperature. It is understood, that increasing concentration of carbon dioxide in an atmosphere (in year 2021 up to 410 ppm) and backward long wave radiation emitted by carbon dioxide molecules can contribute to the surface temperature increase and to the change of the heat balance structure. But, this phenomenon is only one of many reasons of the Earth surface temperature increasing (Novák, 2021). To preserve conditions suitable for life on the Earth, it is necessary to eliminate, or mitigate rapid change of climate. The necessary precondition of such activity is identification and quantification of the most important reasons of climate change. Greenhouse effect of an atmosphere due to increasing concentration of the so called „greenhouse“ gases, like carbon dioxide, water vapour and methane, is an important reason of climate change. But, to the climate change are significantly contributing the land - use changes. Mankind, trying to manage suitable conditions to preserve their existence on the Earth, is increasing agricultural and industrial production leading to increasing demand for water, raw materials, food and energy. A result of this activity, is the increase in agricultural land area (mostly arable land), as well as areas covered by dwelling facilities, industrial and transportation infrastructure. Such surfaces are impermeable (to water) surfaces. Precipitation impacting such surfaces are rapidly flowing out, not infiltrating into the soil, and consequently not evapotranspirating and not

consuming latent heat to change the liquid to vapour phase. This is leading to the additional heating of boundary layer of an atmosphere and increasing its temperature. Well known are the so called „heat islands", as areas of higher air temperatures in and around big cities; the differences between air temperatures in the city and those temperatures above the natural surfaces are some degrees of Celsius.

Increasing population of the Earth

Increasing population itself is not the direct reason of global changes. But pressure on consumption of water, raw materials, food and energy is increasing pressure on land use exploitation efficiency. Such a rapid increase of inhabitants number of the Earth leads to land use changes. People are changing the properties of land and thus changing the structure of water and energy fluxes in the boundary layer of an atmosphere. The question is, how many people could be supplied by the available Earth resources.

In the year 2022 number of people on the Earth reached 8×10^9. It is assumed that in the year 2050 on the Earth will be living 10×10^9, and in the year 2100, we can reach 10.9×10^9 inhabitants (The European state and outlook, 2015). It is assumed that 2000 years ago on the Earth lived about 1.8×10^8 people, in the year 1820, it was 1×10^9 and 110 years later (1930) on the Earth lived 2×10^9 inhabitants. Since then, during the 90 years the gain of population of the Earth was 6×10^9. Approximately, 6×10^9 live in Asia and Africa. Currently, population explosion in Africa is generating gain higher than 3%, i.e. 50 million annually. It is assumed, that in Subsaharan Africa and in some countries of Asia will be living more than 75% inhabitants of the Earth. Subsaharan Africa and some states of Asia (known as developing countries) with low GDP will be faced to the increasing pressure to food production as well as to raw materials and energy. The lack of water, food, arable land and fertilizers as well as lack of resources needed to agriculture intensification in such countries is one of the main reason of massive emigration, mostly to the Europe.

The influence of carbon dioxide concentration on the energy fluxes in the boundary layer of atmosphere

The role of carbon dioxide as a „greenhouse gas" was early understood, but the problem was to quantify the influence of this phenomenon on long – wave energy fluxes (Novák, 2021). A few years ago, there were published results of long – term measurements to estimate long wave energy fluxes emitting by the molecules of carbon dioxide back to the surface (Feldmann et al., 2015). From results of numerous measurements in Oklahoma and Alaska during the decade 2000–2010 was estimated that the contribution of the long wave energy flux due to increasing carbon dioxide concentration is 0.02 Wm^{-2} per year. Since the beginning of the „industrial revolution" the contribution of the carbon dioxide on the back flux of long wave radiation was estimated by 1.82 Wm^{-2}. Is this significant value contributing to the climate change? The average income of solar energy by the Earth surface is 350 Wm^{-2}. To find an answer, it is necessary to compare this value to the extra fluxes of energy due to land use change.

Earth surface structure and its properties

The planet Earth surface area is 520×10^6 km^2, dry land surface is less than one third of Earth surface area (149×10^6 km^2). Arable land surface is less than 12% of land, (19.8×10^6 km^2), and represents ecosystem, which is the main source of food for mankind, Interestingly, the area of deserts over the Earth is (19.85×10^6 km^2), which is close to the area of arable land. Even more interesting is that dryland glaciers are covering approximately the same area (15.7×10^6 km^2) as arable land, or deserts. The basic area is covered by forests (60×10^6 km^2), which represents 38% of dryland area (Rejmers, 1985). Tre rest of the land is covered by steppes and savannas, by vegetationless areas in the Arctic, dwelling infrastructure, industrial areas, water bodies and impermeable surfaces, like buildings and communications. To preserve existing ecosystems temperature regime, it is important to use the maximum part of the incoming solar energy, by evapotranspiration. Energy, not used for evapotranspiration is heating boundary layer of an atmosphere, and dryland surface and thus increasing its temperature.

Key role in stabilizing of ecosystem temperature play water surfaces (seas and oceans), because they cover more than 70% of Earths surface, and for evapotranspiration are utilizing about 90% of incoming solar energy. Tropical (rain) forests (RF) have similar consumption structure of solar energy to evapotranspiration, i.e. they can consume up to 90% of incoming solar energy (Shuttleworth, 1988), and therefore is the role of RF in the formation of climate so important. Another important factor is, that continents are mostly located north of equator (Europe, Asia, Africa, and North America) and south of equator (South America, Australia), therefore, water surfaces with the highest income of solar energy and with highest evaporation rates are mostly located between the tropics and thus contributing to decrease air (and water) temperature. If the trend of increasing air temperature will be preserved, it could lead to the glaciers thawing and to increase of the water surfaces area. Hypothetically, from the increased sea surfaces due to thawing, it can be expected evaporation increasing and cooling of an environment. The autoregulation could work and evaporation can decrease. The higher evaporation is, the higher can be cooling effect due to this phenomenon. Properties of water surface are not changing, but land surfaces are changing significantly. Therefore, it is important to quantify land use changes and their influence on climate and its change.

To minimize the temperature of the boundary layer of atmosphere, it is necessary to maximize energy consumption. It means, to create conditions for maximum evapotranspiration. Process of evapotranspiration consumes basic part of solar energy reaching the Earth surface, due to extremely high latent

heat of evaporation ($L=2.5\times10^6$ J kg^{-1}). Evapotranspiration from land consumes about 51% of net radiation (energy reaching land surface), evaporation from seas and oceans consumes more than 82% of net radiation reaching the water surface (Budyko, 1974). Results of measurements showed (Shuttleworth, 1988), the ratio of consumed energy by evapotranspiration to the incoming one in rain forests (RF) and in tropical seas approximately equals, is up to 0.9.

An attempt to quantify the influence of land use changes on transport of water and energy

The basic problem to quantify the influence of different surfaces and their changes on transport of water and energy in the soil – plant – atmosphere continuum (SPAC) is lack of information, characterizing different surfaces. Satellite photographies can give detailed information about the objects and their distribution in ecosystem, but to estimate quantitative information about evaporation surfaces and their changes is not easy even by ground measurements. To quantify the influence of land use changes on water and energy fluxes, it is necessary to evaluate their quantitative characteristics, like temperature, albedo, leaf area index (LAI), wind velocity, soil properties and meteorological characteristics of the area. Because such information are not available, scientists are trying to use qualified estimates and use methods of quantifications with minimum input data. In this paper an attempt is made to evaluate the influence of land surface and their changes on energy fluxes in the boundary layer of an atmosphere and compare those changes with known changes of energy fluxes by emissions of carbon dioxide.
The most important water and energy fluxes change in the boundary layer of an atmosphere are changes of surfaces in subtropical and tropical areas, because sums of precipitations as well as solar radiation are maximum here, and can significantly modify water and energy fluxes of the Earth. Therefore, to quantify the influence of changed evaporation surfaces on energy fluxes, effort will be focused on decreasing area of rain forests (RF), progressive desertification in sub Sahara region (SH) and on the increasing area of impermeable surfaces (IA, buildings, communications), which are products of mankind.

Decreasing area of rain forests

The area of rain forests (RF) of the Earth is estimated as 15×10^6 km^2, it covers approximately one tenth of dryland area. During the last 21 years, the area of RF was decreased by clearing approximately about 2.6×10^6 km^2 (Global Forest Rev., 2021). Realistic average annual clearing area of RF is 100,000 km^2. Annual evapotranspiration total of RF was estimated by 2700 mm (90% of total annual precipitations). It is assumed, that clearing will decrease evapotranspiration approximately to one half, i.e. to ΔE = 1350 mm per year. Incoming solar radiation, not consumed by evapotranspiration (and therefore „saved“) and heating the environment is $L\times\Delta E = 4.81\times10^9$ J m^2 year^{-1}, (latent heat of water evaporation is $L= 2.5\times10^6$ J kg^{-1}). The average heat flux due to unused energy for evapotranspiration per year (R_s) can be calculated by dividing $L\times\Delta E$ by number of seconds per year ($t = 3.153\times10^7$s); then, $R_s = 1.070\times10^2$ Wm^{-2}, or $R_s = 107$ Wm^{-2}. If this „saved“ energy flux will be regularly distributed across the Earth surface (assuming the homogeneous distribution due to global circulation), then $R_g = 0.0206$ Wm^{-2}. This value (R_g) is the average flux of energy not consumed by evapotranspiration, but heating the environment as a result of clearing of 100,000 km^2 rain forests annually.
The change of land properties, due to RF area decrease is influencing climate globally, but the main effect can be observed locally, i.e. on the area where RF was cleared. The surface soil layer properties change will lead to the surface temperature increase as a result of different plant canopies and other surface, increasing albedo and decreasing of surface roughness. It was estimated decrease of precipitation during the vegetation period by 16–24% depending on properties of changed evaporation surface (pastures, soy). The process of soil devastation, mainly due to cattle breeding is accelerating too (Sampaio, et al., 2007, Kenderessy, 2022).

Desertification of sub Sahara region

The increasing area of Earth´s deserts is reality. Results of measurements showed that the south boundary of Sahara desert moved southwards about 250 kilometers during the last 100 years and desert area increased by 1.62×10^6 km^2. At Sahara desert there were found old anchors (Balek, 2006), so the desert did not always cover this area, but the process of desertification was lasting hundreds of years. It is known from history, that north Africa was important source of food for Roman Empire.
The aim of this chapter is to evaluate the Sahara desert area increasing and its influence on energy fluxes in this area and its contribution to climate change. One hundred years ago, the desert area was smaller at about 1.62×10^6 km^2, and this area was covered by savanna. According to Palmer et. al., (2015), the average annual evapotranspiration total of savanna is $E_s = 379$ mm year^{-1}. After savanna desertification, it is assumed the decrease of average annual evapotranspiration approximately to one half, i.e. $E_d = 200$ mm year^{-1}. Corresponding energy flux decrease needed for evapotranspiration is $R_d = 5.2\times10^8$ J m^{-2} year^{-1} and the average flux of energy not used as latent heat of evaporation (which can heat boundary layer of an atmosphere) of deserted area was calculated by dividing R_d by number of seconds per year (t); resulting value is $R = 16.5$ Wm^{-1}. Sum of energy not consumed by evapotranspiration (because evapotranspiration was decreased by desertification of savanna) is 26.73×10^6 MW. It was calculated by multiplication of energy flux R by the area of „desertificated“ savanna. Assuming homogeneous distribution of the energy, „saved“ by lower evapotranspiration, the resulting value of energy flux is $R_g = 5.24\times10^{-2}$ Wm^{-2}.

Impermeable surfaces

Impermeable surfaces, are covering the surface of

dryland with an increasing speed. Their properties are quite different than permeable (to water) or covered by vegetation. Precipitation falling on the impermeable surfaces basically outflows, only small part of it covers impermeable surfaces by thin layer of water, which evaporates quickly. It means, that basic part of energy reaching such impermeable surface is not used as latent heat of evaporation, but will be heating impermeable surface and adjoining layer of atmosphere. Impermeable surfaces (roofs, asphalt) are usually dark with low albedo, which means high ratio of solar energy absorption (Brutsaert, 1982; Novák, 2012).

To make it more difficult, there are not known shares of impermeable surfaces on total dryland area of the Earth and their shares in particular continent. According to serious estimates based on satellite information, in industrial states of Europe, the share of impermeable surfaces area on total surfaces area is about 5 percent. The same situation can be observed even in Slovakia. According to data of UN up to 0.6 of Earth´s area is disturbed by mankind activity. There are not known quantitative data, therefore it is difficult to use them to calculate its influence on climate change. Globally, it can be assumed the impermeable surfaces (A_i) share is about one percent of dryland area (A_s); ($A_i = 0.01\ A_s$). Using this assumption, we shall try to quantify the influence of impermeable surfaces on energy (and water) flux in ecosystem.

Dryland surface area is $A_s = 149\times10^6$ km^2; one percent of it is $A_i = 0.01A_s = 1.49\times10^6$ km^2, or 1.49×10^{12} m^2. To calculate the influence of one percent impermeable surface of the Earth on evaporation change, the average annual evapotranspiration total from the dryland surface should be known. According to Babkin (1984), average dryland evapotranspiration total per year is 71,000 km^3, or $E_s = 7.1\times10^{13}$ m^3. The average evapotranspiration total per year and unit surface area can be evaluated by dividing it by dryland area, so $E_s = 475$ mm year^{-1}; ($E_s = 475$ kg m^{-2} year^{-1}). Assuming decrease of evaporation from the impermeable surfaces in comparison to the permeable one to one half, (expressed by water layer height) $E_s = 240$ mm year^{-1}, or in weight units ($E_s = 240$ kg m^{-2} year^{-1}), then, the total decrease of evaporation from impermeable layers is $\Delta E_s = 3.57\times10^{14}$ kg year^{-1}.

The average energy flux not used by evapotranspiration ΔR_{se} is calculated by multiplication of „saved“ annual sum of evapotranspiration (ΔE_s) by latent heat of evaporation (L), and by its dividing by number of seconds per year (t). Then $\Delta R_{se} = (\Delta E_s \times L) / t$, and $\Delta R_{se} = 2.94\times10^{13}$ W.

The maximum additional energy flux „saved“ by decreasing evapotranspiration from impermeable surfaces which can heat boundary layer of an atmosphere corresponds to the situation when it is heating the area of impermeable surfaces only. This is maximum contribution to the boundary layer temperature increase. This energy flux ΔR_{si} can be calculated by dividing ΔR_{se} by impermeable surface area $A_i = 0.01A_s$, $\Delta R_{si} = \Delta R_{se} / A_i = 19.73$ W m^{-2}.

The average „saved“ energy flux (or energy not used for evapotranspiration) divided by the Earth surface area (A_g), is $\Delta R_{si} / A_g = 0.0565$ W m^{-2}. The realistic value of additional energy which can contribute to the heating of the boundary layer of an atmosphere ΔR could vary within the range $0.0565\ \text{W m}^{-2} \leq \Delta R \leq 19.73\ \text{W m}^{-2}$.

Comparison of the land use changes and carbon dioxide on energy fluxes in SPAC

In the previous part of this study, an attempt was made to quantify the influence of land use changes (represented by different surfaces) on energy fluxes in the boundary layer of an atmosphere. Analysis was concentrated on such types of land use changes, which are significantly modifying the energy fluxes of the Earth globally and contributing to climate change. The most important changes of the surface types are rain forests (RF) areas clearing, areas impermeable (for water) surfaces, like buildings and communications (IS) and desertificated areas in sub Sahara region (SH). Interesting is, that those three types of surfaces are approximately equal, and their total area is 4.26×10^6 km^2. Their ratio to the dryland of the Earth is relatively small (0.0285), but their changes can significantly contribute to climate changes. The above mentioned selection is not complete, the aim of this selection is to demonstrate the influence of land use changes (artificial or natural) on evapotranspiration and transport of water and energy in ecosystems. We would like to demonstrate the influence of land use changes on energy fluxes as comparable (or even more important) to the role of greenhouse gases.

Discussion

Due to land use changes, land surface properties are changing too. Changes of albedo of the modified surfaces, aerodynamic roughness, leaf area index, soil properties, meteorological characteristics of boundary layer of an atmosphere reflect land use change, and is followed by modified fluxes of water and energy in the soil – plant – atmosphere system. Characteristic feature of land use changes is the decrease of area covered by canopies (plants) and increase of bare areas, like desertificated areas, impermeable areas for water and cleared areas.

From the above described results of analysis it follows that long-wave energy fluxes in the boundary layer of an atmosphere to the land surface are of the same order as those due to the increased concentration of carbon dioxide, emitted by fossil fuel burning. Table 1 presents the value of long wave energy contribution due to increased concentration of carbon dioxide to the Earth surface $R = 1.82$ W m^{-2} (Feldmann et al., 2015). The influence of three types of „modified“ land surfaces (RF, IS, SH), on increase of long –wave radiation fluxes to the surface was estimated as $R = 5.76$ W m^{-2}. The ratio of energy fluxes to the surface due to increased carbon dioxide concentration $R = 1.82$ W m^{-2} and due to land use change $R = 5.76$ W m^{-2} is 0.31. It means, that the contribution of the effect of carbon dioxide concentration on the long wave radiation to the lad surface is less than one third of the effect of land use changes analysed according to used scenario. Analysed land use changes represent only part of reality, because

Table 1. **The contribution of land use changes and increasing concentration of carbon dioxide in an atmosphere on increasing of long – wave energy fluxes (*R*) heating boundary layer of an atmosphere and upper layer of the Earth.**

	RF	IS	SH	CD
		R [W m^{-2}]		
1	107	19.73	16.5	–
2	0.0718	0.197	0.175	–
3	0.0206	0.0565	0.0524	0.02
4	0.2620	2.82	2.62	1.82
5		5.64		1.82
6		7.46		

RF – the influence of rain forest area decrease to energy fluxes change, IS – the influence of increased impermeable surfaces area to energy fluxes change, SH – the influence of increased area of Sahara desert and decrease of savanna area to energy fluxes change. CD – the influence of the increase of carbon dioxide concentration in an atmosphere on long –wave energy fluxes.
1. Increased energy flux (W m^{-2}) due to change of area RF, IS, SH and by carbon dioxide concentration increase CD. 2. Increased energy flux recalculated to the dryland area. 3. Energy flux recalculated to the Earth surface. 4. Contribution of different surfaces to the energy fluxes to the Earth during the past one hundred years (IS, SH), and by 21 years (RF). Calculation of cumulative energy fluxes was assumed to increase linearly (starting from zero value), up to actual energy fluxes. Contribution of CD to the energy fluxes was calculated since the industrial revolution start (Feldmann et al., 2015). 5. Total of energy fluxes (long wave radiation) to the soil surface from three sources (RF, IS, SH), and contribution of increased concentration of carbon dioxide (CD). 6. Total of energy fluxes (long wave radiation) to the soil surface from four sources (RF, IS, SH, CD).

detailed information about actual changes of land use are not known.

Contribution of identified land use changes to long wave radiation in soil surface direction was estimated as $R = 7.56$ W m^{-2} (Table 1). Is it a lot or is it a negligible value? It is difficult to give the definite answer. The average income of solar radiation to the Earth surface is 350 W m^{-2}, but the surface of Slovakia is reaching an average flux of energy 125 W m^{-2} (Chrgijan, 1978). From analysis it follows, that the changes of surface properties, and following energy fluxes changes are felt mostly locally. Contributions of the energy fluxes as a result of land use changes are integrating, as it can be seen in the Table 1, line 4.

The area of seas and oceans is covering more than two thirds of the Earth surface, they are basic stabilizing element of our planet climate. Water bodies are absorbing part of additional heat, thus integrating heat fluxes produced by the discussed land use changes (RF, IS, SH), and partially absorbing high energy fluxes from the areas where consumption of energy by evapotranspiration was decreased. It seems realistic, to explain majority of climate change by land use changes with significant contribution of carbon dioxide concentration increase.

Conclusions

Current land use changes, and resulting evapotranspiration rates decrease means less energy consumption and additional long – wave energy fluxes, comparable, or higher than energy fluxes due to carbon dioxide concentration increased by emissions. Both are contributing to the increase of the temperature of the boundary layer of atmosphere. Reasons of estimated increased long – wave energy fluxes in boundary layer of atmosphere and air temperature increasing can be of various origin. But the contribution of rain forests (RF) clearing, sub Sahara region desertification (SH) and increasing ratio of impermeable surfaces (IS) are dominant. The average rate of additional fluxes of long – wave radiation due to estimated land use changes is 5.64 W m^{-2}, during the last century. It is significantly higher, than flux estimated due to concentration of carbon dioxide increasing – 1.82 W m^{-2} – since the beginning of the industrial revolution. Our results are based on available data of land use changes and they illustrate how those processes participate in redistribution of energy in an atmosphere. It was shown land – use changes can increase water and energy fluxes even more than increasing concentration of carbon dioxide in an atmosphere.

Acknowledgement

This contribution was supported by the Scientific Grant Agency VEGA, Project No 2/0150/20.

References

Brutsaert, W. (1982): Evaporation into the atmosphere. Doortrecht, D. Riedel Publ. Comp.

Babkin, V. I. (1984): Evaporation from water surface. Leningrad, Gidrometeoizdat, pp. 72. (In Russian)

Balek, J. (2006): Hydrological consequences of global changes. J. Hydrol. Hydromech.v. 54, 4, 357–370.

Budyko, M. I. (1974): Climate and life. Leningrad, Gidrometeoizdat. (In Russian)

The European state and outlook (2015): Asessment of global megatrends, EEA, Copenhagen. Denmark.

Feldman, D. R., Collins, W. D., Gero, P. J., Torn, M. S., Mlawer, E. J., Shippert, T. J. (2015): Observational determination of surface radiative forcing by CO_2 from 2000–2010. Nature. 519, 339–343.

Global Forest Rev. (2021): https://research.wri.org/gfr/global-forest-review

Chrgijan, A. Ch. (1978): Physics od atmosphere I., II. Gidrometeoizdat, Leningrad. (In Russian)

Kenderessy, P. (2022): Land use change and the role of forests in current climate change. In: Zmena klímy I. Bratislava, Slovenská akadémia vied, 69–81. (In Slovak)

Kirchner, I. G., Stenchikov, H. F., Graf, A. A, Robock, J. A. (1999): Climate model simulation of winter warming and summer cooling following the 1991 Mount Pinatubo volcanic erruption. J. Geophys. Res.,104, 19,039- 19,055.

Kučera, A. (2021): Global climate change and Solar activity. Is Sun the reason of climate change? In: Zmena klímy I. Bratislava, Slovenská akadémia vied, 46–53. (In Slovak)

Kutílek, M., Nielsen, D. R. (2010): Facts about global warming. Catena, Reiskirchen, pp. 227.

Milankovich, M. (1930): Matematische Klimalehre und Astronomische Theorie der Klimaschwankungen. Handbuch der Klimatologie, Band 1. Teil A. Gebrűder Bornträger, Berlin.

Nemešová, I. (2007): Climate change as a part of global change. Meteorol. Zprávy, 60, 1–6. (In Czech)

Novák, V. (2012): Evapotranspiration in the Soil – Plant – Atmosphere System. Springer Science + Business Media, Dordrecht, 253 p.

Novák, V. (2021): Ecosystems and global changes. Acta Horticult. Regiotext. Spec. issue, 70–79.

Palmer, A., Wiedeman, C., Finca, A., Hanam, N., Everson, C., Ellery, W. (2015): Modeling annual evapotranspiration in a semiarid African savanna: Functional convergence theory, MODIS LAI and the Penman-Monteith equation. African J. Range Forage Sci. v.32, p.23.

Rejmers, N. F. (1985): The vocabulary of nature: Biosfphere. Horizont, Praha, 176 p. (In Czech)

Shuttleworth, W. J. (1988): Evaporation from the Amazonian rainforest. Proc. Roy. Soc., London, B233, 321–346.

Sampaio, G., Nobre, C., Costa, M. H., Satyamury, P., Soares-Filho, B. S., Cardoso, M. (2007): Regional climate change over eastern Amazonia caused by pasture and soybean cropland expansion. Geophys. Res. Letters, v.34, 17.

Ing. Viliam Novák, DrSc. (*corresponding author, e-mail: viliamnovak42@gmail.com)
Institute of Hydrology SAS
Dúbravská cesta 9
841 04 Bratislava
Slovak Republic

DOI: 10.31577/ahs-2023-0024.01.0002

ACTA HYDROLOGICA SLOVACA

Volume 24, No. 1, 2023, 9 – 13

Impact of the biochar fraction sizes on the selected hydrophysical properties of silty loam soil

Lucia TOKOVÁ*, Natália BOTKOVÁ, Justína VITKOVÁ, Lenka BOTYANSZKÁ, Kamil SKIC, Angelika GRYTA

Biochar is a widely known soil amendment. In the presented study, we aimed to evaluate the effect of biochar produced from Swedish willow ((Salix schwerinii x S. viminalis) x S. viminalis), ground into three different size fractions (<125µm, 125µm–2 mm and >2 mm) on selected hydrophysical properties of silty loam soils. Biochar was applied in the amount of 1.5% per weight of dry matter and the results were compared with pure silty loam soil (control). Data of biochar application impact on the selected hydrophysical properties of silty loam soil were statistically analyzed. In general, our results suggest that applied different size fractions of biochar does not have a statistically significant effect on particle density, however does have an effect on bulk density, porosity and saturated hydraulic conductivity of silty loam soil. With regard to bulk density, a statistically significant decrease *($p<0.05$)* was observed compared to the control and it ranged from 4.18 to 8.13% from the smallest to the largest biochar fraction. The decrease of bulk density further led to a statistically significant increase *($p<0.05$)* in porosity of all three treatments. Saturated hydraulic conductivity tended to increase as the size fraction of the biochar used was progressively reduced. This increase ranged from 63.77% (for biochar with size fraction >2 mm) to 112.42% (for biochar with size fraction <125µm) compared to pure silty loam soil (control).

KEY WORDS: hydrophysical properties, silty loam soil, biochar fraction size

Introduction

Biochar is a carbon–rich product made from biomass by pyrolysis process that takes place at high temperatures ranging from 300°C up to 900°C under low oxygen or no oxygen conditions (Spokas, 2010; Lehmann and Joseph, 2015). The positive impact of biochar was discussed in agricultural journals and scientific papers until it was developed into commercial products as a form of fertilizer in the first half of the 19th century. Current interest in this material has been primarily motivated by research in the Amazon (Terra Preta de Indio) (Lehmann and Joseph, 2015). Biochar, as a stable carbon-rich material (Lehmann and Joseph, 2015), is being investigated to mitigate global warming; and it may also have promising properties in relation as a soil amendment.

The benefits of biochar application also in terms of its impact on other agro–environmental parameters of soils such as bulk density, porosity, hydraulic conductivity, water retention, pH, organic carbon content, organic matter content, soil structure and soil aggregate stability was discussed in many scientific papers (Peng et al., 2011; Ajayi and Horn, 2016). These functions in only one product are possible, because the biochar is composted by aromatic moieties that give biochar its black color and are responsible for its stability, which makes biochar an interesting compound for carbon sequestration (Zhu et al., 2019).

The properties of biochar, to a large extent depend on the characteristics of the input raw materials (feedstock) and on the conditions of pyrolysis (Antunes et al. 2017). The subsequent effects of the biochar application on the hydrophysical properties of the soil are dependent on the biochar amount, pyrolysis conditions, feedstock type and biochar particle size (Liu et al., 2012).

In most biochar experiments, biochar has been added to the soil without selecting specific particle sizes. A likely reason for this is the added cost of sorting biochar particles (Verheijen et al., 2019). Whereas, discrete particle size experiments can provide valuable insights into multiple mechanisms occurring simultaneously. Few studies have focused on the effect of biochar particle sizes on the hydrophysical properties of the soil (Blanco–Canqui, 2017; Duarte et al., 2019). Duarte et al. (2019) states, that small particle size of biochar can reduce the volume of soil pores (<0.15 mm diameter). However, it can increase the volume of mesopores (0.15–0.50 mm diameter) and macropores (>0.50 mm diameter). Changing the volume of mesopores and macropores in the soil plays an important role (Lehmann and Joseph, 2015; Liu et al. 2017). The high volume of mesopores

in the soil can increase the area of water available for plants (Mollinedo et al., 2015). Some studies states that biochar addition can increase saturated hydraulic conductivity in clay soils and loamy soils (Dan et al., 2015) by increasing the number of connected macropores.

This paper aims to analyze the impact of three different biochar fraction sizes on selected hydrophysical properties of the silty loam soil in the concentration of 1.5% per weight of dry matter in laboratory conditions. In our study we hypothesized that biochar application will decrease bulk density, soil porosity and saturated hydraulic conductivity.

Material and methods

Soil and biochar mixtures laboratory set up

The silty loam soil used for this laboratory experiment was collected from the area of Dolna Malanta (Nitra, Slovakia). The soil on average contained 36.04% of sand, 48.83% of silt and 15.13% of clay and is classified as a silty loam texture (WRB, 2015). The average soil organic carbon content and soil pH (KCl) was 10.2 g kg^{-1} and 5.58, respectively (Kondrlova et al., 2018).

The willow biochar used in this experiment was produced in the UNYPIR reactor, which is part of the AgroBioTech Centre belonging to the Slovak University of Agriculture in Nitra. The input material was Swedish willow, variety Tordis ((Salix schwerinii x S. viminalis) x S. viminalis). A more detailed description of the reactor operation is given by Gaduš and Giertl (2019). Basic chemical analysis of biochar was performed by the Dionýz Štúr State Institute of Geology (Table 1). Biochar was produced at a pyrolysis temperature of 300°C and a pressure of 101 kPa. The produced biochar was ground on an electric grinder and sieved on 2 mm and 125 µm mesh sieves into three size fractions (Fig. 1).

Mixtures of the silty loam soil and the willow biochar were prepared in laboratory conditions with a biochar concentration 1.5% (which is equivalent to 20 t ha^{-1} in field conditions) in Kopecky cylinders with a volume of 100 cm^3. Overall, three treatments, representing different particle size fractions (<125 µm, 125 µm–2 mm and >2 mm), were prepared. For each treatment were prepared 3 replications of soil and biochar mixtures. These prepared mixtures were compared with the control treatment (without amendment), which was prepared in 3 replicates as well. The following treatments of the laboratory experiment were prepared:

- silty loam soil – control (3 replications)
- soil + willow biochar (<125µm) (3 replications)
- soil + willow biochar (125µm–2 mm) (3 replications)
- soil + willow biochar (>2 mm) (3 replications)

Table 1. Basic chemical analyses of the willow biochar

	C [%]	H [%]	N [%]	Ash [%]	pH [–]
biochar	82.2	2.74	0.86	6.16	9.14

Fig. 1. Biochar fraction sizes a) <125µm, b) 125µm–2mm and c) >2mm.

Determination of the selected hydrophysical properties

The bulk density (BD), particle density (PD), soil porosity (P) and saturated hydraulic conductivity (K) of the samples (control samples, samples treated with biochar) were determined by three replications using standard laboratory methods. Prepared soil samples (100 cm^3) were dried in the oven at 105°C until the samples were at a constant weight. BD was calculated based on the sample weight and core section volume (Brogowski et al., 2014; Obidike–Ugwu et al., 2022). PD was measured with an air pycnometer method. This procedure determines the volume of solid phase of the soil (Eijkelkamp Soil and Water, 2020). Consequently, the BD and PD were used to calculate P of the soil samples. K of the samples was determined in the laboratory conditions using an empty extension cylinder placed on the top of saturated soil sample and filled with water creating a variable hydraulic slope (falling–head method) (Igaz et al., 2017). We performed 3 measurements on each soil sample (n=9).

Statistical analysis

In our study we used Microsoft Excel program for descriptive statistics (Mean, Standard deviation – SD) to describe and summarize the basic feature of the given dataset. Consequently, the effect of biochar application on PD, BD, P and K of the silty loam soil was evaluated using a one-factor analysis of variance (One-Way ANOVA). Statistically significant effects at $p<0.05$ were determined by LSD test. All analyses were performed using Statgraphics Centurion XV. I software (Statpoint Technologies, Inc., Warrenton, VA, USA).

Results and discussion

In general, our results indicate that applied willow biochar does not have a statistically significant effect on PD, but does have an effect on BD, P and K (Table 2). Regarding BD, there we observed a statistically significant reduction ($p<0.05$) on all three biochar treatments compared to the control treatment (Table 2). Biochar itself is a porous material (Adekiya et al., 2020), and when it is added into the soil, it decreases BD and increases P (Nyambo et al., 2018). Biochar has also ability to improve structural properties of soil (Šimanský et al., 2019). Gradual oxidation of biochar in soil also increases the number of functionality groups on its surface (Obia et al., 2016), which can absorb soil particles and minerals, which can turn contributes to the formation of soil aggregates and to reduction of BD. Biochar is a highly porous material with low BD (Adekiya et al., 2020) and therefore its application to soil can increase P. According to Hseu et al. (2014) the change of P in soils treated with biochar is mainly due to the formation of macropores and rearrangement of soil particles. We observed a statistically significant increase ($p<0.05$) in P compared to control treatment (Table 2), which is therefore to be expected after BD reduction. Our results are in agreement with other studies in this area (Githinji, 2014). Very important soil property in solving the problems with soil water regime is also K (Blanco-Canqui, 2017). We observed a statistically significant increase ($p<0.05$) in K values compared to the control treatment (Table 2). Our results are in agreement with other results (Dan et al., 2015; Esmaeelnejad et al., 2017). The changes in K are associated with changes in P, aggregation, and water retention capacity.

By the results, we can further see that biochar produced from willow has different effects on selected soil characteristics at different size fractions (Table 2). If we look at the results, we notice that the BD values tend to decrease gradually as the size fraction of biochar increases. This decrease ranges from 4.18% (biochar with a fraction <125µm) to 8.13% (biochar with a fraction >2mm) compared to the control. Consequently, the P-values tend to increase as the size fraction of biochar is gradually increased. This increase is from 4.27% (biochar with a fraction <125µm) to 7.95% (biochar with a fraction >2 mm) compared to the control. Similar results were reported by Duarte et al. (2019) for loamy soil, explaining that the increase in the particle size reduces the homogeneity of the pore distribution and increases the P. In the case of K, the measured values tend to increase as the size fraction of the biochar used is

Table 2. Effect of biochar application on the selected hydrophysical properties of silty loam soil (SD – standard deviation)

	PD (n=3) [g cm^3]		BD (n=3) [g cm^3]		P (n=3) [%]		K (n=9) [cm h^{-1}]	
	Mean	*SD*	*Mean*	*SD*	*Mean*	*SD*	*Mean*	*SD*
silty loam soil (control)	2.566^{a}	0.004	1.316^{d}	0.006	48.697^{a}	0.171	0.966^{a}	0.558
soil + willow biochar (<125µm)	2.562^{a}	0.044	1.261^{c}	0.000	50.776^{b}	0.863	2.052^{b}	0.732
soil + willow biochar (125µm–2 mm)	2.552^{a}	0.094	1.235^{b}	0.001	51.570^{bc}	1.801	1.878^{b}	1.146
soil + willow biochar (>2 mm)	2.563^{a}	0.036	1.209^{a}	0.001	52.815^{c}	0.700	1.582^{ab}	0.537

Note: Different letters (a, b, c) indicate that treatment means are significantly different at p <0.05 according to least significant difference test (one–way ANOVA).

progressively reduced. This increase can be expressed as a percentage from 63.77% (biochar with a fraction >2 mm) to 112.42% (biochar with a fraction <125μm) compared to the control. According to Esmaeelnejad et al. (2017), finer biochar fractions can better fill the spaces between soil particles.

Conclusion

Our results showed that the hydrophysical properties of soil, such as bulk density, porosity and saturated hydraulic conductivity were depended on the biochar particle size. The results indicated that biochar produced from willow can statistically significantly ($p<0.05$) reduce bulk density, increase soil porosity and increase saturated hydraulic conductivity of silty loam soil. The most significant trend towards a reduction of bulk density (8.13%) was observed in the treatment with biochar fraction size >2 mm compared with control. At the same time, the application of the biochar increased soil porosity up to 7.95%. Positive effect of the saturated hydraulic conductivity was also observed. In this case, the highest increase was showed in treatment with a lowest fraction size <125μm, this increase was 112.42% compared to the control treatment. Based on the results observed in our laboratory experiment, by using willow biochar, we can conclude that the application of biochar leaded to positive trends in changes of studied silty loam soil hydrophysical properties. For agricultural producers, to obtain improvement in the selected hydrophysical properties, the biochar can be used by the largest fraction >2 mm with the concentration 1.5% of the willow biochar, because of its biggest changes in bulk density and porosity. In the case of saturated hydraulic conductivity, was observed the smallest increase (63.77%) compared to the finest biochar applied, but it was enough to improve soil properties. We assume, that the biochar application results in an improvement of the soil structure and in the interconnection of the soil pores.

Acknowledgement

This paper was produced with financial support by the VEGA 2/0155/21 and PAS-SAS-2022-05 projects.

References

Adekiya, A. O., Agbede, T. M., Olayanju, A., Ejue, W. S., Adekanye, T. A., Adenusi, T. T., Ayeni, J. F. (2020): Effect of biochar on soil properties, soil loss, and cocoyam yield on a tropical sandy loam Alfisol. The Scientific World Journal, vol. 2020, 1–9.

Ajayi, A. E., Horn, R. (2016): Modification of chemical and hydrophysical properties of two texturally differentiated soils due to varying magnitudes of added biochar. Soil and Tillage Research, vol. 164, 34–44.

Antunes, E., Schumann, J., Brodie, G., Jacob, M. V., Schneider, P. A. (2017): Biochar produced from biosolids using a single-mode microwave: Characterisation and its potential for phosphorus removal. Journal of Environmental Management, vol. 196, 119–126.

Blanco-Canqui, H. (2017): Biochar and Soil Physical Properties. Soil Science Society of America Journal, vol. 81, 687–711.

Brogowski, Z., Kwasowski, W., Madyniak, R. (2014): Calculating particle density, bulk density, and total porosity of soil based on its texture. Soil science annual, vol. 65, no. 4, 139.

Dan, T., Zhong-Yi, Q., Mang-Mang, G., Bo, L., Yi-Jia, L. (2015): Experimental Study of Influence of Biochar on Different Texture Soil Hydraulic Characteristic Parameters and Moisture Holding Properties. Polish Journal of Environmental Studies, vol. 24, no. 3, 1435–1442.

Duarte, S., Glaser, B., Pellegrino Cerri, C. E. (2019): Effect of biochar particle size on physical, hydrological and chemical properties of loamy and sandy tropical soils. Agronomy, vol. 9, no. 4, 165.

Eijkelkamp Soil and Water (2020): Air Pycnometer according to Langer. https://en.eijkelkamp.com/products/laboratory-equipment/air-pycnometer-according-to-langer.html

Esmaeelnejad, L., Shorafa, M., Gorji, M., Hosseini, S. M. (2017): Impacts of woody biochar particle size on porosity and hydraulic conductivity of biochar-soil mixtures: an incubation study. Communications in soil science and plant analysis, vol. 48, no. 14, 1710–1718.

Gaduš, J., Giertl, T. (2019): Výroba biopalív termickou konverziou. Vykurovanie 2019. Bratislava: Slovenská spoločnosť pre techniku prostredia ZSVTS, 225–228. ISBN 978–80–89878–42–0.

Githinji, L. (2014): Effect of biochar application rate on soil physical and hydraulic properties of a sandy loam. Archives of Agronomy and Soil Science, vol. 60, no. 4, 457–470.

Hseu, Z. Y., Jien, S. H., Chien, W. H., Liou, R. C. (2014): Impacts of biochar on physical properties and erosion potential of a mudstone slopeland soil. The Scientific World Journal, vol. 2014. 1–10.

Igaz, D., Kondrlová, E., Horák, J., Čimo, J., Tárník, A., Bárek, V. (2017): Základné merania v hydropedológií, SPU, Nitra, 110 p. ISBN 978-80-552-1686-7.

World Reference Base for Soil Resources IUSS (2015): World reference base for soil resources 2014. International soil classification system for naming soils and creating legends for soil maps – Update 2015. FAO: Rome, Italy. 203, 2015.

Kondrlova, E., Horak, J., Igaz, D. (2018): Effect of biochar and nutrient amendment on vegetative growth of spring barley ('Hordeum vulgare' L. var. Malz). Australian journal of crop science, vol. 12, no. 2, 178–184.

Lehmann, J., Joseph, S. (2015): Biochar for environmental management: science, technology and implementation. Routledge. 2nd ed. London: Rountledge, Taylor and Francis Group, 976 p. ISBN 978-0-41570415-1.

Liu, J., Schulz, H., Brandl, S., Miehtke, H., Huwe, B., Glaser, B. (2012): Short-term effect of biochar and compost on soil fertility and water status of a Dystric Cambisol in NE Germany under field conditions. Journal of Plant Nutrition and Soil Science, vol. 175, no. 5, 698–707.

Liu, Z., Dugan, B., Masiello, C. A., Gonnermann, H. M. (2017): Biochar particle size, shape, and porosity act together to influence soil water properties. Plos one, vol. 12, no. 6, e0179079.

Mollinedo, J., Schumacher, T. E., Chintala, R. (2015): Influence of feedstocks and pyrolysis on biochar's capacity to modify soil water retention characteristics. Journal of Analytical and Applied Pyrolysis, vol. 114, 100–108.

Nyambo, P., Taeni, T., Chiduza, C., Araya, T. (2018): Effects of maize residue biochar amendments on soil properties and soil loss on acidic Hutton soil. Agronomy, vol. 8, no. 11, 256.

Obia, A., Mulder, J., Martinsen, V., Cornelissen, G., Børresen, T. (2016): In situ effects of biochar on aggregation, water retention and porosity in light-textured tropical soils. Soil and Tillage Research, vol. 155, 35–44.

Obidike-Ugwu, E. O., Ogunwole, J. O., Eze, P. N. (2023): Derivation and validation of a pedotransfer function for estimating the bulk density of tropical forest soils. Modeling Earth Systems and Environment, vol. 9, no. 1, 801–809.

Peng, X. Y. L. L., Ye, L. L., Wang, C. H., Zhou, H., Sun, B. (2011): Temperature-and duration-dependent rice straw-derived biochar: Characteristics and its effects on soil properties of an Ultisol in southern China. Soil and tillage research, vol. 112, no. 2, 159–166.

Spokas, K. A. (2010): Review of the stability of biochar in soils: predictability of O : C molar ratios. Carbon management, vol. 1, no. 2, 289–303.

Šimanský, V., Šrank, D., Jonczak, J., Juriga, M. (2019): Fertilization and application of different biochar types and their mutual interactions influencing changes of soil characteristics in soils of different textures. Journal of Ecological Engineering, vol. 20, no. 5. 149–164.

Verheijen, F. G., Zhuravel, A., Silva, F. C., Amaro, A., Ben-Hur, M., Keizer, J. J. (2019): The influence of biochar particle size and concentration on bulk density and maximum water holding capacity of sandy vs sandy loam soil in a column experiment. Geoderma, vol. 347. 194–202.

Zhu, X., Liu, Y., Li, L., Shi, Q., Hou, J., Zhang, R., Zhang, S., Chen, J. (2019): Nonthermal air plasma dehydration of hydrochar improves its carbon sequestration potential and dissolved organic matter molecular characteristics. Science of The Total Environment, vol. 659, 655–663.

Ing. Lucia Toková, PhD. (*corresponding author, e-mail: tokova@uh.savba.sk)
Ing. Natália Botková
Ing. Justína Vitková, PhD.
Ing. Lenka Botyanszká, PhD.
Institute of Hydrology SAS
Dúbravská cesta 9
841 04 Bratislava
Slovak Republic

Ing. Natália Botková
Institute of Landscape Engineering
Faculty of Horticulture and Landscape Engineering, SUA
Hospodárska 7
949 76 Nitra
Slovak Republic

Kamil Skic, Dr.
Angelika Gryta, M.Sc.
Institute of Agrophysics, Polish Academy of Sciences
Doświadczalna 4
20-290 Lublin
Poland

DOI: 10.31577/ahs-2023-0024.01.0003

ACTA HYDROLOGICA SLOVACA

Volume 24, No. 1, 2023, 14 – 23

Characterization of leakage water flows in the subsoil of Beni Haroun dam by hydrogeological approach

Lynda CHEBBAH*, Abdesselem KABOUR

Dams are designed and built to withstand severe destabilising conditions, including seepage problems, which are very often linked to localized discontinuity stress in the rock foundations, or in the banks. This situation allows water to take different circulation paths, and consequently jeopardizes the stability of the dam and reduces its useful capacity. The Beni Haroun dam, located in the North-Eastern part of Algeria on the Oued El-Kebir, with a water storage capacity of about 1 billion m^3, the dam is located on a Ypresian (Karst) limestone mass with an estimated annual leakage volume of 31.536 hm^3. The present work focuses on the identification of the water leakage origin in the Beni Haroun dam, using a hydrogeological approach, which consists in interpreting the correlation between the water level in the reservoir and that in the piezometers installed around the dam, for the period 2003 to 2021. The results revealed some interesting findings.

KEY WORDS: dam, leakage, piezometer, karst, Beni Haroun

Introduction

Dams are essential infrastructure for water supply and have served human societies for 5000 years (ICOLD, 2013). Dams are the cornerstone of water resources management by providing water for irrigation, domestic and industrial uses, flood control, aquaculture, navigation and recreation. However, the failure and breach of dams can have catastrophic results (Torabi Haghighi et al., 2014).

The problem of water leakage is very complex as it threatens the quantities of water accumulated in most dams around the world and causes concern about the stability of these structures especially if this problem persists (Benfetta et al., 2017).

Seepage rate is an important performance indicator of the dam structural behaviour, as it can provide insight into physical changes in the dam structure. The effect of seepage through the foundation area and banks on the dam safety has become a matter of concern for this reason, the prediction and analysis of recorded seepage data at dam sites is an essential operation in their monitoring tasks, to properly assess the situation and plan corrective actions (de Rubertis, 2018).

Leakage is recognised as having a direct impact on the dams safety. Therefore, it is important to monitor the uplift pressure and leakage rate to identify the risks, and the long-term behaviour of concrete dams and especially in the presence of cracks (Hu et al., 2017).

The Beni Haroun dam is built on limestone formations, which in itself presents a significant challenge to the construction and operation of this large dam. The water-soluble carbonate structure of this type of limestone can lead to the development of cracks and fractures that can eventually extend into conduits and even caves and grottos; a process known as karstification (Milanovic, 2017; Ford and Williams, 2007). As a result, water in a dam reservoir can easily seep through its foundations and banks and thus affect the stability of the dam. Seepage into the foundations of the Beni Haroun dam is estimated at $1 m^3 s^{-1}$, and on a yearly scale it loses 31.536 hm^3, which represents a fairly large volume (ANBT: Agence Nationale des barrages et transferts, 2002).

The objective of this case study is to detect the origin and path of the leakage recorded at the foundations and banks of the dam. This is done by a spatial and temporal piezometric analysis and also an analysis of the leakage rates in the different drainage points as a function of the water level in the lake.

Materials and methods

Presentation of the study site

The Béni-Haroun dam is located on the Oued El Kébir in the wilaya of Mila (East Algeria), (Fig. 1). It is fed by the Oued Rhumel and the Oued Endja (Fig. 2). It is part of the large Kebir-Rhumel basin with a surface area of 6595 km^2. This basin is naturally limited by the limits of

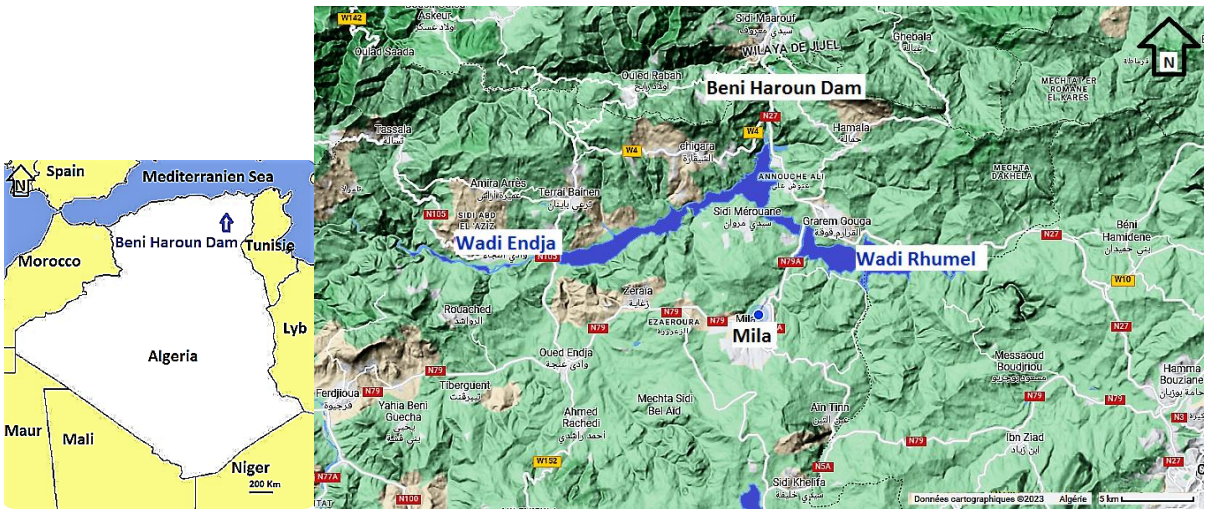

Fig. 1. Geographical location of the Beni Haroun dam (reservoir) (Chebbah and Kabour, 2018).

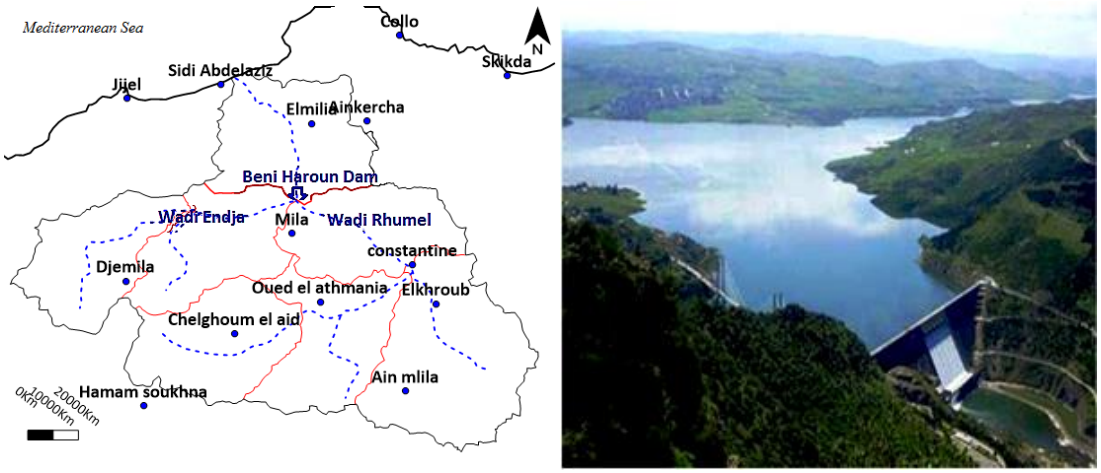

Fig. 2. Watershed and downstream view of Beni Haroun dam (Chebbah and Kabour, 2018).

the Kebir-Rhumel which are: to the North, the basins of the western Constantinois coast and the central Constantinois (BV n°03); to the South, the catchment area of the Constantinois high plateaux (BV n°07); to the West, the Soummam basin (BV n°15) and to the East the Seybouse basin (BV n°14) (Mebarki and Benabbes, 2008).

The structure is of the rectilinear weight type, in BCR (Roller Compacted Concrete) (Fig. 2), with a crest length of 710 m, levelled at elevation 216.3 m, an order height of 118 m above the foundations, and the direction of the axis of the dam is approximately North to South. The lake of the reservoir hugs the captured part of Oued El Kebir and the two valleys of Oued Rhumel and Oued Endja, on a surface of 39.29 km², that is to say nearly 4 000 ha. The rainfall-reservoir balance makes it possible to determine a net destocking by evaporation, equivalent to an average annual tranche of 350 mm. The reservoir can store 963 hm^3 of water, i.e. a useful volume of 732 hm^3, and can regulate an annual inflow of 435 hm^3, with a reserve of 1 billion m^3 of water reached on 12 February 2012. The dam was put into operation in 2003 (Mebarki and Benabbes, 2008).

Geological complexity and constraints

The Beni Haroun area is part of the Tellian domain and is mainly occupied by Paleogene formations (Vila, 1980), which start with the black Paleocene marls, easily friable to silty from colluvial deposits, and sometimes with traces of calcite filling clogging the joints. These Paleocene marls are overlain by Lutheran limestones and marls. The Beni Haroun dam is directly founded on the Ypres limestone (Fig. 3 and 4) (ANBT, 1999). The Ypresian limestone is characterised by the presence of spheroidal to elliptical black flint nodules, the thickness of this series is approximately 100 m (Vila, 1980). In the field, the rock is characterised by beds of

decimetric to metric thickness, it is dark grey to black with a micrite texture (fine grain). The Ypresian limestone is hard to very hard and weather resistant, because some layers are dolomitic or even siliceous, while the other layers contain black flint (ANBT, 2002). Examination of the drill cores recovered during the investigation phase revealed some traces of karst dissolution in this limestone bedrock; these traces of karst developed mainly along certain sub-vertical joints. The opening of the karstified zones could reach 30 to 50 cm. However, during construction, all karst problems were treated by grouting (Fig. 5) (ANBT, 2002).

With regard to the subsurface studies, the Beni Haroun dam site was investigated in two phases using 32 boreholes reaching a maximum depth of 124 m. The first 20 boreholes were drilled during the first phase (1984) by Harza Engineering, and during the second phase in 1997, the remaining 12 boreholes were drilled by Tractebel. The borehole logs were used to draw geological cross-sections (Fig. 4) (Kebab et al., 2021).

The local geology is part of a complex tectonic context of thrusting and faults or detachments, characterised by plastic deformations (folding) and brittle deformations (faults, fractures) of the lithological units of the site. These units are schematically made up of a competent limestone base (with rigid – brittle – behaviour) from100 m to 150 m thick, framed by two incompetent marl series (with plastic – folded – tectonised – behaviour) (Fig. 3 and 4) (Mebarki and Benabbes, 2008). This basic tectonic architecture, already complex in

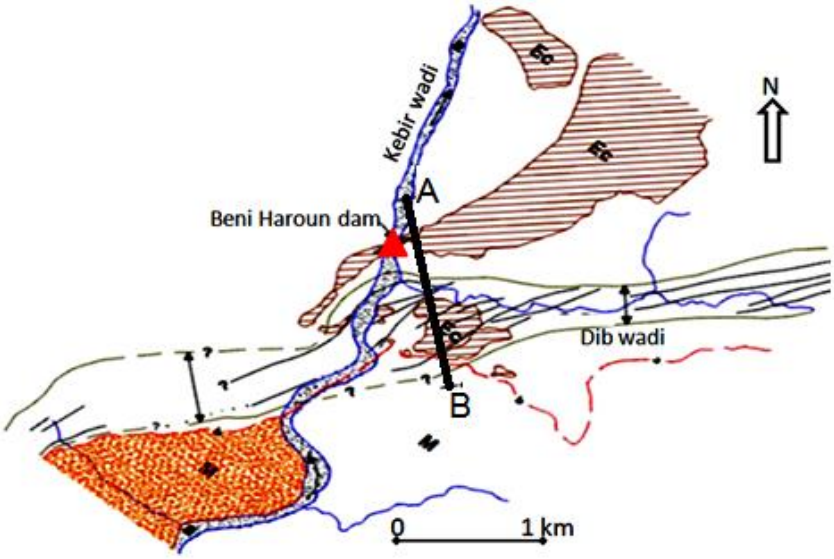

Fig. 3. Geological map of the site (Harza, 1984).

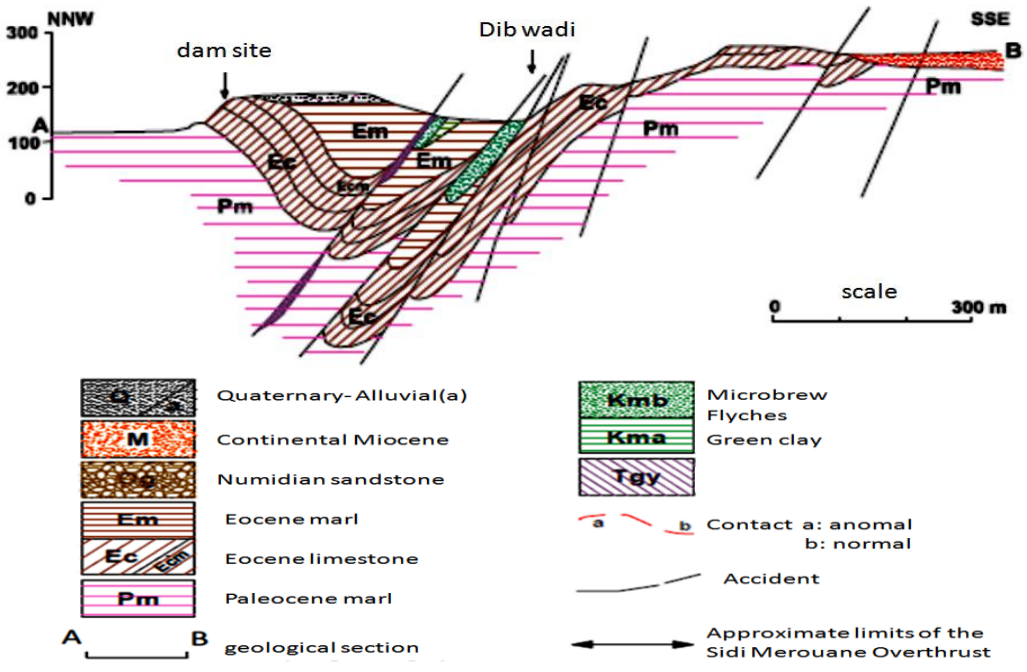

Fig. 4. Geological cross section in the Beni Haroun dam site (Harza, 1984).

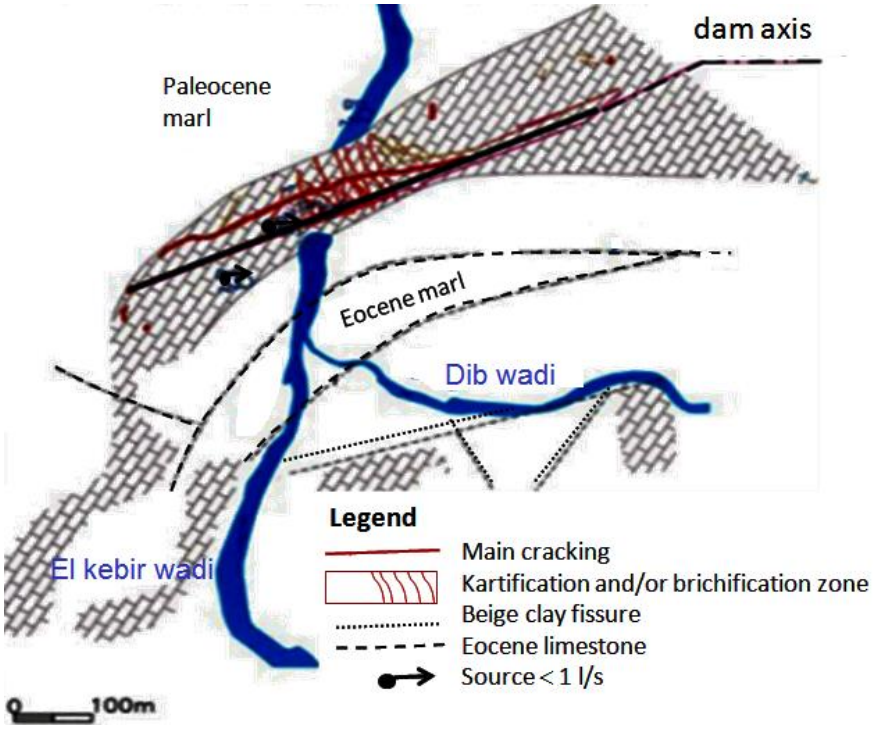

Fig. 5. Location of the karst aquifer (ANBT, 1999).

itself, is complicated by the presence of faults with a strong north-north-west plunge (shear zones) and North-South fractures (observed in the dam foundation). There is every reason to believe that these are traction fractures linked to the torsion of the limestone banks mentioned. (Fig. 4) (ANBT, 2007).

The limestones have a synclinal structure, the dam being entirely founded on its northern flank. Along the left bank of the reservoir, extend into a boat shape, the limestone banks have a sub-vertical or even slightly upward plunge (towards the interior of the slope), and are therefore subject to mowing (or rocking of the heads of the layers). This gravitational phenomenon results in a progressive dislocation of the rock, until it develops into an instability of the settlement, rockfall or landslide type, such as that observed just upstream of the dam (mirador landslide). These phenomena of superficial stretching of the rock mass are accompanied by an opening of the fracture systems, and therefore by a strong increase in permeability (Fig. 4) (Kebab et al., 2021).

The marls surrounding the limestones have similar or comparable characteristics from a hydrogeological point of view. From a geo-mechanical point of view, however, the Paleocene marls, being more calcareous, have more favourable characteristics than the Eocene marls.

Results and discussions

Leakage problem

The Beni Haroun dam showed an "original" deficiency during its first impoundment, December 2003 – January 2004, resulting from particular and complex geological conditions. It is about important leaks in the left wing and abnormally high pressures in this part of the structure (under pressure). This problem, immediately identified by ANBT, and its consulting engineer, who had designed the structure, was analysed in detail (the dam is equipped with an efficient monitoring system) and led to the definition of judicious reinforcement measures: extension of the waterproofing curtain and drainage in the foundation (Benchabane, 2015).

Piezometry

Whatever the type of dam, its foundations and supports are subject to pressures due to the flow of water through the rock. These can be quantified locally using piezometers.

Piezometry is very useful in determining faulty areas in the banks and foundation of the dam. The variation of the piezometric level and the lake level over time allows to deduce the anomalies that occur in the area crossed by the piezometer (Labadi and Achour, 2011).

The piezometers installed in the Beni Haroun dam site show a piezometric control of the reservoir lake in relation to the limestone aquifer on the left and right banks and in the syncline (Fig. 6).

In order to show the influence of the lake shoreline on the water level in the piezometers we plot the piezometer shoreline against the lake shoreline. The good correlation indicates that there is a strong water circulation between the represented piezometers and the lake. On the other hand, the steepness of the regression line indicates the permeability of the area between the lake and the piezometer (Toumi and Remini, 2006).

Monitoring data from the piezometers over the period (2003–2021) have clearly shown the performance of the various seepage control measures (Fig. 7).

Right bank

The water level in the piezometers located in the right bank (piezometers, POI 1, POIII 1, POIII 2, POIII 3, POIV 1) (Fig. 6) showed a good correlation (R^2 between 0.557 and 0.608) with the water level in the reservoir (Fig. 7), from the graphs (Fig. 7) we notice an average correlation between the studied parameters, and also that the slope of the regression lines undergo an increase for all the concerned piezometers which indicates a strong water circulation which is due either to the entrainment of the clogging materials by the flow created by the hydraulic load, or to the chemical dissolution of the components of the rock mass (Toumi and Remini, 2018). But for the piezometers (PUIT 124 RD3, PUIT 124 RD4, POIV 2, PO II 3, POI 2) we have a weak correlation (R^2<0.304), which allows us to see that there is no water circulation between the lake and the piezometers, and that the slopes of the regression lines undergo a rather increasing variation, which indicates the existence of water circulation under the effect of simple cracks and deterioration of the layers crossed by the piezometers**.**

Left bank

For the piezometers located on the left bank, a strong correlation is recorded (PO RG A2 and PORG A1) (R^2>0.9); for the piezometers located upstream of the dam axis, a good correlation is observed for PO VII 1 (R^2=0.582), for PUITS 124 RG 2 (R^2=0.529) and for PO VI 1 (R^2=0.952).

For the rest of the piezometers (POV 1, POV 2, POVII 2, POVI 2, PO 124 RG 1), a very weak correlation (R^2<0.4) between the parameters presented is noted, which informs us of the absence of water circulation in the zones located between the lake and these piezometers (Fig. 7).

On the basis of the data observed, we have noted that the various works undertaken have enabled a significant reduction in the under-pressures of the dam. On the other hand, we can say that the dam in these conditions is in full safety except that in the event of a strong flood, the under-pressures can increase in this case, it is necessary to increase the pumping capacity of the drainage pumps.

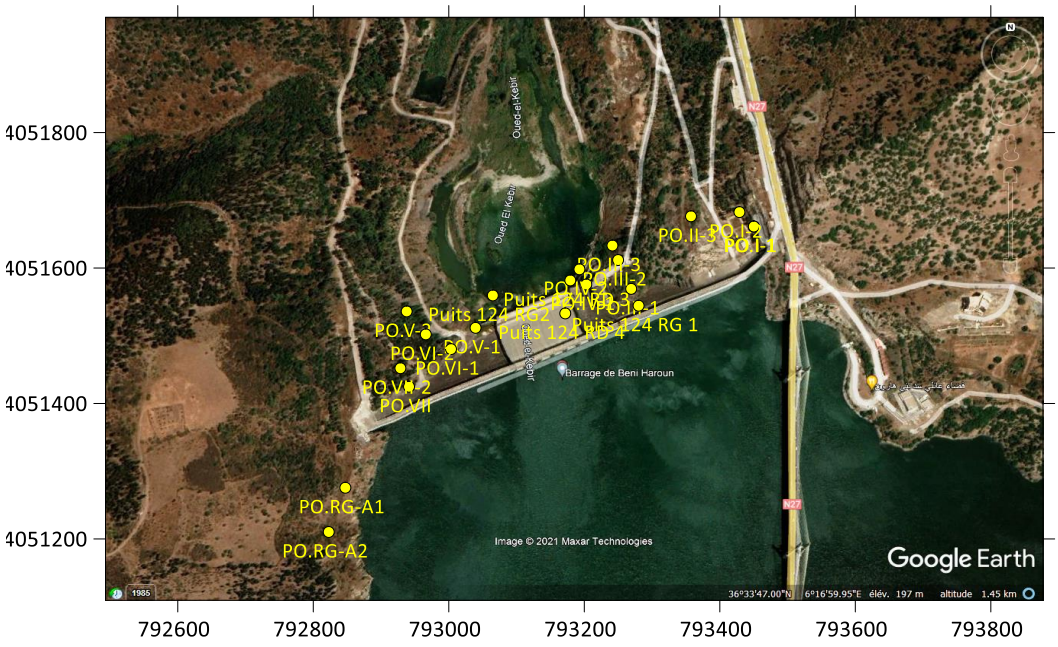

Fig. 6. Location of piezometers around the Beni Haroun dam.

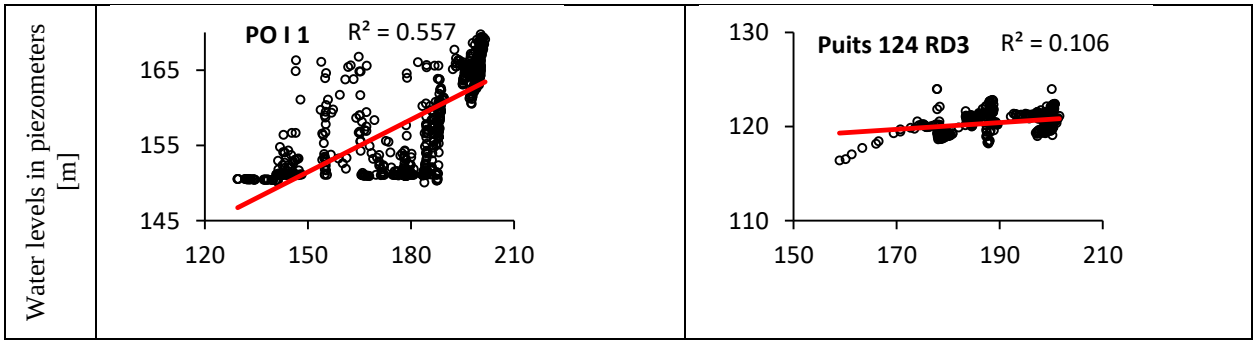

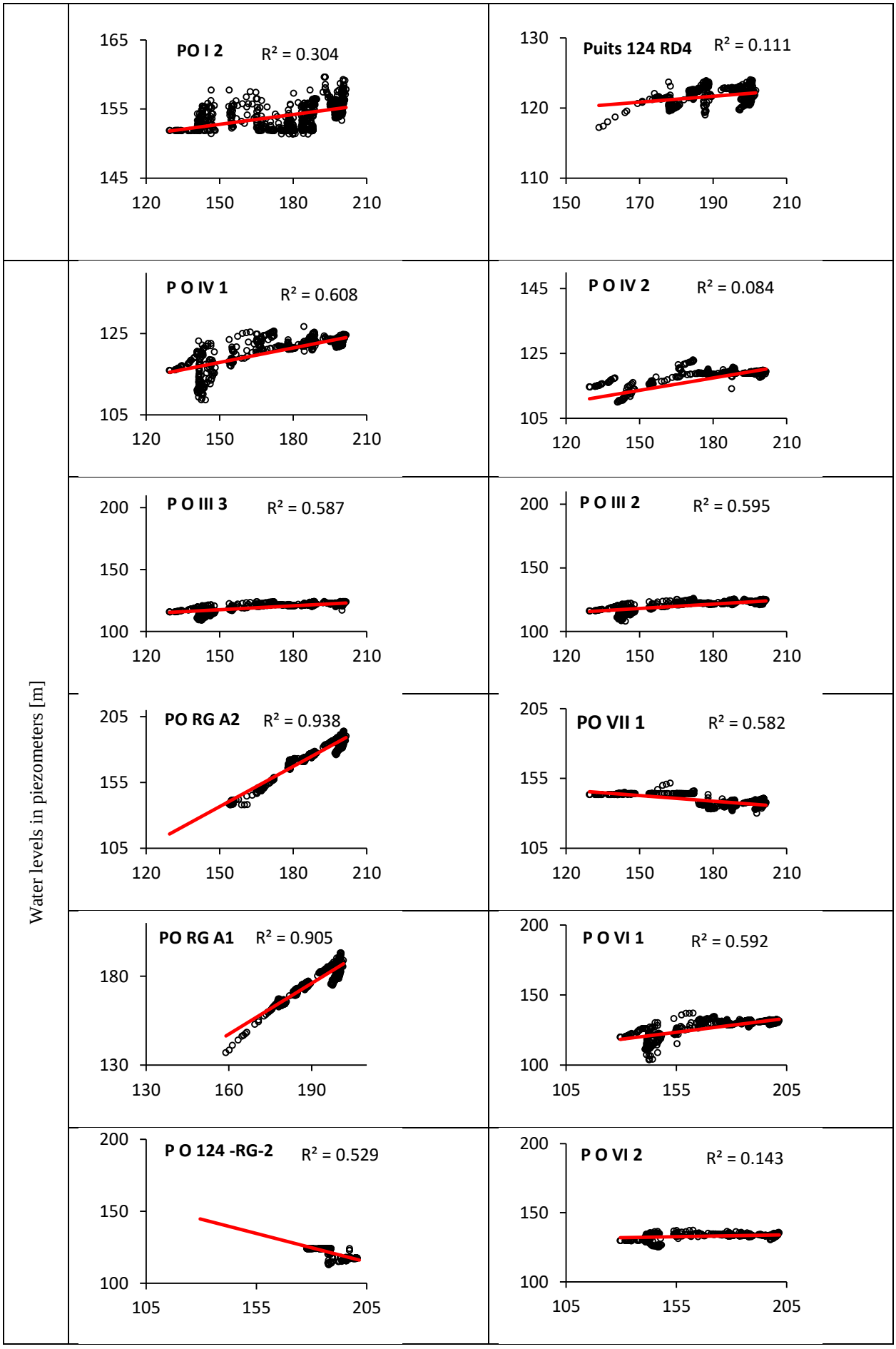
Water levels in piezometers [m]
PO I 2
R² = 0.304
Puits 124 RD4
R² = 0.111
P O IV 1
R² = 0.608
P O IV 2
R² = 0.084
P O III 3
R² = 0.587
P O III 2
R² = 0.595
PO RG A2
R² = 0.938
PO VII 1
R² = 0.582
PO RG A1
R² = 0.905
P O VI 1
R² = 0.592
P O 124 -RG-2
R² = 0.529
P O VI 2
R² = 0.143

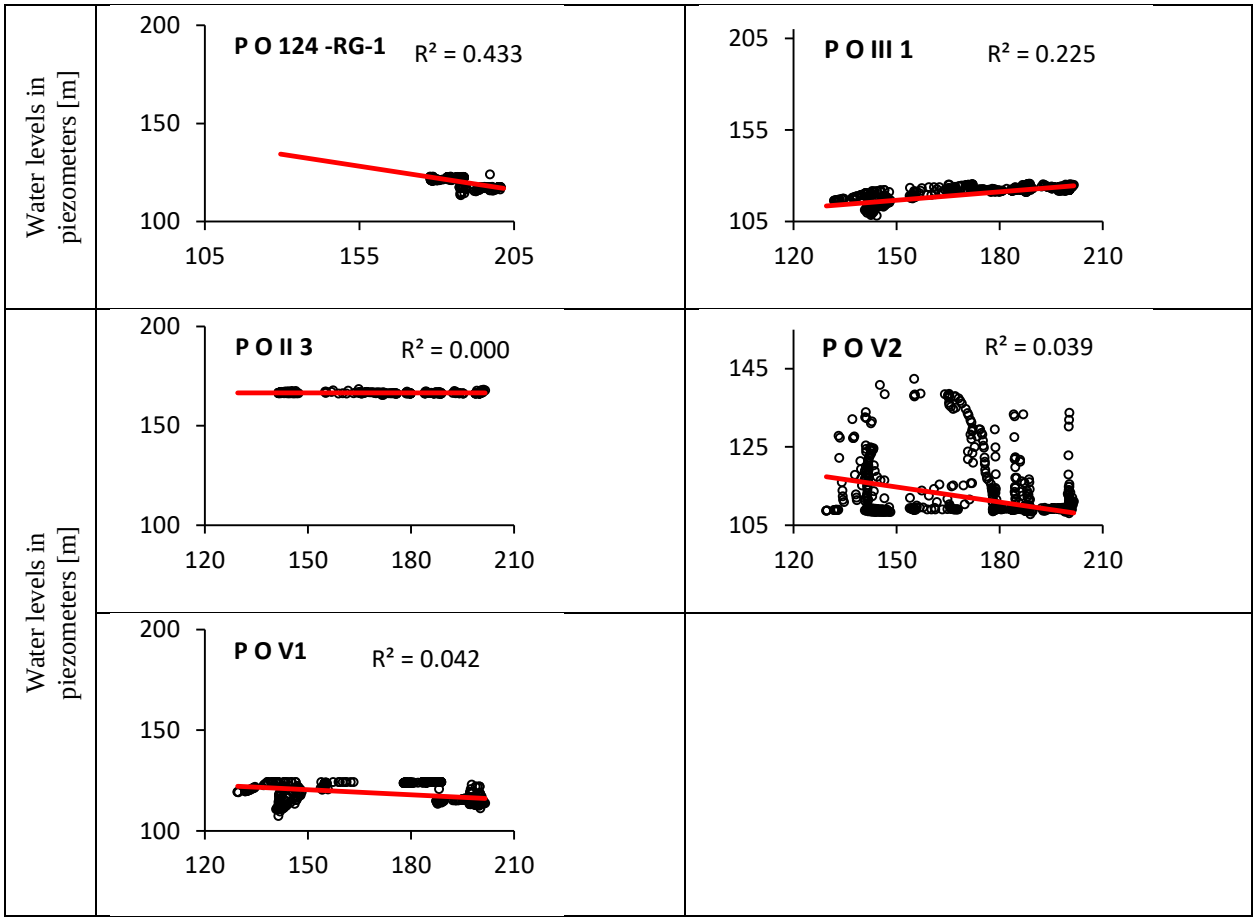

Fig. 7. Correlation between the water level observed in the reservoir and that of the piezometers around the Beni Haroun dam (2003–2021).

Spatial evolution

Piezometry during the construction of the dam

The synclinal structure has a steep western termination, marked by the limestone outcrops on the left bank. Gravity flow has been able to exploit submeridian discontinuities in these limestones to bypass the marly core of the syncline (Fig. 8) (ANBT, 1999). Circulations are fed in a concentrated way under the alluvium of the left bank. They follow two types of drainage axes: firstly, the contact between the limestone wall and the Paleocene black marl to the northwest; secondly, the network of breccias and fracture discontinuities, which jointly direct the gravity flows towards the spring area of the dam site (ANBT, 2007; Benchabane, 2015).

The installation of the dam caused the karst aquifer discharge threshold to rise from 105 m, the approximate altitude of the talweg, to more than 200 m, the approximate altitude of the dam's scouring sills (ANBT, 2007).

The hydraulic gradient was increased to 60–70 m and the spillway was moved to the left bank, on the natural path of the gravity flows that bypass the marl core of the syncline, by reusing the drainage axes abandoned during the digging of the cluse (ANBT, 2007).

The flow pattern in the limestones implies a long pathway, confirmed by a delay of at least 50 days, and on average about 100 days, between the temperature cycles in the reservoir and those observed downstream on the left bank. (Benchabane, 2015).

Piezometry after the implementation of the dam

There is a slow flow from south to north along the dam from a level of 135 m to 115 m (Fig. 9). On the right bank the flow direction is East-West towards the river. From the piezometric data, it can be seen that, even if the water level in the reservoir increases, the water level in most of the piezometers does not move, except for small disturbances during the rainy seasons (Fig. 9). In piezometers POI1 and POI2 a different response is observed, i.e. the water level is higher than in the other piezometers, and the level rises at the time of flooding, which means that there is a relationship with rainfall and that infiltration is rapid in limited areas. On the left bank, the curves are tight with a South East-North West flow direction, which indicates the existence of a rapid flow from a water table (fissured limestone) and the lake water. A hydraulic gradient likely to maintain underground circulation between the lake and the downstream side of the dam, which is expressed preferentially on the left bank. This bank presents a remarkable differentiation compared to the right bank, this difference is located at the level of the piezometers PORG A1, PORG A42 where the water level in these

piezometers evolves with that of the water level of the dam, this means the existence of a direct dam-groundwater relationship.

It is concluded that the piezometric observations on the left bank of the dam show that the permeability of these limestones is anisotropic, it is higher parallel than transversal to the layers, implying circulations parallel to the stratification. The under pressure of the dam is more developed on the left bank than on the right bank.

Leaks

It is clear that one of the major problems encountered when building a dam on fractured limestone soils is the sealing of the reservoir. The most important leakage from the reservoir corresponds to circulation through pre-existing natural drainage networks. The leakage rates are limit by the head losses that can occur throughout the limestone mass.

Conversely, for the same hydraulic load, flows can increase if there is a decrease in head losses following geometric and morphological modifications of the fractures. These modifications can have two origins; either erosion or entrainment of clogging materials, or chemical or mechanical erosion of the rock matrix (Labadi and Achour, 2011). The correlation of the seepage rates at the shoreline with the lake level (Fig. 10) clearly shows that the seepage rates increase strongly with the load and this for a lake level of about 178 m, for the left shore. For the right bank, the variation

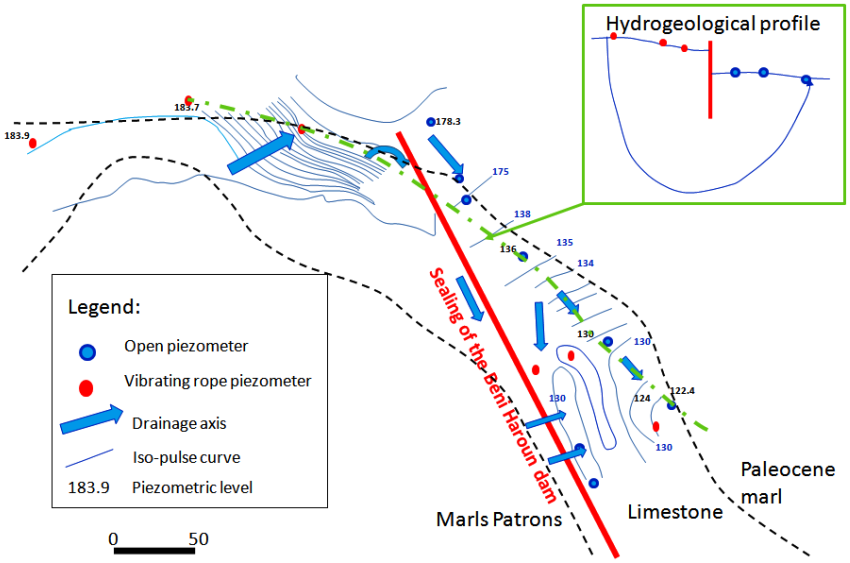

Fig. 8. Groundwater flow in the limestone aquifer during dam construction (ANBT, 1999; Benchabane, 2015).

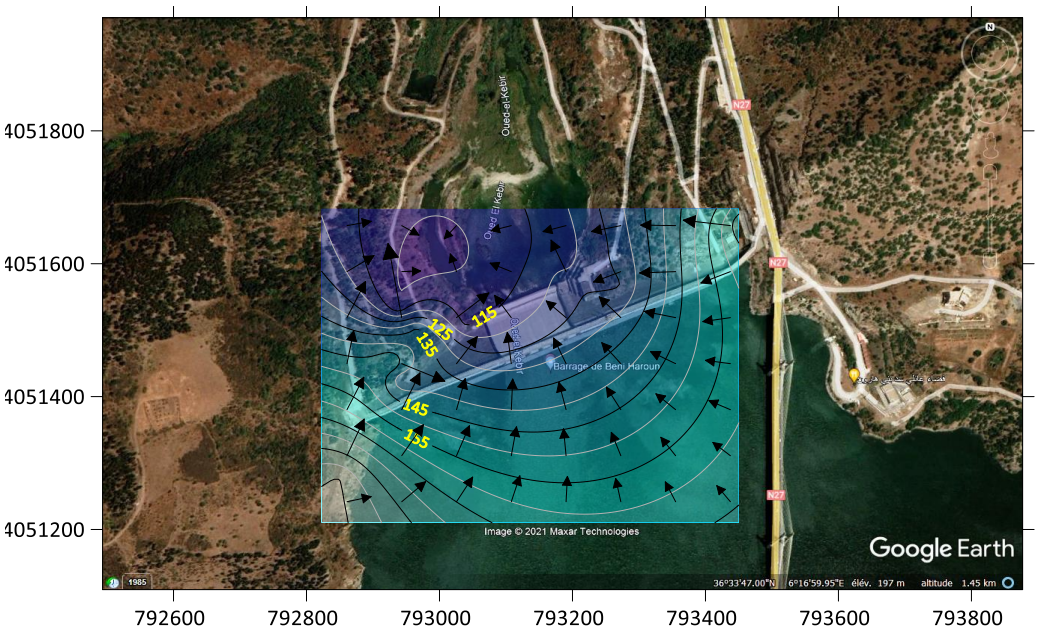

Fig. 9. Piezometry of Beni Haroun dam foundations (February 2019).

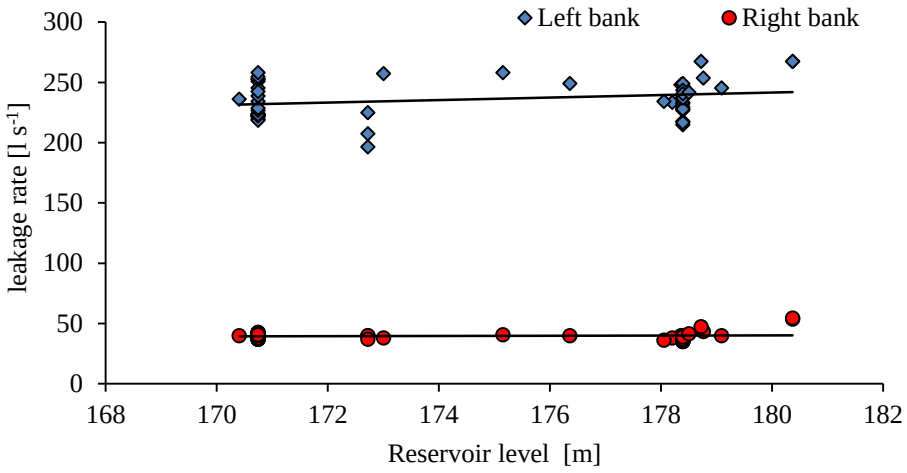

Fig. 10. Variation of leakage rates as a function of reservoir elevation.

of the lake level has no influence on the leakage rates on this bank, and they are stabilised around a value of 40 and 50 l s^{-1}.

It can also be seen that the leakage flows in the left bank are greater than those from the right bank, and there is no relationship between the leakage flows from the right bank and the left bank (Fig. 10).

Conclusion

The majority of dams around the world are confront with the problem of water leakage through the banks and foundations. The study of this phenomenon is of great importance, as it can endanger the stability of the dam and reduce its useful capacity.

The study of the relationship between the piezometric level and the water level of the reservoir allowed us to highlight the existence of a very pronounced relationship between the reservoir and the various piezometers. Thus, the following results were retained:

– The left bank is more cracked than the right bank.
– There are preferred directions of water flow within the limestone massif with a spatial variation in the degree of fissuring.
– The two banks have no relation to each other in terms of underground water circulation.

Based on these observations, we can say that actually we are in the presence of continuous flow channels in which the water will flow from upstream to downstream in a South East–North West direction for the left bank and East-West for the right bank.

References

ANBT (1999): Transfert de Beni Haroun. Rapport de Synthèse. Tractebel, Ingénierie, volume l. Alger.

ANBT (2002): Barrage de Beni Haroun sur L'oued Kebir. Monographie volume 1 Textes. Tractebel Engineering, 363 p.

ANBT (2007): Barrage de Beni Haroun (wilaya de Mila, Algérie). Rapport final de la compagne géophysique.

Benchabane, N. I. (2015): Relation barrage-nappes. Etude de cas barrage de Beni Haroun. Wilaya de Mila, Mémoire de Magister, Université de Constantine, Algérie, 113 p.

Benfetta, H., Achour, B., Ouadja, A. (2017): Les fuites d'eau dans les barrages dans le monde: quelques exemples Algériens. Larhyss Journal. 31, 195–218.

Chebbah, L., Kabour, A. (2018): Impact de la retenue d'un barrage sur le régime climatique local : cas de Béni Haroun (Est algérien). Geo-Eco-Trop, 42–1, 173–186.

ICOLD (International Commission on Large Dams) (2013): Historical review on ancient dams. Bulletin 143. International Commission on Large Dams, Paris, 68 p.

de Rubertis, K. (2018): Monitoring Dam Performance: Instrumentation and Measurements. Virginia. American society of civil engineers, 422 p.

Ford, D., Williams, P. W. (2007): Karst hydrogeology and geomorphology. Chichester, England, A Hoboken, NJ: John Wiley & Sons.

Harza Engineering Company (1984): Etude technico-économique conduisant au choix du site. November, Vol. 3, Annexe B- Géologie.

Hu, J., Ma, F., Wu, S. (2017): Comprehensive investigation of leakage problems for concrete gravity dams with penetrating cracks based on detection and monitoring data: A case study. Struct Control Health Monit. 25–4, 1–18

Kebab, H., Boumezbeur, A., Rivard, P. (2021): Rock mass properties and their suitability as a foundation for a rolled compacted concrete gravity dam: case study of Beni Haroun dam (Mila, NE Algeria), Bulletin of Engineering Geology and the Environment, 80, 1729–1743.

Labadi, A., Achour, S. (2011): Apport de l'analyse piézométrique dans l'étude des fuites du barrage voûte a assises calcaires de Foum El Gherza, Biskra, Algérie, courrier de savoir, 11, 25–32.

Mebarki, A., Benabbes, C. (2008): Le système Beni-Haroun (Oued Kebir-Rhumel, Algérie) aménagements hydrauliques et contraintes morpho-géologiques. Ann-geographies, 105. 37–51.

Milanovic, P. (2017): Water resources engineering in Karst. CRC Press. The Annual Meeting of International Commission on Large Dams July 3–7, Prague, Czech Republic PRAGUE.

Torabi Haghighi, A., Marttila, H., Kløve, B. (2014): Development of a new index to assess river regime impacts after dam construction. Global Planet Change, 122.186–196.

Toumi, A., Remini, B. (2006): La problématique des fuites

d'eau du barrage Hammam-Grouz (Algérie), Larhyss Journal, 05, 41–48.

Toumi, A., Remini,B. (2018): The problem of water in Beni Haroun Reservoir (Algeria). Jordan Journal of Civil Engineering, 12–3, 402–423.

Vila, J. M. (1980): La chaîne alpine d'Algérie Orientale et des confins Algéro-tunisiens. PhD thesis of Sciences, Univ. P & M. Curie, Paris VI, 665 p.

Lynda Chebbah, MCB, (*corresponding author, e-mail: cheblyn@yahoo.fr)
Abdesselem Kabour, MCA.
Department of Civil and hydraulic engineering
University Centre of Abdelhafidh Boussouf
Laboratory of Modeling and Socio-Economic Analysis in Water Science – MASESE Lab.
BP 25, Mila
Algeria

DOI: 10.31577/ahs-2023-0024.01.0004

ACTA HYDROLOGICA SLOVACA

Volume 24, No. 1, 2023, 24 – 32

Long-term forecasting of appearance dates of ice phenomena and freeze-up at the Dnipro Cascade reservoirs by teleconnection indicators

Borys KHRYSTIUK, Liudmyla GORBACHOVA*

Long-term forecasting of the ice regime of water bodies is a difficult task and is still unresolved in the part of improving the accuracy of forecasts. The objective of this paper is the development of the long-term forecasting methods of appearance dates of ice phenomena and freeze-up at the Dnipro Cascade reservoirs by teleconnection indicators. The research was carried out based on the observation data of 38 water gauges, which are located on 6 reservoirs of the Dnipro Cascade. The appearance dates of ice phenomena and freeze-up for the period from the observation beginning at each water gauges to 2020, inclusive, were used. In addition, in the research were also used the information about the teleconnection indicators, namely 34 atmospheric indices, sea surface temperature indices, teleconnection indices and patterns, that are determined by the National Weather Service (NWS) of the National Oceanic and Atmospheric Administration of United States of America (NOAA USA). The long-term forecasting methods of the appearance dates of ice phenomena and freeze-up at the Dnipro Cascade reservoirs were developed by searching for the best correlation or regression relationship between dates and teleconnection indicators. The probabilities of acceptable error of the developed methods are in the range of 61–72%, which corresponds to the category of "satisfactory" assessment of the method quality. It makes it possible to recommend them for use in operational forecasting.

KEY WORDS: ice phenomena, freeze-up, Dnipro reservoirs, teleconnection indices and patterns, forecasting equations

Introduction

Reliable and early forecasts of the appearance timing of ice phenomena and freeze-up at the Dnipro Cascade reservoirs are very necessary for the rational use of water resources of the Dnipro River, for establishing the operating regimes of reservoirs taking into account the requirements and interests of various sectors of the economy: hydropower, shipping, fisheries, utilities, etc. (Kaganer, 1976; Scherbak et al. 2007; Khrystiuk and Gorbachova, 2022). Long-term forecasts of the appearance dates of floating ice and freeze-up with forecast lead time at least 1 month are necessary, first of all, to determine the timing and depth of the autumn triggering of the Dnipro reservoirs.

The scientific and methodological base, which is still used by the Ukrainian Hydrometeorological Center for creating of the long-term forecasts and consultations of the ice regime characteristics of water bodies of Ukraine, is represented by developments 30-70 years ago (Guseva, 1947, 1963; Eremenko, 1962). Note that it needs to be fundamentally revised on new scientific and methodological bases and modern approaches. Along with this, there are no methods for the long-term forecasting of the appearance dates of ice phenomena and freeze-up at the reservoirs of the Dnipro Cascade, therefore, such methods need to be developed.

The development problem of the reliable long-term forecasts of the water bodies ice regime is one of the most difficult in hydrometeorology and has not yet received a fully satisfactory solution (WMO, 1975; 1979; 2009; Sutyrina, 2017). The widespread approaches in the long-term forecasting of the ice regime of water bodies are statistical, discriminant, correlation, regression analyses, orthogonal functions for determining optimal predictors of atmospheric processes (WMO, 1979; GOH, 2012; Das et al., 2022). Along with this, two main approaches are used in the long-term forecasting. The first approach is based on finding relationships between the quantitative indicators of atmospheric circulation over the forecasting object or over separate adjacent (large in area) synoptic areas or zones and the terms (dates) of the ice phenomena appearances (more often their deviations from the norm). The second approach is based on physical and statistical methods that use multiple linear regression equations with the representation of hydrometeorological fields when decomposing them by natural orthogonal components or Chebyshev polynomials (WMO, 1979). In recent decades, methods of satellite sensing, teleconnection indices and patterns, and methods of machine learning are intensively developed and used (Massie et al., 2002; Lindenschmidt et al., 2010;

Sutyrina, 2017; Vyshnevskyi and Shevchuk, 2020; Graf et al., 2022).

In papers (Shimaraev, 2007; Sizova et al., 2013; Sutyrina, 2017; Khrystiuk and Gorbachova, 2022) the teleconnection indices were used for the long-term forecasting of the water bodies ice regime and acceptable results were obtained. In the world, the use of the teleconnection indices and patterns is a well-known methodological approach in the hydroclimatic forecasting, which allows forecasting weeks to months in advance (van den Dool, 2007; Chen and Georgakakos, 2014; Chen and Lee, 2017). For the first time, the concept of using teleconnections was proposed by Ångström (1935) who described the correlations between remote oscillations of the atmospheric circulation and anomalies. Later, this approach was widely used for the long-term forecasting of meteorological parameters. Teleconnection indices and patterns are becoming increasingly popular in the hydrological research. So, the teleconnection indicators are used to forecast and analyze the flow of rivers (Peters et al., 2013; Wang et al., 2020), precipitation (He and Guan, 2013; Mekanik et al., 2015), water equivalent of snow cover on the river catchments (Sobolowski and Frei, 2007), droughts (Chiew et al., 1998; Chen and Lee, 2017), ice phenomena (Shimaraev, 2007; Sizova et al, 2013; Sutyrina, 2017; Khrystiuk and Gorbachova, 2022).

The main objective of this research is to develop the long-term forecasting methods of the appearance dates of ice phenomena and freeze-up at the Dnipro Cascade reservoirs using the teleconnection indicators.

Materials and methods

The cascade of the Dnipro reservoirs was created from the end of the 20s to the beginning of the 70s of the 20th century. So, in 1927–1932, the Dnipro Hydro Power Plant (HPP) was built at the Dnipro River. During the Second World War, this station was partially destroyed, but by 1950 it was restored. The construction of Kakhovka HPP lasted from 1950 to 1956, Kremenchuk HPP – during 1954–1960, Kamianske HPP – from 1956 to 1964, Kyiv HPP – during 1960–1964, Kaniv HPP – from 1963 to 1975 (Kaganer, 1976; Khilchevskyi, 2014). So, a total of 6 reservoirs were built on the Dnipro River, which are located in three physiographic zones: forest (Kyiv reservoir), forest-steppe (Kaniv, Kremenchuk, and partially Kamianske Reservoirs) and steppe (Dnipro and Kakhovka and partially Kamianske reservoirs) (Fig. 1) (Kaganer, 1976). The regulation of the Dnipro River by the reservoirs changed the river ice regime compared to its natural regime. Ice phenomena influence the operation of hydrotechnical structures and hydroelectric power plants, duration of navigation, fisheries, etc. Each of the Dnipro reservoirs has own morphometric features, which determine the freezing conditions in its individual sections. The first ice phenomena at the reservoirs appear primarily in the shallow waters, at the mouths of rivers that flow into reservoirs, at the lake areas, where water masses cool earlier due to the shallow depths (Kaganer, 1976; Vyshnevskyi and Shevchuk, 2020). In severe frosts and low wind speed, the ice formation occurs intensively and simultaneously at the all water area of reservoirs. With weak frosts and strong wind speed, when cooling is replaced by warming, the ice formation occurs slowly and extends over a long period of time (Kaganer, 1976).

Systematic observations of the reservoirs ice regime are carried out at coastal water gauges. At the same time, there are no the systematic observations on the water area of reservoirs, sometimes the episodic observations are carried out in the form of expedition surveys, aerial reconnaissance and satellite images. Note that although this information is useful, it cannot replace the systematic observations. The absence of the observations on the water areas of reservoirs makes it difficult to understand the formation conditions of ice phenomena in a spatial section.

Observations of the reservoirs ice regime of the Dnipro Cascade are carried out at 38 coastal water gauges. There are 5 to 8 water gauges on each of the reservoirs (Fig. 1, Table 1). The research used the materials of observations of the hydrological regime of the lakes and reservoirs of the Dnipro River basin contained in various published reference materials prepared by the Central Geophysical Observatory named after Borys Sreznevsky (Kyiv).

An electronic database is created in MS Excel tables, which includes the information about the appearance dates of ice phenomena and freeze-up for the period from the beginning of observations at each water gauge to 2020, inclusive. At the Dnipro Cascade reservoirs the dates of their first appearance in the current winter period were taken for the appearance dates of ice phenomena and freeze-up.

National Weather Service (NWS) of the National Oceanic and Atmospheric Administration of United States of America (NOAA USA) defines the following teleconnection indicators: atmospheric indices, sea surface temperature indices, teleconnection indices and patterns. The NOAA determined the atmospheric indices and sea surface temperature indices for the Pacific region and, partially, the Atlantic region. Teleconnection indices and patterns are calculated for different areas of the Earth. Mean monthly values of all these teleconnection indicators are listed on the website: https://www.cpc.cep.noaa.gov/products/MD_index.php. In our research 34 teleconnection indicators and their standardized values were used.

Usually, at the Dnipro Cascade reservoirs the processes of ice formation are considered from the point of view of the influence of weather conditions (air temperature, speed and direction of wind, etc.), heat supplies in the reservoirs and intensity of their return to the atmosphere, as well as wind waves and flows that mix water masses (Kaganer, 1976). At the Dnipro Cascade reservoirs, the first ice phenomena are usually observed during the invasion of cold arctic air masses on the territory of Ukraine in the autumn-winter period. From year to year the calendar dates of such incursions vary widely and depend on the general atmospheric circulation in the Northern Hemisphere (Guseva, 1947, 1963; Eremenko, 1962; Kaganer, 1976). At the same time, according to modern ideas, the formation of hydrological, including ice, regime of water bodies is the result of complex

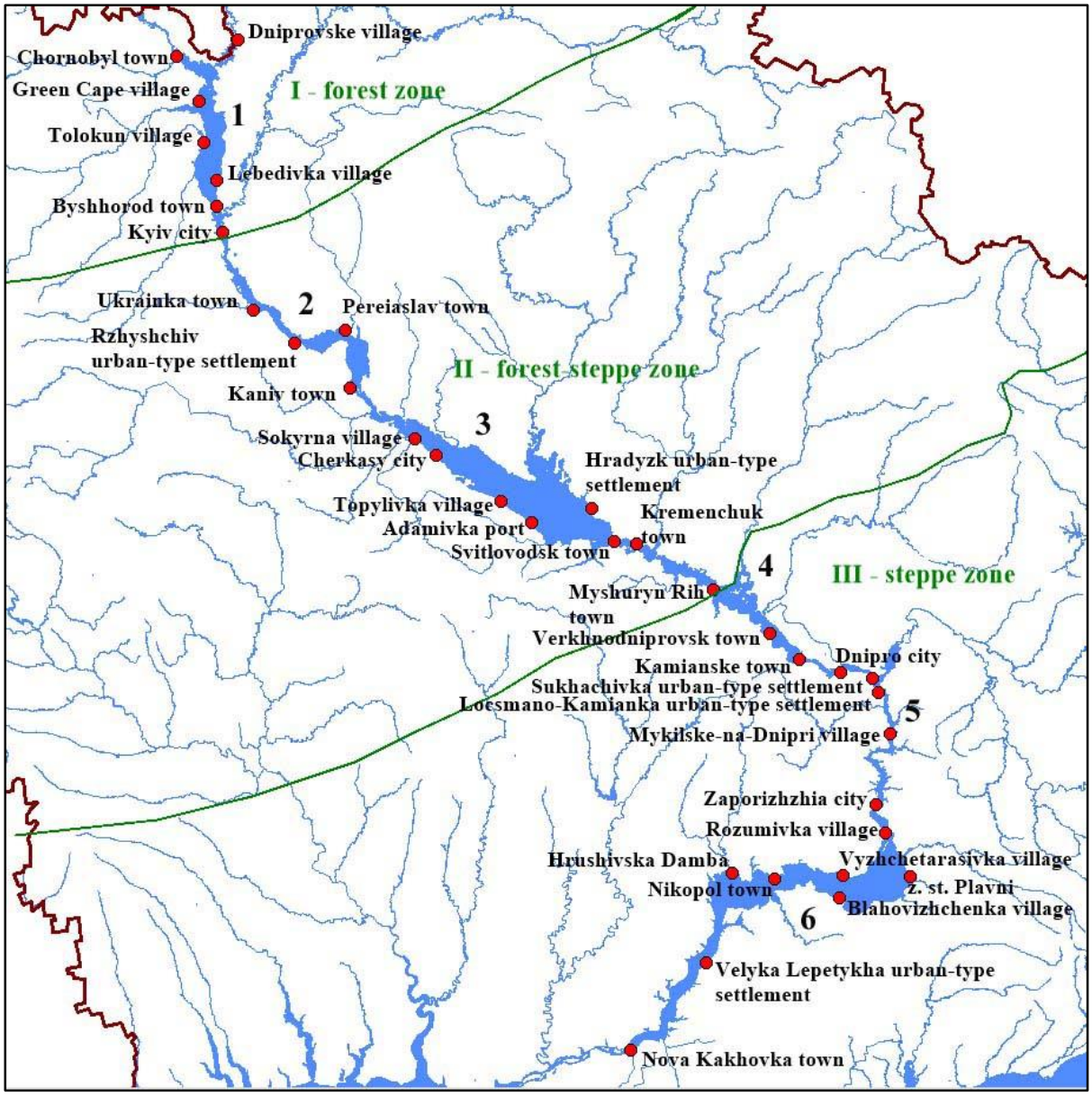

Fig. 1. Scheme of the Dnipro Cascade reservoirs and location of the water gauges on the them (numbering of reservoirs corresponds to Table 1).

processes of climatic and hydrological interactions, which are caused by the circulation of the atmosphere and ocean on the Earth (Wang et al., 2020). So, the basis of the forecasting concept by the teleconnection indicators is the idea of the influence of remote atmospheric circulation fluctuations on the formation of ice phenomena. At the same time, the state of atmospheric circulation is characterized by the various quantitative indices and patterns both in space and time (Sutyrina, 2017). At the Dnipro Cascade reservoirs, the methods of long-term forecasting of the appearance timing of ice phenomena and freeze-up are developed by searching for the best correlation or regression relationship between their dates and teleconnection indicators of the NOAA USA. Along with this, one water gauge-indicator was selected for each reservoir for which a forecasting method was developed. These water gauge-indicators were chosen from among others as those at which the ice phenomena appear annually first. The delay of the ice phenomena appearance at other water gauges is determined by the location of these gauges near the deep-water parts of the reservoir, where significant masses of heat are concentrated; near hydrotechnical structures that violate the natural regime of the reservoir; near the mouths of rivers that flow into the reservoir; in areas with significant water flow, which prevents ice formation.

The assessment of the regression equations quality and accuracy of the long-term forecasting of the appearance timing of ice phenomena and freeze-up at the Dnipro Cascade reservoirs was carried out by the dependent data in accordance to (GOH, 2012). So, the method quality of hydrological forecasting is determined by indicators according to Table 2.

Table 1. List of water gauges at the Dnipro Cascade reservoirs

№	The reservoir name	The year of reservoir filling	The water gauges number	The water gauges name
1	Kyiv reservoir	1966	6	Dniprovske village, Chernobyl town, Green Cape village, Tolokun village, Lebedivka village, Vyshhorod town
2	Kaniv reservoir	1976	6	Vyshhorod town, Kyiv city, Ukrainka town, Rzhyshchiv urban-type settlement, Pereiaslav town, Kaniv town
3	Kremenchuk reservoir	1961	7	Kaniv town, Sokyrna village, Cherkasy city, Topylivka village, Adamivka port, Hradyzk urban-type settlement, Svitlovodsk town
4	Kamianske reservoir	1964	5	Svitlovodsk town, Kremenchuk town, Myshuryn Rih village, Verkhnodniprovsk town, Kamianske town
5	Dnipro reservoir	(1932) 1948	6	Kamianske town, Dnipro city, Sukhachivka urban-type settlement, Locsmano-Kamianka urban-type settlement, Mykilske-na-Dnipri village, Zaporizhzhia city
6	Kakhovka reservoir	1958	8	Rozumivka village, z.st. Plavni, Blahovishchenka village, Vyshchetarasivka village, Nikopol town, Hrushivska Damba, Velyka Lepetykha urban-type settlement, Nova Kakhovka town

Table 2. Indicators of quality of the hydrological forecasting method for the series population $n \geq 25$ (GOH, 2012)

Category	Indicators of quality		
	$\bar{S}/\bar{\sigma}$	coefficient of determination *(R)*	probability of acceptable forecast error (δ_a, %)
good	≤ 0.50	≥ 0.87	≥ 82
satisfactory	0.51 – 0.80	0.86 – 0.60	81–60

The mean square deviation of the forecast value ($\bar{\sigma}$) and mean square error of the verification forecasts ($\bar{S}$) were determined by the formulas:

$$\bar{\sigma} = \sqrt{(\sum_1^n \Delta D_i^2)/(n-1)} \quad (1)$$

$$\bar{S} = \sqrt{(\sum_1^n (D - D')^2)/n} \quad (2)$$

where:
ΔD_i – is the deviation of the appearance dates of ice phenomena/freeze-up (D_i) from mean date for multi-year observation period ($\bar{D}$);
n – is the population of the series;
D – is the historical date;
D' – is the forecast date.

Acceptable forecast error was determined by the formula:

$$\delta_a = \pm 0.674\bar{\sigma} \quad (3)$$

Probability of acceptable forecast error was determined by the formula:

$$\delta_p = (N'/N)\ 100\% \quad (4)$$

where:
N' – is the number of forecasts, the error of which did not exceed the acceptable forecast error;
N – is the total number of forecasts.

The numerical expression of the appearance dates of ice phenomena and freeze-up was carried out by determining their deviations from November 30 (a conventional date that is adopted for all reservoirs of the Dnipro Cascade for the convenience of calculations).

Results and discussion

The analysis of the observation series of the appearance dates of ice phenomena and freeze-up at 38 water gauges of the Dnipro Cascade reservoirs made it possible to determine the water gauge-indicators for which the long-term forecasting methods were developed. The Kremenchuk reservoir is divided into two parts – the upper (channel) and the lower (lake) according to morphometric characteristics. So, the methods of the long-term forecasting of the appearance timing of ice phenomena and freeze-up were developed separately for the upper and lower parts of this reservoir.
At the Dnipro Cascade reservoirs, the mean values, early and late of the appearance dates of ice phenomena and

freeze-up naturally change from north to south in accordance with the physical and geographical conditions of their formation and the individual characteristics of the locations of the water gauge-indicators. The appearance dates of ice phenomena and freeze-up are characterized by significant fluctuations. So, the differences between the late and early dates of the appearance of ice phenomena and freeze-up are about 3 months. The calculated acceptable forecast errors have the range from 10 to 13 days (Table 3).

Analysis of correlation and regression relationships of 34 atmospheric indices, sea surface temperature indices, teleconnection indices and patterns of NOAA USA with the appearance dates of ice phenomena and freeze-up at the water gauge-indicators made it possible to find the best such relationships and to determine predictors (indices and patterns) for forecasting. It turned out that the appearance dates of ice phenomena and freeze-up are determined by the values of 15 teleconnection indices and patterns for different months (Table 4, 5). So, at the Dnipro Cascade reservoirs the formation of ice phenomena and freeze-up is caused by the atmospheric circulation processes at the North and the East Atlantic (NATL, EA, SCAND, EATL/WRUS), the Arctic (AO), the Pacific Ocean (Niño 1+2, Niño 3, PNA, TAHITI, SOI, Darwin), and also near the equator (Z500t, EqSOI, repac_slpa, TROPан). The diversity of the atmospheric circulation processes also determines the instability of the ice regime and significant variability of the timing of its main phases at the Dnipro Cascade reservoirs.

The results of the checking of forecast regression equations (Table 4) according to the dependent data show that these dependencies quite satisfactorily reproduce the historical dates of the appearance of ice phenomena and freeze-up at the Dnipro Cascade reservoirs (an example is shown in Fig. 2). Forecast values in most cases do not exceed the acceptable forecast errors. The value of the extreme dates of the appearance of ice

Table 3. Statistical characteristics of the observation series of the appearance dates of ice phenomena and freeze-up at the water gauges- indicators of the Dnipro Cascade reservoirs

The water gauges name	Period and duration of observations years	The mean date	The early date	The late date	ΔA day	δ_a day	P_m
the appearance of ice phenomena							
Kyiv reservoir – Green Cape village	1966–1974, 1978–2020 / 52	November 27	30.10.1979	28.01.2007	90	11	38
Kaniv reservoir – Kyiv city	1977–2020 / 43	December 13	17.11.1993	10.02.2020	85	12	54
Kremenchuk reservoir – Cherkasy city	1976–2020 / 45	December 15	14.11.1993	08.02.2020	86	13	56
Kremenchuk reservoir – Adamivka port	1976–2020 / 45	December 10	13.11.1993	30.01.2007	78	10	51
Kamianske reservoir – Myshuryn Rih village	1954–2020 / 57	December 10	01.11.2000	09.02.2020	100	11	51
Dnipro reservoir – Kamianske town	1963–1986, 1989–2020 / 55	December 21	18.11.1993	09.02.2020	83	13	62
Kakhovka reservoir – Blahovishchenka village	1958–2020 / 63	December 20	12.11.1993	08.02.2020	87	13	61
the appearance date of freeze-up							
Kyiv reservoir – Green Cape village	1966–1974, 1978–2020 / 52	December 1	01.11.1979	28.01.2007	88	12	30
Kaniv reservoir – Pereiaslav town	1977–2020 / 44	December 14	14.11.1993	31.01.2007	78	10	43
Kremenchuk reservoir – Cherkasy city	1976–2020 / 45	December 20	20.11.1993	05.02.2001	77	13	49
Kremenchuk reservoir – Topylivka village	1976–2020 / 45	December 16	13.11.1993	31.01.2007	79	11	45
Kamianske reservoir – Myshuryn Rih village	1954–2020 / 57	December 19	03.11.2014	04.02.2001	93	12	48
Dnipro reservoir – Locsmano-Kamianka urban-type settlement	1964–2020 / 56	December 23	15.11.1993	03.02.2007	80	13	52
Kakhovka reservoir – z.st. Plavni	1968–2020 / 53	December 22	15.11.1993	17.02.2004	91	13	51

Note: ΔA – the difference between the late and the early dates of the appearance of ice phenomena/freeze-up; δ_a – acceptable forecast error; P_m – mean forecast lead time (the forecasts are released October 20 (the appearance dates of ice phenomena) and on November 1 (the appearance dates of freeze-up)).

Table 4. Dependencies for the long-term forecasting of the appearance dates of ice phenomena and freeze-up at the Dnipro Cascade reservoirs

The water gauges name	The forecasting equation	$\overline{S}/\overline{\sigma}$	δ_p [%]
	the appearance of ice phenomena		
Kyiv reservoir – Green Cape village	$\Delta I = -408.63 + 14.48 \cdot NATL_{IX} + 1.13 \cdot Z500t_{IX}$	0.92	67
Kaniv reservoir – Kyiv city	$\Delta I = 12.20 - 12.81 \cdot AO_{VII\text{-}IX} + 2.29 \cdot EqSOI_{II}$	0.96	72
Kremenchuk reservoir – Cherkasy city	$\Delta I = 14.46 + 6.56 \cdot EA_{VI} - 5.14 \cdot AO_{VII\text{-}IX}$	0.92	69
Kremenchuk reservoir – Adamivka port	$\Delta I = 102.21 - 4.21 \cdot SCAND_{VI} - 3.76 \cdot Niño\ 1{+}2_{I}$	0.94	71
Kamianske reservoir – Myshuryn Rih village	$\Delta I = 10.18 - 4.50 \cdot PNA_{II} - 2.50 \cdot repac\_slpa_{IX}$	0.95	67
Dnipro reservoir – Kamianske town	$\Delta I = 20.39 + 7.81 \cdot TAHITI_{IV} - 0.57 \cdot SOI_{IV}$	0.95	64
Kakhovka reservoir – Blahovishchenka village	$\Delta I = 20.70 - 5.71 \cdot EATL/WRUS_{VII\text{-}IX} + 2.82 \cdot SOI_{I}$	0.95	61
	the appearance date of freeze-up		
Kyiv reservoir – Green Cape village	$\Delta F = -947.80 + 13.07 \cdot NATL_{IX} + 21.55 \cdot TPOR_{VIII\text{-}IX}$	0.88	66
Kaniv reservoir – Pereiaslav town	$\Delta F = 14.66 - 4.88 \cdot EA_{I} - 4.53 \cdot PNA_{II}$	0.89	70
Kremenchuk reservoir – Cherkasy city	$\Delta F = 20.72 - 5.30 \cdot SCAND_{V} + 3.38 \cdot EAWR_{I\text{-}II}$	0.94	70
Kremenchuk reservoir – Topylivka village	$\Delta F = -48.85 + 16.96 \cdot TROPan_{IX} + 2.61 \cdot Niño\ 3_{IX}$	0.93	68
Kamianske reservoir – Myshuryn Rih village	$\Delta F = 17.18 - 6.08 \cdot Darwin_{III} - 4.32 \cdot SCAND_{V}$	0.89	69
Dnipro reservoir – Locsmano-Kamianka urban-type settlement	$\Delta F = 22.77 + 4.93 \cdot TAHITI_{IV} + 2.25 \cdot SOI_{IV}$	0.96	64
Kakhovka reservoir – z.st. Plavni	$\Delta F = 21.24 - 4.20 \cdot EATL/WRUS_{VIII} + 6.18 \cdot TAHITI_{IV}$	0.93	67

Note: $\overline{S}$ – mean square error of the verification forecasts; $\overline{\sigma}$ – mean square deviation of the forecast value; δ_p [%] – probability of acceptable forecast error; ΔI, ΔF – the forecast deviations of the appearance dates of the ice phenomena and the freeze-up from the conditional date November 30, days.

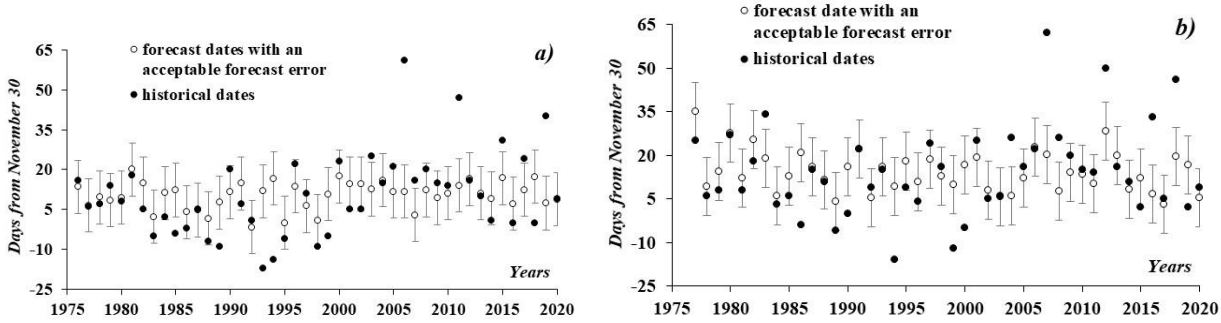

Fig. 2. Historical and forecasted (with an acceptable forecast error) appearance dates of ice phenomena at the Kremenchuk Reservoir near Adamivka port (a) and the appearance dates of freeze-up at the Kaniv Reservoir near Pereyaslav city (b).

phenomena and freeze-up are the exception. It is determining the high values of the ratio of the mean square error of the verification forecasts ($\overline{S}$) to the mean square deviation of the forecast value ($\overline{\sigma}$) (Table 4). At the same time, the probabilities of acceptable errors of the hydrological forecasting methods of the appearance dates of ice phenomena and freeze-up at all water gauge-indicators correspond to the quality assessment "satisfactory" according to (Table 1). This makes it possible to recommend the developed methods for the forecasting of the appearance dates of ice phenomena and freeze-up at the Dnipro Cascade reservoirs.

In the papers (Shimaraev, 2007; Sizova et al, 2013; Sutyrina, 2017) for the long-term forecasting of the ice regime of water bodies using the teleconnection indices, the quality assessments of the developed methods were obtained, which have the "good" category according to (Table 1). The lower quality category of methods for the long-term forecasting of the appearance dates of ice phenomena and freeze-up at the Dnipro Cascade reservoirs is obviously due to the significant variability of atmospheric processes over the territory of Ukraine in the autumn-winter period. Nevertheless, the use of teleconnection indicators as predictors, although it does not fully solve the problem of the long-term forecasting of the appearance dates of ice phenomena and freeze-up at the Dnipro Cascade reservoirs, however, expands its possibilities.

Table 5. Description of teleconnection indicators, which are used as predictors in the forecast dependencies in the Table 4

№	The name of the teleconnection indicator	Short description of the teleconnection indicator	The beginning year of the indicator calculation
1	North Atlantic (5–20°North, 60–30°West), NATL	It is determined for the water surface temperature in the North Atlantic, a rectangle of 5–20°N, 60–30°W	1982
2	Zonally Average 500 MB Temperature Anomalies (Z500t)	It is determined on air temperature anomalies averaged in the 20°N band.–20°S, on the isobaric surface of 500 mb	1979
3	Arctic oscillation (AO) index	It is determined on the values of air pressure anomalies in northern latitudes (norther than 20°N)	1950
4	Equatorial SOI, (EqSOI)	It is determined on atmospheric pressure indicators at sea level in rectangles 80°–130°W, 5°S–5°N and 5°S–5°N, 90°–140°E	1949
5	East Atlantic (EA) pattern	Similar to the North Atlantic Oscillation (NAO) pattern, but the centers of its anomalies are shifted to the southeast	1950
6	Scandinavia pattern (SCAND)	It is determined on the atmospheric circulation nature over Scandinavia, Western Europe and the eastern part of the Russian Federation/western part of Mongolia	1950
7	Niño 1+2 (0–10°South) (90°West–80°West)	It is determined on the temperature of the water surface of the Pacific Ocean in the rectangle 0–10°S, 90–80°W	1950
8	Pacific - North American (PNA) index	It is determined on the atmospheric circulation nature over the northern part of the Pacific Ocean and the North American continent	1950
9	repac_slpa	It is determined on the atmospheric pressure at sea level in the eastern equatorial region of the Pacific Ocean in the rectangle 5°S–5°N, 80°–130°W	1949
10	Tahiti Sea Level Pressure	It is determined on atmospheric pressure at sea level at the Tahiti station (an island in the Pacific Ocean)	1951
11	Southern Oscillation Index (SOI)	It is determined on atmospheric pressure at sea level at Darwin and Tahiti stations	1951
12	East Atlantic/ West Russia (EATL/WRUS) pattern	It is determined on the atmospheric circulation nature over Europe, the northern part of China, the center of the North Atlantic and the northern part of the Caspian Sea	1950
13	Global Tropics (10°South-10 North, 0-360), TROPта TROPан	It is determined on the temperature of the water surface of the Pacific and Atlantic oceans in the band of 10°S–10°N, 0–360°	1982
14	Niño 3 (5°North–South) (150°West–90°West)	It is determined on the surface temperature of the Pacific Ocean in the rectangle 5°N–5°S, 150–90°W	1950
15	Darwin Sea Level Pressure	It is determined on atmospheric pressure at sea level at the Darwin station (Australia)	1951

Conclusion

For the first time, for the Dnipro Cascade reservoirs the methods for the long-term forecasting of the appearance dates of ice phenomena and freeze-up using 34 teleconnection indicators, namely atmospheric indices, sea surface temperature indices, teleconnection indices and patterns were developed. The forecast equations contain 15 teleconnection indicators for different months which is describe the atmospheric circulation processes in the North and the East Atlantic, the Arctic, the Pacific Ocean, and also near the equator. The verification of the developed methods based on dependent data showed that the probabilities of acceptable errors is within 61–72%, which corresponds to the assessment of the method quality as "satisfactory". This makes it possible to recommend them for use in the operational forecasting. Forecasts can create for the ice phenomena appearance at October 20 and for the freeze-up appearance at November 1, provided that the values of the teleconnection indicators are published on the website of the NOAA USA. The mean forecasts lead time ranges

from 38 to 62 days for the appearance dates of ice phenomena and from 64 to 70 days for the appearance dates of freeze-up.

At the Dnipro Cascade reservoirs, the development of the long-term forecasting methods of the appearance dates of ice phenomena and freeze-up is complicated by their significant fluctuations, due to the significant variability of atmospheric processes over the territory of Ukraine in the autumn-winter period.

The use of the teleconnection indicators for the long-term forecasting of the appearance dates of ice phenomena and freeze-up at the Dnipro Cascade reservoirs provides the acceptable results. Therefore, a similar approach can be used to develop the methods of the long-term forecasting of other characteristics of the ice regime, for example, the timing of freeze-up break-up and ice phenomena disappearances at the reservoirs and rivers of Ukraine.

Acknowledgement

This research was conducted within project № 5/21 "Development of a system for long-term forecasting of the appearance of ice regime phases of the reservoirs of the Dnipro River basin" of the Ukrainian Hydrometeorological Institute (state registration № 0121U108580).

References

Ångström, A. (1935): Teleconnections of Climatic Changes in Present Time. Geografiska Annaler, Vol. 17, 242–258.

Chen, C.-J., Georgakakos, A. P. (2014): Hydro-climatic forecasting using sea surface temperatures: methodology and application for the southeast US. Climate Dynamic, Vol. 42, 2955–2982. https://doi.org/10.1007/s00382-013-1908-4

Chen, C.-J., Lee, T.-Y. (2017): An Investigation into the Relationship between Teleconnections and Taiwan's Streamflow. Hydrology and Earth System Sciences Discussions, Vol. 21, 3463–3481. https://doi.org/10.5194/hess-21-3463-2017

Chiew, F. H. S., Piechota, T. C., Dracup, J. A., Mcmahon, T. A. (1998): El Nino/Southern Oscillation and Australian rainfall, streamflow and drought: links and potential for forecasting. Journal of Hydrology, Vol. 204, no. 1–4, 138–149. https://doi.org/10.1016/S0022-1694(97)00121-2

Das, A., Budhathoki, S., Lindenschmidt, K.-E. (2022): Stochastic modelling approach to forecast real-time ice jam flood severity along the transborder (New Brunswick/Maine) Saint John River of North America. Stochastic Environmental Research and Risk Assessment, Vol. 36. 1903–1915. https://doi.org/10.21203/rs.3.rs-748153/v1

Eremenko, L. V. (1962): Method of the rivers freezing forecasting of the Upper and Middle Dnipro based on the analysis of atmospheric processes (report). Kyiv: Department of Hydrometeorological Service of Ukrainian SSR. (in Russian)

Graf, R., Kolerski, T., Zhu, S. (2022): Predicting Ice Phenomena in a River Using the Artificial Neural Network and Extreme Gradient Boosting. Resources, Vol. 11, no. 2, 12. https://doi.org/10.3390/resources11020012

Guidelines for operational hydrology (GOH) (2012): Forecasts of the land water regime. Hydrological support and service. K.: PP "Verlan". (in Ukrainian)

Guseva, A. A. (1947): Analysis of the synoptic conditions of the opening and freezing of the rivers of Ukraine and its application in hydroprognostication of these phenomena (report). Kyiv: Department of Hydrometeorological Service of Ukrainian SSR. (in Russian)

Guseva, A. A. (1963): Method of long-term rivers freezing forecasting of the Upper and Middle Dnipro basin based on the analysis of atmospheric processes (report). Kyiv: Department of Hydrometeorological Service of Ukrainian SSR. (in Russian)

He, X., Guan, H. (2013): Multiresolution analysis of precipitation teleconnections with large-scale climate signals: A case study in South Australia. Water Resources Research, Vol. 49, no. 10, 6995–7008. https://doi.org/10.1002/wrcr.20560

Kaganer, M. S. (eds). (1976): Hydrometeorological regime of lakes and reservoirs of the USSR. Cascade of the Dnieper reservoirs. Leningrad: Gidrometeoizdat. (in Russian)

Khilchevskyi, V. K. (eds). (2014): Water fund of Ukraine. Artificial reservoirs. Reservoirs and ponds. Kyiv: Interpress LTD. (in Ukrainian)

Khrystiuk, B. F., Gorbachova, L. O. (2022): Application of the Natl Index for Long-Term Forecasting of Freeze-Up Appearance Date at the Kyiv Reservoir. Proceedings of the XVI International Scientific Conference «Monitoring of Geological Processes and Ecological Condition of the Environment», Kyiv, Ukraine, November 15–18, 2022. European Association of Geoscientists & Engineers (EAGE), Vol. 2022, 1–5. https://doi.org/10.3997/2214-4609.2022580071

Lindenschmidt, K., Syrenne, G., Harrison, R. (2010): Measuring ice thicknesses along the Red River in Canada using RADARSAT-2 satellite imagery. Journal of Water Resource and Protection, Vol. 2, 923–933. https://doi.org/10.4236/jwarp.2010.211110

Massie, D. D., White, K. D., Daly, S. F. (2002): Application of neural networks to predict ice jam occurrence. Cold Regions Science and Technology, Vol. 35, 115–122. https://doi.org/10.1016/S0165-232X(02)00056-3

Mekanik, F., Imteaz, M. A., Talei, A. (2015): Seasonal rainfall forecasting by adaptive network-based fuzzy inference system (ANFIS) using large scale climate signals. Climate Dynamics, Vol. 46, no. 9–10, 3097-3111. https://doi.org/10.1007/s00382-015-2755-2

Peters, D. L., Atkinson, D. E., Monk, W., Tenenbaum, D. E., Baird, D. J. (2013): A multi-scale hydroclimatic analysis of runoff generation in the Athabasca River, western Canada. Hydrological Processes, Vol. 27, no. 13, 1915–1934. https://doi.org/10.1002/hyp.9699

Scherbak, A. V., Zelenskaya, M. V., Haidai, Yu. M. (2007): The ice regime of Ukraine rivers (ice formation and its characteristics). Proceeding of Ukrainian Hydro-meteorological Institute, Vol. 256, 214–222. Available at: https://uhmi.org.ua/pub/np/256/3-Sherbak_Zelen.pdf (in Ukrainian with English abstract)

Shimaraev, M. N. (2007): Circulation factors of changes in the ice-thermal regime of the Lake Baikal. Geography and natural resources, Vol. 4, 54-60. (in Russian)

Sizova, L. N., Kuimova, L. N., Shimaraev, M. N. (2013): Influence of the atmospheric circulation on ice-thermal processes on Baikal during 1950–2010. Geography and natural resources, Vol. 34, 158–165. https://doi.org/10.1134/S187537281302008X

Sobolowski, S., Frei, A. (2007): Lagged relationships between North American snow mass and atmospheric teleconnection indices. International Journal of Climatology, Vol. 27, no. 2, 221–231. https://doi.org/10.1002/joc.1395

Sutyrina, E. N. (2017): Long-term forecasting techniques for the terms of the complete disappearance of ice on reservoirs of the Angara-Yenisei cascade. Geographical Bulletin, Vol. 1, no. 40, 66–72. https://doi.org/10.17072/2079-7877-2017-1-66-72 (in Russian)

van den Dool, H. (2007): Empirical methods in short-term climate prediction. Oxford University Press Publ.

Vyshnevskyi, V. I., Shevchuk, S. A. (2020): Use of remote sensing data to study ice cover in the Dnipro Reservoirs. Journal of Geology, Geography, and Geoecology, Vol. 29, no. 1, 206–216. https://doi.org/10.15421/112019

Wang, J., Wang, X., Lei X., Wang H., Zhang X., You J., Tan Q., Liu X. (2020): Teleconnection analysis of monthly streamflow using ensemble empirical mode decomposition. Journal of Hydrology, Vol. 582, 124411. https://doi.org/10.1016/j.jhydrol.2019.124411

World Meteorological Organization (WMO) (1975): Hydrological forecasting practices. Operational Hydrology. Report No. 6. WMO-No. 425, World Meteorological Organization, Geneva, Switzerland.

World Meteorological Organization (WMO) (1979): Methods of long-term forecasts of ice phenomena on rivers and reservoirs. Technical report to the Commission for Hydrology-No. 09, World Meteorological Organization, Geneva, Switzerland.

World Meteorological Organization (WMO) (2009): Guide to Hydrological Practices, Vol. II, Management of Water Resources and Application of Hydrological Practices, sixth edition, WMO-No. 168, World Meteorological Organization, Geneva, Switzerland.

Prof. Liudmyla Gorbachova, Dr.Sc. (*corresponding author e-mail: gorbachova@uhmi.org.ua)
Assoc. Prof. Borys Khrystiuk, PhD.
Ukrainian Hydrometeorological Institute
37, Prospekt Nauky
03028, Kyiv
Ukraine

DOI: 10.31577/ahs-2023-0024.01.0005

ACTA HYDROLOGICA SLOVACA

Volume 24, No. 1, 2023, 33 – 42

Analysis of seasonal changes of thermal stratification in reservoir for drinking water supply (Slovakia, Turček reservoir)

Adrián VARGA*, Yvetta VELÍSKOVÁ, Marek SOKÁČ,
Valentín SOČUVKA, Pavol MIKULA

Water reservoirs are important source in supplying inhabitants with drinking water of high–quality. In total, there are 8 reservoirs in Slovakia for drinking water supply purpose. The youngest of them is the Turček reservoir located in the middle of Slovakia, which is also the object of this study. In the article, we deal with the thermal stratification in it during 3 seasons (spring, summer, autumn). Based on the analysis of data provided by the operator of the reservoir from its operation start, it came out that the thermal stratification in the reservoir occurs significantly during the summer. In the given hydro–climatic conditions, it starts at the end of April and ends in October. We also analyzed the existence of the thermocline layer, which occurs mainly in the summer, but also in spring and in autumn, but not so significantly and regularly. Thermal stratification can be classified also by Thermocline Strength Index (TSI) that indicates the steepness of the thermocline or the average gradient of the thermocline layer, so the part of the study was focused also to this indicator.

KEY WORDS: water reservoir, water temperature, stratification, thermocline

Introduction

Thermal stratification is a phenomenon in water bodies such as lakes and reservoirs where the epilimnion and hypolimnion are separated by strong vertical density gradients (metalimnion or thermocline) as a result of seasonal temperature variations (Boehrer and Schultze, 2008; James et al., 2017). Stratification plays a vital role in reservoir water quality management, as it can significantly influence the hydrodynamics and water quality regimes (Lee et al., 2013), eutrophication and sediment transport processes (Scheu et al., 2015; Zhang et al., 2020) and nutrient and phytoplankton dynamics (Liu et al., 2009).

Thermal stratification is one of the primary physical processes in lakes and reservoirs, resulting from the thermal expansion of water by solar heating (Woolway and Merchant, 2019). This stratification is crucial for water quality and ecological processes assessment in deep lakes and reservoirs and can be substantially affected by meteorological and hydrological processes in the catchment (Liu et al., 2020).

The degree of stratification depends on climatic factors, as well as on morphology, and in the case of reservoirs flow rates. In temperate zones, a lake is isothermal with typical temperatures at about 4°C in early spring. As the season progresses, lakes begin to warm and differential absorption of heat induces stratification forming the so-called epilimnion and hypolimnion. Later during cooling periods, when the temperature of the water at the surface begins to decrease, convective mixing occurs through the unequal density of the water. Strong circulation and mixing of water can eventually destroy thermal stratification. Water turnovers are especially pronounced when surface waters reach 4°C, i.e. maximum water density. Wind mixing also contributes to water temperatures distribution (Meyer et al., 1994).

Impacts of global climate changes may cause modifications of stratification regimes. The impact of rainfalls on the thermal stratification and dissolved oxygen in riverine zone was more impressive than that in transitional and lacustrine zones of reservoirs (Liu et al., 2020). According to the hydro–meteorological data from the Turček reservoir, there are no frequent occurrences of storms or heavy rains there – storms occur 2–3 times per year – so a strong influence on stratification at the given site is unlikely.

Anyway, many studies have highlighted that increasing air temperature has led to the rapidly warming of water (Bajtek et al., 2022; Vyshnevskyi and Shevchuk, 2022) and stronger thermal stratification (Kraemer Benjamin et al., 2015; Onderka, 2004; O' Reilly et al., 2015; Piccolroaz et al., 2018; Valerio et al., 2015; Woolway

and Merchant, 2019). On the other side, decreasing wind speed coupled with increasing air temperature led to increased thermal stability and reduced water column mixing in Lake Tanganyika (O' Reilly et al., 2003). So, there are still many questions without clear answers to them.

Aim of this study is the analysis of seasonal changes of thermal stratification in the Turček reservoir, which was started to build as a reservoir for drinking water supply in 1993 and put in the full operation in 1998. This study aims to gain a good understanding of the thermal regime changes of a reservoir on the base of data analysis from the reservoir operation start and on that base (outcome information) it will be able to predict trends in different future conditions.

Layers of stratification

Stratification is defined as the act of sorting data, people or objects into distinct groups or layers. In case of the thermal stratification in reservoirs it means the dividing of water volume of reservoir in general to three layers.

The upper layer, epilimnion is constantly mixed by wind and a wave generated with it, and is warmed by sun. The epilimnion thickness is not constant over the stratification period. In spring, a thin layer is formed, which throughout the summer gradually gains thickness because of wind action. It is not until autumn, that colder water from the water body surface can erode the stratification to the hypolimnion at a larger rate. During this later period of thermal stratification, substances dissolved in hypolimnetic waters, such as nutrients, become available in the epilimnion again. If surface temperature falls enough, epilimnion and hypolimnion can be mixed, and the entire water body is homogenized (circulation period) to one layer, the so-called mixolimnion. (Boehrer and Schultze, 2008)

The next layer, metalimnion, is described by a steep temperature gradient in a body of water (Liu et al., 2020). This layer is the middle layer between the mentioned epilimnion and the deepest layer, hypolimnion (see Fig. 1). As it was mentioned above, water temperature in the metalimnion changes steeply with water depth. Some authors define this middle part, where the water temperature changes by the steepest way, as the thermocline. Thermocline is a relatively thin part of the metalimnion layer in which temperature decreases rapidly with depth increase. The thermocline has been defined for partial unification, but on a strictly arbitraty basis, as a layer of water in which the temperature decrease 1° or more along 1 meter of the depth. A decrease in temperature is accompanied by an increase in density and a corresponding increase in resistance to mixing. (Kittrell, 1965)

The bottom layer of the reservoir is the hypolimnion. Water in this layer is excluded from the atmosphere influence by the overlying metalimnion and epilimnion. Only few light and heat from the sun penetrates these depths, and there is very little temperature rise once the stratification is formed. Most of the increase takes place in the upper part of the hypolimnion, which produces a slight temperature gradient from top to bottom. (Kittrell, 1965)

Description of locality

The Turček Water Reservoir was built from 1993 to 1996. The main task of the Turček Water Reservoir is the accumulation and supply of raw water for later drinking water treatment process. Its secondary mission is flood protection of the downstream part of the Turiec brook basin, to ensure ecologically stable flow throughout the year, and to produce electricity in small hydroelectric power plants. The reservoir is located at the confluence of the Turiec and Ružový brook streams above the Turček village. The dam profile is placed below the confluence of both streams. The width of the valley is approximately 120 m and the elevation in the dam profile is 719 asl. The total volume of the reservoir is 10.8 million m^3, while its storage volume is 9.1 million m^3 and the constant volume is 0.3 million m^3 of water. The strength of the dam is ensured by its retaining wall, which has a height of 59 m

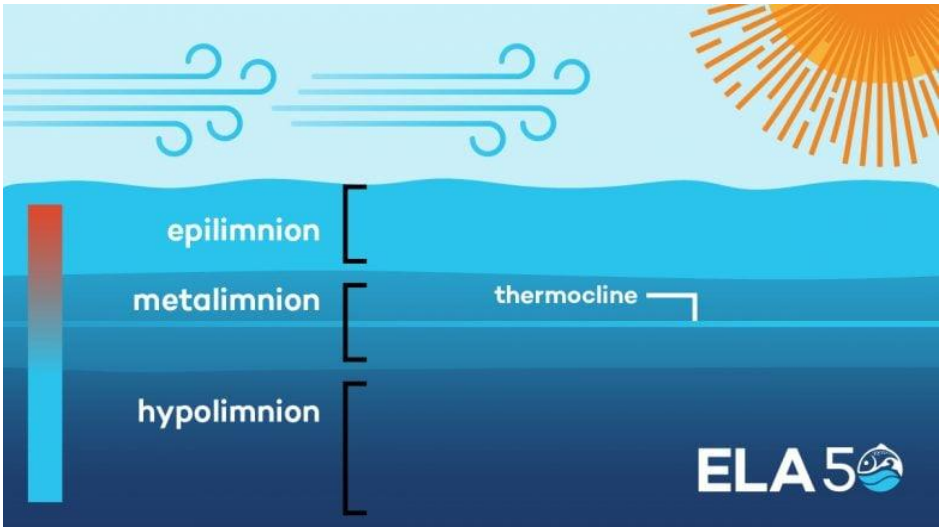

Fig. 1. Layers of water stratification (Source: Fafard, 2018).

and a crown length of 287.6 m. The total area of the basin is 29.85 km^2. The amount of water supplied to the water treatment plant is 15.8 million m^3 per year. The Turček water reservoir was put into operation on May 15, 1996. (Chmelár, 1998) Mean annual precipitation is 960 mm with maximal values in June and July, mean air temperature is 6.4°C with maximal values in July and August (Rules of manipulation, 2019). Current bathymetry of the reservoir from own measurements is shown in Fig. 2.

Method

Data on air temperature and water quality were provided to us by the water reservoir operator, the Slovak Water Management Enterprise, from its archives for period 1997–2022. Data was in the paper form, so for the next use and analysis, it was necessary to digitize them.

Water quality is monitored at 4–5 monitoring localities/points inside the reservoir in vertical direction at several horizons (Fig. 3, Table 1), with taking samples in each 5 m depth and by in situ measurements (pH, dissolved oxygen, water conductivity, water temperature) which was performed directly on the water surface from a boat equipped with a motor for maintaining the position and the GPS device for locating points. This kind of measurement was made in each meter of depth. A selected range of physiochemical, microbiological and hydrobiological indicators was monitored in the reservoir 3 times per year (spring, summer, autumn) (Mikula, 2022).

Monitoring dates were as follows: spring sampling was carried out from the end of April (because of ice cover) to mid-May, summer sampling was carried out during July, and autumn sampling was carried out from mid-October to the beginning of November.

Vertical water temperature profiles were evaluated analytically and also graphically for each measurement campaign, based on this evaluation, the distribution of epilimnion, metalimnion and hypolimnion layers was determined for each case where thermal stratification was formed. At the same time, based on the definition of the thermocline, it was determined where the thermocline layer was located in individual years during the monitored period.

Thermal stratification can be classified also by the Thermocline Strength Index (TSI) (Yu et al., 2010). This indicator can be computed using the equation:

$$TSI = \frac{\Delta T}{\Delta h} \quad (1)$$

where

ΔT – is the difference of water temperature [°C],

Δh – is and the difference of water depth [m].

TSI simply indicates the steepness of the thermocline or the average gradient of the thermocline layer (Liu et al., 2019).

Existence of a thermocline is recognized if TSI > 1 [°C m^{-1}] and the stratification becomes more pronounced with a higher TSI value (Horne and Goldman 1994).

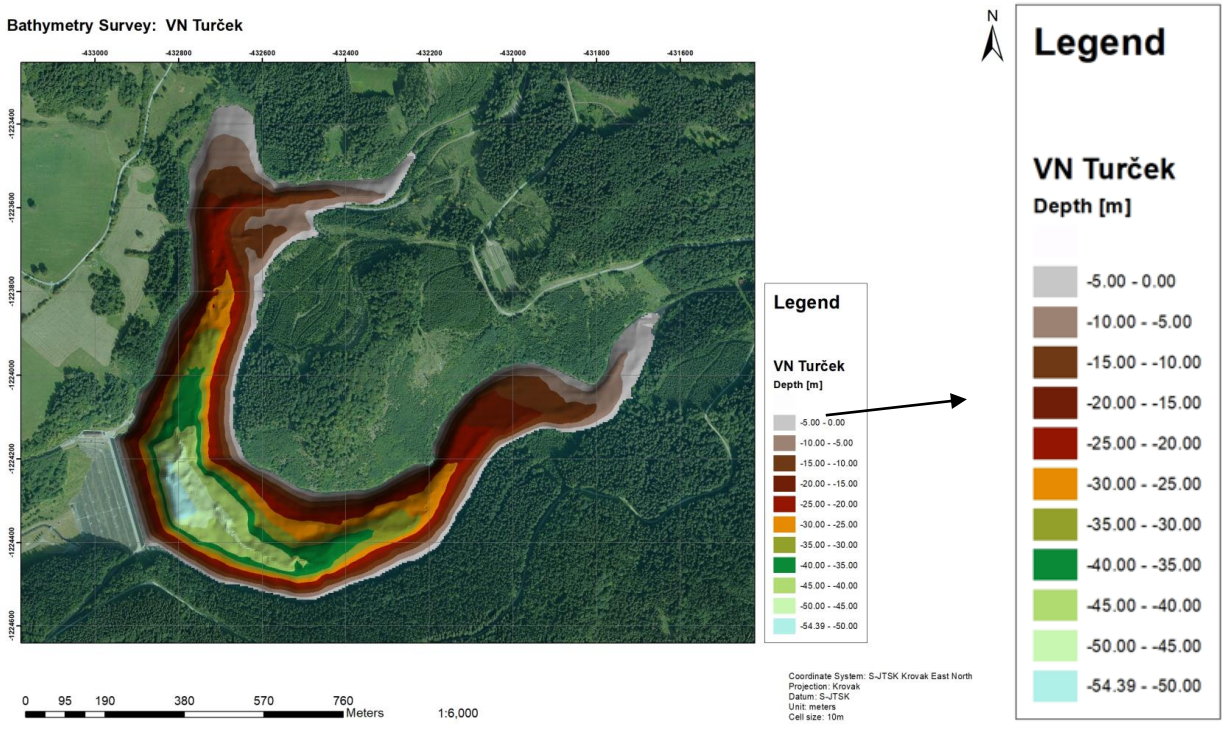

Fig. 2. Map of the Turček reservoir bathymetry.

Table 1. Coordinates and depths of 5 monitoring sites

Monitoring site	Coordinates (N / E)	Max depth
1	48.763159 / 18.939620	47 m
2	48.763666 / 18.945901	27 m
3	48.765962 / 18.949415	13 m
4	48.764264 / 18.937379	40 m
5	48.768097 / 18.938869	24 m

Fig. 3. Monitoring sites for measuring water quality parameters.

Results and discussion

In general, three vertical thermal profiles averaging temperature from 5 monitoring points could be determined for each year in evaluated period 1997–2022, one for each season. Anyway, in the years 2015, 2017 and 2020, data from some seasons were missing. In the study, we do not report all vertical water temperature profile graphically, but only mention some peculiarities, anomalies that occurred during the monitored period (Fig. 4). An example of an atypical distribution of temperatures is the year 1997. It is logical, because this year was the year of gradual filling of the reservoir, so there was no possibility of creating classic thermal stratification. On the other hand, the thermal stratification was fully created in the next years. Atypical water temperature profile was obtained in the autumn 2010, when de facto the water temperature distribution along the water column was constant. This case should be analyzed in connection with time series of hydro–meteorological data (air temperature, wind) in the locality and evaluate the reality of this phenomenon or whether it is a measurement error. A somewhat similar situation arose also in the years 2002 and 2021, but not so pronounced. Spring season has also some case when the thermal stratification has not even begun to form, for example in 2006, 2008, 2018, 2021 and 2022, It could be caused by later beginning of spring and ice cover melting. Anyway, again it should be analyzed in connection with hydro-meteorological data analysis.

Next task of this study was the determination of the thermocline in case of thermal stratification creation. This stratification was always created in summer season. As we can partially see in Fig. 4, the water temperature was stratified even in 1998–2000, but we do not know exactly at what depth the thermocline was formed during summer, as the data from these years were measured in the depth interval of 5 m. Anyway, we determined the depth of the thermocline in partial measured points for each season separately in all years when

it was possible. and the thermal stratification was formed. Results are shown in Fig. 5. For each year, it was determined also the thermocline depth by averaging measuring points during the season to see what inaccuracy we would incur in using such a value given the results from specific points. From Fig. 4 and mainly Fig. 5, we can see that during the spring season the thermocline occurs mainly in the range of 2–7 meters of depth.

In the middle part of Fig. 5 – graphic summary of depths

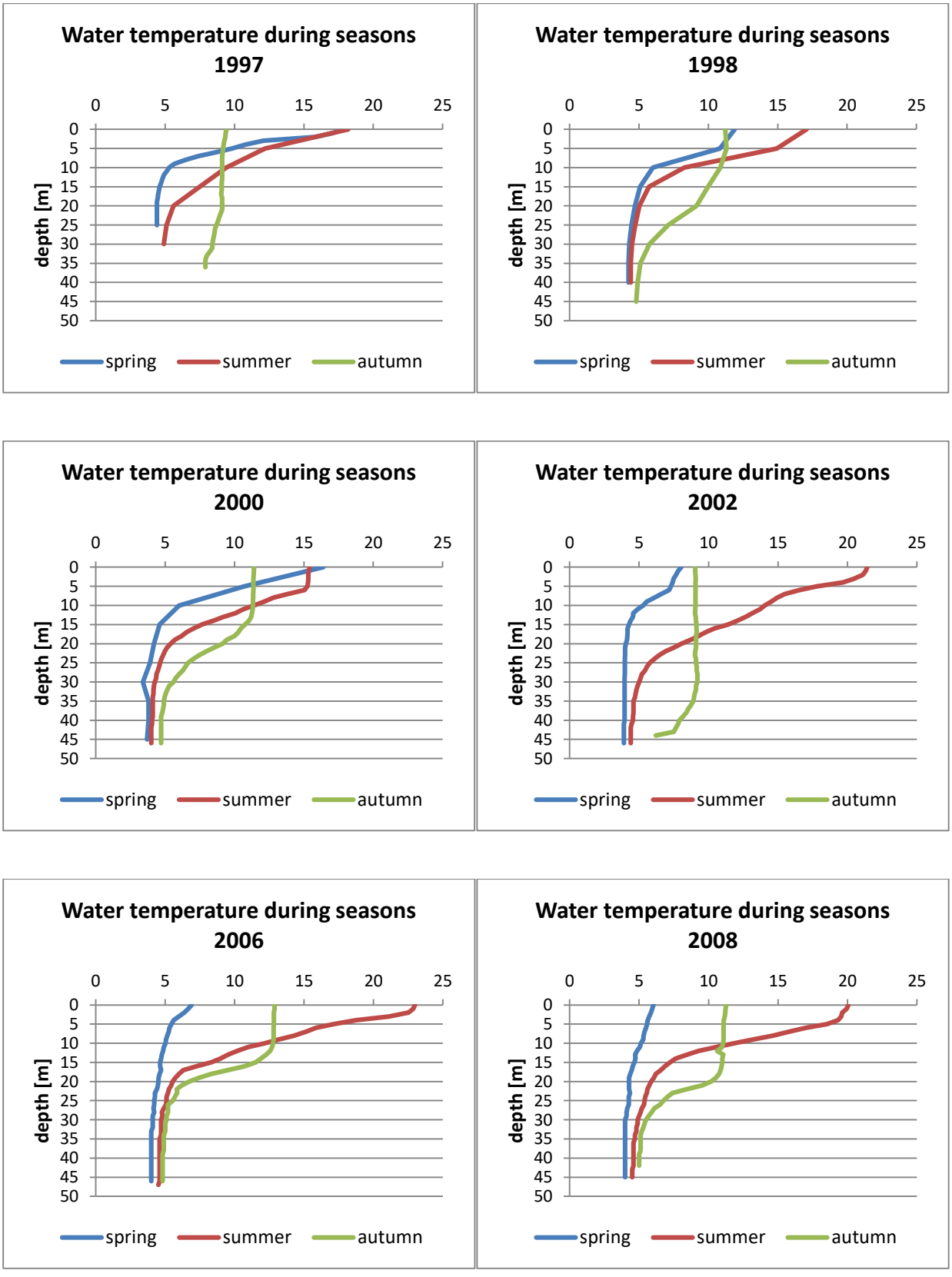

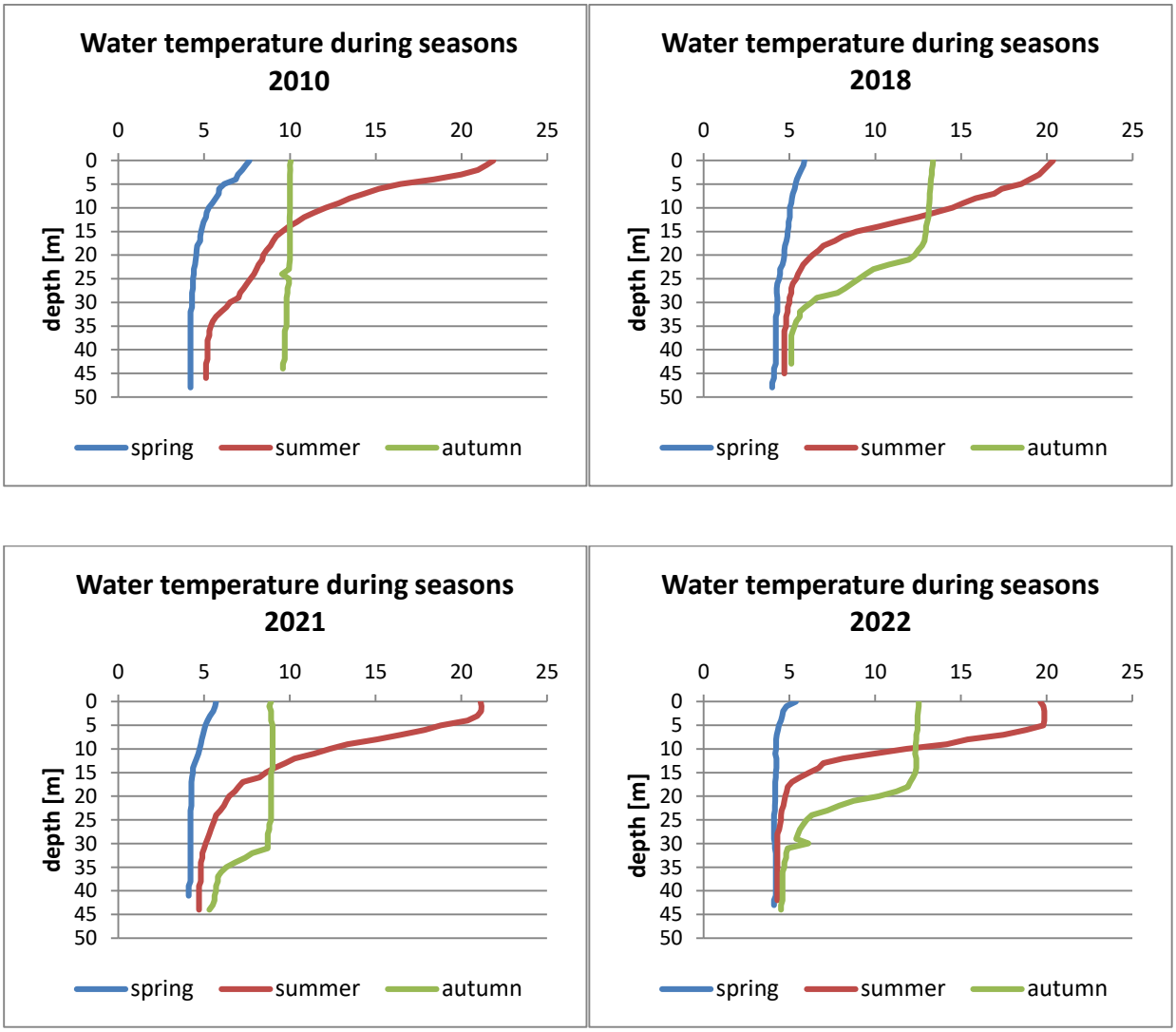

Fig. 4. Vertical water temperature profiles [°C].

of thermocline for the summer season, the course of the thermocline layer with its upper and lower edges is drawn. It was intended for the summer season, because spring and autumn are periods when temperature stratification of water does not form for many years. Based on this course, we can conclude that the thermocline in the initial years of monitoring occurred mainly in the depth range of 5–10 meters in the summer seasons. However, in recent years (approximately since 2013), the depth of the thermocline has been increasing, and in some years, the extent of this thermal stratification layer has been expanding. The least amount of data on water temperature was from the autumn seasons; so the course of the thermocline depths from this season is only slightly informative and illustrative. However, it is evident that the thermocline is deeper in this season from 17 m to 33 m.

In more details, if we take into account that the thermocline is a layer in which the temperature drops by 1°C or more per 1 meter of the depth, then during the spring seasons in case of 11 years, the thermocline was not formed in the early measurement period in April. In the years when the thermocline layer was formed, it occurred on average at depths of 4–6 m. During the summer season, when the water in the reservoir is stratified in each year, this layer occurred on average from 5–8 m, with its average value at the depth of 6m. If we look at the autumn season, a temperature drop of 1°C or more was recorded only in 10 years out of the entire 25-year period. Compared to the summer season, we can see a decrease in the thermocline, with an average depth of 23–24 m, and only in points 1, 2, 4 and 5, as point 3 is located in the shallow area of the reservoir. In 2006, the depth of the thermocline was the smallest one and appeared at the deepest measured points 1, 2 and 5, at depths of 15–19 m. The greatest depth of the thermocline was recorded in 2013, in the depth range of 32–33 m, but only at point 1, which is located on the sampling tower in the deepest part of the reservoir.

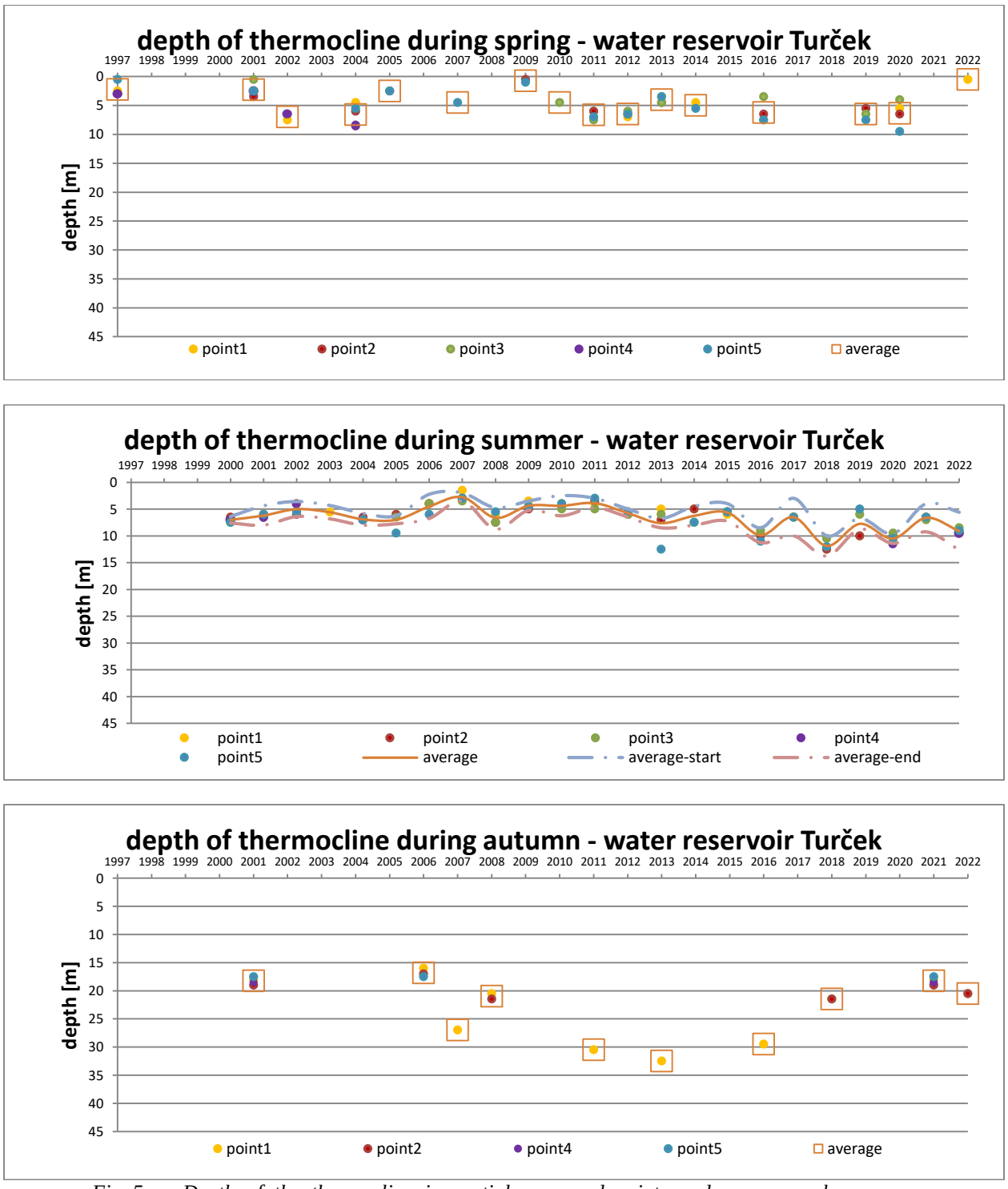

Fig. 5. Depth of the thermocline in partial measured points and average value from 5 measuring points during 3 seasons – spring, summer, autumn – in the period 1997–2022.

As a next indicator of the thermal stratification we evaluated values of TSI. This indicator was determined for each season separately and summary of results are shown in Fig. 6. Overall, the fewest observations are in point 4, which were omitted from monitoring in some years for operational reasons. Value of this index was in majority not higher than 2 – in the autumn seasons it never exceeded this value, but as we said above, this season is not covered enough by measured data. The most and the highest exceeding of this value was observed in the summer season, in the spring season there was only twice. Higher TSI values were observed in the part of the reservoir where the Turiec stream (left tributary) flows into it.

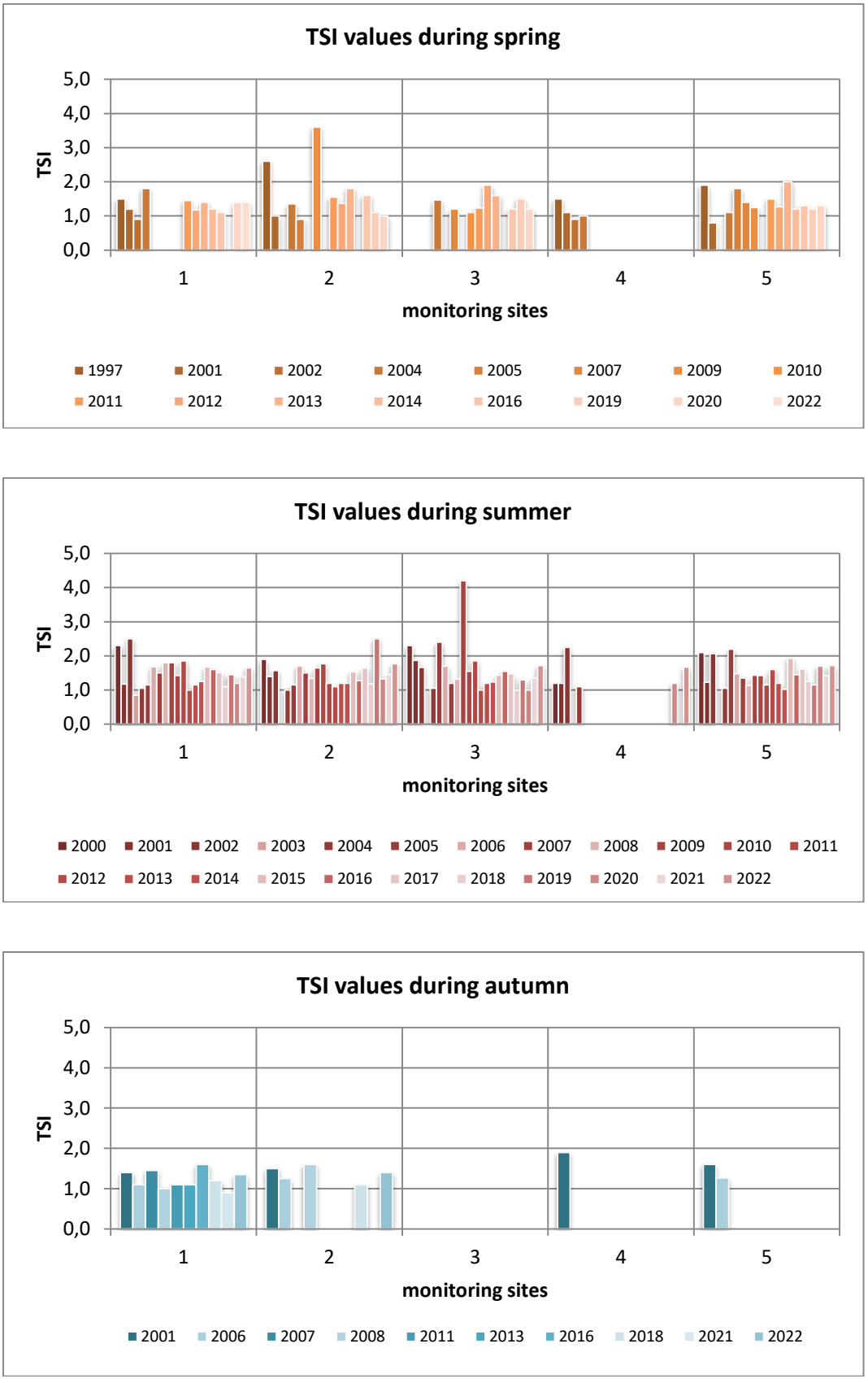

Fig. 6. Thermocline strength index during seasons for 5 monitoring sites during 1997–2022.

Conclusion

This study deals with analysis of seasonal changes of thermal stratification in the Turček reservoir. This reservoir was built primarily for drinking water supply, but also for flood protection of downstream part of the basin and for ensuring ecological discharges, as well. Thermal stratification has an important impact on the cycling of reservoir water quality. Uneven vertical distribution of water quality factors, such as dissolved oxygen and nutrients, occurs during seasonal stratification, which creates chemical stratification. Typically, thermocline and chemocline characteristics vary across different reservoirs, so it is important to study them in valid natural conditions of each reservoir separately.

Results of this study are based on analysis of water temperature values monitored during the whole operating time of the Turček reservoir. The most pronounced thermal stratification was formed in summer, in the given hydro–climatic conditions it starts at the end of April and ends in October. We also analyzed the existence of the thermocline layer, which occurs mainly in the summer, but also in spring and also in autumn, but not so significantly and regularly. The value of TSI, as an indicator of steepness of the thermal stratification, was in majority not higher than 2.

The results presented here are not applicable to reservoirs in general in terms of thermocline structure and variability. However, for objective characterization purposes and monitoring the thermocline as a boundary influencer of biological and chemical processes in this reservoir, these results are useful and helpful for further analysis focused on the development of chemistry in this reservoir, mainly in connection with its purpose to supply the population in the region with drinking water.

Acknowledgements

This work was supported by the project APVV – 18–0205.

References

Bajtek, Z., Pekárová, P., Jeneiová, K., Ridzoň, J.: Analysis of the water temperature in the Litava River, Acta Hydrologica Slovaca, Vol. 23, No. 2, 2022, 296–304. doi:10.31577/ahs-2022-0023.02.0034

Boehrer, B., Schultze, M. (2008): Stratification of lakes, Rev. Geophys., 46, RG2005, doi:10.1029/2006RG000210.

Chmelár, V. (1998): Drinking water reservoir Turček. Žilina: Electa. ISBN 80–88689–07–4 (in Slovak)

Fafard, P. (2018): How and Why Lakes Stratify and Turn Over: We explain the science behind the phenomena [online] 16.5.2018, IISD [cited 4.4.2023] https:// www.iisd.org/ela/blog/commentary/lakes–stratify–turn–explain–science–behind–phenomena/

Horne, A. J., Goldman, C. (1994): Limnology, McGraw Hill. New York 576 pp.

James, S. C., Arifin, R. R., Craig, P. M., Hamlet, A. F. (2017): Investigating summer thermal stratification in Lake Ontario. In AGU Fall Meeting Abstracts (Vol. 2017, EP11C–1570).

Kittrell, F. W. (1965). Thermal stratification in reservoirs. In Symposium on Stream-flow Regulation for Quality Control (57–67). Robert A. Taft Sanitary Engineering Center.

Kraemer Benjamin, M., Anneville, O., Chandra, S., Dix, M., Kuusisto, E., Livingstone David, M.,...McIntyre Peter, B. (2015): Morphometry and average temperature affect lake stratification responses to climate change. Geophysical Research Letters, 42(12), 4981–4988. https://doi.org/ 10.1002/2015GL064097

Lee, H., Chung, S., Ryu, I., Choi, J. (2013): Three–dimensional modeling of thermal stratification of a deep and dendritic reservoir using ELCOM model. Journal of Hydro–environment Research, 7(2), 124–133. doi.org/ 10.1016/j.jher.2012.10.002

Liu, M., Zhang, Y., Shi, K., Zhang, Y., Zhou, Y., Zhu, M., Zhu, G., Wu, Z., Liu, M. (2020): Effects of rainfall on thermal stratification and dissolved oxygen in a deep drinking water reservoir. Hydrological Processes. 2020; 34: 3387–3399. https://doi.org/10.1002/hyp.13826

Liu, M., Zhang, Y., Shi, K., Zhu, G., Wu, Z., Liu, M., Zhang, Y. (2019): Thermal stratification dynamics in a large and deep subtropical reservoir revealed by high–frequency buoy data. Science of the Total Environment, 651, 614–624.

Liu, W. C., Chen, W. B., Kimura, N. (2009): Impact of phosphorus load reduction on water quality in a stratified reservoir–eutrophication modeling study. Environmental monitoring and assessment, 159, 393–406. doi.org/ 10.1007/s10661–008–0637–3

Meyer, G. K., Masliev, I., Somlyody, L. (1994): Impact of Climate Change on Global Sensitivity of Lake Stratification. IIASA Working Paper. IIASA, Laxenburg, Austria: WP–94–028

Mikula, P. (2022): Occurrence of cyanobacteria at the Turček reservoir, Vodohospodársky spravodajca 7–8/2022, 65, 16–21. ISSN: 0322–886X (in Slovak)

Onderka, M. (2004): Factors influencing water quality development in the Liptovská Mara water reservoir, Acta Hydrologica Slovaca, Vol. 5, No. 2, 2004, 319–324 (in Slovak)

O' Reilly, C. M., Alin, S. R., Plisnier, P. D., Cohen, A. S., McKee, B. A. (2003): Climate change decreases aquatic ecosystem productivity of Lake Tanganyika, Africa. Nature, 424(6950), 766–768. https://doi.org/10.1038/ nature01833

O'Reilly, C. M., Sharma, S., Gray, D. K., Hampton, S. E., Read, J. S., Rowley, R. J., Schneider, P., Lenters, J. D., McIntyre, P. B., Kraemer, B. M., et al. (2015): Rapid and highly variable warming of lake surface waters around the globe, Geophys. Res. Lett., 42, 10,773–10,781, doi:10.1002/2015GL066235.

Piccolroaz, S., Healey, N. C., Lenters, J. D., Schladow, S. G., Hook, S. J., Sahoo, G. B., Toffolon, M. (2018): On the predictability of lake sur–face temperature using air temperature in a changing climate: A case study for Lake Tahoe (U.S.A.). Limnology and Oceanography, 63(1), 243–261. https://doi.org/10.1002/lno.10626

Rules of manipulation for the Turček reservoir (2019): Slovenský vodohospodársky podnik, š.p., July 2019 (in Slovak)

Scheu, K. R., Fong, D. A., Monismith, S. G., Fringer, O. B. (2015): Sediment transport dynamics near a river inflow in a large alpine lake. Limnology and Oceanography, 60(4), 1195–1211. doi.org/10.1002/lno.10089

Valerio, G., Pilotti, M., Barontini, S., Leoni, B. (2015): Sensitivity of the multiannual thermal dynamics of a deep

pre–alpine lake to climatic change. Hydrological Processes, 29(5), 767–779. https://doi.org/10.1002/hyp.10183

Vyshnevskyi, V., Shevchuk, S. (2022): Impact of climate change and human factors on the water regime of the Danube Delta, Acta Hydrologica Slovaca, Vol. 23, No. 2, 207–216. doi: 10.31577/ahs-2022-0023.02.0023

Woolway, R. I., Merchant, C. J. (2019): Worldwide alteration of lakemixing regimes in response to climate change. Nature Geoscience, 12, 271–276. https://doi.org/10.1038/s41561–019–0322–x

Yu, H., Tsuno, H., Hidaka, T., Jiao, C. (2010): Chemical and thermal stratification in lakes. Limnology, 11, 251–257.

Zhang, F., Zhang, H., Bertone, E., Stewart, R., Lemckert, C., Cinque, K. (2020): Numerical study of the thermal structure of a stratified temperate monomictic drinking water reservoir. Journal of Hydrology: Regional Studies, 30, 100699. doi.org/10.1016/j.ejrh.2020.100699

Ing. Adrián Varga (*corresponding author, e-mail: varga@uh.savba.sk)
Ing. Yvetta Velísková, PhD.
Assoc. Prof. Ing. Marek Sokáč, PhD.
Ing. Valentín Sočuvka, PhD.
Institute of Hydrology SAS
Dúbravská cesta 9
841 04 Bratislava
Slovak Republic

Ing. Adrián Varga
Institute of Landscape Engineering
Faculty of Horticulture and Landscape Engineering SUA in Nitra
Tulipánová 7
949 76 Nitra
Slovak Republic

Ing. Pavol Mikula
Slovak Water Management Enterprise
Corporate Directorate
Martinská 49
821 05 Bratislava – Ružinov
Workplace: Department of water management laboratories
Kuzmányho 10
012 05 Žilina
Slovak Republic

DOI: 10.31577/ahs-2023-0024.01.0006

ACTA HYDROLOGICA SLOVACA

Volume 24, No. 1, 2023, 43 – 51

Dynamics of water temperature in a small mountain catchment

Patrik SLEZIAK*, Martin JANČO, Michal DANKO

Water temperature has a significant effect on the river fauna and flora and changes the quality of the aquatic ecosystem. Water temperature similar to other physical and chemical indicators of water quality enters into the assessment of the ecological status of surface waters in accordance with the requirements of the framework directive on water (RSV EU). Therefore, it is important to monitor it and also to know to what extent it is influenced by other factors.

The aim of this work was to evaluate the short-term water temperature development and also to analyse its regime with respect to influencing factors, especially air temperature and altitude. The study is conducted in the foreland and mountain part of the Jalovecký Creek catchment in Slovakia and uses hourly data from the hydrological year 2022 (November 1, 2021 – October 31, 2022). We performed field water temperature measurements along the entire Jalovecký creek (six sites at altitudes from 560 to 1,110 m a.s.l.) to better evaluate the water temperature regime. Seasonality of water temperature was analyzed by statistical analysis of time series. We used scatter-plots to assess the relationship among water temperature, air temperature and altitude. The analysis of the water temperature measurements showed that the highest mean hourly/daily water temperature was recorded at Ondrašová site (22.3°C/18.3°C), and the lowest was measured at the Hlboká valley (-1.2°C/-1.5°C). This fact resulted both from the altitude of the stations (Ondrašová 560 m a.s.l., Hlboká valley 1,110 m a.s.l.). The lowest mean monthly air temperature was measured in December (-0.2°C), while the highest was observed in July (15.7°C). The highest variations of the mean monthly water temperatures among the studied sites were observed during summer (June – August), when mean monthly temperature range reached even 8.0°C. The relationship between water and air temperature did not differ significantly among the investigated sites. However, the higher correlations were found for higher altitude (i.e., Hlboká valley). The results of the work could contribute to a better understanding of temperature conditions in high mountain streams.

KEY WORDS: water temperature, air temperature, altitude, mountain stream

Introduction

Changes in the runoff regime, low water levels during the summer season, as well as atmospheric warming significantly affect the water temperature in the streams. Water temperature is an important physical characteristic of water. It has a significant impact on river fauna and flora and conditions the quality of the water ecosystem. During extreme and long-lasting heat and droughts, there is a dangerous rise in water temperature. Longer-term overheating of water in streams combined with low flows can cause undesirable processes that lead to the death of fauna and flora. Water temperature like other physico-chemical indicators of water quality is included in the assessment of the ecological status of surface waters in accordance with the requirements of the framework directive on water – RSV EU (WFD, 2000). This directive stipulates the obligation of EU member states to assess the development of water quality in streams depending on the type of water body (alpine, forested, agricultural catchments, etc.).

Hydrological research in small catchments plays an important role in improving the understanding of hydrological processes. Investigation of changes in the hydrological regime of Slovak rivers deals with the work of Poórová et al. (2023). Small experimental catchments serve the purpose of research precisely because they are mostly upper watersheds and only small landscape changes occur in them. In addition, it is easier to create a dense network of observations in them and thus obtain quality data (Schumann and Herrmann, 2010). Due to the fact that water temperature measurements do not require demanding measurement techniques, water temperature as a basic indicator of water quality is monitored for a long time in selected streams in Slovakia as well as in the world. The first continuous measurements of water temperature in Slovak streams are dated from 1924 to 1926 (Danube: Bratislava – 1926, Hron: Banská Bystrica – 1925, Starohorský potok: Motyčky – 1924, Nitra: Nitrianska Streda – 1925, Váh: Sereď – 1930). Dmitrijeva and Pacl (1952) for the first time processed the basic characteristics of water temperature on the Danube River at the Bratislava station. Horváthová and Vanetianerová (1963),

Horváthová (1964) and Horváthová and Dávid (1969) also dealt with the processing of water temperature data up to 1960 in their works. The water temperature of Czechoslovak streams until 1960 was comprehensively evaluated by Čermák (1965). Dulovič (1989) in his study dealt with the processing of long-term characteristics of water temperature up to 1980. In recent years, the authors Lešková and Škoda (2003) analyzed the development of water temperature regime in Slovak streams. They evaluated daily water temperatures from selected water measuring stations and monthly temperatures from selected climatological stations. Their results showed that the highest water temperatures in Slovak streams occur in August/July, lowest in January.

The influence of the hydrological regime of streams on water temperature is evident from the work of Pekárová et al. (2008), where the thermal flow of the Danube water was evaluated in the Bratislava profile. Another work on the assessment of water temperature in the Danube (Bratislava profile) for the period 1931–2005 is the work of Škoda et al. (2007). The dependence of water temperature on air temperature is evaluated in the work of Bajtek et al. (2022a; b).

In recent decades, the question of air temperature increases due to the strengthening of the atmosphere's greenhouse effect, as well as the question of the influence of the phenomena of the North Atlantic Oscillation (NAO) and the Arctic Oscillation (AO) on temperature fluctuations, has come to the fore. The influence of the Severoatlantic Oscillation on the multiple variability of water temperature in Vienna, Salzach and Traune was studied by Webb and Nobilis (2007). The authors found out that a statistically significant increase in water temperature occurred during the 20th century at all the following stations. Changes in water temperature values are closely related to the development of air temperatures. The expected increase in air temperature will also be reflected in the increase in water temperature in streams (Bonacci et al., 2008). Since water has an order of the magnitude higher thermal capacity than air, an increase in the temperature of the water in the stream could be a significant signal of the warming of the watershed (Pekárová et al., 2008).

Since water temperature is a basic physico-chemical characteristic indicating water quality, its future development is extremely important. In order to eliminate human influence on water temperature, it is necessary that monitoring is also carried out in catchments with a natural regime. In our study, the water temperature dynamics is evaluated at six sites with different altitudes in the foreland and pristine mountain part of the Jalovecký Creek catchment, located in the Jalovecká valley in northern Slovakia. The aim of this study is (a) to evaluate experimental measurements of water temperature in the studied catchment, (b) to analyze the seasonality of water temperature (hourly, daily and monthly course), (c) to assess the relationship between water temperature and influencing factors, especially air temperature and altitude.

Study area and data

This study is carried out in the the Jalovecký Creek catchment located in northern Slovakia (Fig. 1). In 1986,

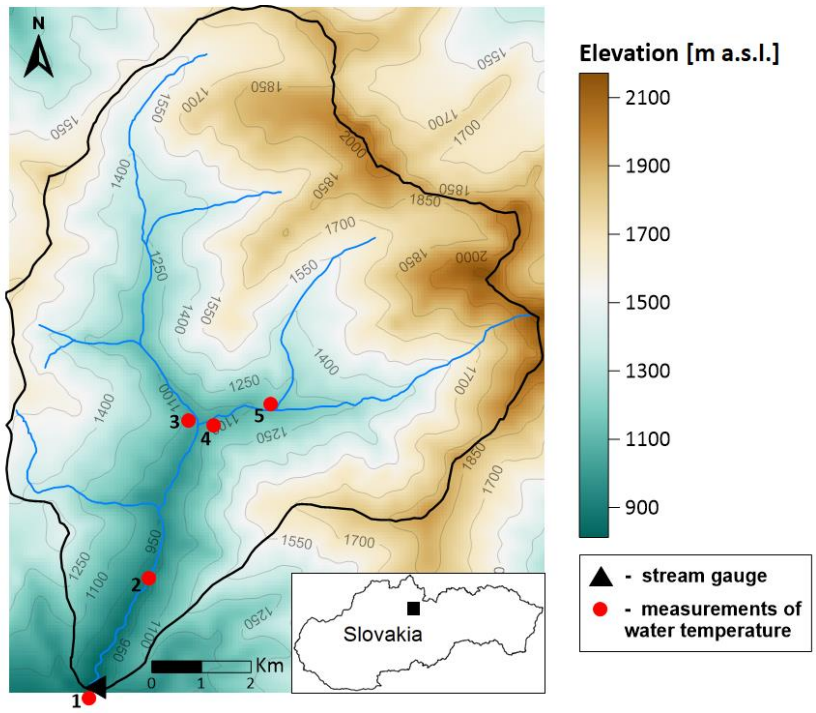

Fig. 1. Topography of the Jalovecký Creek catchment and location of selected water temperature measurement sites (numbers 1 – 5 (the red points), 1 – Catchment outlet, 2 – Jalovecká valley, 3 – Bobrovecká valley, 4 – Parichvost valley, 5 – Hlboká valley, one station called Ondrašová is located outside the catchment). The map also includes location of the stream gauge at the outlet of the catchment (the black triangle).

the Institute of Hydrology of Slovak Academy of Sciences (IH SAS) established an extended workplace in Liptovský Mikuláš – the Experimental Hydrological Base. The Jalovecký Creek catchment in the West Tatras was chosen as a representative research catchment. The main content of the workplace is the research of the water balance components in the mountains and as well as the experimental research of hydrological processes that determine the formation of water sources and runoff.

Jalovecký creek is a typical mountain stream. It is formed by the confluence of two streams of Parichvost and Bobrovecký creek at an altitude of 1,000 m a.s.l., Jalovecký creek flows into the river Váh. The mouth of the stream is located at an altitude of 560 m a.s.l. in the town district of Liptovský Mikuláš (part Liptovská Ondrášová). The catchment is led on both sides by the ridge of the Western Tatras. Catchment area is 45 km^2 and it is composed of two parts: the upper part (called mountain part) and the lower part (called foothill part).

The mountain part of the catchment is located in the Tatra National Park (TANAP), which implies that human activities here are limited to tourism and the occasional removal of wood after calamities. Its area is 22.2 km^2, the elevation ranges between 820 and 2,178 m a.s.l. (mean 1,500 m a.s.l.) and mean slope 30°. The bedrock is dominantly formed by granodiorite and gneiss that are covered by fluvioglacial sediments and slope debries. About 7% of the catchment is formed by Mesozoic rocks dominated by limestone and dolomite. Soil cover is represented by cambisols, podsols, rankers and lithosols. Forests dominated by spruce cover 44% of catchment area, dwarf pine covers 31% and alpine meadows and bare rocks cover the rest 25%.

The foothill part of the catchment is located in the Liptov Basin. Geology is represented by the low permeability claystones and sandstones (at some places Carphatian flysch dominated by claystone) that are covered in the valley by the alluvium of Jalovecký creek. The soil is represented by fluvisols.

The water temperature in the Jalovecký creek was evaluated from hourly measurements at six locations (Fig. 1, 2. and Table 1) during the hydrological year 2021/22 (November 1, 2021 – October 31, 2022). The air temperature at three locations was evaluated from hourly measurements too. From the measured water temperatures, hourly, daily, and monthly mean water temperature values were calculated for each location. These measurements were also used in evaluating the dependence of water temperature on altitude and air temperature. The list of sites and their location in the catchment and their associated altitude for water temperature and air temperature is shown in Table 1.

Fig. 2. The water temperature measurement sites in the Jalovecký Creek catchment.

Methods

From November 2021, we started measuring the water temperature along the creek (stream) at six locations at different altitudes (560–1,110 m a.s.l.) in the mountain catchment of the Jalovecký creek. We named the measurement sites according to the positions where the water temperature sensors were located, namely: Ondášová, Catchment outlet of the Jalovecká valley, Jalovecká valley, Bobrovecká valley, Parichvost valley and Hlboká valley (Fig. 1, 2). The water temperature sensors in the upper part of the catchment were placed in such a way as to cover the area of the Bobrovecká valley, through which the Poliansky creek flows and the Hlboká valley, through which the Hlboký creek flows. The Poliansky and Hlboký creek subsequently flow into the Jalovecký creek, which flows through the Parichvost valley. The water temperature sensors were placed on the left sides of the creek, so that access to them was possible. During the installation, the following criteria were observed: the water temperature sensors were placed in flowing water so that they were always below the water surface and were placed in shaded areas to avoid increased influence of solar radiation. Shading was provided by riparian vegetation.

We used Minikin Tie temperature sensors from the EMS Brno company to record the water temperature at five locations. These are durable and waterproof devices that measure and record water temperatures in intervals from 30 seconds to 4 hours. The datalogger case is manufactured from high-density polyethylene terephthalate. The data was downloaded via a portable field computer, Mini32 software and an IrDA cable (Fig. 3). At the catchment outlet of the Jalovecká valley, we took the water temperature data from the MicroStep-MIS automatic station. Data from this station is available to us online. We took air temperature data from three locations, namely Ondrašová (560 m a.s.l.), Priemstav (750 m a.s.l.) and Hlboká valley (1,400 m a.s.l.). At the Ondrašová location, the air temperature is recorded by means of the MicroStep-MIS automatic station. At the Priemstav and Hlboká valley sites, air temperatures are recorded using Minikin THi or Minikin RTHi devices with radiation shield (EMS Brno), which, like Minikin Tie temperature sensor, record air temperature in intervals from 30 seconds to 4 hours.

Table 1. The water/air temperature measurement sites and their corresponding altitude in the Jalovecký Creek catchment

Water temperature [°C] Locality	Altitude [m a.s.l.]	Air temperature 2 m [°C] Locality	Altitude [m a.s.l.]
Ondrašová	560	Ondrašová	560
Catchment outlet	850	Priemstav	750
Jalovecká valley	960	Hlboká valley	1,400
Bobrovecká valley	1,009	-	-
Parichvost valley	1,015	-	-
Hlboká valley	1,110	-	-

Fig. 3. Equipment for downloading water temperature data (portable field computer, Minikin Tie temperature sensor and IrDA cable).

Results and discussion

Hourly, daily and monthly dynamics of water temperature

The hourly course of water temperature during the day was analyzed on the basis of data from hydrological year 2022 (Fig. 4, Table 2). The highest variation in hourly water temperature (from -1.0°C to 22.3°C) was recorded at site Ondrašová, and the lowest differences (from -0.4°C to 10.5°C) were recorded at the Bobrovecká valley. As altitude increases, the variation in hourly water temperature decreases (up to altitude 1009 m a.s.l.).
Minima occur in the morning at sunrise and maxima in the afternoon. The highest averages of the mean water temperature were recorded at site Ondrašová (6.7°C), and the lowest were recorded at the Bobrovecká valley (4.1°C). Similar mean hourly water temperature values were also recorded at Jalovecká valley (4.2°C) and Parichvost valley (4.2°C). In the winter months, the water temperature during the day has a lower amplitude (not shown here). The winter averages of the mean water temperature at lowest altitude (560 m a.s.l.) ranged from -1.0°C to 12.6°C and the summer temperatures were between 4.1°C and 22.3°C. The winter temperature at highest altitude (1,110 m a.s.l.) varied from -1.2°C to 7.9°C and the summer temperatures ranged from 2.1°C to 15.1°C.
Fig. 5 shows the daily course and dynamics of fluctuations in the measured water temperature during the hydrological year 2022. Basic statistics of the mean daily water temperatures is given in Table 3. We can see that the course of water temperature represents a long-known sinusoid. Generally, the water temperature should range from 0°C to 25°C during the year in a temperate climate zone.
The averages of the mean daily temperatures range from 4.1°C (Bobrovecká valley) to 6.7°C (Ondrašová). The highest mean daily water temperature was recorded at Ondrašová (18.3°C), and the lowest was measured at the Hlboká valley (-1.5°C). This fact resulted both from the altitude of the stations (Ondrašová 560 m a.s.l., Hlboká valley 1,009 m a.s.l.). The minimum daily water temperature dropped to or below 0°C at all sites (except

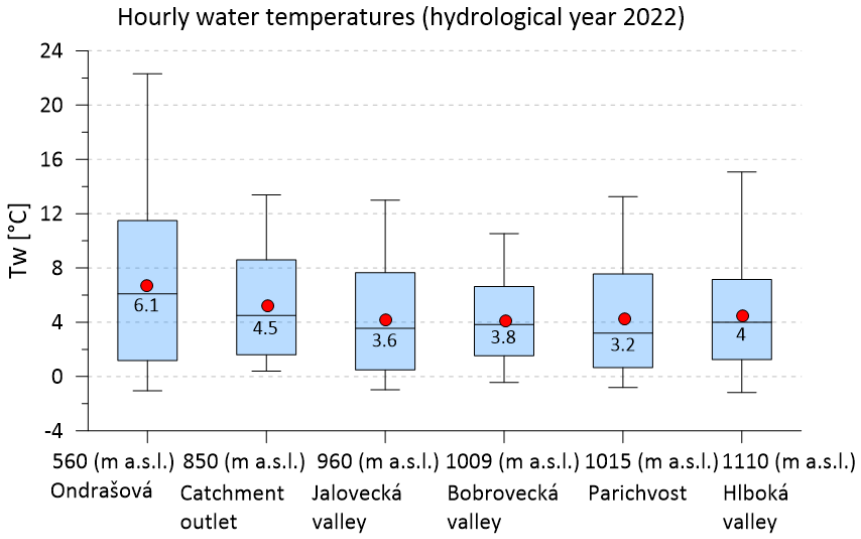

Fig. 4. Hourly water temperatures (Tw) measured at different sites and altitudes. The whiskers represent minima and maxima; the boxes show 25% and 75% percentiles; the line shows the median of the water temperature; the red point indicates the mean water temperature value.

Table 2. Basic statistics of hourly water temperatures measured at different sites and altitudes in the foreland and mountainous part of the Jalovecký Creek catchment in the hydrological year 2022 (November 1, 2021 – October 31, 2022)

Locality	Altitude [m a.s.l.]	Minimum [°C]	Maximum [°C]	Median [°C]	Mean [°C]
Ondrašová	560	-1.0	22.3	6.1	6.7
Catchment outlet	850	0.4	13.4	4.5	5.2
Jalovecká valley	960	-1.0	13.0	3.6	4.2
Bobrovecká valley	1,009	-0.4	10.5	3.8	4.1
Parichvost valley	1,015	-0.8	13.3	3.2	4.2
Hlboká valley	1,110	-1.2	15.1	4.0	4.5

for the Catchment outlet). Interestingly, the water temperature course varies more between Bobrovecká valley and Parichvost valley in the summer. This can be caused by a different subsoil (dolomites vs granite). Daily fluctuations are, in general, higher in deforested areas, where the bank vegetation does not prevent water against overheating during the day.

Mean monthly water temperatures can be described as one of the important sources that is provided to various sectors of the water management. This is because they very clearly show changes in water temperature during the year and represent a balanced value, without substantial distortion by random influences, as is the case with daily water temperatures. Changes in water temperature distribution on the Jalovecký Creek at 6 selected locations were analyzed for the hydrological year 2022 (Fig. 6). Mean monthly values were calculated from measurements in hourly time step for the evaluated period and they are summarized in Table 4. The water temperature rose especially markedly in July and August, which corresponds to an increase of the air temperature. The highest mean monthly water temperature was measured in July (15.7°C) at Ondrašová site, while the lowest was observed in December (-0.2°C) at the same site and also at Jalovecká valley. The monthly water temperature dynamics had a clear seasonal pattern; the highest variations of water temperature among the studied sites were observed during summer (June – August), when mean monthly temperature range reached even 8.0°C, while the lowest were observed in January, February, March and April with the mean monthly range approximately of 1°C. The largest difference between the lowest (560 m a.s.l.) and highest (1,110 m a.s.l.) altitudes is observed in July, when mean monthly temperature range reached even 6.7°C.

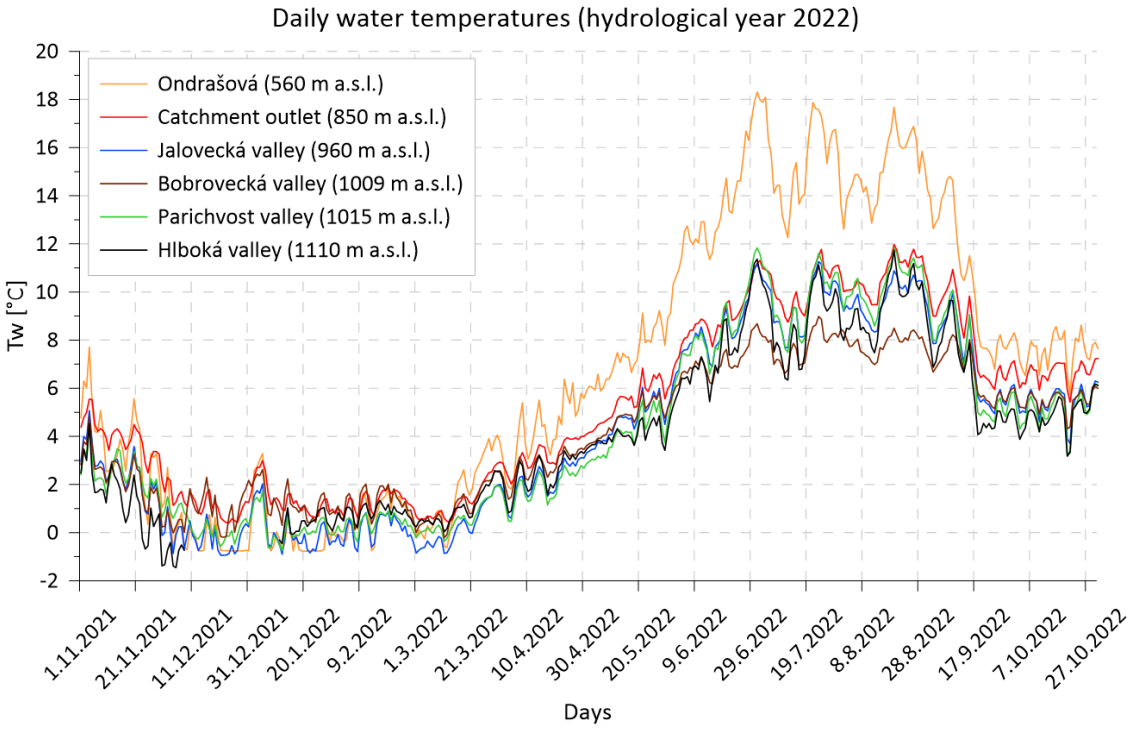

Fig. 5. Mean daily water temperatures (Tw) measured at different sites and altitudes.

Table 3. Basic statistics of the mean daily water temperatures measured at different sites and altitudes in the foreland and mountainous part of the Jalovecký Creek catchment in the hydrological year 2022 (November 1, 2021 – October 31, 2022)

Locality	Altitude [m a.s.l.]	Minimum [°C]	Maximum [°C]	Median [°C]	Mean [°C]
Ondrašová	560	-0.8	18.3	6.0	6.7
Catchment outlet	850	0.4	12.0	4.5	5.2
Jalovecká valley	960	-0.9	11.3	3.7	4.2
Bobrovecká valley	1,009	-0.2	9.0	3.8	4.1
Parichvost valley	1,015	-0.8	11.8	3.2	4.2
Hlboká valley	1,110	-1.5	11.7	4.0	4.3

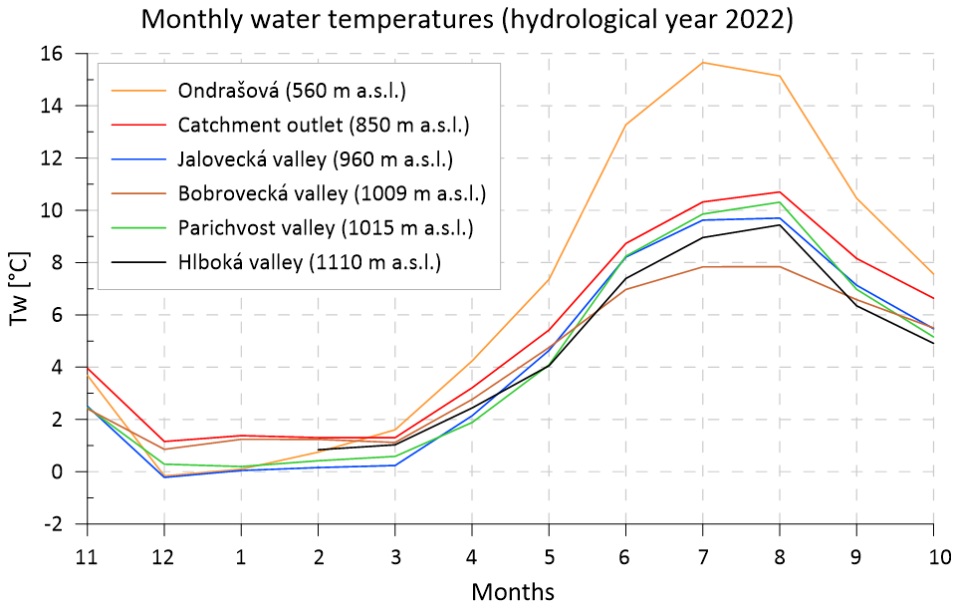

Fig. 6. Mean monthly water temperatures (Tw) measured at different sites and altitudes.

Table 4. The mean monthly water temperatures measured at different sites and altitudes in the foreland and mountainous part of the Jalovecký Creek catchment in the hydrological year 2022 (November 1, 2021 – October 31, 2022)

Months	Ondrašová (560 m a.s.l.)	Catchment outlet (850 m a.s.l.)	Jalovecká valley (960 m a.s.l.)	Bobrovecká valley (1,009 m a.s.l.)	Parichvost valley (1,015 m a.s.l.)	Hlboká valley (1,110 m a.s.l.)
November	3.7	4.0	2.5	2.4	2.5	1.6
December	-0.2	1.2	-0.2	0.9	0.3	-
January	0.1	1.4	0.0	1.2	0.2	-
February	0.7	1.3	0.2	1.2	0.4	0.8
March	1.6	1.3	0.2	1.1	0.6	1.0
April	4.2	3.2	2.1	2.8	1.9	2.4
May	7.4	5.4	4.6	4.8	4.1	4.1
June	13.3	8.7	8.2	7.0	8.2	7.4
July	15.7	10.3	9.6	7.8	9.9	9.0
August	15.1	10.7	9.7	7.8	10.3	9.4
September	10.5	8.2	7.1	6.6	7.0	6.3
October	7.6	6.6	5.5	5.5	5.2	4.9

Dependence of water temperature on influencing factors – altitude and air temperature

The relationship among air temperature, water temperature and altitude was assessed by scatterplots and correlation coefficients. The correlations were evaluated for three sites with different altitudes (560 m a.s.l., 750 m a.s.l., 1,400 m a.s.l.) as shown in Fig 7. A value of the correlation coefficient (r) close to 1 indicates a strong dependence between the variables. It is evident, that there is a high dependence between air and water temperatures (r for summer and winter seasons above 0.9).

The results indicate that the correlations between air and water temperatures do not differ significantly between the seasons. Higher correlations were found at higher elevations, particularly at the Hlboká valley site. For instance, the summer correlation between water temperature (*Tw*) and air temperature (*Ta*) at the Ondrašová site (560 m a.s.l.) was about 0.82, while it was around 0.87 at the Hlboká valley site. This could be attributed to the fact that the water temperature increases gradually along the entire length of the stream, resulting in lower correlations at lower altitudes (such as the Ondrašová site) and higher correlations at higher altitudes (such as the Hlboká valley site).

In winter season, the correlations are as follows: 0.80 (Ondrašová), 0.85 (Catchment outlet – Priemstav), 0.86 (Hlboká valley). In general, the air temperature is higher than the water temperature, particularly at higher altitudes.

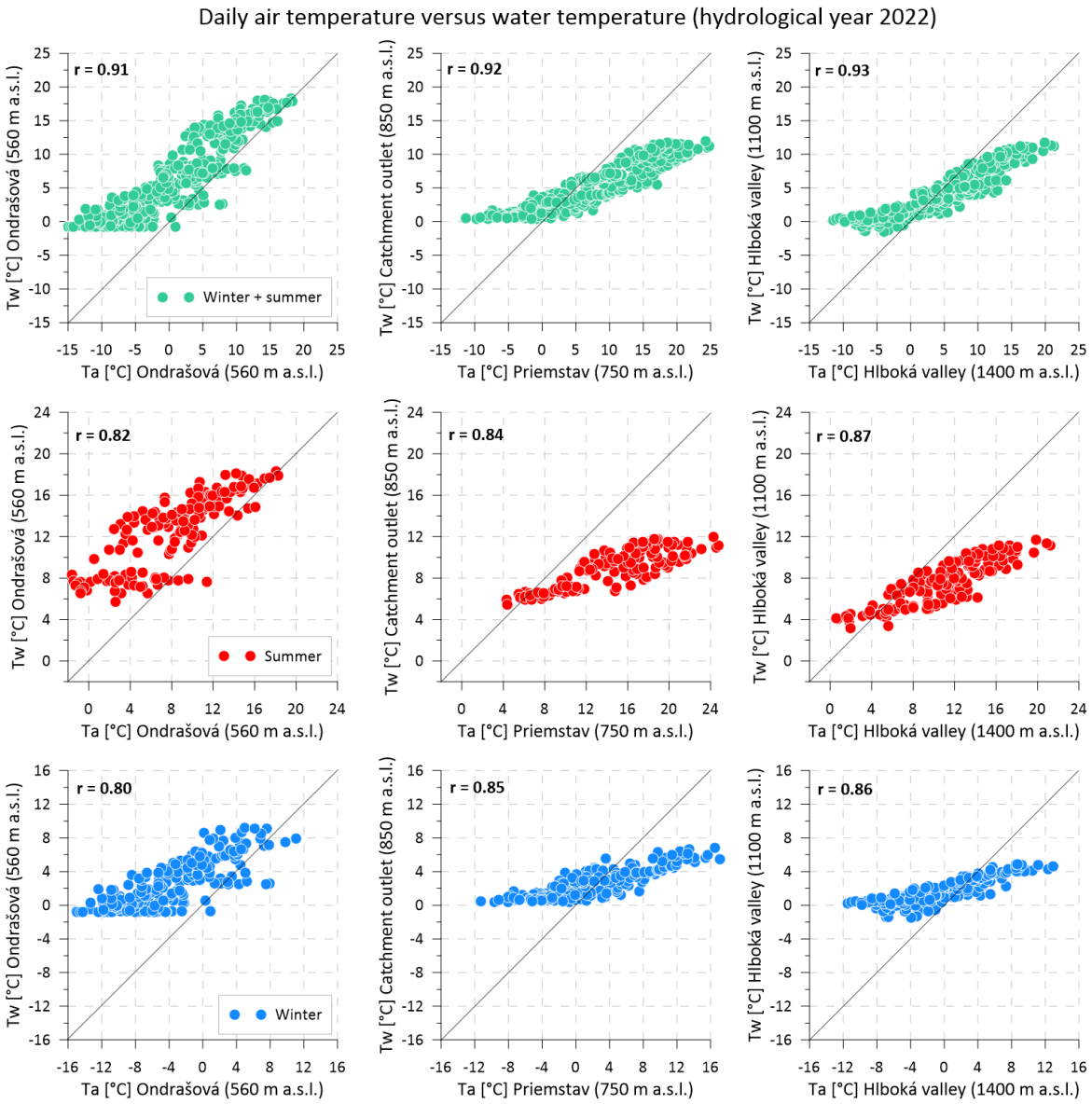

Fig. 7. Measured daily air temperature (Ta) versus water temperature (Tw) at different elevations in the hydrological year 2022 (November 1, 2021 – October 31, 2022) and its warm (June–October) and winter season (November–May); the diagonal represents the 1:1 line.

Conclusion

Data on water temperature and air temperature measured at different altitudes in the Jalovecký Creek catchment confirm the differences between the mountain and foothill parts of the studied catchment.

The highest mean hourly/daily water temperatures were recorded at lower altitudes (560 m a.s.l.), while the lowest were measured at higher altitudes (1,110 m a.s.l.). The lowest monthly water temperature variations were observed in the winter, they increased in the spring to reach maximum values early summer, and then decreased again in the autumn. Water temperature at the studied sites followed the air temperature pattern. The higher dependence between the water and air temperatures were found for higher altitudes.

The measurements may serve to determine the limit values of the water temperature for a good ecological condition for altitudes between 560 and 1,100 m above sea level in small mountain catchments.

The monthly values could be used when classifying the water of high mountain streams into individual water quality classes with regard to water temperature. Although it would be necessary to evaluate a longer series of measurements to determine the boundaries, these values provide us with at least indicative values for flows little affected by human activity in high mountain environments.

Acknowledgement

This study was supported by the grants from the Slovak Academy of Sciences (project VEGA No. 2/0019/23) and from the Slovak Research and Development Agency (project APVV No. 20- 0374).

References

Bajtek, Z., Pekárová, P., Jeneiová, K., Ridzoň, J. (2022a): Analysis of the water temperature in the Litava River. Acta Hydrologica Slovaca, 23(2), 296–304.

Bajtek, Z., Pekárová, P., Jeneiová, K., Ridzoň, J. (2022b): Stream temperature analysis in the Krupinica river. In Transport of water, chemicals and energy in the soil – plant –atmosphere system in conditions of the climate variability: book of Abstracts. 1. vydanie. – Bratislava: Institute of Hydrology of the Slovak Academy of Sciences in Bratislava, 2022, 38–38. ISBN 978-80-89139-54-5.

Bonacci, O., Trninić, D., Roje-Bonacci, T. (2008): Analyses of water temperature regime at Danube and its tributaries in Croatia. Hydrolog. Process. 22, 7, 1014–1021.

Čermák, M. (1965): Teploty vody Československých tokov, Vodohospodársky časpois, 13 (3), 296–304.

Dmitrijeva, M., Pacl, J. (1952): Príspevok k poznaniu vodného režimu Dunaja v Bratislave. Zemepisný sborník SAV, roč. IV, 1–2, 63–88.

Dulovič, L. (1989): Dlhodobé charakteristiky teploty vody. Zborník prác SHMÚ 29/I, ALFA Bratislava, 381–413.

Horváthová, B., Vanetianerová, M. (1963): Teplota vody slovenských tokov, Praha.

Horváthová, B. (1964): Teplotný režim slovenských tokov. Vodohospodársky časopis. 12(1), 5–15.

Horváthová, B., Dávid, A. (1969): Ročný rytmus zmien teploty riečnej vody. Vodohospodársky časopis. 17(2), 117–130.

Lešková, D., Škoda, P. (2003): Temperature series trends of Slovak rivers. Meteorologický časopis, 6, 2, 13–17.

Pekárová, P., Halmová, D., Miklánek, P., Onderka, M., Pekár, J., Škoda, P. (2008): Is the Water Temperature of the Danube River at Bratislava, Slovakia, Rising? J. Hydrometeorol. 9(5), 1115–1122.

Poórová, J., Jeneiová, K., Blaškovičová, L., Danáčová, Z., Kotríková, K., Melová, K., Paľušová, Z. (2023): Effects of the Time Period Length on the Determination of Long-Term Mean Annual Discharge. Hydrology, 10(4), 88.

Schumann, S., Herrmann, A. (2010): 60 years of the Bramke research basins: history, major hydrological results and perspectives. In: Status and Perspectives of Hydrology in Small Basins (proceedings of the workshop held at GoslarHahnenklee, Germany, 30 March–2 April 2009). IAHS 336.

Škoda, P., Kučárová, K., Majerčáková, O. (2007): Zhodnotenie teploty vody a ľadových úkazov na Dunaji v Bratislave, Zborník z konferencie Ľadový a teplotný režim tokov a nádrží, ISBN: 978-80-89090-27-3, Banská Bystrica.

Webb, B. W., Nobilis, F. (2007): Long-term changes in river temperature and the influence of climatic and hydrological factors. Hydrol. Sci. J., 52 (1), 74–85.

WFD (2000): Directive 2000/60/EC of the European Parliament and of the Council of 23 October 2000 establishing a framework for Community action in the field of water policy. Official Journal of the European Communities.

Ing. et Ing. Patrik Sleziak, PhD. (*corresponding author, e-mail: sleziak@uh.savba.sk)
Ing. Martin Jančo, PhD.
Ing. Michal Danko, PhD.
Institute of Hydrology SAS
Dúbravská cesta 9
841 04 Bratislava
Slovak Republic

DOI: 10.31577/ahs-2023-0024.01.0007

ACTA HYDROLOGICA SLOVACA

Volume 24, No. 1, 2023, 52 – 62

Investigation of water temperature changes in the Hron River in the context of expected climate change

Veronika BAČOVÁ MITKOVÁ*, Pavla PEKÁROVÁ, Dana HALMOVÁ

The water temperature is one of the physico – chemical indicator of water quality that plays a crucial role in affecting the biological processes in surface water. In the context of the climate changes, there are also changes in the temperature of the water in the streams. The paper presents an analysis of long-term data of the water temperature in the Hron River at two selected gauging stations: Banská Bystrica and Brehy, during the period of 1962–2020. The analysis was conducted using a long series of water temperature measurements. The aim of the study is to detect whether significant trends occur in the time series of water temperature. The first part of the paper dealt with the trend analyses of monthly and annual water temperature. The following section is focused on determination, investigation and evaluation of 1-, 3-, 7-day maximum water temperatures. The impact of rising air temperatures on water temperature is critical for protecting water resources and ensuring water quality. In the last part of the study, the monthly water temperature of the Hron River at two gauging stations was modeled using air temperature. The best for Hron at B. Bystrica was the model: SARIMA$(1,0,0)x(0,1,1)_{12}$ + 1 regressor, and for Hron at Brehy the best was the model: SARIMA$(1,0,0)x(1,0,2)_{12}$ + 2 regressors, with a high correlation coefficient of 0.983 at B. Bystrica and 0.985 at Brehy. Results showed that a 1°C increase in air temperature caused the water temperature to rise by 0.35°C at Banská Bystrica and 0.57°C at Brehy, while a 3°C increase resulted in a rise of 1.05°C at Banská Bystrica and 1.75°C at Brehy. The study concludes that the SARIMA model can effectively simulate changes in water temperature based on changes in air temperature.

KEY WORDS: Climate change, Hron River, water temperature, air temperature, trends, stochastic models

Introduction

Climate change and anthropogenic activity have an impact on the components of the hydrological regime of rivers, potentially leading to negative effects on the quantity and quality of water. Therefore, monitoring changes in the quantity and quality of water in streams is essential in quantifying the potential threat to their balanced regime. Understanding and analysing the relationship between the quality and quantity of water also deserves attention. Much less attention is paid to the long-term water temperature behaviour in natural streams and rivers. Till the end of 2000, a lack of suitable data hinders such studies and, for example, relatively few analyses of detailed water temperature records covering periods of a decade or longer have been published (Vannote and Sweeney, 1980; Webb and Walling, 1985; Beschta et al. 1987; Ludwig et al., 1990). Obtaining a relatively long series of data is necessary to accurately determine the true nature of the thermal regime for a river monitoring station and to assess the response of water temperature to the potential impacts of climate change on river systems.

The European Environment Agency (EEA, 2017) indicates that climate change has increased the water temperature of rivers and lakes. Water temperature is a primary parameter of physical water quality which exerts an important influence on the ecology of freshwaters, low flows in conjunction with high water temperatures can directly threaten life in rivers. It is a key abiotic variable that models the chemical composition of water and organisms in rivers and streams (St-Hilaire et al., 2012). The resulting temperature of water in rivers is influenced mainly by atmospheric temperature, as well as other factors such as the amount of water in the stream, orographic conditions of the basin (e.g., altitude of the basin, size of the basin, presence of lakes in the basin), and human activity in the basin (Liptay, 2022; Okhravi et al, 2022).

The assessment of the consequences of environmental changes on the temperature regime of rivers and their impact on water quality has been a frequently discussed topic in many professional studies in recent years (Webb and Walling, 1992; Webb and Nobilis, 1997; Ptak et al., 2019). Due to the air and stream temperature relationships, increases in air temperature expected from future climatic changes are thought to raise stream temperatures. The goal of several research papers in

the past was not to develop a model, but to determine how stream temperatures in general can be explained by air temperatures, and whether the relationship can be expected to be linear, particularly at high air temperatures (Mosheni and Stefan, 1999). However, the potential of these future stream temperature increases has, to date, not been systematically explored. A fundamental question still remains is, how long and detailed water temperature information provides a good ability to characterize the long-term temperature behaviour of water, investigate the occurrence of recent trends in the thermal regime, and predict likely increases in stream and river temperatures as a consequence of global warming. Webb and Walling (1992) studied the long term water temperature in catchments of England and according to their study the long term water temperature behaviour between catchments appeared primarily to reflect the influence of different land use characteristics. In Poland, the analysis of data for six gauging stations along the Warta river by Ptak et al. (2019) showed, that over the last fifty years there has been a significant transformation of the thermal regime manifesting itself in a successive increase in water temperature. In the case of the analysed gauging stations it was found that the observed changes were caused mainly by climatic factors, which is confirmed by strong relations between water temperature and air temperature. The transformation of thermal conditions of stream and river waters is particularly important in the context of global warming. The importance of thermal changes occurring in rivers start to be within a broad range of interest, subject to research in the scope of various scientific disciplines.

Watercourses in Slovakia have a variable hydrological regime with relatively frequent occurrence of extreme flows, both in time and space. Their variability is determined by physical-geographic and climatic conditions. Long periods of drought are increasingly occurring, alternating with intense rainfall causing flash floods (Poórová et al., 2017; Lešková and Škoda, 2003; Martincová et al., 2011). For example, in the autumn of the extremely dry year 2003, there was a mass death of fish in the river Váh, due to the high water temperature in the river (low oxygen content in the water). Authors Martincová et al. (2011) describe the methodology for classification scheme determination of water temperature, in order to evaluate status of the surface water bodies in selected Slovakian high-mountain, highland and lowland basins. Development of the methodology was based on statistical processing of long-term water temperature trends in selected Slovak rivers and used continuous 40 yearly series (time period 1964–2003) of the daily water temperature data, from six stations, that represent several altitude positions.

On 19 November, 2004, a strong wind-throw destroyed the riparian vegetation along the channel of the Bela River. Pekárová et al. (2011) attempted to point out if, and possibly to what extent, the remove riparian vegetation affected the temperature regime of the Bela River. The result is, that after the wind-throw in the Bela River watershed, the variability of daily water temperature increased – maxima are higher, whereas minima are lower on the daily time scale.

The objective of this study was to analyse changes in long-term data of the water temperature in the Hron River at two selected gauging stations, Banská Bystrica and Brehy, during the period of 1962–2020. The next objective of the study was to determine the maximum water temperatures for 1-, 3-, 7-day periods, and to analyse changes in their long-term trends. Analysis of water temperature trends can be a reliable tool for decision-makers, as it provides insight into potential threats to the aquatic ecosystem. The impact of increasing air temperatures on water temperature is critical for safeguarding water resources and maintaining water quality.

Due to the strong correlation between air temperature and water temperature, the final objective of the study was to predict the effect of a hypothetical increase in average monthly air temperature (*Ta*) on the average monthly water temperature (*To*).

Material and methods

Study area and data

The Hron River is the second longest river in Slovakia. It is 298 km long with basin area of 5 465 km^2. The Hron River flows only through the territory of Slovakia and feeds into the Danube near Štúrovo. The Hron springs in the Horehronie valley, connected to the Low Tatras and the Spiš-Gemer Karst and can be characterized as a nivo-pluvial river. The location of the selected river in area of Slovak territory illustrates Fig. 1. The Hron River at Banská Bystrica drains into a basin of 1 766.48 km^2. The long-term average daily flow reached 24.76 m^3 s^{-1} at Banská Bystrica for the period 1962–2020. The Hron River at Brehy drains into a basin of 3 821.35 km^2. The long-term average daily discharge reached 44.59 m^3 s^{-1} at Brehy for the period 1962–2020. The location of the Hron River within the Slovak territory is presented in Fig. 1, and basic location characteristics of the selected gauging stations are listed in Table 1.

The analysis was conducted using a long series of water temperature measurements. The first measurements in the Hron River at Banská Bystrica started in 1925, while measurements at Brehy began in 1961. However, it should be noted that the available long-term data are incomplete. Therefore, we analysed series of daily water temperatures for period of 59-years (1962–2020) in this study. The course of daily water temperatures and long-term mean monthly water temperature To_m at Banská Bystrica and Hron for the period 1962–2020 are presented in Fig. 2. Table 2 lists the descriptive statistical characteristics of daily water temperature series for analysed period 1962–2020. The daily maximum temperature was measured in June 1963 (20°C, Hron: Banská Bystrica) and in August 1989 (25.5°C, Hron: Brehy).

The long-term mean water temperature at the Banská Bystrica reached value 7.96°C, and at Brehy it reached value of 9.51°C. From monthly water temperature point of view, the maximum long-term water temperatures

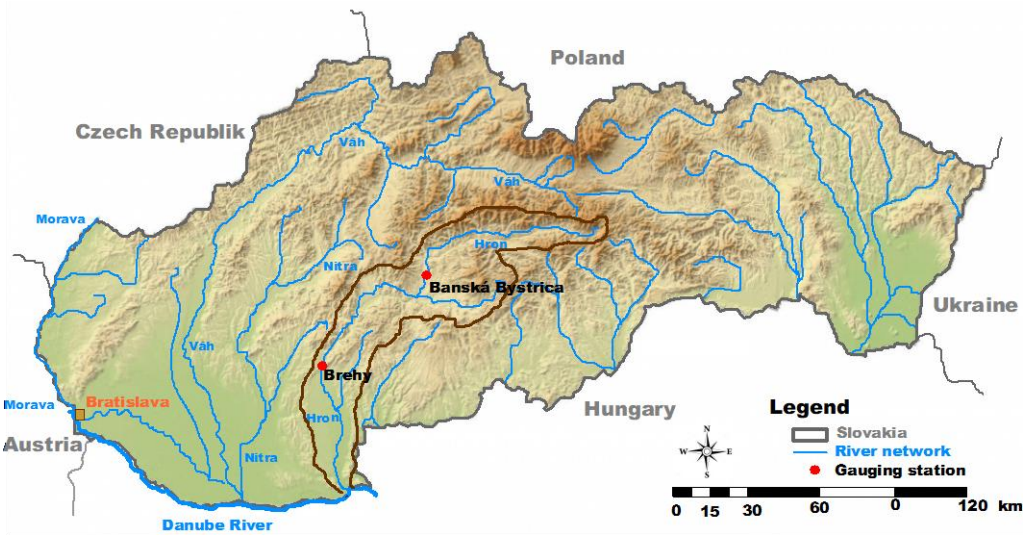

Fig. 1. Scheme of the Hron river basin location in Slovak territory and gauging stations' locations on the Hron River.

Table 1. Basic location characteristics at the selected gauging stations in the Hron river basin

River	Gauging station	Area [km^2]	River kilometer [rkm]	Elevation [m a.s.l]
Hron	Banská Bystrica	1766.48	175.2	334.21
	Brehy	3821.35	93.9	194.25

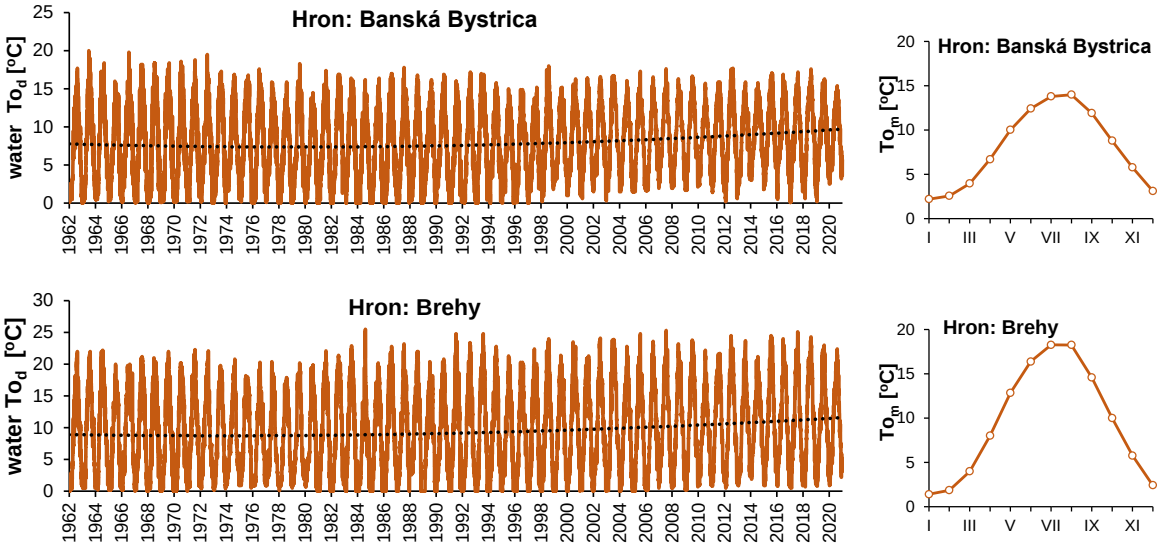

Fig. 2. Daily water temperature To_d of the Hron River observed at 7:00 am, and long-term mean monthly water temperature To_m at Banská Bystrica and Brehy for the period 1962–2020.

Table 2. Basic statistical characteristics of daily water temperature at the selected gauging stations in the Hron River

River	Gauging station	Period	Average [°C]	max [°C]	min [°C]	Median	c_v	Stnd. Deviation
Hron	Banská Bystrica	1962–2020	7.96	20	0.0	8	0.58	4.45
	Brehy	1962–2020	9.51	25.5	0.0	9.1	0.69	6.61

occur in month of August, with temperatures of 14°C for the Hron River at Banská Bystrica and 18.3°C for the Hron River at Brehy.

Methods

Analysis of the water temperature changes in the Hron River at Banská Bystrica and Brehy gauging stations

First, we tested the homogeneity of daily water temperatures for the period of 1962–2020 and corrected the data for Banska Bystrica station from 2003–2010. The Mann-Kendall nonparametric trend test (M-K test) was used for determining the significant trends detection in yearly time series. The nonparametric tests are more suitable for the detection of trends in hydrological time series, which are usually irregular, with many extremes (Hamed, 2008; Gilbert, 1987). The study performs two types of statistical analyses: 1) the presence of a monotonic increasing or decreasing M-K test trend and 2) the slope of a linear trend is estimated with the non-parametric *Sen's method*, which uses a linear model to estimate the slope of the trend and the variance of the residuals should be constant in time. We tested the null hypothesis *H0* of no trend, i.e. the observations To_m against the alternative hypothesis *H1*, where there is an increasing or decreasing monotonic trend. The significance of trends was assessed at the four tested significance levels. The following symbols were used in the analysis:

*** if trend at α = 0.001 significance level – *H0* seems to be impossible;
** if trend at α = 0.01 significance level – 1% mistake if we reject the *H0;*
* if trend at α = 0.05 significance level – 5% mistake if we reject the *H0;*
\+ if trend at α = 0.1 significance level – 10% mistake if we reject the *H0;*
Blank: the significance level is greater than 0.1, cannot be excluded that the *H0* is true.

The most significant trend is assigned three stars (***), with a gradual decrease in importance, the number of stars also decreases (Salmi et al., 2002).

Simulation and prediction of water temperature

Multiple regression and SARIMA models were created to predict water temperature based on monthly air temperature in the Hron River. The SARIMA (Seasonal Autoregressive Integrated Moving Average) model is a time series forecasting model that incorporates both autoregressive (AR) and moving average (MA) components, as well as differencing and seasonal components. The model is designed to capture and account for patterns and trends within the time series data, including seasonality and periodicity. The seasonal component is particularly important in the SARIMA model, as it allows for the modelling of data with seasonal fluctuations or cycles. The model involves fitting a regression equation to the data, where the dependent variable is the time series data, and the independent variables are lags of the series and lagged errors. The model is typically estimated using maximum likelihood estimation, and the accuracy of the model can be evaluated using various statistical measures such as AIC (Akaike Information Criterion) and BIC (Bayesian Information Criterion) (Pekárová, 2009).

The general form of the SARIMA(p,d,q)x(P,D,Q)L model takes the following form:

$$\varphi(B)\,\Phi(B^L)\,\nabla^d\,\nabla_L^D\,Y_t = \Theta(B)\,\Theta(B^L)E_t \qquad (1)$$

where

E_t – independent and normally distributed random variable with zero mean value μ=0 and variance σ_E^2;
p – trend autoregressive order;
d – trend difference order;
q – trend moving average order.
P – seasonal autoregressive order;
D – seasonal difference order;
Q – seasonal moving average order;
L – the number of time steps for a single seasonal period (an L of 12 for monthly data suggests a yearly seasonal cycle.
B – reversion shift operator defined as $BY_t = Y_{t-1}$;
∇^d – the backwards difference operator;
φ – the regular AR (auto-regressive) operator of the order p;
Θ – is the regular SMA (moving average) operator of the order q.
∇_L^D – the seasonal backwards difference operator;
Φ – is the regular SAR (seasonal auto-regressive) operator of the order P;
Θ – is the regular SMA (seasonal moving average) operator of the order Q.

In order to identify this model it is necessary to analyse the particular components of the time series in the following sequence:

- identification of a trend (differentiating of order d) and seasonality (seasonal differentiating of order D);
- selection of a model type (AR, MA, ARMA) and determination of the model's order;
- estimation of model parameters;
- verification of the model.

Monthly air temperatures from the Banská Štiavnica station (1991–2020) were used as climatic input data for the model. To predict the increase in water temperature, two scenarios of average monthly air temperatures were created. The first scenario (SCEN+1) was created by adding 1°C to the measured monthly air temperature. The second scenario (SCEN+3) was created by adding 3°C to the measured monthly air temperature.

Results and discussion

Long-term trends of the monthly and annual water temperatures in the Hron River

Initially, we examined the average monthly water temperatures, as well as the long-term annual water temperature fluctuation at the selected gauging stations. The average monthly water temperatures show an increase in long-term trends in all months over the analysed period 1962–2020 at both gauging stations. The increasing in long-term trends of average monthly temperatures To_m, with significance level $\alpha = 0.001$ were calculated during winter months from November to February, and during spring months of March and of April, at Hron: Banská Bystrica. Additionally, significant increasing trends were observed in the summer months from June to August at Hron: Brehy.

The results of long-term trends significance test of mean monthly water temperatures To_m in the Hron River at Banska Bystrica and at Brehy gauging stations during the period of 1962–2020 is listed in Table 3. The course of the mean monthly water temperatures for the Hron River at Banská Bystrica and Brehy during the period 1962–2020 is illustrated in Fig. 3 a–b.

The course of long-term mean annual water temperatures for the Hron River at Banská Bystrica and at Brehy during the period 1962–2020 are illustrated in Fig. 4 a–b. The long-term mean annual water temperature To_y showed an increasing in long-term trend at $\alpha = 0.001$ significance level during the analysed period 1962–2020. Table 4 lists conclusion of trend significance test of long-term mean annual water temperature To_y in the Hron River at Banská Bystrica and at Brehy gauging station during the period 1962–2020.

Long-term trends of the M-day maximum water temperatures in the Hron River

Multi-day summer heatwaves during low-flow periods cause a lack of oxygen in the water, which leads to the death of aquatic organisms. Therefore, in the next section, we focused on evaluating the long-term development of water temperature in the Hron River during several days. In our study the 1-, 3-, and 7-day maximums were taken from moving averages of the appropriate length calculated for every possible period that is completely within the year.

The 1-day maximum water temperatures showed decreasing long-term trend at significance level of $\alpha = 0.001$ (Fig. 5) for the Hron River at Banská Bystrica during the period 1962–2020. On the other hand, the 1-, 3-, 7-day maximum water temperatures showed a significant an increasing long-term trends with significance level of $\alpha = 0.001$ (Fig. 5) for the Hron River at Brehy during the same period. The conclusion of the long-term trend significance test of M-day maximum water temperature in the Hron River at Banská Bystrica and at Brehy gauging station during the period 1962–2020 (with $\alpha = 0.001$) are listed in Table 5.

Table 3. Conclusion of long-term trend significance test of mean monthly water temperature Toy in the Hron River at Banska Bystrica and at Brehy gauging station during the period 1962–2020 (with *α = 0.001, **α = 0.01 and *α = 0.05)**

River	Gauging station	Month	Period	*n*	Signif.	slope	Correlation R^2
Hron	Banská Bystrica	January	1962–2020	59	***	0.050	0.357
		February	1962–2020		***	0.051	0.349
		March	1962–2020		***	0.054	0.411
		April	1962–2020		***	0.053	0.417
		May	1962–2020		*	0.023	0.114
		November	1962–2020		***	0.040	0.203
		December	1962–2020		***	0.048	0.370
	Brehy	January	1962–2020	59	*	0.025	0.137
		February	1962–2020		*	0.028	0.127
		March	1962–2020		***	0.045	0.278
		April	1962–2020		***	0.053	0.323
		May	1962–2020		**	0.034	0.147
		June	1962–2020		***	0.046	0.170
		July	1962–2020		***	0.054	0.260
		August	1962–2020		***	0.061	0.283
		September	1962–2020		***	0.050	0.216
		October	1962–2020		***	0.045	0.191
		November	1962–2020		**	0.045	0.121
		December	1962–2020		**	0.038	0.155

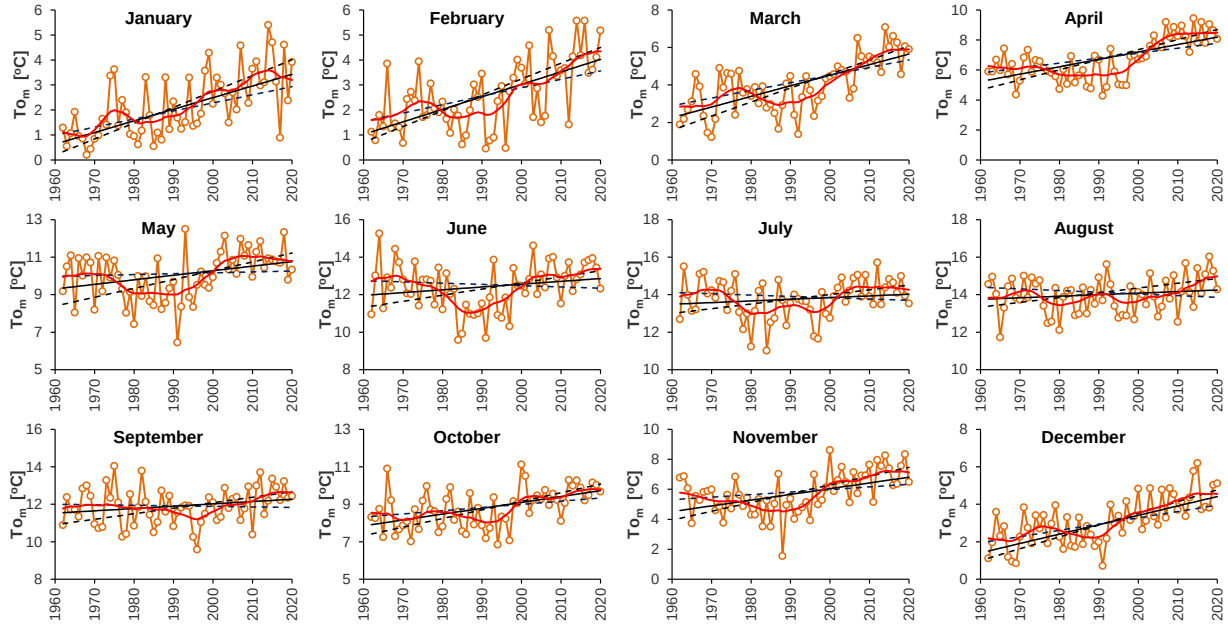

a)

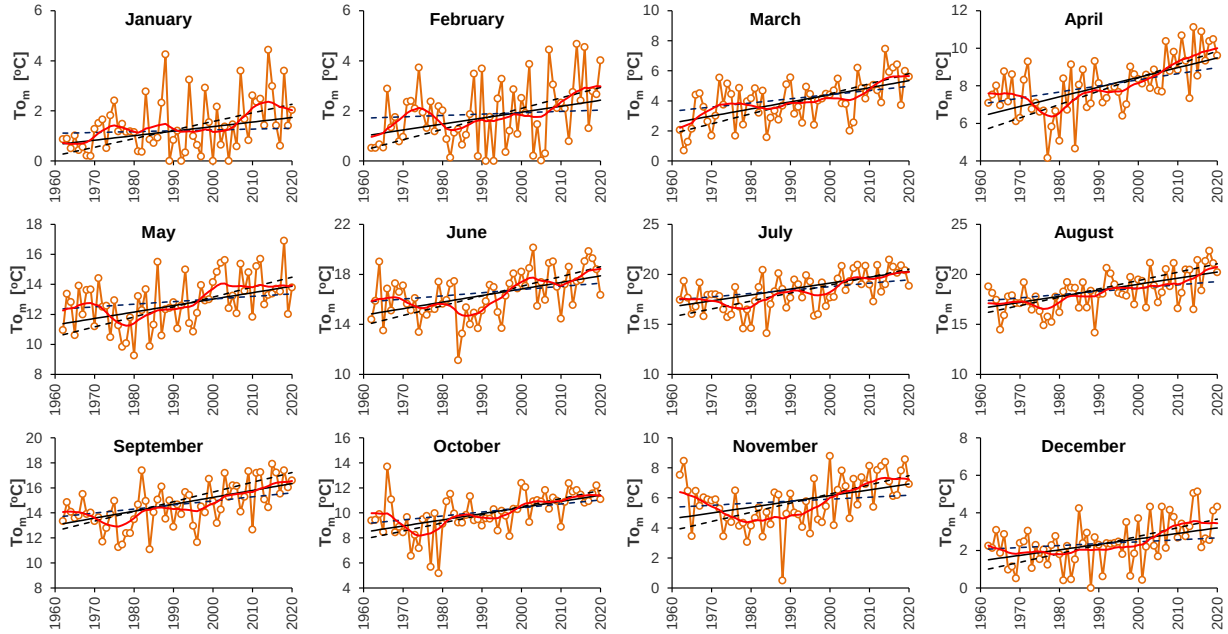

b)

Fig. 3. Course of monthly water temperature To_m, 7-year moving averages (red line), and long-term linear trend (black line) with confidence limits 95% (dot line) of the Hron River a) at Banská Bystrica and b) at Brehy for the period 1962–2020.

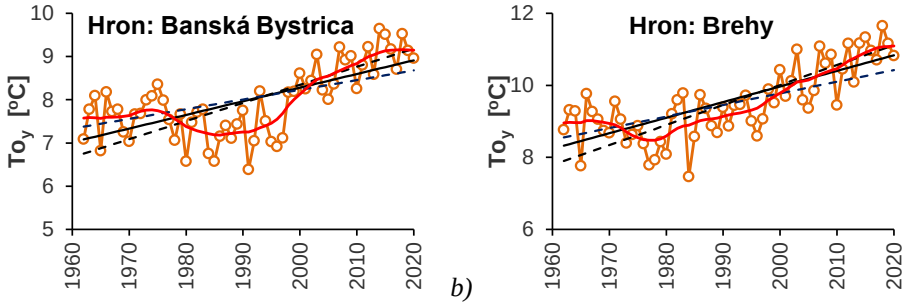

a) b)

Fig. 4. Course of long-term mean annual water temperature To_y, 7-year moving averages (red line), and long-term linear trend (black line) with confidence limits 95% (dot line) of the Hron River a) at Banská Bystrica; b) at Brehy. Period 1962–2020.

Table 4. **Conclusion of trend significance test of long-term mean annual water temperature To_y in the Hron River at Banská Bystrica and at Brehy gauging station during the period 1962–2020 (***α = 0.001)**

River	Gauging station	First year	Last year	*n*	Significance	slope	Correl. R^2
Hron	Banská Bystrica	1962	2020	59	***	0.032	0.452
	Brehy	1962	2020	59	***	0.043	0.563

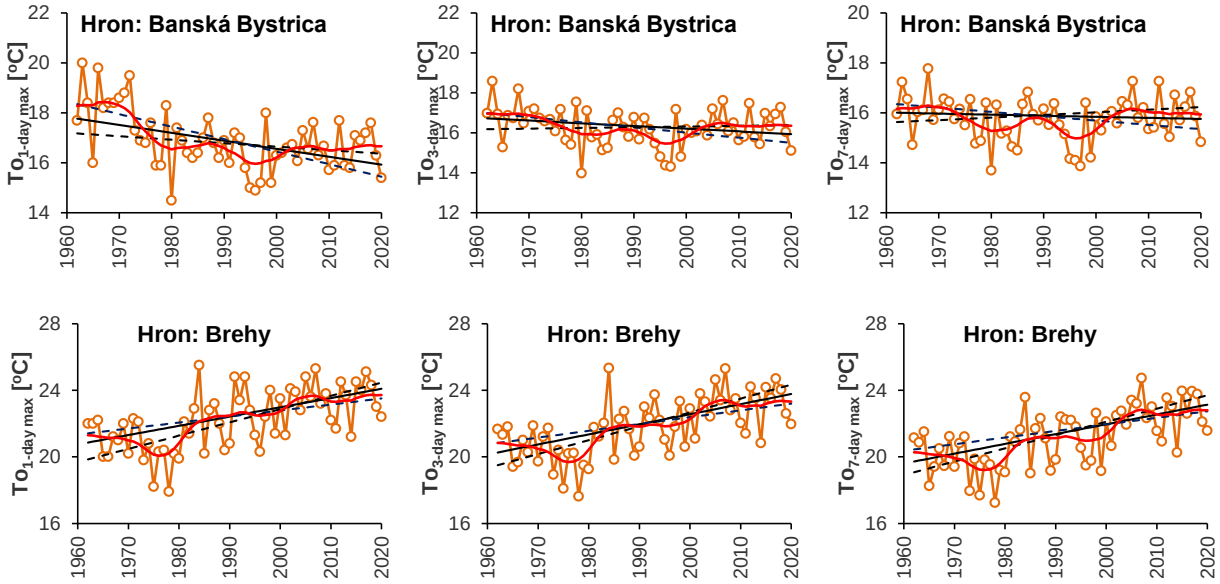

Fig. 5. Course of M-day maximum water temperature $To_{M\text{-}day\ max}$, 7-year moving (red line), and long-term linear trend (black line) with confidence limits 95% (dot line) of the Hron River a) at Banská Bystrica and b) at Brehy for the period 1962–2020.

Table 5. **Conclusion of long-term trend significance test of M-day maximum water temperature $To_{M\text{-}day\ max}$ in the Hron River at Banská Bystrica and at Brehy gauging station during the period 1962–2020 (with ***α = 0.001)**

River	Gauging station	M-day max *To* [°C]	Period	*n*	Significance	slope	Correl. R^2
Hron	Banská Bystrica	1-day	1962–2020	59	***	-0.032	0.226
		3-day	1962–2020	59	No	-0.011	0.042
		7-day	1962–2020	59	No	-0.003	0.004
	Brehy	1-day	1962–2020	59	***	0.059	0.338
		3-day	1962–2020	59	***	0.062	0.368
		7-day	1962–2020	59	***	0.061	0.368

Simulating the impact of air temperature changes on monthly water temperature in the Hron River using SARIMA model

The measured monthly water temperature *To* (Hron: Banská Bystrica and Hron: Brehy) and monthly air temperature *Ta* (Banská Štiavnica station) from the period 1991–2020 were used to model calibration. Several autoregressive models of the monthly water temperature *To* were selected (with monthly air temperature *Ta* as regressor). The best for Hron at B. Bystrica was the model: SARIMA(1,0,0)x$(0,1,1)_{12}$ + 1 regressor (the model with the lowest value of the AIC=-1.27). For Hron at Brehy the best was

the model: SARIMA(1,0,0)x(1,0,2)$_{12}$ + 2 regressors (the model with the lowest value of the AIC=-0.41).
The process of model selection is presented on water temperature data from gauging stations Hron: Banská Bystrica and Brehy. The resulting parameters of the model simulation SARIMA are given in Table 6. The marginal significance levels of each model parameter (*P*-value) were less than 0.05, so any parameter of the model has not to be excluded. Relationship between the measured monthly water temperatures at the Hron: Banská Bystrica and at the Hron: Brehy and monthly water temperatures modelled using SARIMA model are illustrated in Fig. 6. The SARIMA model performs very well in modelling the monthly water temperature values, with a high correlation coefficient of 0.983 at B. Bystrica and 0.985 at Brehy. Therefore, it can be effectively used to simulate changes in water temperature for different scenarios of changes in air temperature.
The largest increase in European mean temperature was detected in winter and spring, amounting to 0.5 to 1.0°C per decade during 1977–2001 (Jones and Moberg, 2003). Van der Schrier et al. (2013) note that Europe is warming faster (0.41°C per decade) than global land average (0.27°C per decade) over the period 1980–2010. These values refer to conspicuously enhanced warming in Europe at the end of the twentieth century compared with other continents. The Ministry of the Environment of the Slovak Republic (ME SR, 2018) formulates the general conclusions of the further development of the climate in Slovakia in a study. This study states, that the in comparison to the period between 1951 and 1980 the average air temperature may gradually increase by from 2°C to 4°C – the so-far inter-annual and inter-seasonal weather fluctuation may remain.
Therefore, two hypothetical scenarios of average monthly air temperatures were created:

1. The first scenario (SCEN+1) was created by adding 1°C to the measured monthly air temperature;
2. The second scenario (SCEN+3) was created by adding 3°C to the measured monthly air temperature (Fig. 7).

Comparison of the monthly increase in water temperature for scenarios (SCEN+1) and (SCEN+3) in the Hron River at Banská Bystrica and at Brehy is illustrated in Fig. 8.
According to the SARIMA model simulation results, the annual average increase in water temperature is smaller than the increase in air temperature. Results showed that a 1°C increase in air temperature caused the water temperature to rise by 0.35°C at Banská Bystrica and 0.57°C at Brehy, while a 3°C increase resulted in a rise of 1.05°C at Banská Bystrica and 1.75°C at Brehy. The differences in water temperature between selected stations is very pronounced, the difference in maximum water temperature reached in average value of 5°C during the period of 1962–2020. It may be caused by elevation and geographical location of the stations.
It is interesting to note that the increase in temperature in individual months varies. The highest increase is observed in October, while for the spring months, it occurs in April (Fig. 8).

Table 6. Summary Parameters for the model SARIMA(1,0,0)x(1,0,2)$_{12}$ + 2 regressors *TaBS* for water temperature at Hron: Brehy station and for the model SARIMA (1,0,0)x(0,1,1)$_{12}$ + 1 regressor *TaBS* for water temperature at Hron: Banská Bystrica station (*TaBS* -monthly air temperature at B. Štiavnica climatic station)

		Hron: Brehy		
Parameter	Estimate	Stnd. Error	t	P-value
AR(1)	0.46083	0.0482463	9.55162	0.000000
SAR(1)	1.00236	0.00617557	162.311	0.000000
SMA(1)	0.894541	0.0534495	16.7362	0.000000
SMA(2)	-0.14739	0.0505729	-2.9145	0.003798
TaBS	0.385112	0.0297479	12.9458	0.000000
TaBS*TaBS	0.0085917	0.0014794	5.80741	0.000000
Mean	5.188	1.07511	4.82556	0.000002
Constant	-0.0066115			
		Hron: Banská Bystrica		
Parameter	Estimate	Stnd. Error	t	P-value
AR(1)	0.7239173	0.0391153	18.5072	0.000000
SMA(1)	0.867648	0.0255945	33.8998	0.000000
TaBS	0.350164	0.0137955	25.3826	0.000000

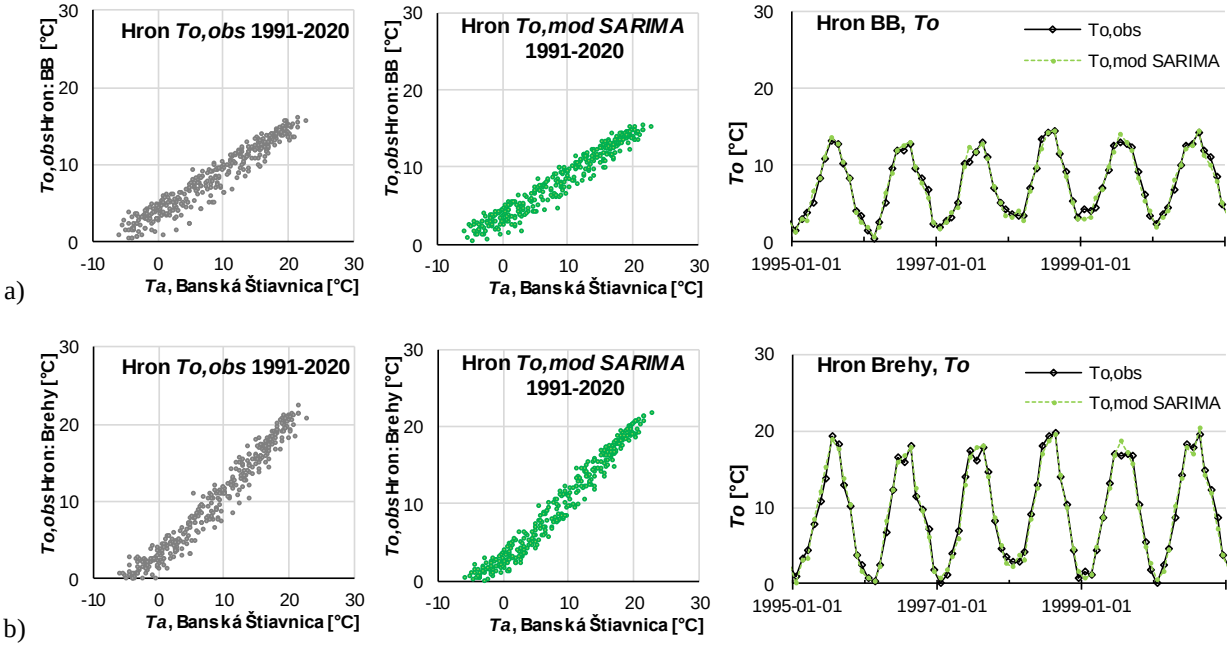

Fig. 6. a) Relationship between observed monthly water temperatures (To,obs) at Hron: B. Bystrica and monthly water temperatures modelled using SARIMA model (left graphs), and comparison of the monthly water temperatures modelled using SARIMA model (To,mod) (right graph) for the period 1995–2000. b) The same relationship for Hron: Brehy station.

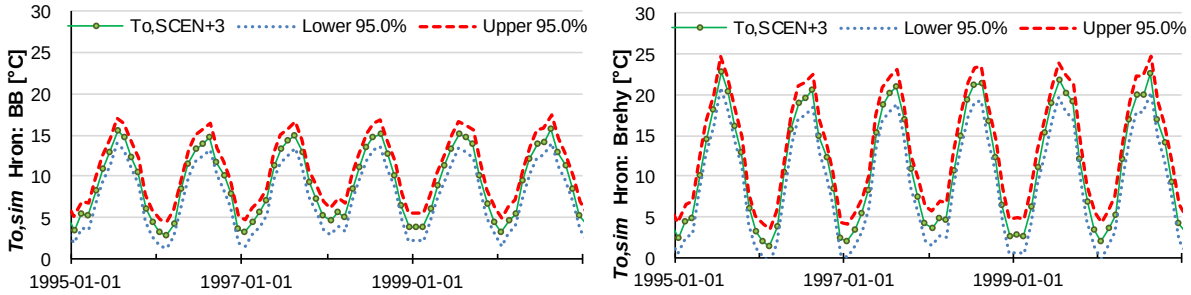

Fig. 7. Simulation of monthly water temperatures using SARIMA model, along with upper and lower 95% confidence limits. Results for the second scenario (SCEN+3). Left figure shows results for Hron: Banská Bystrica, while the right figure shows results for Hron: Brehy.

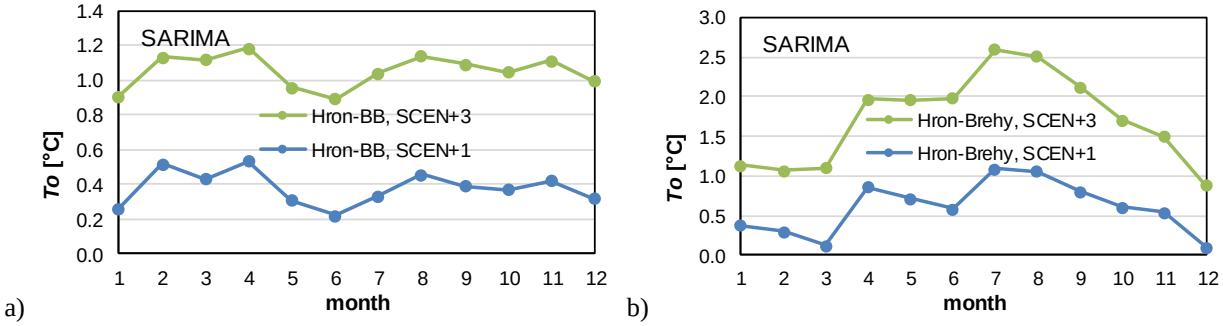

Fig. 8. Comparison of the predicted monthly increase in water for scenarios (SCEN+1) and (SCEN+3) in the Hron River at Banská Bystrica and at Brehy.

Conclusion

The first part of the present study was aimed to evaluate the long-term trend development of water temperature in the Hron River at two selected stations, Banská Bystrica and Brehy. A trend analysis was made for the period of the last 59 years (1962–2020). The results of the trend analyses are presented in Tables 3–5. The result showed a significant increasing of long-term trends in mean monthly water temperatures, especially in spring and winter months ((Hron: Banská Bystrica) and in spring and summer months (Hron: Brehy). In the case of long-term mean annual water temperatures, there is also a significant increasing in long term trends for both stations.

Significant increasing long-term trends were also recorded for the 1-, 3-, and 7-day maximum water temperatures at the Hron: Brehy station. Conversely, the Banská Bystrica station showed a significant decreasing long-term trend for the 1-day water temperature and no significant long-term trend for the 3- and 7-day maximum water temperatures.

With regard to the significant trend changes occurring in water temperature values, it is necessary to base the assessment of water quality and subsequent prediction of quality in Slovak rivers on data from the last 30 years at most or on the data since the period when started measuring with the automatic sensors of water temperature in hourly steps. Taking into account the results of the trend analysis, we attempted to model and predict the development of water temperature depending on the changes in air temperature.

To model the monthly water temperature (*To*) of the Hron River at two gauging stations (Banská Bystrica and Brehy) the monthly air temperature (*Ta*) as a regressor from 1991 to 2020 were used. The SARIMA$(1,0,0)x(1,0,2)_{12}$ model with 2 regressors was selected as the best fit model at Brehy, with significant parameters at p-value < 0.05 and a good fit indicated by a high correlation coefficient R^2 of 0.985. The SARIMA$(1,0,0)x(0,1,1)_{12}$ model with 1 regressors was selected as the best fit model at Banská Bystrica, with significant parameters at p-value < 0.05 and a good fit indicated by a high correlation coefficient R^2 of 0.983. The SARIMA model was then used to predict the impact of changes in air temperature on water temperature, with two scenarios of air temperature increase created: SCEN+1 (1°C increase) and SCEN+3 (3°C increase). Based on the simulation results of the SARIMA model, the yearly average rise in water temperature is lower than the increase in air temperature. A 1°C elevation in air temperature causes the water temperature at B. Bystrica station in the Hron River to rise by 0.35°C, and at the Brehy station, it rises by 0.57°C. In addition, a 3°C increase in air temperature results in a rise of water temperature by 1.05°C at Banská Bystrica and 1.71°C at Brehy. Tang and Garcia (2023) obtained similar results in the Mississippi River, where they found that the mean water temperature increased by 1.3°C, 1.5°C, and 1.8°C in the northern, central, and southern zones of the Mississippi River Basin, respectively, under a hypothetical uniform air temperature increase of 3.0°C. Our results showed that an increase in air temperature led to a corresponding increase in water temperature, with a greater increase observed at Brehy than at Banská Bystrica. The highest increase in water temperature occurred in August, while for the spring months, it occurred in April. Overall, the study concludes that the SARIMA model can be used to effectively simulate changes in water temperature based on changes in air temperature.

The findings of the study provide valuable information for water management and conservation strategies.

Acknowledgement

This work was supported by the project VEGA No. 2/0015/23 "Comprehensive analysis of the quantity and quality of water regime development in streams and their mutual dependence in selected Slovak basins"; project APVV-20-0374 "Regional detection, attribution and projection of impacts of climate variability and climate change on runoff regimes in Slovakia"; and project WATSIM "Water temperature simulation during summer low flow conditions in the Danube basin".

References

Beschta, R. L., Bilby, R. E., Brown, G. W., Holtby, L. B., Hofstra, T. D. (1987): Stream temperature and aquatic habitat: fisheries and forestry interactions. In: Stream-Side Management: an Interdisciplinary Symp. on Forestry and Fisheries Interactions (ed. E. F. Salo, Cundy T.), 191 p.(https://www.fs.usda.gov/rm/boise/AWAE/labs/awae_flagstaff/Hot_Topics/ripthreatbib/beschta_etal_streamtempaquahab.pdf)

European Environment Agency (2017): Climate Change, Impacts and Vulnerability in Europe 2016. An Indicator-based Report. Publications Office of the European Union. (https://www.eea.europa.eu/publications/climate-change-impacts-and-vulnerability-2016)

Gilbert, R. O. (1987): Statistical Methods for Environmental Pollution Monitoring. John Wiley & Sons, Inc., New York.

Hamed, K. H. (2008). Trend detection in hydrologic data: The Mann-Kendall trend test under the scaling hypothesis. Journal of Hydrology, 349(3–4), 2008, 350–363.

Jones, P. D., Moberg, A. (2003): Hemispheric and large-scale surface air temperature variations: an extensive revision and an update to 2001. J. Clim., Vol. 16, 206–223. https://doi.org/10.1016/j.gloplacha.2018.08.015

Lešková, D., Škoda, P. (2003): Temperature series trends of Slovak rivers. Meteorologický časopis. Vol. 6, no. 2, 13–17. (https://www.shmu.sk/File/ExtraFiles/MET_CASOPIS/MC_6-2003_2.pdf)

Liptay, Z. (2022). Neurohydrological prediction of water temperature and runoff time series. Acta Hydrologica Slovaca, 23(2), 190–196. 2644-6291 (printed until 2018). DOI: https://doi.org/10.31577/ahs-2022-0023.02.0021

Ludwig, Ch., Ranner, H., Kavka, G., Kohl, W., Humpesch, U. (1990): Long term and seasonal aspects of the water quality of the River Danube within the region of Vienna (Austria). In: Water Pollution Control in the Danube Basin (ed. M. Miloradov), 51–58.

International Association on Water Pollution Research and Control. https://doi.org/10.2166/wst.1990.0009

Martincová, M., Kučárová, K., Škoda, P., Pekárová, P. (2011): Long term trend of water temperature in Slovak Rivers. In XXVth Conference of the Danubian Countries on the Hydrological Forecasting and Hydrological Bases of Water Management: Conference Proceedings. (Ed. G. Bálint, M. Domokos). Budapest: VITUKI, pp. 11. ISBN 978-963-511-152-7.

Ministry of the Environment of the Slovak Republic. (2018): Strategy of adaptation of the Slovak Republic to climate change. Executive Summary, Bratislava, 145 p. https://climate-adapt.eea.europa.eu/repository/11273729.pdf

Mohseni, O., Stefan, H. G. (1999): Stream Temperature-Air Temperature Relationships: A Physical Interpretation. Journal of Hydrology, vol. 218, no. 3–4, 128–141. http://dx.doi.org/10.1016/S0022-1694(99)00034-7.

Okhravi, S., Sokáč, M., Velísková, Y. (2022): Three-dimensional numerical modeling of water temperature distribution in the Rozgrund Reservoir, Slovakia. Acta Hydrologica Slovaca, 23(2), 305–316. 2644-6291. DOI: https://doi.org/10.31577/ahs-2022-0023.02.0035

Pekárová, P. (2009): Multiannual runoff variability in the upper Danube region. Dizertačné doktorské práce (DrSc.). Bratislava: IH SAS, 2009. p. 151.

Pekárová, P., Miklánek, P., Halmová, D., Onderka, M., Pekár, J., Kučárová, K., Liová, S., Škoda, P. (2011): Long-term trend and multi-annual variability of water temperature in the pristine Bela River basin (Slovakia). J. Hydrology, vol. 400, no. 3–4, 333–340. https://doi.org/10.1016/j.jhydrol.2011.01.048

Poórová, J., Melová, K., Lovásová, Ľ., Blaškovičová, L., (2017): The effect of the selected Water Reservoirs manipulation on the flow with regard to the dry season. (In Slovak: Vplyv manipulácie na Vybraných Vodných nádržiach na tok so zreteľom na obdobie sucha. In conference Water reservoirs 2017, Brno ČR 3-4.10.2017, 169–177. (https://www.shmu.sk/File/Hydrologia/Publikacna_cinnost/2017/2017_Vodni_nadrze_2017_Poorova%20a%20kol_Vplyv%20VN.pdf)

Ptak, M., Sojka, M., Kałuza, T., Choinski, A., Nowak, B. (2019): Long-term water temperature trends of the Warta River in the years 1960–2009. Ecohydrology & Hydrobiology, vol. 19, no. 3, 441–451, https://doi.org/10.1016/j.ecohyd.2019.03.007.

Salmi, T., Määttä, A., Anttila, P., Ruoho-Airola, T., Amnell, T. (2002): Detecting trends of annual values of atmospheric pollutants by the Mann-Kendall test and Sen's slope estimates MAKESENS–The excel template application. Finish Meteorological Institute, Helsinki.

St-Hilaire, A., Ouarda, T. B. M. J., Bargaoui, Z., Daigle, A., Bilodeau, L. (2012): Daily river water temperature forecast model with a k-nearest neighbour approach. Hydrol. Process. 26, 9, 1302–1310. https://doi.org/10.1002/hyp.8216

Tang, Ch., Garcia, V. (2023): Identifying stream temperature variation by coupling meteorological, hydrological, and water temperature models. JAWRA Journal of the American Water Resources Association 00 (0): 1–16. https://doi.org/10.1111/1752-1688.13113

Van der Schrier, G., van den Besselaar, E. J. M., Klein Tank, A. M. G., Verver, G. (2013): Monitoring European average temperature based on E-OBS gridded data set. J Geophys Res Atmos. Vol: 118, 5120–5135. https://doi.org/10.1002/jgrd50444

Vannote, R. L., Sweeney, B. W. (1980): Geographic analysis of thermal equilibria; a conceptual model for evaluating the effect of natural and modified thermal regimes on aquatic insect communities. Am. Naturalist, vol. 115, no. 6, 667–695. https://doi.org/10.1086/283591

Webb, B.W., Nobilis, F. (1997): Long-Term Perspective on the Nature of the Air-Water Temperature Relationship: A Case Study. Hydrological Processes 11(2): 137–47. https://doi.org/10.1002/(SICI)1099-1085(199702)11:2<137: AID-HYP405>3.0.CO;2-2.

Webb, B. W., Walling, D. E. (1985): Temporal variation of river water temperatures in a Devon river system. Hydrological Sciences Journal, vol. 30, no. 4, 449–464. https://doi.org/10.1080/02626668509491011

Webb, B. W., Walling. D. E. (1992): Long-Term Water Temperature Behaviour and Trends in a Devon, UK, River System. Hydrological Sciences Journal, vol. 37, no. 6, 567–80. https://doi.org/10.1080/0262666929492624.

Ing. Veronika Bačová Mitková, PhD. (*corresponding author, e-mail: mitkova@uh.savba.sk)
RNDr. Pavla Pekárová, DrSc.
Ing. Dana Halmová, PhD.
Institute of Hydrology SAS
Dúbravská cesta 9
841 04 Bratislava
Slovak Republic

DOI: 10.31577/ahs-2023-0024.01.0008

ACTA HYDROLOGICA SLOVACA

Volume 24, No. 1, 2023, 63 – 72

Understanding the impact of drought on Topľa River discharge seasonality

Wael ALMIKAEEL*, Luara Cunha de ALMEIDA, Lea ČUBANOVÁ, Andrej ŠOLTÉSZ, Jakub MYDLA, Dana BAROKOVÁ

This study examines the effect of drought on the discharge seasonality of the Topľa River from 1988 to 2020. Each year is classified into dry, normal, or wet years using the water-bearing coefficient as a drought index. The Seasonal and Trend decomposition using the Loess time series decomposition method was used to compare discharge patterns between these groups. The results demonstrate a significant impact of drought on the seasonal discharge of the Topľa River, with substantially lower discharge and affected seasonality during dry years. The study findings demonstrate that the impact of the drought is altering the seasonal discharge pattern of the river. This highlights the importance of considering the effects of drought in water management and resource planning, particularly in the face of climate change and increasing water scarcity. These findings provide valuable insights for informing water management policies and practices in the region and can guide future research on the impact of drought on river systems.

KEY WORDS: time series decomposition, drought analysis, seasonality analysis, climate change, water resources

Introduction

Climate change has had a profound impact on water resources and water management strategies globally, with hydrological drought being a particular challenge. There is growing evidence to suggest that climate change is exacerbating hydrological drought conditions in many regions of the world. As temperatures rise, evapotranspiration rates increase, leading to higher rates of water loss from soils and vegetation (Vicente-Serrano et al., 2014). This, coupled with changes in precipitation patterns, can lead to reduced water availability and increased frequency and severity of hydrological drought. Climate change can also alter the frequency and intensity of extreme weather events such as hurricanes, floods, and heat waves, which can further exacerbate the impacts of hydrological drought. Addressing climate change through mitigation and adaptation measures is essential for reducing the risks associated with hydrological drought and ensuring sustainable water management for present and future generations (Gu et al., 2022).

Hydrological drought is a significant issue in Europe, affecting many regions and posing challenges for water management and adaptation (Vicente-Serrano et al., 2014). The changing climate in Europe has led to a more frequent occurrence of drought events, and the recent decades have seen a significant increase in the duration, severity, and spatial extent of hydrological drought in many parts of the continent (Spinoni et al., 2018; Sýs et al., 2021). In Slovakia, the impacts of hydrological drought have been particularly severe, with the country experiencing multiple episodes of low river discharge, reduced groundwater levels, and agricultural losses in recent years (Zeleňáková et al., 2018; Fendeková et al., 2018a). These impacts have been attributed to a combination of factors, including climate change, land-use changes, and water abstraction for various purposes. The hydrological drought situation in Slovakia highlights the need for effective monitoring and management of water resources, as well as the development of drought-resilient infrastructure and policies. It also underscores the importance of international cooperation and coordination to address the transboundary nature of water resources in Europe (Özerol et al., 2016).

Slovakia's surface runoff regime exhibits a notable increase in spring runoff, with the mountainous regions at higher altitudes experiencing slower snowmelt and consequently, delayed enhanced spring runoff when compared to lowland streams (Fendeková et al., 2018b; Velísková et al., 2017). During the summer-autumn season, most streams in Slovakia exhibit low water content, with the months between August and October being a crucial period for the growing season. In mountainous regions, the winter low-water period is of significant importance, particularly during the months of December to February (Almikaeel et al., 2022). Snowfall

is a contributing factor to the low-water season, which does not immediately generate runoff during periods of sub-zero temperatures resulting from partial or complete freezing of the stream (Wang, 2019).

Understanding seasonal patterns of river flow is crucial for sustainable water management and agriculture (Serrano et al., 2020; Duchan et al., 2022). It can impact the quality and quantity of available water resources, affecting water supply, agriculture, and other water-dependent industries (Serrano et al., 2020; Khan et al., 2009). Hydrologists and agriculture can optimize their water use by comprehending seasonal changes in river flows, reducing losses, and increasing productivity, particularly in regions with limited water resources (Khan et al., 2009). A better understanding of the seasonality of river flows can also inform climate adaptation strategies (Laizé et al., 2016) and drinking water demand (Varga and Velísková, 2021). Seasonality can exacerbate drought conditions as precipitation patterns correlate with water availability, amplifying the effects of low rainfall or prolonged drought (Romano et al., 2020). This can result in reduced water availability during times of high demand, such as during the growing season for crops. Similarly, seasonality plays a role in exacerbating flood disasters, as seasonal patterns of precipitation and snowmelt can concentrate high-flow occurrences at particular times of the year, increasing the likelihood and severity of flooding (Serrano et al., 2020; Sivapalan et al., 2005).

Climate change has had a profound impact on water resources and water management strategies globally, with hydrological drought being a particular challenge (Vicente-Serrano et al., 2014; Rao and Patil, 2016). Changing precipitation patterns, increasing temperatures, and altered seasonal cycles have resulted in more frequent and severe drought events, leading to reduced water availability and quality (Rao and Patil, 2016). Moreover, innovative approaches that account for the impacts of climate change on water resources, including changing precipitation patterns, temperature, and water availability, are crucial in developing sustainable water management strategies that can cope with the increasingly frequent and severe drought events resulting from climate change (Rao and Patil, 2016).

Effective water resources management under extreme climate conditions requires an understanding of seasonal flow discharge patterns. The influence of water management can be significant as it extends beyond borders, and this is due to the fact that water does not recognize boundaries. Climate change has led to alterations in seasonal cycles and precipitation patterns, resulting in more frequent and severe hydrological droughts (Van Loon et al., 2014; Tomaszewski, 2014). Consequently, understanding the timing and variability of water flows in different seasons has become critical for managing water resources sustainably. By considering seasonal flow discharge patterns, water resources management strategies can be designed to catch and store water during high-flow periods, improving water availability during low-flow periods, particularly during droughts (Van Loon et al., 2014).

Study area

The study area – Topľa River in eastern Slovakia, falls within these administrative divisions of Slovakia: Prešovský, and Košický region, and comprises agricultural land and forested areas. It is a right-hand tributary of the Ondava River, and it is classified as an upland/lowland type of river, with a catchment drainage area of 1,544 km² (Vodohospodárska bilancia SR, 2014) and a length of 129.8 km (Fig. 1). The annual rainfall in the Topľa River basin ranges from 600 to 700 mm in lower elevations to approximately 1000 mm in mountainous areas, and it is situated in the temperate climate zone. It falls within three different climatic regions of Slovakia, based on the classification by Lapin. The warm region covers the lower-lying areas, mostly in the southern part of the basin, and is characterized by an average annual number of summer days of over 50 and a daily temperature maximum of over 25°C. The moderately warm region covers most of the study area and spreads mainly in valleys, uplands, and foothills, with an average July temperature of 16°C or more and an average annual number of summer days of less than 50. The cool region covers the northern and northwestern parts, represented by mountains, with a July mean temperature of less than 16°C (Garaj et al., 2019). According to the available data, July is identified as the month with the highest precipitation rate in the eastern region of Slovakia in period 1997–2017 (Predbežné hodnotenie povodňového rizika, 2018).

According to data from the period 1931–2015, the long-term mean daily discharge amounts in Hanušovce nad Topľou (the lowest gauging station on the Topľa River) station was 8.1 $m^3 \cdot s^{-1}$, with a maximum discharge of 449 $m^3 \cdot s^{-1}$ occurring on 06.04.1932. The seasonal variation of the discharge is the dominant characteristic of the Topľa River's hydrological regime, with the highest discharge usually recorded during the spring snowmelt period and summer rainfall events. On the other hand, low flows and occasional ice cover are witnessed during the winter months. For the purposes of this study data from the Bardejov gauging station (103.5 rkm, catchment area of 325.8 km^2) were used. The Slovak Hydrometeorological Institute (SHMI) reported a mean annual discharge of $Q_{a\ 1967\text{-}2000}$ = 2.978 $m^3\ s^{-1}$ for the Bardejov gauging station (Frandofer and Lehotský, 2014). An in-depth understanding of the hydrological characteristics of the Topľa River is critical for effective water management and the mitigation of extreme events like floods and droughts.

Material and methods

Drought analysis

Drought assessment approaches that are hydrological in nature are valuable tools for detecting potential water shortages, and their use is particularly important in the implementation of drought response strategies. To identify, monitor, and evaluate the severity of drought

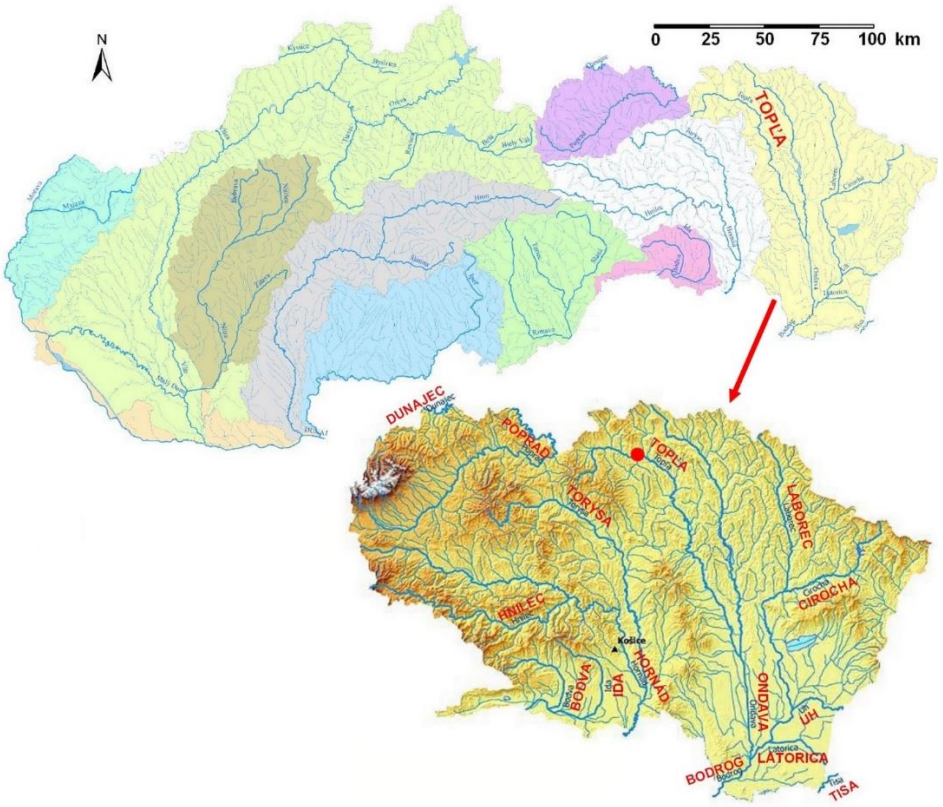

Fig. 1. Map of Slovak Republic – in yellow basin of Bodrog River with subbasin of Topľa River (Plaveniny, 2020), red dot represents gauging station in Bardejov.

events, indices have been developed by researchers worldwide, using several years of meteorological data, including precipitation, air temperature, evapotranspiration, runoff, and soil moisture. Indices provide a way to quantify drought and monitor wet and dry periods. They help to understand the severity, duration, location, and timing of drought events, and they make it easier to communicate this information to diverse audiences. Different indices can be used for various purposes, such as the Palmer Drought Severity Index (PDSI), Standardized Precipitation Index (SPI), Standardized Precipitation Evapotranspiration Index (SPEI), Soil Moisture Anomaly Index (SMAI), Standardized Runoff Index (SRI), and Vegetation Condition Index (VCI). These indices can be used to assess the impact of droughts on agriculture, water resources, and communities and promote sustainable development. Therefore, the use of drought indices is crucial in mitigating the negative effects of drought and providing critical information to manage drought impacts effectively (WMO, 2008; Zhu et al. 2018).

Various hydrological drought indices are utilized to assess and characterize the severity of droughts on water resources. The indices allow for the monitoring of drought's effects on hydrological variables such as streamflow, discharge, and water storage. Standardized Runoff Index (SRI) and the water-bearing coefficient are two frequently utilized hydrological drought indices when only discharge data are available. The SRI is a drought index based on the standard deviation of discharge from the long-term mean, whereas the water-bearing coefficient estimates the available water resources relative to the long-term mean. The water-bearing coefficient is used as the drought index in this study to evaluate the hydrological drought in the study area (Almikaeel et al., 2022, Zhu et. al, 2018).

The water-bearing coefficient method is frequently employed to assess drought. This method calculates the ratio of the annual mean discharge (Q_{avg}) to the long-term mean discharge (Q_a), represented by Q_{avg}/Q_a. The annual mean discharge, Q_{avg}, refers to the average flow of water through a river or stream within a year, while the long-term mean discharge, Q_a, is the average flow of water over a more extended period. This method was applied also in this study for the Topľa River. This coefficient establishes standard values to determine the proportion of mean discharge during a particular period relative to the long-term average. The standard intervals are categorized into three primary groups to identify whether the year is dry, normal, or wet, and subcategories determine the severity of drought and wet years. While the water-bearing coefficient is a useful tool for analyzing drought conditions, other factors such as precipitation patterns, land-use changes, and water demand should be considered to evaluate water availability and management fully (Almikaeel et al., 2022; GWP, 2013). The classification intervals utilized by the Water-Bearing Coefficient method to assess the severity of drought are presented in Table 1.

Table 1. Hydrological status categories according to the water-bearing coefficient values

Standard Intervals	Hydrological Situation
10 – 29	Extreme Drought
30 – 49	Severe Drought
50 – 69	Moderate Drought
70 – 89	Mild Drought
90 – 110	Normal
111 – 130	Mild Wet
131 – 150	Moderate Wet
151 – 170	Severe Wet
171 – 180 More	Extreme Wet

Time series decomposition

In various fields such as business, economics, engineering, environment, medical, earth sciences, hydrology, climatology, and meteorology, time series data are frequently collected through repeated measurements. These data can be discrete values of a variable, averaged over a particular time interval, or continuously recorded across time. Hydrological time series data often contain a deterministic component, which can be a trend, a jump, a periodic component, or a combination of these, placed on a random component. These data are typically collected at regular intervals, such as hour, day, week, month, season, or year. An example of hydrological time series is streamflow or river-stage readings collected hourly, daily, weekly, monthly, or annually. To decompose a hydrological time series into its level, trend, and seasonality, a time series decomposition method is used (Liu et al., 2021).

Seasonal and Trend Decomposition using Loess (STL)

Seasonal and Trend Decomposition using Loess (STL) is a popular method for time series analysis that decomposes a given time series into three main components: a seasonal component, a trend component, and a remainder or residual component. The seasonal component represents the repeating patterns of the time series that occur over a fixed time interval, such as a year or a month. The trend component represents the overall direction or trend of the time series over time. The remainder component represents the random fluctuations in the data that are not accounted for by the seasonal or trend components.

The STL method involves smoothing the time series using a locally weighted regression method called Loess. The Loess method fits a curve through the data points using a weighted average of neighbouring points. The weights are determined by a tuning parameter, which determines the amount of smoothing. The seasonal component is estimated by taking the moving average of the time series after removing the trend component. The trend component is estimated by taking the moving average of the time series after removing the seasonal component. The remainder component is estimated by subtracting the seasonal and trend components from the original time series.

The STL method can be expressed mathematically as follows. Given a time series y_t, the seasonal component S_t, trend component T_t , and remainder component R_t can be estimated by the following equations:

$$S_t = \sum_{i=1}^{m} w_i \left(m_j y_{t+i-m/2} \right) \quad (1)$$

$$T_t = \sum_{i=1}^{n} w_i \left(n_j y_{t+i-n/2} \right) \quad (2)$$

$$R_t = y_t - S_t - T_t \quad (3)$$

where

m – odd window size for the seasonal component,
n – odd window size for the trend component,
w_i – the weights assigned to each data point,
m_j, n_j – the number of non-missing data points in the j-th window.

The weights w_i are determined by the distance between the i-th data point and the central point of the window, with closer points receiving higher weights. The tuning parameters for the method include m, n, and the degree of smoothing for the Loess method (Liu et al, 2021; Theodosiou, 2011; Dokumentov and Hyndman, 2015).

The window size utilized in this study is 365 days, which has been chosen to signify an entire year and satisfy the requirement of an odd-sized window.

The STL method is useful for examining the dynamics of drought as it can separate the underlying trends and seasonal patterns from the noise in the data, which can help identify drought periods and their severity by analyzing the residuals from the decomposition.

Results and analysis

Drought analysis

Further analysis of the Topľa River's discharge data reveals important information about the hydrological

situation of the river over the period of 1988 to 2020 (Fig. 2). By using the water-bearing coefficient, each year was assessed into three main categories: wet, normal, and dry. The results of the analysis confirm that the river experienced wet hydrological status during 8 years (1989, 2001, 2005, 2006, 2008, 2009, 2010, and 2017), with water bearing coefficients ranging between 110% to 196%. Meanwhile, normal hydrological status was observed during 7 years (1991, 1992, 1997, 1999, 2004, 2014, and 2019), with water bearing coefficients ranging from 89% to 104%. On the other hand, the river experienced dry hydrological status during 18 years (1988, 1990, 1993, 1994, 1995, 1996, 1998, 2000, 2002, 2003, 2007, 2011, 2012, 2013, 2015, 2016, 2018, and 2020), with water-bearing coefficients ranging from 53% to 88%. It can be concluded from Fig. 2 that the year 2003 was the worst in terms of drought. This statement is also confirmed in the "Preliminary Assessment of Flood Risk" report from 2018. Furthermore, it was the year with the most severe meteorological drought in Slovakia since 1881.

Overall, the results indicate that the hydrological situation of the Topľa River tended to be dry during the study period, with a maximum 3 sequential years of wet or normal years. However, the period between 2004 and 2010 was the best period in terms of the level of discharges. Interestingly, even though 2007 is considered as a dry year, the water-bearing coefficient was around the boundaries of the normal level. For further analysis, the discharges of each year were grouped according to the hydrological situation. This grouping allows for a more detailed examination of the discharge data and can help in developing appropriate strategies to manage and optimize the use of water resources in the Topľa River basin.

Seasonality analysis

Seasonality analysis is a useful tool to understand the pattern and trend of a time series. In the current study, the STL method was used to perform time series decomposition on four groups of data, including the general data set over the period 1988–2020, dry years data set containing discharges of 18 years, normal years data set containing discharges of 8 years, and wet years data set containing discharges of 7 years. The seasonal decomposition function was used from the statsmodel library, and the period was set to be 365 to represent a whole year, and the model was chosen to be multiplicative. This enabled the study to determine the seasonal pattern of each hydrological group on an annual basis. The seasonal pattern was extracted from each group and then compared to the seasonality over the whole period. The results showed that the seasonal pattern of the general data set was characterized by a clear peak in discharge during the spring season, followed by a gradual decrease during the summer and autumn seasons, and a relatively low discharge during the winter season. In contrast, the seasonal pattern of the dry years data set showed a gradual increase in discharge from the winter season to the spring season, followed by a sharp decrease during the summer and autumn seasons. The normal years data set showed a seasonal pattern similar to that of the general data set, with a clear peak in discharge during the spring season, followed by a gradual decrease during the summer and autumn seasons, and a relatively low discharge during the winter season. Finally, the wet years data set showed a seasonal pattern with a clear peak in discharge during the spring season, followed by a gradual decrease during the summer season, and a relatively low discharge during

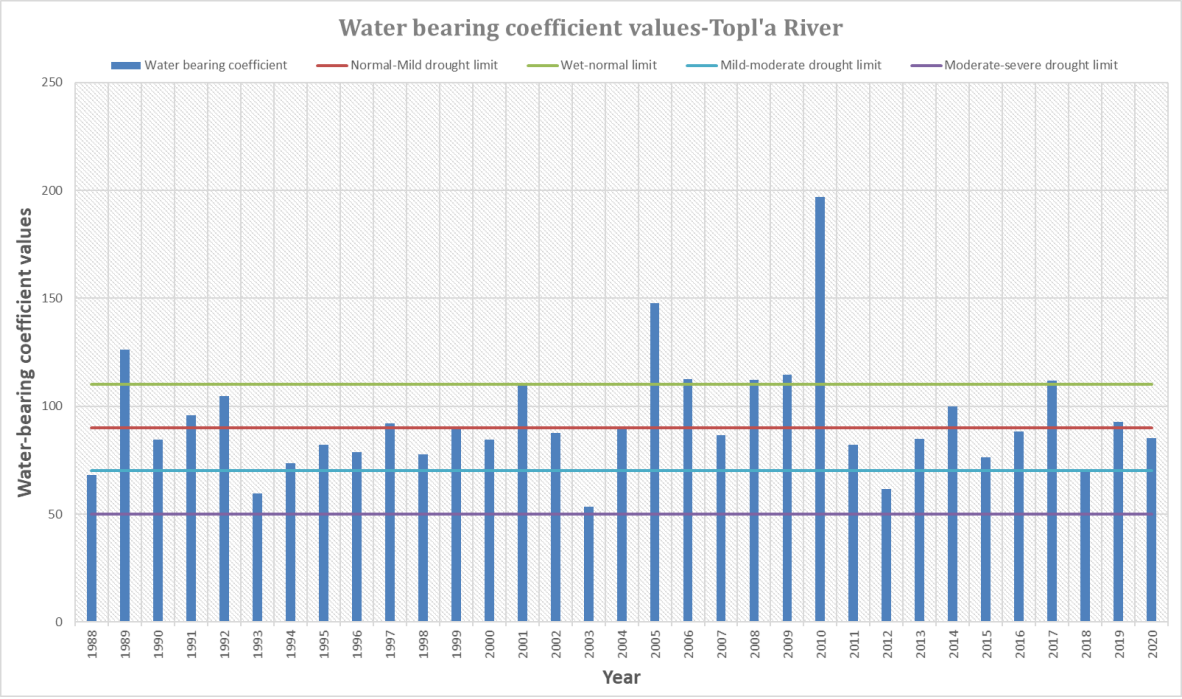

Fig. 2. Water bearing coefficient and its standard values for Topľa River, period 1988–2020.

the autumn and winter seasons. These results indicate that the seasonal pattern of the discharge data varies depending on the hydrological situation of the year.

Based on the analysis of the seasonal discharge of the dry years compared to the general seasonal discharge, it can be concluded that the seasonality of the two groups is very similar. Both groups have relatively low seasonal discharge during the first two months of the year, followed by a steady increase that reaches its peak in mid-April, which is most likely due to the onset of the spring snowmelt in the catchment area. From mid-April to mid-May, the seasonal discharge component decreases slowly, followed by two peaks in May and June, where a significant increase in the seasonal discharge component is observed. However, it is uncertain whether the increase in June can still be attributed to ice melting, as summer storms may especially contribute to the increase in discharge during this time. Additionally, the seasonal discharge component decreases slightly after mid-June, reaching another significant peak in the last week of July and the first week of August, which dominates the discharge component during this period. Following this peak, the seasonal discharge component decreases until it reaches its minimum in October, with a slight increase observed in November and December. The main difference between the dry and general seasonality seems to be the peak in mid-June, which is slightly higher in the general seasonality, and a small peak of discharge in July for the dry seasonality seems to be shifted to August in the general one. Furthermore, the seasonal discharge in late April or the first of May seems to be higher in the general seasonality compared to the dry seasonality (Fig. 3).

The seasonal discharge patterns of the normal and general data sets are quite similar, with some slight differences. Both seasonalities show a relatively low seasonal discharge during the first two months of the year, which can be attributed to low precipitation and snow accumulation during this period. After mid-February, the seasonal discharge component increases slowly, reaching its first peak in late February for the normal seasonality, while in the general seasonality, this peak is less significant. There is a large peak in late February in the normal seasonality, which is absent in the general seasonality, indicating a higher rate of precipitation during this month in normal years than the average rate during the study period. From late February to mid-April, the seasonal discharge component decreases slowly, followed by a significant increase in mid-April that reaches its peak in the first week of May. This peak is most likely due to the onset of the spring snowmelt in the catchment area.

Moreover, there are two significant peaks in seasonal discharge in the normal seasonality, occurring in late April and the beginning of August. These peaks have a higher magnitude compared to the general seasonality, indicating a higher rate of precipitation during these periods. The late April peak is likely related to the spring snowmelt and heavy rainfall, while the August peak may be correlated to summer storms. From mid-May to mid-June, the seasonal discharge component decreases slightly, followed by a peak in late June, which is higher in the general seasonality compared to the normal one. After mid-June, the seasonal component of the discharge decreases slightly, reaching another significant peak in the last week of July and the first week of August, which dominates the discharge component during this period. The seasonal discharge component then decreases until it reaches its minimum in October, with a slight increase observed in November and December. These results demonstrate the impact of precipitation and snowmelt on

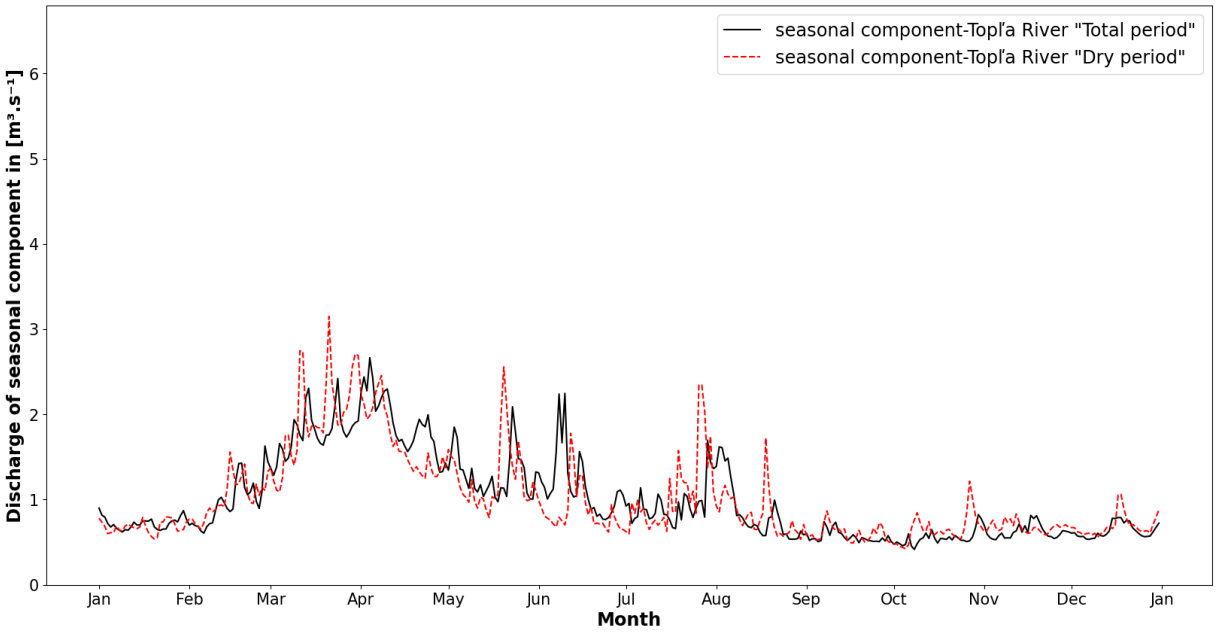

Fig. 3. Comparison of seasonal discharge patterns in dry years and over the whole study period.

the seasonal discharge patterns of both normal and general data sets but also highlight the significance of certain peak periods in the normal seasonality that indicate higher precipitation rates during those periods (Fig. 4).

A comparison of the wet seasonality to the general seasonality indicates significant differences in the seasonal discharge patterns. Although February and late March exhibit slightly higher seasonal discharge in the general period, the wet seasonality shows extremely high seasonal discharge peaks in April and June, significantly higher than those in the general seasonality. The June peak, slightly higher than the April peak in the wet period, demonstrates the combined effect of snow melting and summer storms on the seasonal discharge, affecting the hydrological situation of the river. Additionally, mid-April and mid-July show relatively larger peaks of seasonal discharge in the wet period compared to the general seasonality. Overall, these results emphasize the significance of understanding the hydrological dynamics of the river catchment and the role of precipitation and snow melting in predicting the seasonal discharge patterns. The wet seasonality's analysis highlights the impact of precipitation and snowmelt rate on the seasonal discharge pattern, exhibiting a distinct pattern of seasonal discharge with significant differences in the magnitude and timing of the peaks. While February and late March exhibit slightly lower seasonal discharge components in the wet seasonality, April and June exhibit extremely higher seasonal discharge peaks, suggesting the importance of snow melting and summer storms in shaping the seasonal discharge pattern. Mid-April and mid-July also show relatively larger peaks of seasonal discharge in the wet seasonality, indicating a higher rate of precipitation during these periods. These findings suggest that the wet seasonality of the river is highly influenced by hydro-climatic conditions such as snow accumulation, precipitation, and temperature, affecting the rate of snowmelt and onset of summer storms (Fig. 5). Findings of this study correlates with results stated in other studies dealing with hydrological aspects of Slovak streams, e.g. (Predbežné hodnotenie povodňového rizika, 2018).

The results of the hydrological assessment of the Topľa River over the period 1988–2020 indicate that most of the years can be classified as dry hydrological, as compared to the long-term average discharge of the river. However, it is worth noting that the drought situation in 79% of these dry years is considered as mild drought, with only 21% being classified as a moderate drought. This finding suggests that although the river tends to have a lower-than-average discharge in most years, the severity of drought is not extreme. Nevertheless, the shift of the long-term average towards the dry situation can be correlated to the increasing effect of climate change, and the lack of precipitation and snow in the area. This trend is consistent with the findings of other studies that indicate an overall decrease in water resources in many parts of the world due to climate change. It is essential to continue monitoring the hydrological status of the Topľa River and other water resources in the region to evaluate the impacts of climate change and identify appropriate adaptation measures. The results of this study can provide valuable information for water resource management and planning in the region and could help to mitigate the potential impacts of climate change on water availability.

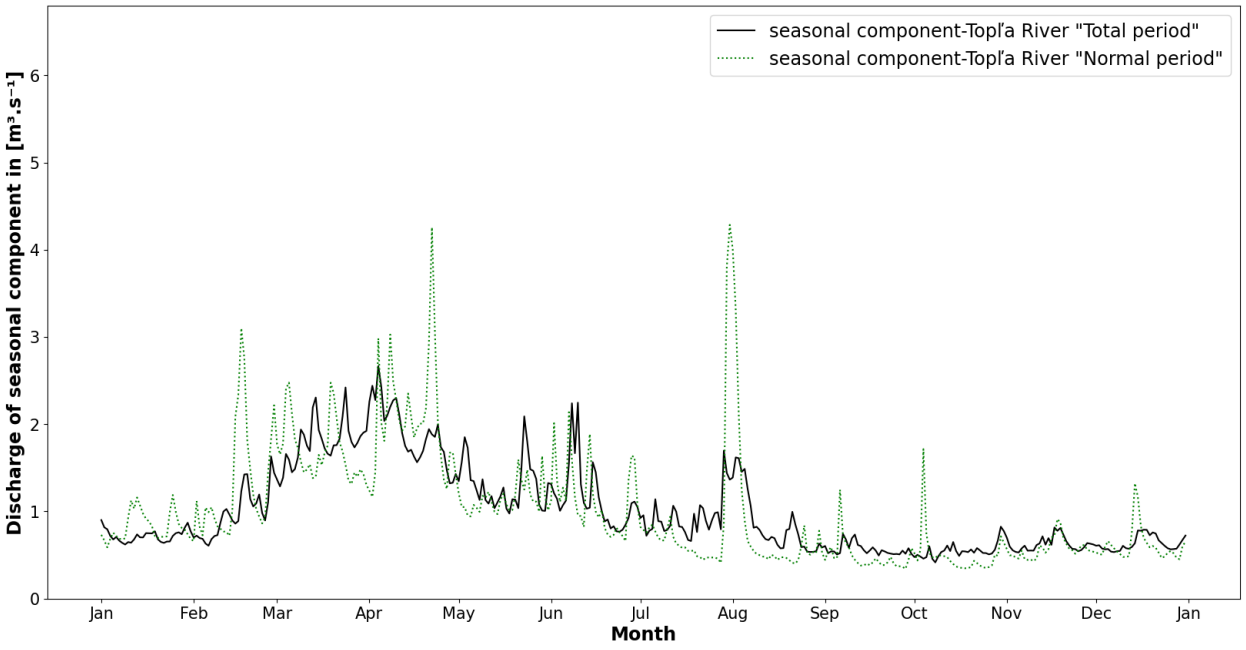

Fig. 4. Comparison of seasonal discharge patterns in normal years and over the whole study period.

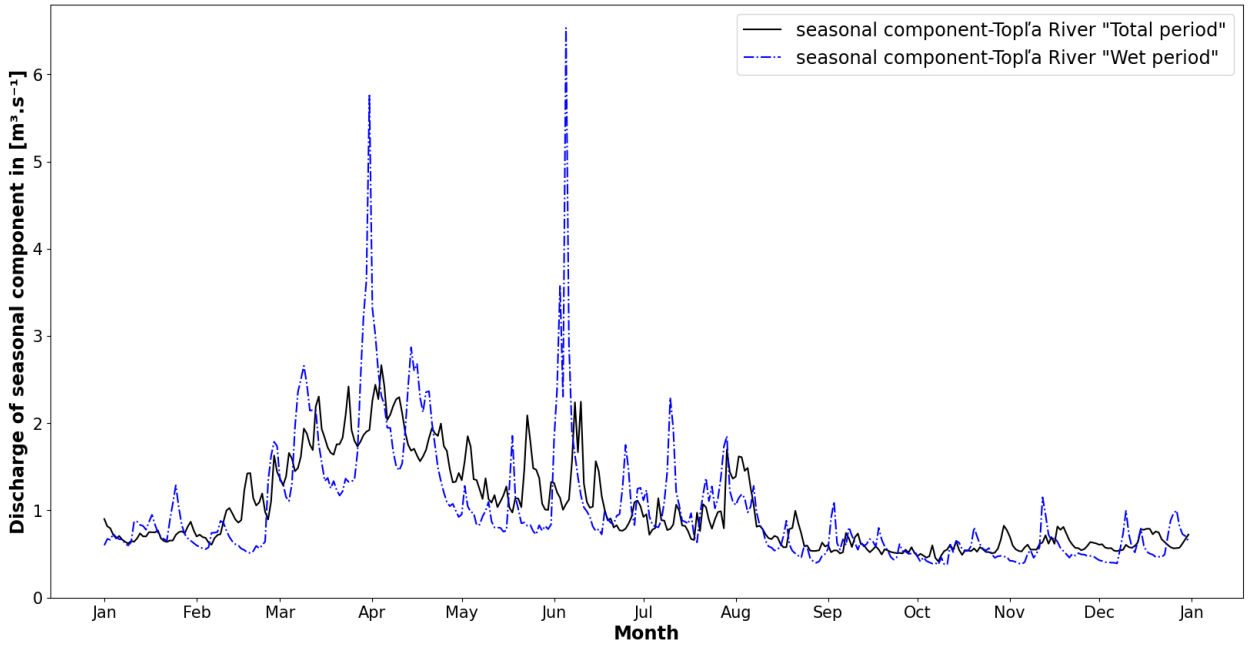

Fig. 5. Comparison of seasonal discharge patterns in wet years and over the whole study period.

Conclusion and discussion

In conclusion, the analysis reveals that the Topľa River's seasonality is undergoing a gradual shift towards dry seasonality, and the results suggest that perhaps changes in the magnitude of precipitation, snowmelt, and summer storms are the key factors behind the changes in seasonal discharge patterns, but these data were not available to assess. The drought analysis supports these findings, with more than half of the study period classified as dry. This shift towards dry seasonality raises concerns about the potential impacts of climate change and global warming on hydrological systems, as rising temperatures can affect snow accumulation and snowmelt, causes heavy storms or flash floods, leading to changes in the distribution of discharge throughout the year. Therefore, further research and monitoring of the hydrological dynamics of the Topľa River and other river systems are essential to better understand the effects of climate change on water resources and to develop effective management strategies to mitigate and adapt to these changes.

It is worth noting that the data set used in this study is imbalanced due to the unequal number of dry, wet, and normal years. While this may limit the conclusions drawn from analyzing the wet and normal groups, the results of the dry group analysis are more reliable due to its homogenous data set and good size. Therefore, the findings related to the dry hydrological status should be given more weight and considered in decision-making processes related to water resource management in the study area. However, future studies should aim to increase the number of wet and normal years to provide a more balanced data set for analysis by adding simulated data.

Very important is to have appropriate data from a long time period, except discharges, it means other hydrological data such as temperatures, precipitations, evaporation, evapotranspiration, snow cover correlated to geology, to terrain slopes, basin agricultural utilization, land cover, water management measures (reservoirs) etc. But these are often not available, or only short time of observation is accessible. This is mostly problem, data insufficiency of small basins, but their influence on the hydrological assessment in larger scale is not negligible. Therefore, in term of these statements, understanding of changed hydrological cycle in climate change conditions is important for the planning of water management strategies.

Such management strategies may include improving water storage and management practices, promoting water-efficient technologies, and reducing greenhouse gas emissions to limit the effects of climate change on hydrological systems. The shift towards the dry seasonality of the Topľa River also highlights the significance of studying other environmental indicators such as groundwater level, precipitation, temperature, and other relevant factors to achieve a comprehensive understanding of the hydrological dynamics of the river. The implications of the shift towards dry seasonality for the ecology of the river and the surrounding environment, as well as for human activities such as agriculture and hydropower generation, are substantial and require immediate attention. Therefore, it is necessary to develop effective policies and management strategies to ensure the sustainable use and management of the river systems in the face of changing climate and hydrological conditions.

Acknowledgement

This contribution was developed within the framework and based on the financial support of the APVV-19-0383 project, "Natural and technical measures oriented to water retention in sub-mountain watersheds of Slovakia", together with APVV-20-0023 project, "Research on hydraulic characteristics of fish passes with regard to ichthyological requirements" and Vega project No.1/0728/21 "Analysis and prognosis of impact of construction activities on ground water in urbanized territory".

References

Almikaeel, W., Čubanová, L., Šoltész, A. (2022): Comparison of mean daily discharge data for under-mountain and highland-lowland types of rivers. Acta Hydrologica Slovaca, vol. 23, no. 1, 73–81.

Dokumentov, A., Hyndman, R. J. (2015): STR: A seasonal-trend decomposition procedure based on regression. Department of Econometrics and Business Statistics, Monash University, Australia, 32 p.

Duchan, D., Julínek, T., Říha, J. (2022): Multicriterial analysis used for the optimisation of dike system management. Journal of flood risk management, vol. 15, issue 4.

Fendeková, M., Gauster, T., Labudová, L., Vrablíková, D., Danáčová, Z., Fendek, M., Pekárová, P. (2018a): Analysing 21st century meteorological and hydrological drought events in Slovakia. Journal of Hydrology and Hydromechanics, 66, 393–403.

Fendeková, M., Horvát, O., Blaškovičová, L., Danáčová, Z., Fendek, M., Bochníček, O. (2018b): Prognosis of climate change driven drought in the Poprad, Torysa and Topľa river basins. Acta Hydrologica Slovaca, vol. 19, no. 2, 234–243.

Frandofer, M., Lehotský, M. (2014): Morfologicko-sedimentová diferenciácia horského vodného toku a jeho odozva na povodňové udalosti. Geomorphologia Slovaca et Bohemica, vol 14, issue 1, 86 p.

Garaj, M., Pekarova, P., Pekar, J., Miklanek, P. (2019): The changes of water balance in the eastern Slovakia. IOP Conference Series: Earth and Environmental Science, vol. 362, WMESS 2019.

Gu, L., Yin, J., Slater, L. J., Chen, J., Do, H. X., Wang, H., Chen, L., Jiang, Z., Zhao, T. (2022): Intensification of Global Hydrological Droughts Under Anthropogenic Climate Warming. Water Resources Research, vol. 59, issue 1.

GWP (Global Water Partnership (Central and Western Europe)) Slovakia. (2013): Guidelines for Drought Management Plan Milestone 2: Slovak case study report. Retrieved April 15, 2023, from http://www.shmu.sk/File/Hydrologia/Projekty_hydrologia/projekt11_Slovak_case_study_report_IDMP.pdf

Khan, S., Ahmad, A., Malano, H. M. (2009): Managing irrigation demand to improve seasonality of river flows. Irrigation and Drainage, vol. 58, issue 2, 157–170.

Laizé, C. L., Meredith, C. B., Dunbar, M. J., Hannah, D. M. (2016): Climate and basin drivers of seasonal river water temperature dynamics. Hydrology and Earth System Sciences, vol. 21, issue 6, 3231–3247.

Liu, Z., Zhu, Z., Gao, J., Xu, C. (2021): Forecast Methods for Time Series Data: A Survey. IEEE Access, vol. 9, 91896–91912.

Özerol, G., Stein, U., Troeltzsch, J., Landgrebe, R., Szendrenyi, A., Vidaurre, R. (2016): European Drought and Water Scarcity Policies. In H. Bressers, N. Bressers, & C. Larrue (Eds.), Governance for Drought Resilience: Land and Water Drought Management in Europe, Springer, 17–43.

Plaveniny – Hodnotenie plaveninového režimu na slovenských tokoch, 2020. SHMÚ, Bratislava, 2021, 92 p. Retrieved April 15, 2023, from https://www.shmu.sk/File/Hydrologia/Monitoring_PV_PzV/Monitoring_kvantity_PV/PVkvant2020/Hodnotenie_plaveninoveho_rezimu_2020.pdf

Predbežné hodnotenie povodňového rizika v čiastkovom povodí Bodrogu – aktualizácia 2018. MŽP SR, 2018, 200 p. Retrieved April 15, 2023, from https://minzp.sk/files/sekcia-vod/hodnotenie-rizika-2018/bodrog/phpr-bodrog.pdf

Rao, P., Patil, Y. (2016): Reconsidering the Impact of Climate Change on Global Water Supply, Use, and Management. IGI Global, USA.

Romano, N., Allocca, C., Deidda, R., Nasta, P. (2020): Assessing the impact of rainfall seasonality anomalies on catchment-scale water resources availability. Hydrology and Earth System Sciences, vol. 24, issue 6, 3211–3227.

Serrano, L. D., Ribeiro, R. B., Borges, A. C., Pruski, F. F. (2020): Low-Flow Seasonality and Effects on Water Availability throughout the River Network. Water Resources Management, 34, 1289–1304.

Sivapalan, M., Blöschl, G., Merz, R., Gutknecht, D. (2005): Linking flood frequency to long-term water balance: Incorporating effects of seasonality. Water Resources Research, vol. 41, issue 6.

Spinoni, J., Vogt, J. V., Naumann, G., Barbosa, P. M., Dosio, A. (2018): Will drought events become more frequent and severe in Europe? International Journal of Climatology, 38 (4), 1718-1736.

Sýs V., Fošumpaur P., Kašpar T. (2021): The Impact of Climate Change on the Reliability of Water Resources. Climate, 9 (11): 153.

Theodosiou, M. (2011): Forecasting monthly and quarterly time series using STL decomposition. International Journal of Forecasting, vol. 27, issue 4, 1178–1195.

Tomaszewski, E. (2014): Seasonality level of hydrological drought in rivers and its variability. Conference proceedings: 2nd International Conference – Water resources and wetlands. 11–13 September, 2014 Tulcea (Romania), 278–284.

Van Loon, A. F., Tijdeman, E., Wanders, N., Van Lanen, H., Teuling, A.J., Uijlenhoet, R. (2014): How climate seasonality modifies drought duration and deficit. Journal of Geophysical Research: Atmospheres, vol. 119, issue 8, 4640–4656.

Varga, A., Velísková, Y. (2021): Assessment of time course of water and air temperature in the locality of the Turček reservoir during its operation in the period 2005–2019. Acta Hydrologica Slovaca, vol. 22, no. 2, 304–312.

Velísková, Y., Dulovičová, R., Schügerl, R. (2017): Impact of vegetation on flow in a lowland stream during the growing season. Biologia, vol. 72, no. 8, 840–846.

Vicente-Serrano, S. M., López-Moreno, J. I., Beguería, S., Lorenzo-Lacruz, J., Sanchez-Lorenzo, A., García-Ruiz, J. M., Azorín-Molina, C., Morán-Tejeda, E., Revuelto, J., Trigo, R. M., Coelho, F., Espejo, F. (2014): Evidence of increasing drought severity caused by temperature rise in southern Europe. Environmental Research Letters, 9, 044001.

Vodohospodárska bilancia SR – Vodohospodárska bilancia množstva povrchových vôd za rok 2013. SHMÚ, Bratislava, 2014, 114 p. Retrieved April 15, 2023, from https://www.shmu.sk/File/Hydrologia/Vodohospodarska_bilancia/VHB_kvantita_PV/VHB_KnPV_2013_text.pdf

Wang, S. (2019): Freezing Temperature Controls Winter Water Discharge for Cold Region Watershed. Water Resources Research, Vol. 55, Issue 12, 10479–10493.

World Meteorological Organization (WMO). (2008). Manual on low-flow estimation and prediction | e-library. Retrieved April 15, 2023, from https://library.wmo.int/index.php?lvl=notice_display&id=7978

Zeleňáková, M., Soľáková, T., Purcz, P., Simonová, D. (2018): Hydrological Drought Occurrence in Slovakia. In: Negm, A., Zeleňáková, M. (eds) Water Resources in Slovakia: Part II. The Handbook of Environmental Chemistry, vol 70. Springer, Cham.

Zhu, N., Xu, J., Li, W., Li, K., & Zhou, C. (2018): A Comprehensive Approach to Assess the Hydrological Drought of Inland River Basin in Northwest China. Atmosphere, volume 9(10), 370 p. MDPI AG. Retrieved from http://dx.doi.org/10.3390/atmos9100370

Ing. Wael Almikaeel (*corresponding author, e-mail: wael.almikaeel@stuba.sk)
Luara Cunha de Almeida
Ing. Lea Čubanová, PhD.
Prof. Ing. Andrej Šoltész, PhD.
Ing. Jakub Mydla
Assoc. Prof. Ing. Dana Baroková, PhD.
Department of Hydraulic Engineering
Faculty of Civil Engineering
Slovak University of Technology in Bratislava
Radlinského 2766/11
810 05 Bratislava
Slovak Republic

DOI: 10.31577/ahs-2023-0024.01.0009

ACTA HYDROLOGICA SLOVACA

Volume 24, No. 1, 2023, 73 – 81

On future changes in the long-term seasonal discharges in selected basins of Slovakia

Zuzana SABOVÁ*, Silvia KOHNOVÁ

Climate change and its impact on hydrological characteristics is a research topic of increasing interest. Studies that examine historical, current or future changes in hydrological regimes are important for understanding future changes in the water balance and its components. This study analyses changes in long-term discharges in the summer and winter half-year and the baseflow index for eight selected river basins in Slovakia till 2100. For the analysis, data observed from the period 1981–2010 were used to calibrate the HBV-type rainfall-runoff TUW model. To simulate future discharges up to the 2100 horizon, two climate scenarios were used, i.e., the Dutch KNMI and the German MPI. The analysis was performed for four selected periods with a duration of 30 years. The results point to the most significant changes in the increase in long-term seasonal discharges in the winter half-year by 2100. In the future, the summer period will probably be characterised by a reduction in long-term seasonal discharges and decrease in the base flow index in all of the basins analysed.

KEY WORDS: seasonal discharges, baseflow index, the KNMI and MPI climate scenarios, the HBV model, the TUW model

Introduction

The impact of climate change on river runoff is increasingly being investigated due to changes in various factors, including the air temperature, amount of precipitation, evaporation, and evapotranspiration. These changes have resulted in an increased occurrence of extreme events, i.e., floods, droughts, heat, heavy rain, and intense cyclones. More extreme events associated with global warming could have an intense impact on changes in the hydrological cycle, thereby leading to socio-economic consequences (Vyshnevskyi and Donich, 2021; He et al., 2022; Meresa et al., 2022).

Global and regional models are essential when explaining the annual, seasonal, and daily characteristics of precipitation and air temperatures. Forecasts for climate models differ due to different parametrisation methods and the underlying network structure. This fact makes it challenging to develop accurate and reliable climate data. The differences in the results should be corrected by the so-called 'calibration' before their further use in projections of hydrological extremes in hydrology. Most hydrological models consist of physical mechanisms or empirical equations that describe basins. Rainfall-runoff models often comprise a series of equations that describe simplified hydrological processes from small to large basins (Meresa et al., 2022). Hydrological models are widely used to analyse and determine changes in hydrological environments, including modifications and improvements in different areas. Many models with various structures are applied to basins with different climatic or geographical conditions. The most significant advantage of hydrological models is that they are used to predict hydrological dynamics by combining them with climate scenarios (Yang et al., 2022). Rainfall modelling is often used in water management simulation analyses to predict the future course of floods, droughts, and climate change. It must be taken into account that, in the period simulated, the climate conditions can differ from the calibration conditions when uncertainties arise that may affect the accuracy of outputs (Sleziak et al., 2017).

Meresa and Romanowicz (2017) addressed uncertainties in projecting hydrological regimes. They pointed to increased uncertainty in hydrological models that result in further uncertainty in climate models, leading to increased risks for the adaptation, planning, and management of water resources for future extreme hydrological events. Yang et al. (2022) studied the effect of calibration conditions on the accuracy of conceptual hydrological models under different climatic conditions. Huntington (2003) studied the relationship between the average annual temperature, precipitation, and evapotranspiration in the New England region of the USA. He found that annual runoff decreased by 11–13% for the historical periods in the selected basins until 2003. Various analyses have been performed for the territory of Slovakia that were devoted to hydrological changes (Ďurigová et al., 2020), changes in water balance and soil moisture (Rončák et al., 2021), and an evaluation of

average monthly discharges (Pekárová et al., 2007; Ďurigová et al., 2019; Majerčáková et al., 2007). The impact of climate change on the Hron, Váh, and Laborec River basins using the KNMI, MPI and ALADIN-Climate climate data in the period 1961–2100 was addressed by Štefunková et al. (2013). The team focused on the impact of climate change on the territory of Slovakia using an HBV-type rainfall-runoff TUW model by Sleziak et al. (2016; 2018), who pointed out changes in simulated runoff that are related to changes in precipitation, but stressed the need to recalibrate conceptual HBV models if climate conditions change.

This study deals with an analysis of future changes in long-term seasonal discharges; it is divided into two groups, i.e., the summer half-year (April–September) and the winter half-year (October–March). Data from the KNMI and MPI climate scenarios are input in the HBV-type rainfall-runoff TUW model to predict future discharge changes up to 2100. The 30-year future periods were compared with a historical one, which forms the reference period from 1981 to 2010. An analysis of changes in the baseflow index's average annual values within the periods examined until 2100 was also carried out.

Material and methods

For the study, eight basins in the territory of Slovakia were selected; they differ in their area, altitude, and location (Table 1 and Fig. 1). The river basins have an area from 238.5 to 2093.7 km^2, with a mean elevation from 361.7 to 1090.1 m a.s.l., a minimum elevation from 163 to 568 m a.s.l, and a maximum elevation from 792 to 2489 m a.s.l

The data observed from the gauging stations provided by the Slovak Hydrometeorological Institute were used to create the modelled data using the HBV-type rainfall-runoff TUW model. The model´s calibration parameters simulated the daily discharges up to 2100 and the modelled data (MODEL HBV) were created (Table 2).

The HBV-type TUW model is a conceptual semi-distributed rainfall-runoff model, which was used for modelling changes in the daily discharges (Fig. 2). The basic structure of the HBV consists of three modules, i.e., snow, soil, and runoff. The HBV model has 15 parameters for the calibration. The model needs daily discharges, precipitation, the air temperature, and evapotranspiration as the input data for the calibration.

Table 1. Characteristics of the selected gauging stations

River basin / Gauging station	ID	Basin area [km^2]	Mean basin elevation [m a.s.l.]	Min. – Max. elevation [m a.s.l.]
Myjava / Jablonica	5022	238.45	361.7	206 – 792
Nitra / Nitrianska Streda	6730	2093.71	419.5	175 – 1179
Hron / Banská Bystrica	7160	1766.48	844.4	332 – 2030
Turiec / Martin	6130	827.00	716.0	403 – 1456
Poprad / Chmeľnica	8320	1262.41	878.1	510 – 2489
Váh / Liptovský Mikuláš	5550	1107.21	1090.1	568 – 2387
Laborec / Humenné	9230	1272.40	421.7	166 – 917
Topľa / Hanušovce nad Topľou	9500	1050.05	435.4	163 – 1077

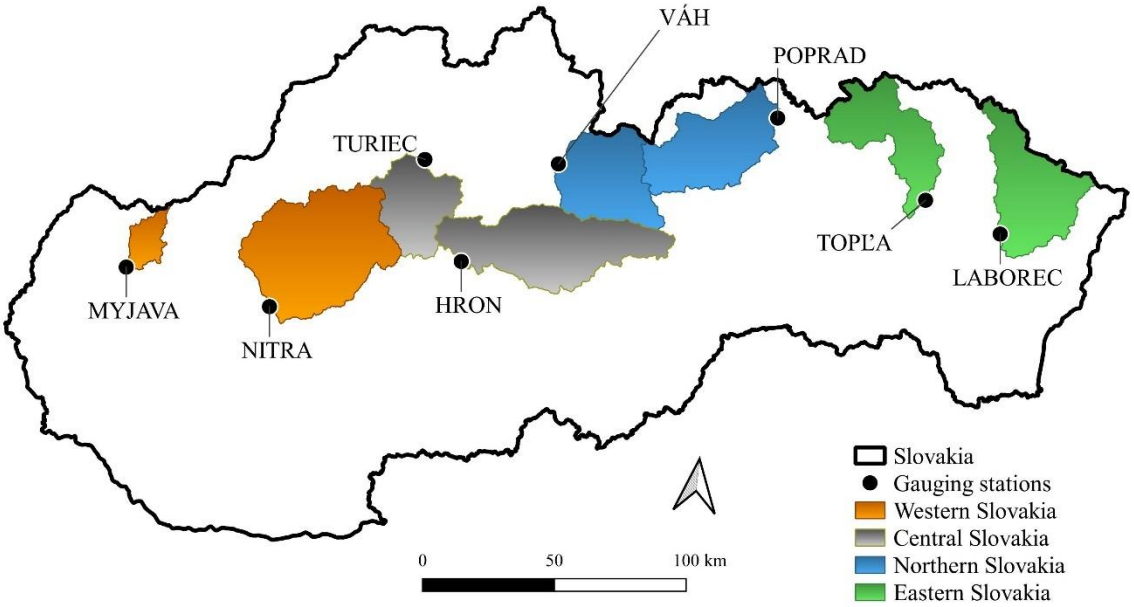

Fig. 1. Location of selected basins within the territory of Slovakia.

Table 2. Distribution of the time period examined concerning the use of data

Time period analysed	Group of data
1981–2010	Observed mean daily discharges
	Modelled mean daily discharges using the HBV-type rainfall-runoff TUW model
	Simulated mean daily discharges according to the KNMI climate scenario´s data
	Simulated mean daily discharges according to the MPI climate scenario´s data
2011–2040	Simulated mean daily discharges according to the KNMI climate scenario´s data Simulated mean daily discharges according to the MPI climate scenario´s data
2041–2070	
2071–2100	

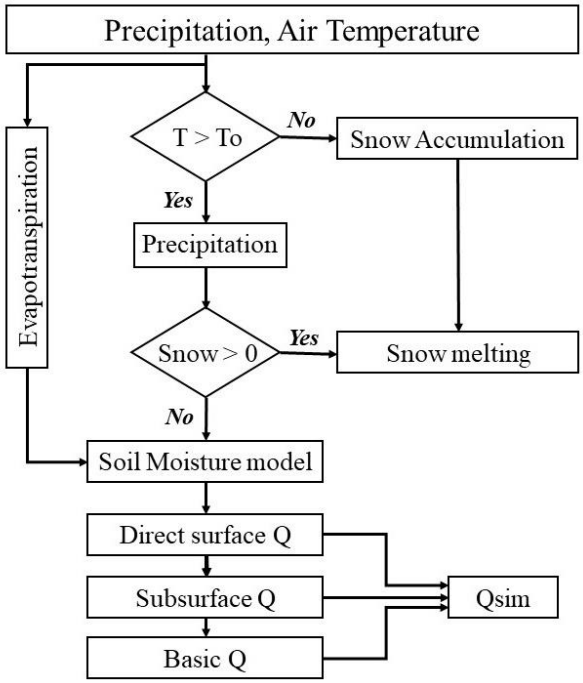

Fig. 2. Basic scheme of the HBV-type rainfall-runoff TUW model (T – air temperature, To – air temperature of melting snow, Q – runoff, Qsim – simulated discharge).

More details about the model can be found in, e.g., Výleta et al., 2020; Sleziak, 2017.

Daily precipitation and temperature data from two climate scenarios, i.e., the Dutch KNMI and the German MPI, were used to model discharges for the future periods. Both climate scenarios belong to regional circulation models that were scaled for the territory of Slovakia in a daily step with a resolution of 25x25 km. They have 190 grid points with detailed topography in and around Slovakia. Their outputs were processed for the period 1951–2100.

The period of 1981 to 2100 investigated in our study was divided into four 30-years periods to determine in which period the most significant changes in long-term seasonal discharges could be expected. The following periods were compared: 1981–2010, 2011–2040, 2041–2070, and 2071–2100. For a better representation of the changes in the discharges, the relative deviation in percentages was calculated according to the formula:

$$RO = \frac{CS - MODEL\ HBV}{MODEL\ HBV} * 100 \quad [\%] \qquad (1)$$

where:

RO – relative deviations [%];

CS – long-term seasonal discharges simulated using the KNMI/MPI climate scenarios in all the periods selected;

MODEL HBV – long-term seasonal discharges simulated using the HBV model in the period 1981–2010.

In this study, changes in the base flow index for the hydrological characteristics are analysed. This was estimated as the ratio of the 7-day minimum discharge to the average annual discharge using the Indicators of Hydrologic Alteration program. The resulting values of the base flow index were also calculated according to Equation (1) to represent the results of the work.

Results and discussion

The study compared changes up to 2100 in the long-term seasonal discharges in the summer and winter half-years and the average annual baseflow index within the simulated discharges according to the KNMI and MPI climate scenarios. The results were processed using graphic representations and in tabular form.

a) Long-term seasonal discharges in the summer and winter half-years

In the graphic processing of the seasonal discharges for the selected river basins in Slovakia, it can be seen that in the summer half-year, a decrease in long-term seasonal discharges, and in the winter half-year, an increase in long-term seasonal discharges, up to 2100 is expected (Figs. 3 and 4). The increase in discharges in the winter months may be caused due to the continuation of more intense snowmelt, e.g., in the Hron River basin in an earlier period (February–March). For the Váh and Poprad River basins, the results indicate higher values of seasonal discharges in the summer than in the winter until 2100, despite the fact that the values of the seasonal discharges in the basins will decrease in the future. The reason could be the maintenance of snow cover, increased precipitation, or snow melting in the higher areas of the basins in April and May.

For a better representation of the future changes predicted using data from the KNMI and MPI climate scenarios, Tables 3a (KNMI) and 3b (MPI) were created; they consist of the resulting values of the long-term seasonal discharges in the summer half-year for the discharges modelled by the HBV-type rainfall-runoff TUW model (MODEL HBV) and for the simulated discharges using the climate scenarios by 2100. The tables also contain the percentage changes in the simulated discharges from the discharges modelled. Blue indicates the most significant decreases, and red indicates the highest increase in long-term seasonal discharges in the summer half-year. According to the simulated discharges using the MPI climate scenario for western Slovakia, an increase in long-term seasonal discharges in the summer half-year by 23% (the Myjava River basin) and 30% (the Nitra River basin) until 2070 is expected. We can assume that this will be caused by increases in

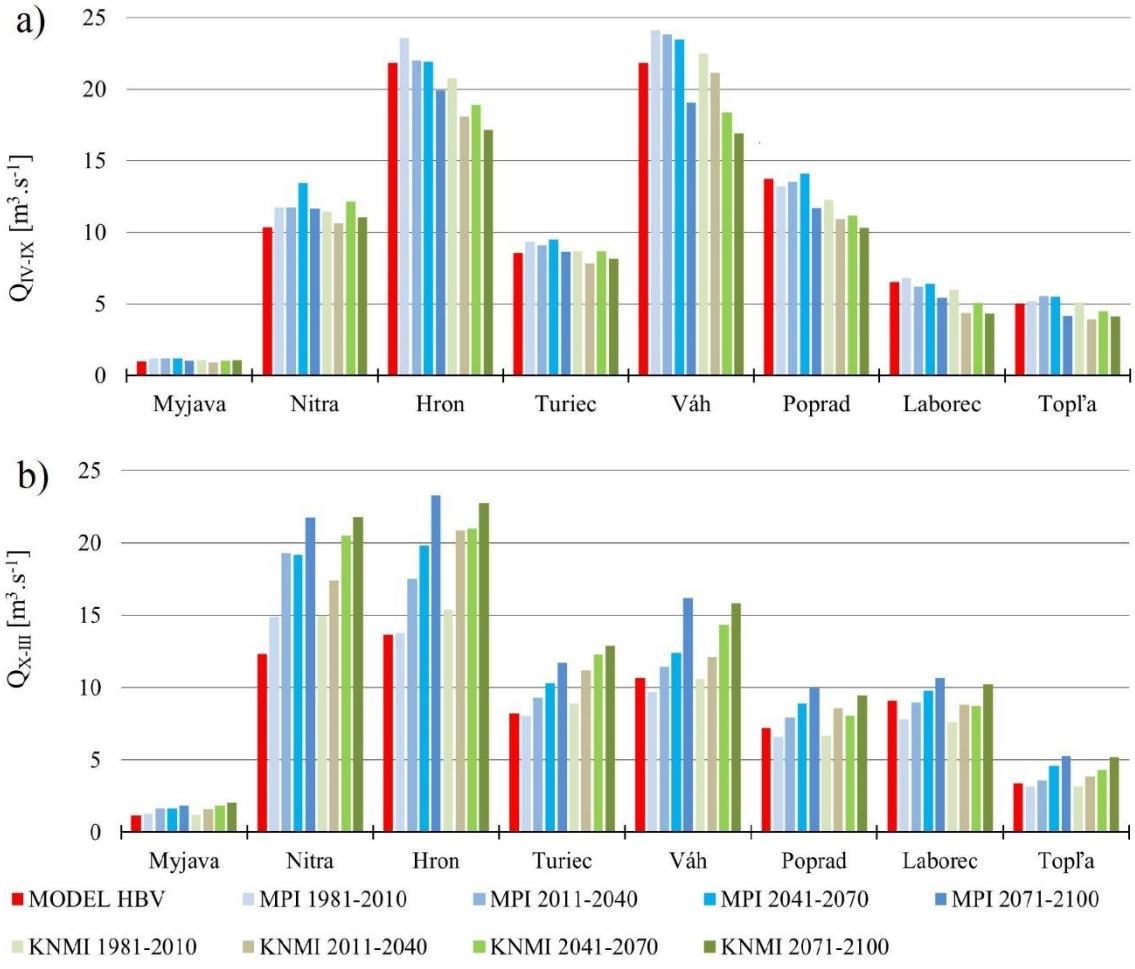

Fig. 3. Comparison of temporal changes in the long-term seasonal discharges for the discharges modelled by the HBV-type rainfall-runoff TUW model (MODEL HBV) and simulated discharges according to the KNMI and MPI climate scenarios for the selected periods analysed: a) in the summer half-year; b) in the winter half-year.

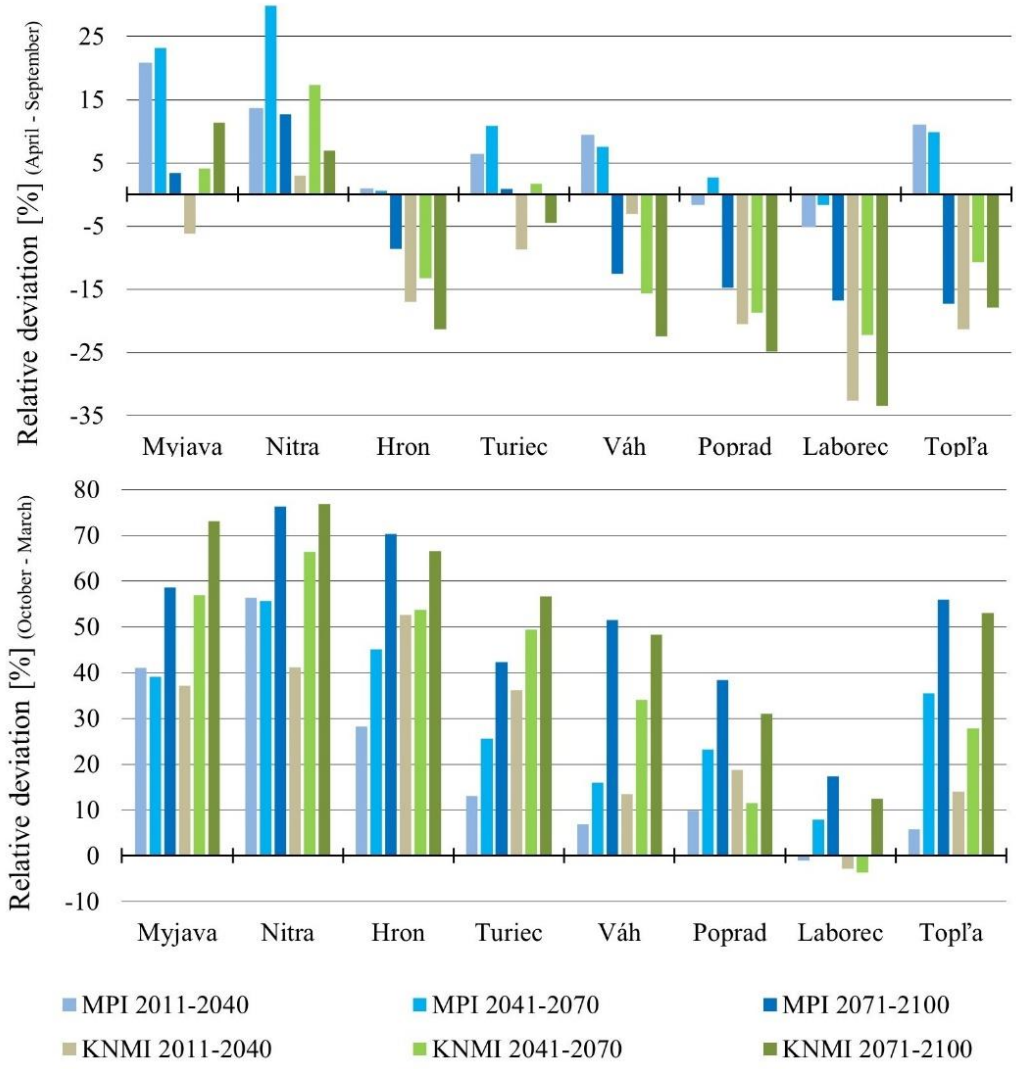

Fig. 4. Graphic representation of the relative deviations of the simulated long-term seasonal discharges of the KNMI and MPI climate scenarios from the modelled long-term seasonal discharges of the HBV-type rainfall-runoff TUW model for the summer half-year.

Table 3a. Resulting values of the long-term seasonal discharges by 2100 in the summer half-year [$m^3 s^{-1}$] and their relative deviations [%] of the simulated discharges according to the KNMI climate scenario

River basin	MODEL HBV	KNMI					
	1981–2010	2011–2040		2041–2070		2071–2100	
	[$m^3 s^{-1}$]	[$m^3 s^{-1}$]	[%]	[$m^3 s^{-1}$]	[%]	[$m^3 s^{-1}$]	[%]
Myjava	0.98	0.92	**-6.18**	1.02	4.15	1.09	**11.34**
Nitra	10.34	10.65	3.00	12.13	**17.31**	11.05	6.89
Hron	21.82	18.10	-17.03	18.92	-13.30	17.15	**-21.37**
Turiec	8.56	7.81	**-8.69**	8.70	**1.71**	8.17	-4.50
Váh	21.82	21.16	-3.02	18.39	-15.70	16.92	**-22.45**
Poprad	13.72	10.90	-20.53	11.16	-18.70	10.31	**-24.84**
Laborec	6.51	4.39	-32.64	5.06	-22.24	4.34	**-33.42**
Topľa	5.01	3.94	**-21.35**	4.48	-10.69	4.12	-17.86

Table 3b. Resulting values of the long-term seasonal discharges by 2100 in the summer half-year [$m^3 s^{-1}$] and their relative deviations [%] of the simulated discharges according to the MPI climate scenario

River basin	MODEL HBV	MPI					
	1981–2010	2011–2040		2041–2070		2071–2100	
	[$m^3 s^{-1}$]	[$m^3 s^{-1}$]	[%]	[$m^3 s^{-1}$]	[%]	[$m^3 s^{-1}$]	[%]
Myjava	0.98	1.18	20.67	1.20	**23.15**	1.01	3.43
Nitra	10.34	11.75	13.59	13.43	**29.89**	11.66	12.71
Hron	21.82	21.99	0.79	21.94	0.54	19.94	**-8.61**
Turiec	8.56	9.09	6.26	9.48	**10.86**	8.63	0.84
Váh	21.82	23.85	9.31	23.47	7.55	19.08	**-12.57**
Poprad	13.72	13.52	-1.49	14.09	**2.65**	11.70	**-14.72**
Laborec	6.51	6.18	-5.04	6.40	-1.67	5.42	**-16.80**
Topľa	5.01	5.56	**10.93**	5.50	9.84	4.15	**-17.25**

convective and long-term cyclonic events in the summer season.

According to the KNMI climate scenario, simulated discharges for the territory of central Slovakia mainly indicate a decrease in the value of long-term seasonal discharges in the summer half-year until the year 2100 (by 21% in the Hron River basin), with the exception being the period from 2041 to 2070 in the Turiec River basin, when the resulting values of the hydrological characteristics are expected to grow. According to the simulated discharges of the MPI climate scenario, an increase in the long-term seasonal discharges of the summer half-year in central Slovakia is expected to reach 11% in the Turiec River basin.

Northern Slovakia is characterised by high altitudes since the High Tatra mountains are in the territory. Changeable weather in the summer half-year there can also affect the size of the discharges in the respective basins. According to the study presented, a decrease in long-term seasonal discharges in the Poprad and Váh River basins in the summer half-year is expected to occur by approximately 23–25% until 2100 according to the simulated discharges of the KNMI climate scenario. Also, according to the data from the MPI climate scenario, a decrease of approximately 13–14%, compared to the modelled data from the HBV-type rainfall-runoff TUW model, can be observed.

The most significant decreases are recorded in the Laborec and Topľa River basins, which are located in eastern Slovakia. More precisely, this is the highest decrease in long-term seasonal discharges in the summer half-year, according to the simulated discharges of the KNMI climate scenario (a decrease of 21–33%). Simulated discharges of the MPI climate scenario predict a decrease in long-term seasonal discharges by up to 17% in the summer half-year by 2100.

The long-term seasonal discharges for the winter half-year indicate changes utterly different from those in the summer half-year in the future. These are mainly significant increases in the long-term seasonal discharges of the winter half-year according to the simulated discharges of the KNMI and MPI climate scenarios (Tables 4a and 4b). The exception is the Laborec River basin in 2011–2040, where only a slight decrease in long-term seasonal discharge values is expected from October to March, according to both climate scenarios.

For the river basins of western Slovakia, the highest increase in long-term seasonal discharges in the winter half-year is by 73–77% according to the simulated discharges of the KNMI climate scenario and by 59–77% according to the simulated discharges of the MPI climate scenario. Part of central Slovakia is characterised by approximately the same values of the changes in the long-term seasonal discharges of the winter half-year as in western Slovakia by 2100. In the basins of northern Slovakia, the expected change in long-term seasonal discharges in the winter half-year until 2100 is an increase in the values of the long-term seasonal discharges of the winter half-year by 31–48% for the simulated discharges of the KNMI climate scenario and by 38–52% for the simulated discharges according to the MPI climate scenario. For eastern Slovakia, the predictions for the selected basins differ. Simulated discharges of the KNMI and MPI climate scenarios also indicate a decrease in long-term seasonal discharges in the winter half-year by 1–4% by 2040–2070; the results indicate they will increase again by 2100. Minor changes in the long-term seasonal discharges from the winter half-year are expected in the Laborec River basin.

The results of the summer and winter periods examined differ significantly, and the most notable changes can be expected in the winter half-year. The long-term seasonal discharges can be affected by several extremes throughout the year. Snowmelt floods occur regularly in the spring. In the summer, there are strong storms or prolonged droughts. In recent years, there have also been periods without any precipitation in the winter. In Sabová and Kohnová (2022), the authors analysed average monthly discharges in the territory of Slovakia. Their results showed that in eastern Slovakia, the highest

decrease in average monthly discharges is expected in the summer. On the other hand, the most significant increases in the winter in average monthly discharges are expected for the Nitra, Hron and Topľa River basins.
For the Hron and Váh River basins, decreasing trends in the average monthly discharges in the summer have already been identified in the historical period of 1963–2016 (Ďurigová et al., 2019). Majerčáková et al. (2007) detected the development of maximum discharges in the Poprad River basin for the territory of northern Slovakia. The result of the work confirmed the sensitivity of the basin with regard to the changes in climate.

b) Average annual baseflow index

The baseflow index is a hydrological characteristic that represents the continuous contribution of groundwater to river discharges. From the point of view of future changes, gradual decreases in the values of the base flow index for the selected river basins until 2100 in Slovakia are evident (Table 5). The most extreme changes in base flow decreases are expected in the Myjava, Nitra, and Laborec River basins (a decrease of 43%). The exceptions are the basins of northern Slovakia, that is, the Poprad and Váh River basins, which indicate positive changes in the values in the baseflow indices. For example, according to the simulated discharges from the MPI climate scenario data, an increase in the baseflow index is expected by 38% in the Poprad River basin from 2041 to 2070 (Fig. 5). The simulated discharges of the KNMI climate scenario in most cases assume higher values of the changes in the hydrological characteristics of the baseflow index, in comparison to the MPI climate scenario. The consequences of a decrease in the base flow index in almost all the basins except for the mountainous ones indicate that the basins will be more prone to drying out in the summer and autumn months.

Table 4a. Resulting values of the long-term seasonal discharges by 2100 in the winter half-year [$m^3 s^{-1}$] and their relative deviations [%] of the simulated discharges according to the KNMI climate scenario

River basin	MODEL HBV	KNMI					
	1981–2010	2011–2040		2041–2070		2071–2100	
	[$m^3 s^{-1}$]	[$m^3 s^{-1}$]	[%]	[$m^3 s^{-1}$]	[%]	[$m^3 s^{-1}$]	[%]
Myjava	1.17	1.61	37.10	1.84	56.94	2.03	**73.09**
Nitra	12.32	17.40	41.19	20.51	66.42	21.80	**76.89**
Hron	13.66	20.84	52.57	20.99	53.67	22.75	**66.53**
Turiec	8.22	11.20	36.23	12.28	49.40	12.87	**56.61**
Váh	10.69	12.13	13.48	14.34	34.15	15.85	**48.24**
Poprad	7.21	8.57	18.83	8.04	11.49	9.45	**31.04**
Laborec	9.09	8.82	-2.88	8.75	**-3.72**	10.22	**12.47**
Topľa	3.38	3.86	13.97	4.32	27.76	5.18	**53.06**

Table 4b. Resulting values of long-term seasonal discharges by 2100 in the winter half-year [$m^3 s^{-1}$] and their relative deviations [%] of simulated discharges according to the MPI climate scenario

River basin	MODEL HBV	KNMI					
	1981–2010	2011–2040		2041–2070		2071–2100	
	[$m^3 s^{-1}$]	[$m^3 s^{-1}$]	[%]	[$m^3 s^{-1}$]	[%]	[$m^3 s^{-1}$]	[%]
Myjava	1.17	1.66	41.12	1.63	39.06	1.86	**58.54**
Nitra	12.32	19.27	56.39	19.18	55.66	21.73	**76.35**
Hron	13.66	17.51	28.18	19.82	45.07	23.26	**70.26**
Turiec	8.22	9.30	13.11	10.32	25.52	11.70	**42.34**
Váh	10.69	11.43	6.98	12.40	15.98	16.19	**51.50**
Poprad	7.21	7.92	9.84	8.89	23.18	9.98	**38.38**
Laborec	9.09	9.00	**-0.99**	9.80	7.88	10.66	**17.35**
Topľa	3.38	3.58	5.81	4.58	35.47	5.27	**55.90**

Table 5. **The course of changes in the baseflow indices [–] and their relative deviations [%] for the selected river basins in Slovakia according to the simulated discharges of the KNMI and MPI climate scenarios by 2100**

River basin	MODEL HBV	KNMI						MPI					
	1981–2010	2011–2040		2041–2070		2071–2100		2011–2040		2041–2070		2071–2100	
	[–]	[–]	[%]	[–]	[%]	[–]	[%]	[–]	[%]	[–]	[%]	[–]	[%]
Myjava	0.17	0.14	-18	0.11	-34	0.10	**-42**	0.13	-24	0.13	-19	0.10	**-42**
Nitra	0.30	0.23	-23	0.21	-31	0.18	**-40**	0.24	-22	0.23	-22	0.21	**-30**
Hron	0.33	0.32	-4	0.30	-8	0.28	**-15**	0.32	-3	0.32	-2	0.29	**-11**
Turiec	0.38	0.34	-9	0.32	-15	0.28	**-27**	0.35	-6	0.37	-2	0.29	**-23**
Poprad	0.24	0.25	4	0.29	**24**	0.28	21	0.24	3	0.33	**38**	0.30	27
Váh	0.42	0.46	8	0.48	13	0.48	**14**	0.38	**-10**	0.45	8	0.47	**12**
Laborec	0.20	0.16	-20	0.14	-31	0.11	**-43**	0.17	-15	0.17	-16	0.12	**-38**
Topľa	0.30	0.26	-11	0.25	-14	0.21	**-29**	0.26	-13	0.27	-8	0.24	**-20**

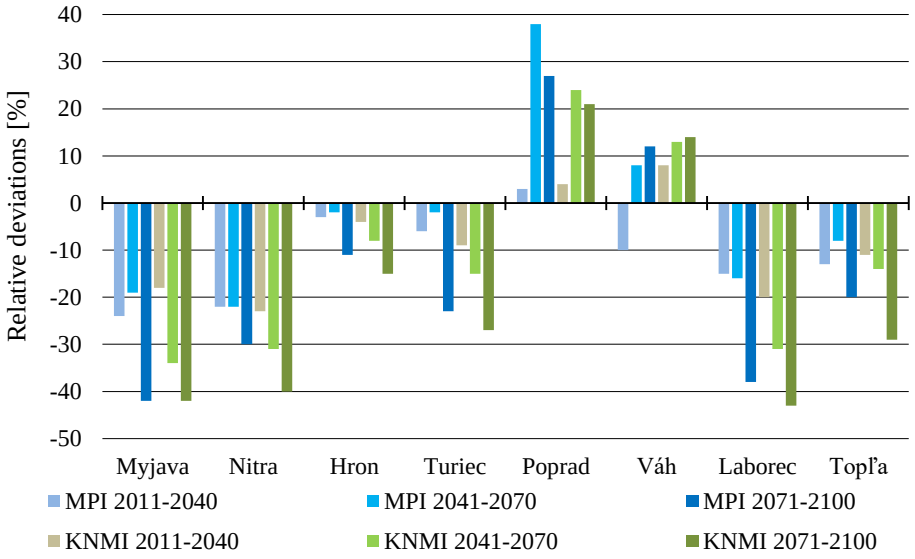

Fig. 5. *Graphic representation of the relative deviations of the simulated baseflow index of the KNMI and MPI climate scenarios by 2100 from the modelled average annual discharges of the HBV-type rainfall-runoff TUW model.*

Conclusion

The study is aimed at analysing changes in the long-term seasonal discharges from the winter and summer half-years up to 2100 using simulated discharges according to the KNMI and MPI climate scenarios. Four groups of basins in Slovakia were created, which were divided in terms of their location. The results for the periods predict the most significant changes for the future in the period 2071–2100 in the winter half-year, when increases in the long-term seasonal discharges of up to 77% are expected (Nitra River basin). The summer half-year shows lower increases in the values of the long-term seasonal discharges. Compared to the winter period, the results indicate that a decrease in the long-term seasonal discharges will also occur more often. The winter half-year is different for Slovakia with respect to the morphological and climatological diversity of the basins (mountain and lowland basins). The winter half-year is different for Slovakia in terms of snowfall because a lack of snow cover occasionally appears in lowland areas; on the other hand, northern Slovakia is affected by heavy snow showers on a yearly basis, which increase the discharges in the water courses. From a general point of view, the survey results indicate a decrease in the summer period and a significant increase in the values of the long-term seasonal discharges in the winter period.

The results of the analyses for the baseflow index indicate decreasing values in the future in most cases of the selected basins, which will have an adverse effect on their hydrological regimes; the best forecasts in terms of the baseflow index were recorded in the basins of northern Slovakia (the Poprad and Váh River basin),

where data predictions from climate scenarios indicate an increase in the baseflow index. When using the climate scenarios, it was found that the simulated discharges under the KNMI climate scenario predicted more extreme changes than those under the MPI climate scenario.

Acknowledgement

This study was supported by the Slovak Research and Development Agency under Contract No. APVV-20-0374 and APVV-19-0340. The study was also supported by the VEGA Grant Agency under Project No. 1/0632/19. The authors are very grateful for their research support.

References

Ďurigová, M., Hlavčová, K., Komorníková, M., Kalická, J., Ballová, D., Bacigál, T. (2019): The change analysis of the mean monthly discharges in Slovakia in recent decades. Acta Hydrologica Slovaca, Vol. 20, No. 1, 10–21. DOI: 10.31577/ahs-2019-0020.01.0002.

Ďurigová, M., Hlavčová, K., Poórová, J. (2020): Detection of Changes in Hydrological Time Series during Recent Decades. Slovak Journal of Civil Engineering, Vol. 28, No. 2, 56–65. https://doi.org/10.2478/sjce-2020-0016.

He, Y., Manful, D., Warren, R., Forstenhäusler, N., Osborn, T. J., Price, J., Jenkins, R., Wallace, C., Yamazaki, D. (2022): Quantification of impacts between 1.5 and 4°C of global warming on flooding risks in six countries. Climatic Change, Vol. 170, No. 15, 21 pp. https://doi.org/10.1007/s10584-021-03289-5.

Huntington, T. G. (2003): Climate warming could reduce runoff significantly in New England, USA. Agricultural and Forest Meteorology, Vol. 117, 193–201. doi:10.1016/S0168-1923(03)00063-7.

Majerčáková, O., Škoda, P., Danáčová, Z. (2007): Selected hydrological and precipitation characteristic of 1961–2000 and 2001–2006 periods in the High Tatra region. Meteorological Journal, Vol. 10, 205–210.

Meresa, A., Romanowicz, R. J. (2017): The critical role of uncertainty in projections of hydrological extremes. Hydrology and Earth System Sciences, Vol. 21, 4245–4258. https://doi.org/10.5194/hess-21-4245-2017.

Meresa, H., Tischbein, B., Mekonnen, T. (2022): Climate change impact on extreme precipitation and peak flood magnitude and frequency: observations from CMIP6 and hydrological models. Natural Hazards, Vol. 111, 2649–2679, https://doi.org/10.1007/s11069-021-05152-3.

Pekárová, P., Miklánek, P., Pekár, J. (2007): Long-term Danube monthly discharge prognosis for the Bratislava station using stochastic models. Meteorological Journal, Vol. 10, 211–218.

Rončák, P., Šurda, P., Vitková, J. (2021): Analysis of a Topsoil Moisture Regime Through an Effective Precipitation Index for the Locality of Nitra, Slovakia. Slovak Journal of Civil Engineering, Vol. 29, No. 1, 9–14. https://doi.org/10.2478/sjce-2021-0002.

Sabová, Z., Kohnová, S. (2022): Seasonal and spatial changes in mean monthly discharges in selected gauging stations of Slovakia. In Kalicz, P., Hlavčová, K., Kohnová, S., Széles, B., Rattayová, V., Gribovszki, Z. HydroCarpath 2022. Hydrology of the Carpathian Basin: synthesis of data, driving factors and processes across scales: proceedings of the conference. Vienna/Bratislava/Sopron, 24. 11. 2022. Sopron: University of Sopron Press, 2022, 104 pp. ISBN 978-963-334-452-1.

Sleziak, P. (2017): Modelling of the rainfall-runoff processes in conditions of changing climatic conditions. Dissertation thesis. Bratislava. SvF-104305-65272, 190 pp.

Sleziak, P., Szolgay, J., Hlavčová, K., Duethmann, D., Parajka, J., Danko, M. (2018): Factors controlling alterations in the performance of a runoff model in changing climate conditions. Journal of Hydrology and Hydromechanics, Vol. 66, 381–392. DOI: 10.2478/johh-2018-0031.

Sleziak, P., Szolgay, J., Hlavčová, K., Parajka, J. (2016): The impact of the variability of precipitation and temperatures on the efficiency of a conceptual rainfall-runoff model. Slovak Journal of Civil Engineering, Vol. 24, No. 4, 1–7. DOI: 10.1515/sjce-2016-0016.

Sleziak. P., Hlavčová, K., Szolgay, J., Parajka, J. (2017): Dependence of the quality of runoff-simulation by a rainfall-runoff model on the differences in hydroclimatic conditions of calibration and validation period. Acta Hydrologica Slovaca, Vol. 18, No. 1, 23–30.

Štefunková, Z., Hlavčová, K., Lapin, M. (2013): Runoff change scenarios based on regional climate change projections in mountainous basins in Slovakia. Contributions to Geophysics and Geodesy, Vol. 43, No, 4, 327–350. doi: 10.2478/congeo-2013-0019.

Vyshnevskyi, V., Donich, O. A. (2021): Climate change in the–Ukrainian Carpathians and its possible impact on river runoff. Acta Hydrologica Slovaca, Vol. 22, No. 1, 3–14. DOI:10.31577/ahs-2021-0022.01.0001.

Výleta, R., Hlavčová, K., Szolgay, J., Kohnová, S., Valent, P., Danáčová, M., Kandera, M., Aleksić, M. (2020): Reevaluation of the structure and methodology of the quantitative water management balance of surface waters. Scientific research analytical study, Bratislava, 282 pp.

Yang, W., Xia, R., Chen, H., Wang, M., Xu, CH.-Y. (2022): The impact of calibration conditions on the transferability of conceptual hydrological models under stationary and nonstationary climatic conditions. Journal of Hydrology, Vol. 613, 128310. https://doi.org/10.1016/j.jhydrol.2022.128310.

Ing. Zuzana Sabová (*corresponding author, e-mail: zuzana.sabova@stuba.sk)
Prof. Ing. Silvia Kohnová, PhD.
Department of Land and Water Resources Management
Faculty of Civil Engineering
Slovak University of Technology in Bratislava
Radlinského 11
811 07 Bratislava
Slovak Republic

DOI: 10.31577/ahs-2023-0024.01.0010

ACTA HYDROLOGICA SLOVACA

Volume 24, No. 1, 2023, 82 – 93

An assessment of the uncertainty of the extremity of flood waves with vine copulas

Roman VÝLETA*, Kamila HLAVČOVÁ, Silvia KOHNOVÁ, Tomáš BACIGÁL, Anna LIOVÁ, Ján SZOLGAY

Flood hazard connected with the failure of hydraulic structures and flood risk associated with areas subject to flooding need to be estimated using flood hydrographs. Multivariate statistics of flood wave parameters enable quantitative conclusions about such flood hazards and risks. This study focuses on uncertainties in their estimates using unbounded and bounded marginal distributions of flood durations in the joint modelling of flood peaks, volumes, and durations with vine copulas. We have respected the seasonality of floods by distinguishing between the durations of summer and winter floods. We propose to use the bounded Johnson's SB distribution to represent the hydrological constraints associated with flood durations. The practical consequences of selecting various unbounded and bounded distributions for modelling flood durations for the joint overall and conditional probabilities of the exceedance of flood peaks, volumes, and durations were demonstrated on data from the Parná River in Slovakia. Differences in modelling joint probabilities due to the tail behaviours of the marginal distributions tested were found. Although these are not critical for practical applications, accepting upper and lower bounds as hydrological constraints improves the quality of the statistical models.

KEY WORDS: vine copulas, assessment of uncertainty, flood wave characteristics, conditional probability, flood hazard

Introduction

Managing flood risks relies, among other inputs, on hydrological design values, which are used for sizing hydraulic structures (reservoir volumes, spillways, flood levees, etc.), protecting residential zoning, and other areas at risk of flooding. The most recognised quantity in hazard estimation is the peak of a design flood, which is assessed by classical flood frequency analysis. Since specific hydraulic structures or flooding zones can only be correctly sized with a design input hydrograph, the knowledge of a such flood hydrograph (or at least of its selected parameters) is advantageous for a reliable design and adequate description of the impact of flooding events (Brunner et al., 2016a; Brunner, 2023; Kotaška and Říha, 2023; Škvarka et al., 2021). Another problem of univariate analysis is, that it does not consider the dependence between the hydrological control variables, e.g., flood peaks and volumes, which leads to inappropriate conclusions about the risks associated with their join impact (Rizwan et al., 2019). Interdependencies inherent among parameters of flood waves, which are of interest for a particular problem, must be accepted and assessed within a multivariate probabilistic framework (Brunner, 2023).

Recently efforts were therefore directed towards a multivariate probabilistic analysis of two or more flood wave characteristics (Xiao et al., 2009). Classical applications of bi- and tri-variate probability distributions were initially preferred. Rizwan et al. (2019) provided a short review of these methods. Unfortunately, their inherent limitations, such as the requirement that the marginal distributions of the constituent variables be identical, are challenging to meet in practice since the suitable marginal distributions of the multi-dimensional analysis usually differ. In addition, the mathematical formulations exceeding two dimensions are increasingly complicated (Rizwan et al., 2019).

Multivariate statistical analysis using the copula functions was introduced as a solution; it provides a convenient framework for estimating overall or conditional joint probabilities. Copulas allow for different marginal distributions of their components. These are connected by the copula function and which accounts for the dependence structure between them in the probability space. For a comprehensive overview of these developments, methods, and applications, see Nazeri Tahroudi et al. (2022); Tootoonchi et al. (2022); Größer and Okhrin (2022). Copula methods efficiently enable the assessment of joint and conditional probabilities of exceedance or return periods of a set of variables. Whereas, probabilities of exceedance in a univariate case, are uniquely defined, in a multivariate case we need to prefer one definition out of several possibilities for the practical problem given; an overview

is provided by Gräler et al. (2013) and Brunner et al. (2016b). In recent years, vine copulas have been suggested as convenient models of higher dimensions (Tosunoglu et al., 2020). They can establish flexible dependence structures by mixing components modelled by bivariate copulas.

Because of its practical convenience, the vine approach has recently received increased attention in studying multivariate hydrological analyses (e.g., Gómez et al., 2018; Brunner et al., 2019; Nazeri Tahroudi et al., 2022; Latif and Simonovic, 2022; Jafry et al., 2022), which has also led to increased efforts to conduct multivariate statistical analyses of entire flood events (e.g. Bačová Mitková et al., 2014; 2023; Ganguli et al., 2013; Requena et al., 2013; Rizwan et al., 2019). For example, Medeiro et al. (2010) described an ensemble of design flood hydrographs given by the peaks and volumes of peak-volume probabilistic spaces. A set of hydrographs with the same joint return period was proposed for a reservoir design, which leads to return periods for water levels for different flood peaks and volume combinations.

However, similarly to the case of design flood peaks, hydrologic flood wave characteristics and their respective parameters are inherently uncertain. The sources of the uncertainty are rooted in the length and quality of the hydrological records, the selection of uni- and multivariate statistical models, and the estimation of the parameters. To guarantee reliable flood wave estimates for designs, such uncertainties must be quantified and communicated to practitioners (Brunner et al., 2018; Liová et al., 2022).

Traditional uncertainty analyses of univariate design variables in hydrology are well established; they focus on many relevant aspects of the problem, such as the choice of the probability distributions, their parameter uncertainties, and comparisons of annual maxima sampling versus peak-over-threshold sampling (Beven and Hall, 2014; Kjeldsen et al., 2014). For a bivariate analysis, the problem becomes more complex. Brunner et al. (2018) presented a complex framework for quantifying and solving uncertainty issues, which could also be generalised to a multivariate case. The framework reflects, among other issues, problems of the length of the record, flood wave sampling, base flow separation, determination of marginal distributions and fitting of probability density functions, dependence modelling between the variables, and estimations of the joint and conditional design variable quantiles.

This study aims to invite the attention of practising risk analysts to one particular aspect of uncertainty associated with this new consistent probabilistic framework not tackled in previous studies. In the dependence modelling of peaks, volumes, and durations with vine copulas, we are only focusing on the consequences of respecting the hydrological constraints connected with modelling flood durations and propose to use the bounded Johnson distribution to describe them. While all sources of uncertainty mentioned above are acknowledged, we are ignoring here these uncertainties. Instead we pragmatically accept results of statistical testing when selecting the dependence structures among the peaks, volumes, and durations of the flood hydrographs modelled by vine copulas their marginal distributions. We are also robustly respecting the hydrologic seasonality of floods by distinguishing between summer and winter floods since flood types of diverse origins have different shapes and consequently exhibit other dependence structures between the characteristics of flood waves (e.g., Gaál et al., 2015; Grimaldi et al., 2016; Szolgay et al., 2015). Finally, the practical consequences for the joint overall and conditional probabilities of the exceedance of flood peaks, volumes, and durations of choosing a bounded distribution for the flood durations are compared with the performance of distributions without an upper bound. The comparison was demonstrated on summer and winter flood data from the Parná River above the Horné Orešany reservoir in Slovakia.

Methods and material

Vine copulas for modelling the joint distribution of flood peaks, volumes, and durations

We are treating the respective flood peaks, volumes, and durations as elements X_i of the random vector X= (X_1, X_2, X_3). Their (cumulative) distribution function (CDF) is defined as the probability of the (simultaneous) non-exceedance of:

$$F_i(x) = Pr(X_i \leq x) \text{ for } i \in (1,2,3) \quad (1)$$

$$F(x_1, x_2, x_3) = Pr(X_i \leq x_1 \wedge X_2 \leq x_2 \wedge X_3 \leq x_3) \quad (2)$$

while their survival function as a probability of the (simultaneous) exceedance,

$$\overline{F}_i(x) = Pr(X_i > x) \quad (3)$$

$$\overline{F}(x_1, x_2, x_3) = Pr(X_i > x_1 \wedge X_2 > x_2 \wedge X_3 > x_3) \quad (4)$$

The formula linking multivariate survival functions to CDF includes all the lower-dimensional marginals:

$$\overline{F}_{ijk} = 1 - F_i - F_j - F_k + F_{ij} + F_{ik} + F_{jk} - F_{ijk} \quad (5)$$

for $i, j, k \in \{1,2,3\}$ and $i \neq j \neq k$.

The joint probability distribution random variables are modelled by a combination of the marginal distributions of X_1, X_2, and X_3, which describe the individual stochastic behaviour of the elements, and a copula, which models their mutual relationship:

$$F(x_1, x_2, x_3) = C[F_1(x_1), F_2(x_2), F_3(x_3)] \quad (6)$$

$$f(x_1, x_2, x_3) = c[F_1(x_1), F_2(x_2), F_3(x_3)] \cdot f_1(x_1) f_2(x_2) f_3(x_3) \quad (7)$$

where F is the joint cumulative distribution function (CDF); F_1, F_2, and F_3 are the marginal CDFs; f_1, f_2, and f_3 are the corresponding densities; and C is a copula having uniform marginals defined on the unit hypercube C: [0,1]3→[0,1] (for the comprehensive details, see

Nelsen (2006). The joint CDF of the X_2, X_3 conditional on X_1 is then given by the formula:

$$F_{23|1}(x_2, x_3, x_1) = \int_{-\infty}^{x_3}\int_{-\infty}^{x_2} c\big(F_1(x_1), F_2(s), F_3(t)\big) f_2(s) f_3(t)\, ds dt \quad (8)$$

although numerical integration is necessary, since the primitive function of the integrand is not available in a closed form.

Here, the vine copula approach is used to construct copula *C* by using a graphic vine tool (see, e.g., Asquith (2022); Czado and Nagler (2022)) and bivariate copulas as building blocks, so that a multivariate copula is obtained through conditioning. Since, in practice, the flood peak is usually considered the most critical flood characteristic, we have chosen this variable as being conditioned upon; then the trivariate density is given by:

$$\begin{aligned} f(x_1, x_2, x_3) &= f_1(x_1) \cdot f_{2|1}(x_1, x_2) \cdot f_{3|12}(x_1, x_2, x_3) \\ &= f_1(x_1) \cdot c_{12}[F_1(x_1), F_2(x_2)] \cdot f_2(x_2) \\ &= c_{32|1}[F_{3|1}(x_3, x_1), F_{2|1}(x_2, x_1)] \cdot \\ &\quad c_{13}[F_1(x_1), F_3(x_3)] \cdot f_3(x_3) \end{aligned} \quad (9)$$

where $f_{i|j}(x_i, x_j) = f(x_i, x_j)/\, f_j(x_j)$ is the conditional density function of X_i given X_j. Further, the copula density c_{ij} couples X_i and X_j, while $c_{ij|k}$ couples the bivariate conditional distributions of $X_i|X_k$ and $X_j|X_k$, where $i, j, k \in \{1,2,3\}$ and $i \neq j \neq k \neq i$. Finally, $F_{i|j}(x_i, x_j) = \partial C_{ij}\big[F_i(x_i), F_j\big(x_j\big)\big]/\partial F_j(x_j)$ is a conditional CDF of X_i given X_j, see Schirmacher and Schirmacher (2008) and Dissmann et al. (2013) for further details.

Bivariate copulas, which are often used in hydrology, such as those from the Archimedean class (the Clayton, Gumbel, Frank, Joe and BB1 to BB8 copula families) with their survival counterparts and copulas of elliptically contoured distributions (Gaussian and Student t-copula), were considered as building blocks of the vine copula. Their selection and estimation of the parameters were made using a sequential procedure based on the AIC criterion and the maximum likelihood method (Dissmann et al., 2013).

The marginal CDFs of flood volume and discharge were selected from several distribution functions often used in the hydrology of extremes, such as the Generalized Extreme Value (GEV), Pearson 3 (p3), Weibull 3 (wb3) and Log-normal 3 (ln3) distributions. The models of the marginal distributions of flood durations considered with two to five parameters were selected from distribution functions with a lower bound, such as Wakeby (wak), Log-normal 3 (ln3), Gamma (gam), Rayleigh (ray), Rice (rice), Exponential (exp), Govindarajulu (gov), and Generalized Pareto (gpa) distributions. The parameters were estimated using the L-moments (Hosking, 1990). Additionally, flood durations were also modelled by the bounded distribution of Johnson (1949), specifically Johnson's SB distribution (joh), which showed that a random variable *X* with an upper and lower bound could be transformed to an approximately normal distribution with the density function given as:

$$f(x) = \frac{\delta}{\sqrt{2\pi}} \frac{\lambda}{(x-\xi)(\xi+\lambda-x)} e^{\left\{-\frac{1}{2}\left[y+\delta\ln\left(\frac{x-\xi}{\xi+\lambda-x}\right)\right]^2\right\}} \quad (10)$$

where $\xi < x < \xi + \lambda, \delta > 0, -\infty < y < \infty, \lambda > 0, \xi \geq 0$. The location parameter ξ, the range parameter λ, and shape parameters γ and δ were estimated by the maximum likelihood method.

The best-fitting distribution function for each flood variable was evaluated based on the CDF plots and the statistical Kolmogorov-Smirnov test (at 0.05 of the level of significance). The mean square error (MSE) between the observed and the simulated flood variables were calculated to evaluate the performance of the distribution functions selected. The statistical analysis and the visualizations were performed using the following R packages: Vine Copula (Nagler et al., 2022); ggplot2 (Wickham, 2016); metR (Campitelli, 2021); and cubature (Narasimhan et al., 2023).

Trivariate flood wave characteristics on the Parná River

The analysis was carried out on the Parná River inflow into the Horné Orešany reservoir located in western Slovakia (Fig. 1). The gauging station is situated above the reservoir on the Parná River at rkm 26.8 and has a basin area of 37.86 km^2. A more detailed description of the basin can be found in Liová et al. (2022). The discharge time series in hourly time steps and the maximum annual discharges used in the analysis were provided by the Slovak Hydrometeorological Institute (SHMI) for the period from 01.11.1988 to 31.12.2021. The precipitation and air temperature data in the daily time step, which were collected from the Dolné Orešany rainfall station and SHMI Modra-Piesok climatological station, were used for a better determination of the duration of the flood wave.

The flood waves analysed differ significantly in their shape, volume, and duration. For example, winter flood waves have a longer duration and greater volume than summer flood waves, which often arise from storm events and are also associated with melting snow or a combination of snowmelt and rain. On the other hand, summer flood waves are slimmer in shape and have a shorter duration. For this reason, flood waves were analysed separately for the summer (June-October) and winter (November-May) seasons. The separation of the flood waves, base flow, and estimations of the flood wave characteristics have been processed by an algorithm used in the FloodSep method (Valent, 2019). Next, we focused on a more detailed analysis of the flood wave durations and their effect on estimating the joint probability of the exceedance of flood characteristics.

Fig. 2 presents the probability density functions and histograms of flood durations in the summer and winter seasons. We can observe a unimodal form of both histograms. The summer flood durations have a range from 1.08 to 8.08 days and a median of 3.5 days.

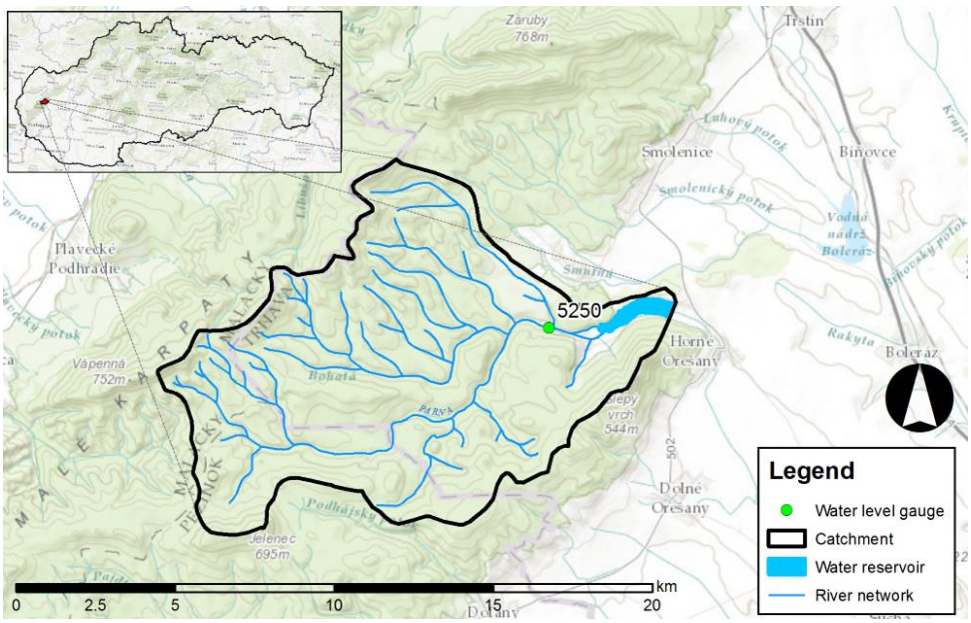

Fig. 1. Location of gauging station on the Parná River and the water reservoir of Horné Orešany within Slovakia.

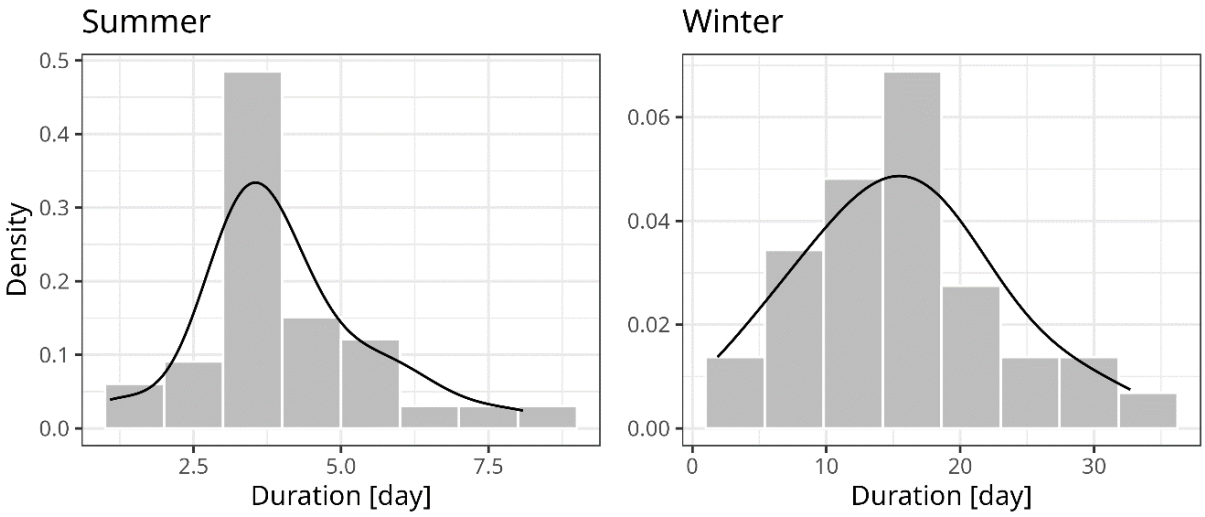

Fig. 2. Empirical probability density functions for durations of floods in the summer (left) and winter (right) seasons on the Parná River.

The winter flood durations are considerably longer in a range from 1.88 to 32.70 days and a median of 15 days, and their histogram is left-skewed. These results already show how different the flood waves are in the seasons selected and confirm the importance of treating them separately.

Results

Estimation of the best-fitting distributions of the flood peaks, volumes and durations and defining marginals

Prior to the modelling, the peak discharges, volumes, and durations were extracted from each flood wave to form the distributions of the extreme values in the summer and winter seasons. The most appropriate distribution functions were then found for the peak discharges, the Generalized Extreme Value distribution (gev), and, for the flood volumes, the Pearson type III distribution (p3). As a means of comparison, the DVWK (1999) methodology, which provided similar results of the distribution fitting, was also used.

For the flood durations, the efficiency of several selected distribution models with a lower bound, which are frequently used in hydrological applications sensitive to extreme values, were evaluated in detail. The validity of

the estimated models was examined based on the goodness of fit (GoF) using the MSE (Fig. 3) and visually on the CDFs of the flood durations (Fig. 4). This was the rationale for adopting the best types of the distributions of the flood durations in the paper. According to the results, the three appropriate distribution functions of the flood durations were selected to assess the uncertainty of the extremity of the flood events. In Fig. 3, these are shown by colour as joh (red point), ln3 (green point) and rice (blue point) distribution.

The Log-normal 3 and Rice distributions represent those with only the lower boundary parameters. However, Johnson's SB distribution can estimate not only the lower bound but also the upper bound of flood durations. The upper bound of the flood durations in the summer season using Johnson's SB distribution at 12 days and in the winter summer season at 37 days was estimated.

Trivariate distribution modeling using the vine copulas and the uncertainty of extremity of the seasonal floods

Modeling of unconditional joint probability of the exceedance of flood characteristics

To analyze the joint probability of the exceedance of the characteristics of maximum summer and winter floods, we evaluated the joint probability of the exceedance of the flood peaks "AND" the flood volumes "AND" the flood durations denoted as (1- $F(Q_{max},V,D)$) for three various distribution functions the duration of floods (see Tables 1, 2).

The most significant differences in the joint probability of the exceedance of flood peak Q_{max}, flood volume V, and flood duration D for summer flood waves were found for those with the longest durations. For example, for the longest flood wave, i.e., No. 25, with a duration

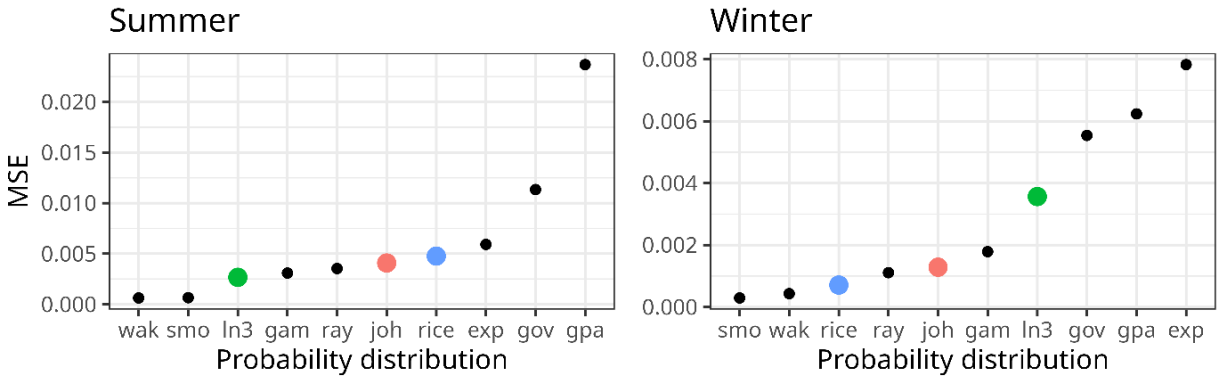

Fig. 3. Performance of various probability models for fitting marginals distributions for flood durations in the summer (left) and winter (right) seasons on the Parná River. The three distribution functions of flood duration selected to assess the uncertainty of the extremity of flood events are marked by colour.

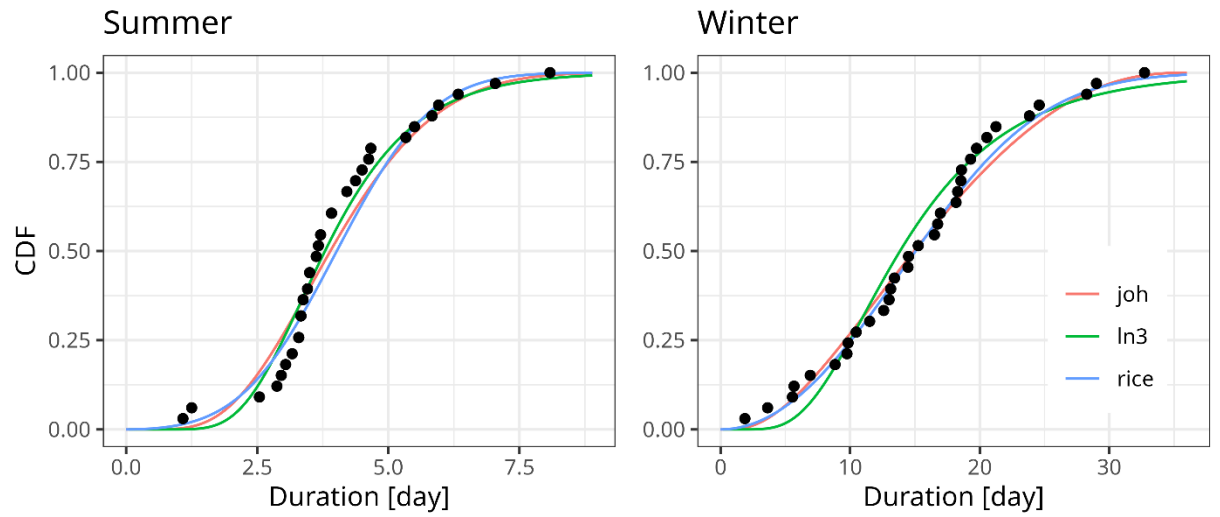

Fig. 4. Fitted marginal distributions for the flood durations in the summer (left) and winter (right) seasons: CDFs of the three selected types of distribution probability on the Parná River.

Table 1. The joint probability of the exceedance of maximum summer floods on the Parná River (probability distribution of flood durations: joh – Johnson's SB, rice – Rice and ln3 - Log-Normal3 distribution)

No. of the wave	Q_{max} [$m^3 s^{-1}$]	Volume [mil.m^3]	Duration [day]	1-$F(Q_{max},V,D)$		
				joh	rice	ln3
1	1.39	0.18	4.38	0.278	0.29	0.252
2	0.56	0.05	3.04	0.661	0.681	0.741
3	0.67	0.11	3.92	0.403	0.424	0.379
4	1.11	0.25	5.33	0.154	0.144	0.135
5	0.88	0.05	3.46	0.527	0.566	0.509
6	0.35	0.05	3.17	0.642	0.670	0.633
7	2.29	0.32	3.33	0.269	0.273	0.266
8	3.28	0.25	4.21	0.184	0.19	0.171
9	**8.63**	**1.59**	**7.04**	**0.007**	**0.004**	**0.008**
10	5.37	0.66	5.83	0.041	0.035	0.037
11	6.02	0.49	3.92	0.098	0.101	0.095
12	0.70	0.05	3.29	0.585	0.609	0.577
13	2.01	0.17	3.29	0.358	0.365	0.352
14	5.89	0.17	2.54	0.140	0.141	0.142
15	0.09	0.02	2.96	0.764	0.763	0.749
16	0.88	0.09	3.67	0.458	0.481	0.436
17	1.37	0.15	3.38	0.417	0.430	0.409
18	1.58	0.10	3.5	0.412	0.430	0.401
19	2.14	0.29	4.67	0.191	0.195	0.172
20	0.60	0.11	5.96	0.104	0.083	0.094
21	1.09	0.14	3.92	0.375	0.396	0.351
22	4.98	0.83	5.50	0.052	0.048	0.047
23	**33.86**	**1.67**	**3.62**	**0.005**	**0.005**	**0.005**
24	0.93	0.05	3.50	0.533	0.546	0.491
25	**2.53**	**0.52**	**8.08**	**0.004**	**0.001**	**0.010**
26	13.99	0.94	4.50	0.023	0.024	0.022
27	3.12	0.33	4.62	0.153	0.156	0.139
28	2.17	0.18	3.71	0.302	0.315	0.295
29	0.89	0.08	2.88	0.588	0.609	0.588
30	9.54	0.28	3.33	0.063	0.065	0.063
31	2.22	0.04	1.08	0.415	0.443	0.411
32	8.83	1.72	6.33	0.011	0.009	0.011
33	0.59	0.02	1.25	0.805	0.787	0.716

of 8.08 days, the values of the joint probability of the distribution of Q_{max}, V and D under various marginal distributions of D were 0.004 for Johnson's SB, 0.001 for Rice, and 0.01 for the Log-Normal 3 distribution; for the flood wave No. 9 with a duration of 7.04 days, the values of the joint probability of exceedance were 0.007, 0.004 and 0.008. However, these two flood waves with the longest D were not significant in either their peaks or volumes. On the contrary, for the flood wave with the highest flood peak and volume, i.e., with a duration of 3.62 days, the joint probability of exceedance was the same as for all three marginal distributions of D, i.e., 0.005.

For winter flood waves, the most significant differences in the joint probability of exceedance were again found for flood wave No. 11 with the longest duration of 32.7 days; the probability of exceedance was 0.002 for Johnson's SB, 0.003 for Rice, and 0.007 for the Log-Normal 3 marginal distribution of D. Here, the differences were also found for the most significant winter floods. Flood wave No. 18, with the highest flood peak and volume and a relatively long duration of 18.54 days, had a value of the probability of exceedance of 0.007 for the Johnson marginal distribution of D, 0.006 for Rice, and 0.005 for the Log-Normal3 marginal distribution. The second largest flood wave in flood peak and volume, i.e., No. 21, with a duration of 23.8 days, had joint probabilities of exceedance of 0.005, 0.005, and 0.004.

Table 2. The joint probability of the exceedance for maximum winter floods on the Parná River (probability distribution of flood duration: joh – Johnson's SB, rice – Rice and ln3 - Log-Normal3 distribution)

No. of the wave	Q_{max} [$m^3 s^{-1}$]	Volume [mil.m^3]	Duration [day]	$1\text{-}F(Q_{max},V,D)$		
				joh	rice	ln3
1	1.49	0.55	8.83	0.623	0.635	0.63
2	1.99	1.11	18.58	0.237	0.225	0.187
3	1.77	0.98	14.50	0.37	0.375	0.328
4	5.51	3.91	20.54	0.037	0.035	0.030
5	3.48	1.68	13.12	0.213	0.217	0.194
6	3.53	2.58	19.75	0.097	0.091	0.077
7	3.43	0.93	9.75	0.299	0.302	0.291
8	5.43	5.15	24.58	0.013	0.012	0.012
9	2.83	2.26	28.25	0.028	0.026	0.034
10	1.45	0.93	13.42	0.439	0.429	0.393
11	**3.70**	**4.59**	**32.71**	**0.002**	**0.003**	**0.007**
12	2.28	1.80	18.29	0.189	0.184	0.155
13	1.95	1.09	14.46	0.347	0.350	0.307
14	1.25	0.77	16.96	0.350	0.340	0.286
15	1.16	0.54	11.5	0.575	0.589	0.568
16	3.93	1.70	12.58	0.190	0.194	0.174
17	7.16	3.00	19.29	0.026	0.025	0.020
18	**11.47**	**5.54**	**18.54**	**0.007**	**0.006**	**0.005**
19	1.36	0.86	18.17	0.299	0.287	0.239
20	1.01	1.24	29.00	0.040	0.040	0.057
21	**9.70**	**5.04**	**23.83**	**0.005**	**0.005**	**0.004**
22	5.39	2.73	16.75	0.070	0.069	0.058
23	7.22	2.32	13.00	0.048	0.049	0.044
24	1.71	0.47	10.46	0.547	0.558	0.532
25	4.26	3.00	21.25	0.059	0.054	0.048
26	2.56	0.25	3.62	0.564	0.556	0.546
27	4.85	2.64	16.50	0.088	0.087	0.074
28	2.26	1.27	9.83	0.401	0.417	0.397
29	1.37	0.76	15.25	0.402	0.404	0.337
30	1.95	0.19	1.88	0.718	0.701	0.752
31	6.37	1.06	5.67	0.104	0.104	0.111
32	2.79	0.41	6.92	0.457	0.454	0.460
33	3.64	0.95	5.54	0.323	0.317	0.318

Modeling of the conditional probability of the exceedance of flood characteristics

In the next step, the uncertainties of the selection of the marginal distribution functions of the flood durations were demonstrated by the joint conditional probability of the exceedance of V and D on the 100-year flood peak Q_{100}, written as $S(V,D/Q_{100})$. From the marginal distribution of the flood peaks, the design discharge with the probability of exceedance 0.01 (100-year flood) was estimated as 32.76 $m^3 s^{-1}$. The results of the conditional probability of exceedance are illustrated by the isolines of $S(V,D/Q_{100})$ in Fig. 5.

From the results illustrated by the isolines of the joint probability of the exceedance of V and D, it can be seen that for summer floods, the differences in the joint probabilities of exceedance $S(V,D/Q_{100})$ due to various marginal distributions of D are visible for flood waves with durations longer than approximately 2 days. With the decreasing of the joint probability of the exceedance of V and D, the flood durations from which the differences are evident are increasing. While for the joint probability of exceedance $S(V,D/Q_{100})$ of 0.9, it is approximately 2 days; for $S(V,D/Q_{100}) = 0.7$, it is 3 days; and for $S(V,D/Q_{100}) = 0.3$, it is 4 days. We can see similar results in the winter season, but the flood durations from which the differences in $S(V,D/Q_{100})$ are visible are longer. Because $S(V,D/Q_{100}) = 0.9$, the flood durations are approximately 2.5 days; for $S(V,D/Q_{100}) = 0.7$, they are approximately 5 days; and for $S(V,D/Q_{100}) = 0.3$; they are approximately 10 days.

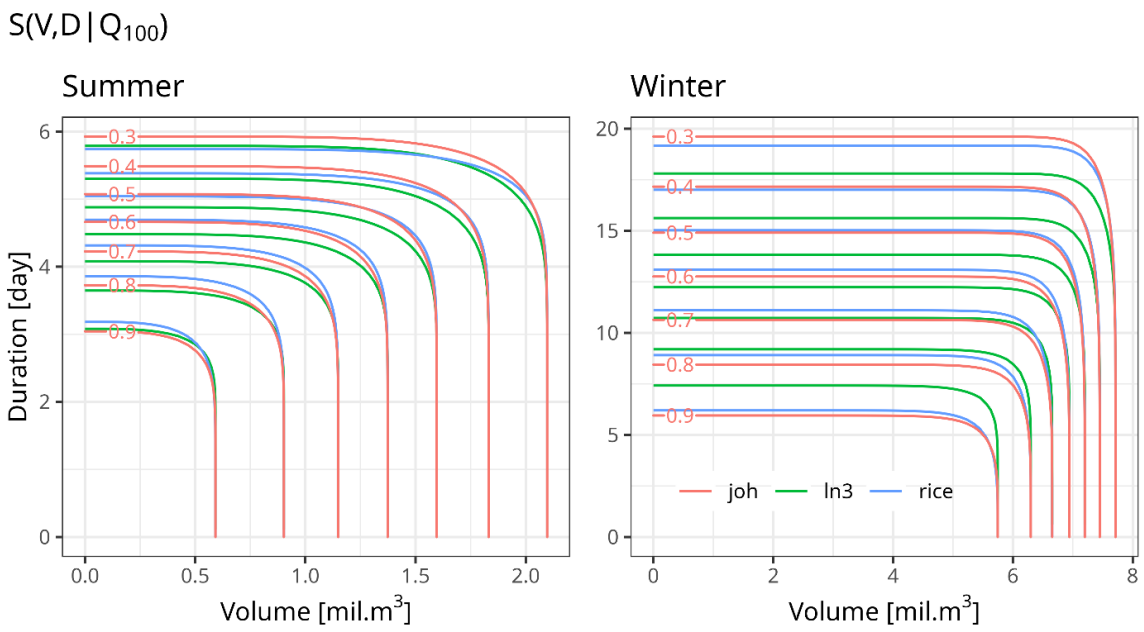

Fig. 5. The isolines of the joint conditional probability of the exceedance of the flood duration with various probability distributions "AND" the volume of the 100-year flood peak in the summer (left) and winter (right) seasons on the Parná River.

Discussion

Besides factors that cause uncertainties in frequency analysis, which are well reflected in the univariate methods (the length of the record, the annual maxima versus the peak- over-threshold sampling, the choice of the probability distributions, and their parameter uncertainties), in the multivariate case additional uncertainty sources occur, such as the sampling of flood waves (including base flow separation), determination of the marginal distributions, and fitting of multivariate probability density functions, dependence modelling between the variables, and estimation of the joint and conditional design variable quantiles (Beven and Hall, 2014; Kjeldsen et al., 2014).

This study aimed only at attracting the attention of practising analysts to one particular hydrological aspect of the uncertainty not tackled in previous studies. We acknowledge the importance of all uncertainty sources listed and treated in detail in Brunner et al. (2018). However, as is usual in a practical hydrological design exercise, we intentionally left out their assessments and pragmatically implemented the results of the basic statistical testing when selecting the appropriate models for the frequency and dependence analysis of the peaks, volumes, and durations of the flood hydrographs observed by vine copulas.

The effect of baseflow considerations on the beginning and end of a flood was not evaluated here, too. We could also have discussed the options for the wave selection, such as the direct runoff separation or taking the entire hydrograph. Instead, the results from the FloodSep method described in Liová et al. (2022) were implemented. Nevertheless, we acknowledge the immense importance of using hydrologically sound and practically relevant flood wave separation methods for the outcomes of the analyses of volumes and durations.

We also restricted the analysis of the typology of flood generation in the pilot catchment only to the basic seasonality of the floods by distinguishing between summer and winter floods. The discharge waves analysed differ significantly in their shape, volume, and duration, which can be seen, e.g., on the bimodal shape of the histogram of the annual maximum flood durations in Fig.6. Winter waves have longer durations associated with melting snow or combinations of snowmelt and rain. Their volumes are more significant than those of summer waves, which often arise from storm events and are slimmer in shape and have a shorter duration. For this reason, the flood waves were analysed separately for the summer (June–October) and winter (November–May) seasons, reaching a median of 3.5 days duration in the summer and 15 days in the winter seasons.

The unimodal frequency histograms of the respective summer and winter flood durations showed that such a simplification might be acceptable in the given catchment. Although the seasonal histograms of flood durations are unimodal, we can also see that they are skewed (see Fig. 2), which could indicate that not all floods may have the same origin; e.g., in the winter, a pattern composed of a mix of flood events caused by snowmelt, prolonged rains, and rain on snow events could be hidden in a histogram. In such and similar cases in basins with a richer flood typology, respecting more flood types (short rain, long rain, rain on snow etc., see Gaál et al. (2015)) than in our method may be required since flood types of diverse origins have

different shapes and consequently exhibit other dependence structures between the parameters of flood waves (Gaál et al., 2015).

We only focused in this analysis on the consequences of respecting or neglecting the obvious hydrological constraints connected with flood durations. To model a flood duration coming from a finite interval, we proposed to use the bounded Johnson's SB distribution to describe them. The SB Johnson distribution proved to be flexible. When respecting its domain of applicability defined through its third and fourth moments, see Johnson (1949) and Parresol (2003), it also enables the use of hydrologically determined upper and lower bounds. Practical consequences for the joint overall and conditional probabilities of the exceedance of the flood peaks, volumes, and durations of choosing a bounded distribution for the flood durations were compared with the performance of distributions without an upper bound, which is a hydrologically erroneous (but often used) assumption, see Figs. 4 and 7.

Differences in the modelling of joint probabilities due to the different tail behaviors of the marginal distributions tested were found. Although these are not located in critical regions of joint probabilities for practical applications, accepting hydrological constraints as upper and lower bounds improves the statistical model's quality and is recommended.

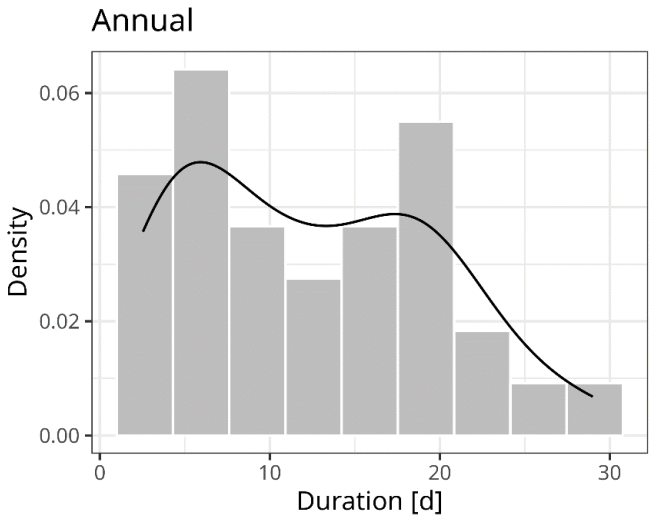

Fig. 6. Bimodal empirical probability density function for flood durations associated with annual maximum discharges on the Parná River.

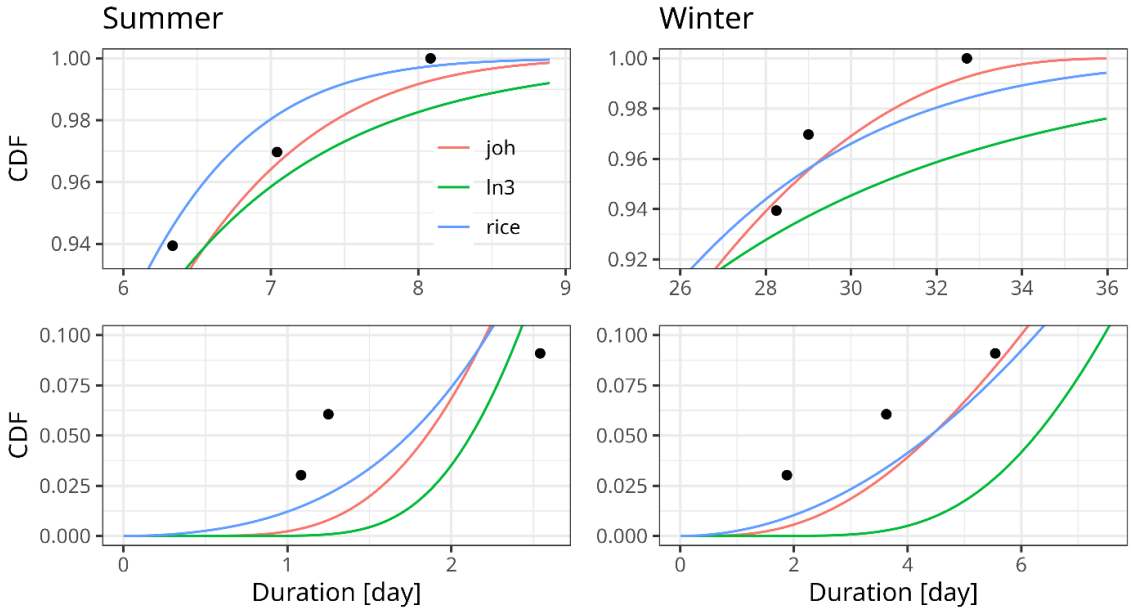

Fig. 7. Details of upper and lower bounds of fitted marginal distributions for flood durations in the summer (left) and winter (right) seasons on the Parná River: CDFs of three selected types of distribution probabilities.

Conclusion

The most recognized quantity in flood hazard estimations is the peak of the design flood. Univariate frequency analysis is used conventionally to assess its value and the associated uncertainties of its estimation. However, specific design tasks require considering the impact of the flood hydrograph, usually described by a set of hydrological control variables, e.g., the flood peaks, volumes or durations. Only by considering the dependence among these variables in the hazard estimation may lead to appropriate conclusions about the risks associated with the joint impact of these in their various combinations. The inherent interdependencies among flood wave shape control variables must be quantified within multivariate statistical assessment frameworks, which can also account for the uncertainties of the estimates (though in a more complex way than in a univariate case). Besides uncertainty-causing factors, which are reflected in univariate cases (such as problems involving the annual maxima versus peak- over-threshold sampling, the choice of the probability distributions, and their parameter uncertainties), additional issues such as flood wave sampling, base flow separation, fitting of multivariate probability density functions, the dependence modelling between the variables, and estimation of the joint and conditional probabilities of the design variable quantiles have to be considered.

As previously mentioned, this study only intended to attract the attention of practising analysts to the uncertainty associated with the joint probabilities assessed within the vine copula probabilistic framework. These must be addressed in practice and in connection with statistical flood duration models. Therefore, our analysis did not consider the statistical sources of uncertainties but illustrated those originating in hydrological sources, which could require attention. These are mostly related to the sampling of flood waves and include the knowledge of flood generation processes (short rains, prolonged rains, rain on snow, snowmelt, etc.), the estimation of the flood volume (direct runoff vs. a whole hydrograph), and the determination of the duration of the flood waves.

Regarding which flood generation processes to consider, using annual maxima in such an analysis may not meet the IID requirements in general. Instead, we recommend to consider the basic seasonality of the flood regime separately and to look within the seasons at a stepwise approach at the frequency histograms of the durations associated with respective flood types of the events sampled (unimodal vs. multimodal, symmetrical vs. skewed, etc.) and the practical goals of the design or risk analysis task. For example, frequency histograms of the respective durations of flood types may support a decision made on an acceptable grouping of sparser flood types (or eventually leaving them out) in the given catchment and for the specific task.

In a decision on the selection of the flood volumes for the analysis, more practical aspects could be preferred and a task-related choice performed. For example, in sizing the retention volumes of multipurpose reservoirs or flood zoning, a whole hydrograph could be required for the design. To only consider direct runoff for flood detentions may not be correct since the detention volume is also filled with the flood's baseflow. On the contrary, direct runoff may be preferred when looking at a regime of event-based rainfall-runoff relationships.

Determining the duration of a flood is connected to the decisions to be made on its volume, and it is not a straightforward task, especially when the whole hydrograph is taken as a flood wave. This determination is especially complicated in the winter season for snowmelt and mixed floods. Methods ranging from baseflow separations up to snowmelt and rainfall runoff modelling may be required for a hydrologically plausible solution. In any case, an upper and lower bound must be considered. The marginal distribution of the duration should preferably respect these bounds since, in the dependence modelling of peaks, volumes and durations, it affects the joint and conditional probabilities of the exceedance associated with any combined hazards. Our case study showed differences in the outcomes of modelling the joint probabilities due to the different tail behaviours of the marginal distributions tested. Although these may sometimes only be critical for practical applications, accepting hydrological constraints as upper and lower bounds improves the statistical model's quality. One computationally and conceptually acceptable option is the four-parameter bounded Johnson’s SB distribution, as was illustrated in our case study.

Acknowledgement

This work was supported by the Slovak Research and Development Agency under Contract No. APVV 15-0497, No. APVV 20-0374 and the VEGA Grant Agency No. VEGA 1/0577/23.

Reference

Asquith, W. (2022): lmomco–L-moments, censored L-moments, trimmed L-moments, L-comoments, and many distributions. R package version 2.4.7. https://cran.r-project.org/web/packages/lmomco/lmomco.pdf

Bačová Mitková, V., Halmová, D. (2014): Joint modeling of flood peak discharges, volume and duration: A case study of the Danube River in Bratislava. Journal of Hydrology Hydromechanics, 62, 186–196. DOI: https://doi.org/10.2478/johh-2014-0026

Bačová Mitková, V., Halmová, D., Pekárová, P., Miklánek, P. (2023): The Copula Application for Analysis of the Flood Threat at the River Confluences in the Danube River Basin in Slovakia. Water, 15(5), 984. DOI: https://doi.org/10.3390/w15050984

Beven, K., Hall, J. (2014): Applied uncertainty analysis for flood risk management. World Scientific. DOI: https://doi.org/10.1142/p588

Brunner, M. (2023): Floods and droughts: a multivariate perspective on hazard estimation: a multivariate perspective on hazard estimation. Hydrology and Earth System Sciences Discussions, 1–26. DOI: https://doi.org/https://doi.org/10.5194/hess-2023-20

Brunner, M., Furrer, R., Favre, A. (2019): Modeling the spatial

dependence of floods using the Fisher copula. Hydrology and Earth System Sciences, 23(1), 107–124. DOI: https://doi.org/10.5194/hess-23-107-2019

Brunner, M. I., Sikorska, A. E., Furrer, R., Favre, A. C. (2018): Uncertainty assessment of synthetic design hydrographs for gauged and ungauged catchments. Water Resources Research, 54(3), 1493–1512. DOI: https://doi.org/10.1002/2017WR021129

Brunner, M., Seibert, J., Favre, A. (2016a): Bivariate return periods and their importance for flood peak and volume estimation. WIREs Water, 3(6), 819–833. DOI: https://doi.org/10.1002/wat2.1173

Brunner, M., Vannier, O., Favre, A., Viviroli, D., Meylan, P., Sikorska, A., Seibert, J. (2016b): Flood volume estimation in Switzerland using synthetic design hydrographs – a multivariate statistical approach. 13th Congress INTERPRAEVENT 2016, Luzern, 30 May 2016 – 2 June 2016, 468-476. DOI: https://doi.org/10.5167/uzh-124430

Campitelli, E. (2021): metR: tools for easier analysis of meteorological fields: tools for easier analysis of meteorological fields. R Package version 0.13.0. DOI: https://doi.org/10.5281/zenodo.2593516

Czado, C., Nagler, T. (2022): Vine Copula Based Modeling. Annual Review of Statistics and Its Application, 9(1), 453–477. DOI: https://doi.org/10.1146/annurev-statistics-040220-101153

Dissmann, J., Brechmann, E., Czado, C., Kurowicka, D. (2013): Selecting and estimating regular vine copulae and application to financial returns. Computational Statistics Data Analysis, 59, 52-69. DOI: https://doi.org/10.1016/j.csda.2012.08.010

DVWK 101 (1999): Wahl des Bemessungshochwassers. Empfehlung zur Berechnung der Hochwasser-wahrscheinlichkeit. DVWK Schriften, Heft 101. Verlag Paul Parey, Hamburg.

Gaál, L., Szolgay, J., Kohnová, S., Hlavčová, K., Parajka, J., Viglione, A., Merz, R., Blöschl, G. (2015): Dependence between flood peaks and volumes: a case study on climate and hydrological controls. Hydrological Sciences Journal, 60(6), 968-984. DOI: https://doi.org/10.1080/02626667.2014.951361

Ganguli, P., Reddy, M. (2013): Probabilistic assessment of flood risks using trivariate copulas. Theoretical and Applied Climatology, 111(1–2), 341–360. DOI: https://doi.org/10.1007/s00704-012-0664-4

Gómez, M., Ausín, M., Domínguez, M. (2018): Vine copula models for predicting water flow discharge at King George Island, Antarctica. Stochastic Environmental Research and Risk Assessment, 32(10), 2787–2807. DOI: https://doi.org/10.1007/s00477-018-1599-9

Gräler, B., van den Berg, M., Vandenberghe, S., Petroselli, A., Grimaldi, S., De Baets, B., Verhoest, N. (2013): Multivariate return periods in hydrology: a critical and practical review focusing on synthetic design hydrograph estimation. Hydrology and Earth System Sciences, 17(4), 1281–1296. DOI: https://doi.org/10.5194/hess-17-1281-2013

Grimaldi, S., Petroselli, A., Salvadori, G., De Michele, C. (2016): Catchment compatibility via copulas: A non-parametric study of the dependence structures of hydrological responses. Advances in Water Resources, 90, 116–133. DOI: https://doi.org/10.1016/j.advwatres.2016.02.003

Größer, J., Okhrin, O. (2022): Copulae: An overview and recent developments. WIREs Comp. Statistics, 14(3). DOI: https://doi.org/10.1002/wics.1557

Hosking, J. (1990): L-Moments: Analysis and Estimation of Distributions Using Linear Combinations of Order Statistics. Journal of the Royal Statistical Society: Series B (Methodological), 52(1), 105–124. DOI: https://doi.org/10.1111/j.2517-6161.1990.tb01775.x

Jafry, N., Suhaila, J., Yusof, F., Mohd Nor, S., Alias, N. (2022): Preliminary Study on Flood Frequency Analysis in Johor River Basin Using Vine Copula. Proceedings of Science and Mathematics, 7, 52–55. https://science.utm.my/procscimath/files/2022/06/52_55_Naqibah_Aminuddin_Jafry.pdf

Johnson, N. (1949): Systems of frequency curves generated by methods of translation. Biometrika, 36(12), 149–176. DOI: https://doi.org/10.2307/2332539

Kjeldsen, T., Lamb, R., Blazkova, S. (2014): Uncertainty in flood frequency analysis. Applied Uncertainty Analysis for Flood Risk Management, 153–197. DOI: https://doi.org/10.1142/p588

Kotaška, S., Říha, J. (2023): Dam incidents and failures- cases in the Czech Republic. Slovak Journal of Civil Engineering, 31(1), 22–33. DOI: https://doi.org/10.2478/sjce-2023-0003

Latif, S., Simonovic, S. (2022): Parametric Vine Copula Framework in the Trivariate Probability Analysis of Compound Flooding Events. Water, 14(14). DOI: https://doi.org/10.3390/w14142214

Liová, A., Valent, P., Hlavčová, K., Kohnová, S., Bacigál, T., Szolgay, J. (2022): A methodology for the estimation of control flood wave hydrographs for the Horné Orešany reservoir. Acta Hydrologica Slovaca, 23(1), 52–61. DOI: https://doi.org/10.31577/ahs-2022-0023.01.0006

Mediero, L., Jiménez-Álvarez, A., Garrote, L. (2010): Design flood hydrographs from the relationship between flood peak and volume. Hydrology and Earth System Sciences, 14(12), 2495-2505. DOI: https://doi.org/10.5194/hess-14-2495-2010

Nagler, T., Schepsmeier, U., Stoeber, J., Brechmann, E., Graeler, B., Erhardt, T. (2022): VineCopula: Statistical Inference of VinCopulas. R package version 2.4.4. https://CRAN.R-project.org/package=VineCopula

Narasimhan, B., Johnson, S., Hahn, T., Bouvier, A., Kiêu, K. (2023): cubature: Adaptive Multivariate Integration over Hypercubes. R package version 2.0.4.6. https://CRAN.R-project.org/package=cubature

Nazeri Tahroudi, M., Ramezani, Y., De Michele, C., Mirabbasi, R. (2022): Trivariate joint frequency analysis of water resources deficiency signatures using vine copulas. Applied Water Science, 12(4). DOI: https://doi.org/10.1007/s13201-022-01589-4

Nelsen, R. (2006): An introduction to copulas, (2nd Ed.), Springer.

Parresol, B. (2003): Recovering parameters of Johnson's SB distribution (Vol. 31): US Department of Agriculture, Forest Service, Southern Research Station. DOI: https://doi.org/10.2737/SRS-RP-31

Requena, A., Mediero, L., Garrote, L. (2013): A bivariate return period based on copulas for hydrologic dam design: accounting for reservoir routing in risk estimation. Hydrology and Earth System Sciences, 17(8), 3023–3038. DOI: https://doi.org/10.5194/hess-17-3023-2013

Rizwan, M., Guo, S., Yin, J., Xiong, F. (2019): Deriving Design Flood Hydrographs Based on Copula Function: A Case Study in Pakistan. Water, 11(8). DOI: https://doi.org/10.3390/w11081531

Schirmacher, D., Schirmacher, E. (2008): Multivariate dependence modeling using pair-copulas. Technical report. https://www.soa.org/4938dc/globalassets/assets/files/resources/essays-monographs/2008-erm-symposium/mono-2008-m-as08-1-schirmacher.pdf

Szolgay, J., Gaál, L., Kohnová, S., Hlavčová, K., Výleta, R., Bacigál, T., Blöschl, G. (2015): A process-based analysis

of the suitability of copula types for peak-volume flood relationships. Proceedings of the International Association of Hydrological Sciences, 370, 183–188. DOI: https://doi.org/10.5194/piahs-370-183-2015

Škvarka, J., Bednárová, E., Miščík, M., Uhorščák, Ľ. (2021): The Domaša reservoir in the spectrum of climate change. Slovak Journal of Civil Engineering, 29(2), 9–15. DOI: https://doi.org/10.2478/sjce-2021-0009

Tootoonchi, F., Sadegh, M., Haerter, J., Räty, O., Grabs, T., Teutschbein, C. (2022): Copulas for hydroclimatic analysis: A practice-oriented overview. WIREs Water, 9(2). DOI: https://doi.org/10.1002/wat2.1579

Tosunoglu, F., Gürbüz, F., İspirli, M. (2020): Multivariate modeling of flood characteristics using Vine copulas. Environmental Earth Sciences, 79(19). DOI: https://doi.org/10.1007/s12665-020-09199-6

Valent, P. (2019): Floodsep: user´s manual, SvF STU in Bratislava.

Wickham, H. (2016): ggplot2: Elegant Graphics for Data Analysis. Springer-Verlag NY. https://ggplot2.tidyverse.org

Xiao, Y., Guo, S., Liu, P., Yan, B., Chen, L. (2009): Design flood hydrograph based on multicharacteristic synthesis index method. Journal of Hydrologic Engineering, 14(12), 1359-1364. DOI: https://doi.org/10.1061/(ASCE)1084-0699(2009)14:12(1359)

Assoc. Prof. Ing. Roman Výleta, PhD. (*corresponding author, e-mail: roman.vyleta@stuba.sk)
Prof. Ing. Kamila Hlavčová, PhD.
Prof. Ing. Silvia Kohnová, PhD.
Ing. Anna Liová
Prof. Ing. Ján Szolgay, PhD.
Department of Land and Water Resources Management
Faculty of Civil Engineering
Slovak University of Technology in Bratislava
Radlinského 11
810 05 Bratislava
Slovak Republic

Assoc. Prof. Ing. Tomáš Bacigál, PhD.
Department of Mathematics and Descriptive Geometry
Slovak University of Technology in Bratislava
Radlinského 11
810 05 Bratislava
Slovak Republic

DOI: 10.31577/ahs-2023-0024.01.0011

ACTA HYDROLOGICA SLOVACA

Volume 24, No. 1, 2023, 94 – 100

Identification of areas with potential significant flood risk using specialized software in the Vistula river basin within Ukraine

Maksym MARTYNIUK*, Valeriya OVCHARUK

In the period of climate change, the frequency of extreme hydrological phenomena increases, therefore, an extremely important problem in the hydrological study of the territory is the determination of areas with potentially significant risks of flooding, as well as the construction of maps of threats and risks of flooding. The basin of the Vistula river within Ukraine, located in the west of Ukraine, is in a zone of sufficient moisture and suffers from floods almost every year. A significant problem of the hydrological study of this basin is the identification of areas with potential significant flood risks, as well as the creation of flood hazard and risk maps. The paper presents the methodological principles and algorithm for using the HEC-RAS software in modeling the flooded territory with the corresponding calculated characteristics of the maximum runoff. The resulting maps of areas with potential significant flood risk (APSFR) in the area of Busk are also presented.

KEY WORDS: Vistula, flood, maximum runoff, HEC-RAS

Introduction

Floods on the Vistula river are a complex phenomenon, caused by several generating mechanisms, with a relative frequency of occurrence specific to the different parts of the basin (Cyberski et. al., 2006), particularly, for Upper Vistula is possible as spring such as rain floods. Flood zoning is one of the three components of Integrated Flood Management (IFRM). A detailed analysis of flood risk and flood damage assessment studies is available (Šugareková and Zeleňáková, 2021). In particular, it is shown, the IFRM method (Wang et. al., 2021) includes the identification, assessment, and management of flood risk with a focus on 3 objectives. First, it's the identification of significant areas with high flood risk. The second one is an assessment of economic damage caused by floods, and the third – is the use of flood risk management to select the best design measures to improve the capacity of the drainage system.

In Ukraine also, at the governmental level, the need to develop maps of flood threats and risks and flood risk management plans (Resolution of the Cabinet of Ministers of Ukraine, 2018). In 2022 was presented the first part of the Vistula river basin management plan (RBMP) was, which will help implement integrated water resources management on a basin basis. The plan was developed by a team of the Ministry of Natural Resources, the State Water Agency, and the Blue Rivers Environmental Consulting project together with experts, including specialists from the Basin Administration for Water Resources of the Western Bug and San rivers. Now presented is only the first part of the management plan for the Vistula river basin. The document contains information about: the characteristics of surface and ground waters; anthropogenic impact on surface and groundwater and their condition; areas to be protected; results of studies of surface and ground waters and their mapping; economic analysis of water use; measures to reduce water pollution.

Thus, the development of cartographic information about the flooding of the territory will play an important role in the further development of the RBMP, which also includes an assessment of areas of possible flooding during the passage of floods. The development of flood hazard and risk maps is carried out by hydrodynamic modeling. Based on the results of such modeling, it is possible to determine the inundation zones, water levels, and depths in the study area. Such maps make it possible to determine the potential damage from flooding in the future.

Material and methods

The Vistula river is the largest river flowing into the Baltic Sea. The Vistula river originates in the Western Beskids in Poland from the confluence of the Black and White Vistula rivers and flows into the Gulf of Gdańsk (Fig. 1). The basin of the Vistula river in Ukraine is

located within the borders of the Lviv and Volyn regions; watersheds run along ridges and hills, so they are clearly defined. The area of the Vistula river basin within Ukraine is 12,892 km^2, which is 2.13% of the country's territory and has 3,112 rivers, the total length of which is 7,356 km. According to the modern hydrographic zoning of the territory of Ukraine, the basin of the Vistula river is represented in a separate district. Its characteristic feature is the only region of the river basin in Ukraine, the flow of which is directed to the Baltic Sea.

The area of the Vistula river basin is divided into two sub-basins: the Western Bug and San rivers. A part of the Poltva river basin, a tributary of the Western Bug river, was chosen for modeling the flooding zone (Fig. 2). The studied area was limited to the water gauging stations (WGS) of the Poltva river – WGS Busk and the Western Bug river – WGS Kamyanka Buzka. This area was chosen as characteristic of the areas with potential significant flood risk (APSFR), and according to the WRBM of the Western Bug and San, it regularly

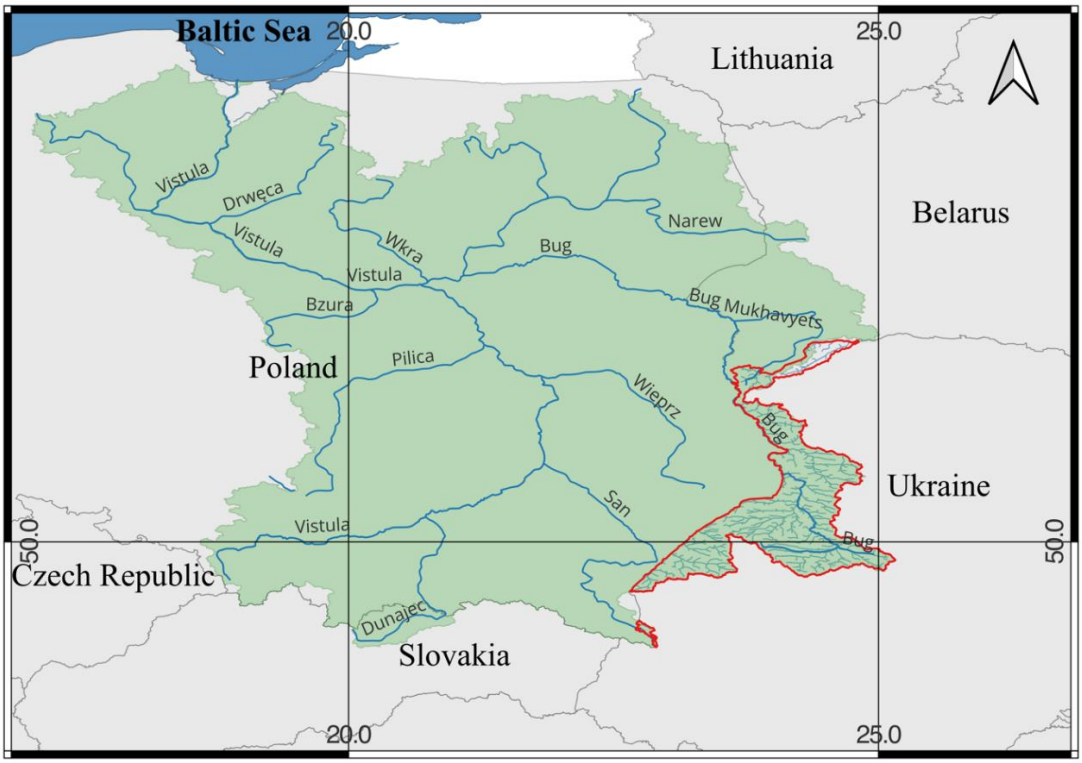

Fig. 1. The Vistula river location in territory of Ukraine.

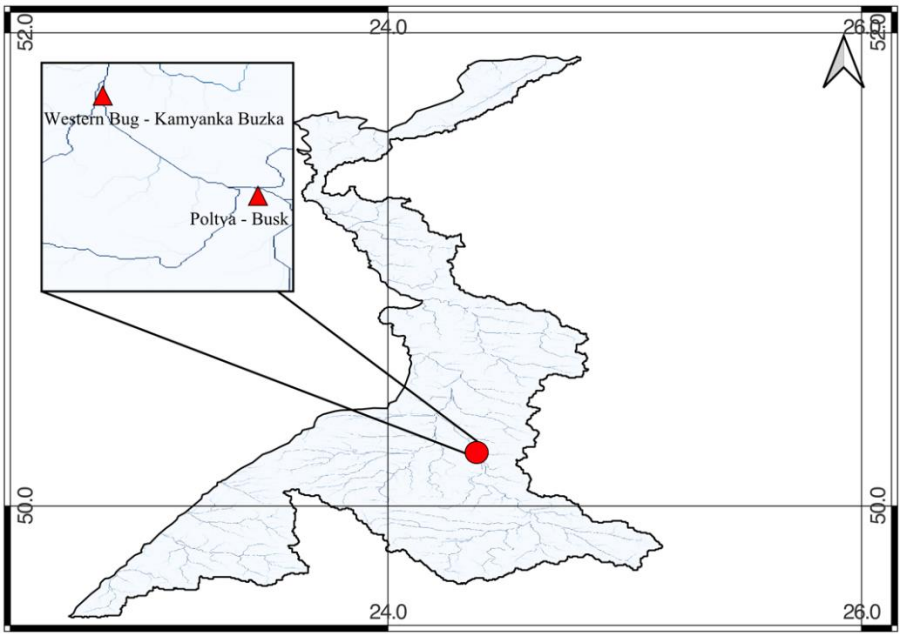

Fig. 2. The study area within Vistula river basin.

suffers from floods both during spring and rain floods.
For the construction, the calculated output data on the maximum runoff during the spring flood period, calculated hydrographs, transverse profiles, and the constructed digital elevation model of the terrain were used.
In this particular case, the water gauging stations located at Busk, which is located upstream, were taken as the upper reach for further calculations; therefore, the characteristics of the maximum runoff explicitly calculated for this WGS were used.
Calculations of the maximum water runoff with a rare probability of exceeding were performed under current regulatory documents (Manual, 1984).
Data on water flows, runoff layers, and runoff modules of the rare probability of exceedance were used, the calculation of which is given in the works (Martyniuk and Ovcharuk, 2020a; 2020b).
The estimated hydrograph is built based on data on the maximum discharges corresponding to the estimated probability of exceeding, in our case – 1%. Estimated hydrographs for spring floods are built based on the average daily water discharge, so it is necessary to switch from the calculated maximum runoff $Q_{1\%}$ to the average daily $Q_{1\%daily}$ using the transition coefficient K_τ according to the formula:

$$Q_{1\%daily} = Q_{1\%}K_\tau \quad (1)$$

Transition coefficient K_τ is determined depending on the studied territory's natural zone, and for the Poltva river basin, K_τ = 1.2 (Manual, 1984).
The form of calculated hydrographs depends on many factors, such as the morphometric characteristics of the basin and the distribution of water discharge time. However, the typical form of the hydrograph is accepted in hydrological calculations.
The hydrograph asymmetry coefficient K_s and the corresponding hydrograph shape factor λ are determined approximately, depending on the catchment area. Determination of the scheme of hydrographs, both for spring and rain floods, according to the equation proposed by Alekseev (1955):

$$Y = 10^{\frac{\alpha(1-x)^2}{x}} \quad (2)$$

where
x – is the relative abscissa of the calculated hydrograph, expressed in fractions of the flood duration;
Y – is the relative ordinate of the calculated hydrograph, expressed as a fraction of the average daily maximum water discharge of a particular supply.

The absolute abscissas of the calculated hydrograph are determined by the formula:

$$t_i = X_i t_r \quad (3)$$

where
t_r – the duration of the rise of spring floods or rain floods is defined as:

$$t_r = \frac{0.0116 \cdot \lambda \cdot Y_{1\%}}{q_{1\%}} \quad (4)$$

where
$Y_{1\%}$ – is the calculated runoff layer of the flood (spring or rain) with a rare probability of exceeding [mm];
$q_{1\%}$ – module of the maximum runoff of flood (spring or rain) [m^3 skm^{-2}];
λ – hydrograph shape factor.

The absolute ordinates of the calculated hydrograph are calculated as follows:

$$Q_t = Y_i Q_{1\%daily} \quad (5)$$

The calculated hydrograph of spring flood on the Poltva river – WGS Busk is shown in Fig. 3.
Transverse profiles of the upper reach (Poltva river – WGS Busk) and the lower reach (Western Bug river – WGS Kamyanka Buzka) were used in the modeling, which is given in special reference publications. Intermediate cross-sections were obtained by interpolating DEM and cross-sections of the upper and lower reaches using HEC-RAS software.

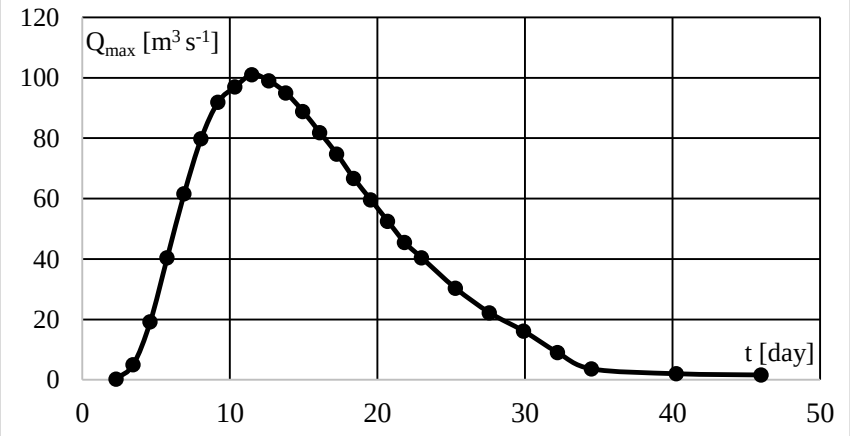

Fig. 3. Estimated hydrograph of the spring flood of the Poltva river – WGS Busk.

Results and discussion

A Digital Terrain Model (DEM) with sufficient accuracy for preliminary modeling of flood zones for large areas can be built from SRTM data. However, analysis of SRTM data accuracy indicates significant errors, up to 2.9 m for a flat area, as considered in (Karwel and Ewiak, 2008) and (Bildirici et al., 2007). The ability to use SRTM images of various resolutions to build a DEM is described by (Nagaveni, 2019). For an accurate study of APSFR, it is necessary to use refined DEMs obtained from LiDAR survey data and survey work directly in field studies. In subsequent calculations, in the absence of field observations and surveys, only SRTM data obtained from the USGS Earth Explorer resource and processed using Quantum GIS were used. The resulting map is shown in Fig. 4.

The HEC-RAS 6.2 software was used to create the flood model. HEC-RAS is a software developed by the US Army Corps of Engineers. The software allows the user to perform 1D steady flow calculations, 1D and 2D transient flow calculations, and other hydrological and hydraulic simulations.

HEC-RAS is also used for dam failure and land flooding simulations. The use of the application and its correctness in different conditions and on different rivers is confirmed by (Farooq et al., 2019; Parhi, 2018; Sathya and Thampi, 2021; Marko et al., 2019).

The first stage of work is creating a new project and working with the integrated GIS RAS Mapper. Importing a pre-prepared DEM and creating a one-dimensional (1D) flow model is necessary. For this purpose, the middle line of the river and coastlines are marked manually and using satellite images.

Next, the flow center lines (Flow Paths) are defined. They are used to calculate the length of sections between cross- sections and are plotted along the downstream coastline. The lines do not reflect and may not coincide with areas of possible flooding but are only an initial geospatial estimate of the relationship of the center of mass of the flow from one cross-section to another.

Cross sections of the river are also being built. They should be placed perpendicular to the flow, often enough for adequate modeling, covering an area considered potentially floodable from upstream to downstream. That is, such cross-sections reflect changes in the relief of the entire floodplain, and in the area of the channel bounded by the banks, they are automatically marked as cross-sections of the stream (Starodub and Havrys, 2015) (Fig. 5).

An example of the built cross section of the upper reach is shown in Fig. 6.

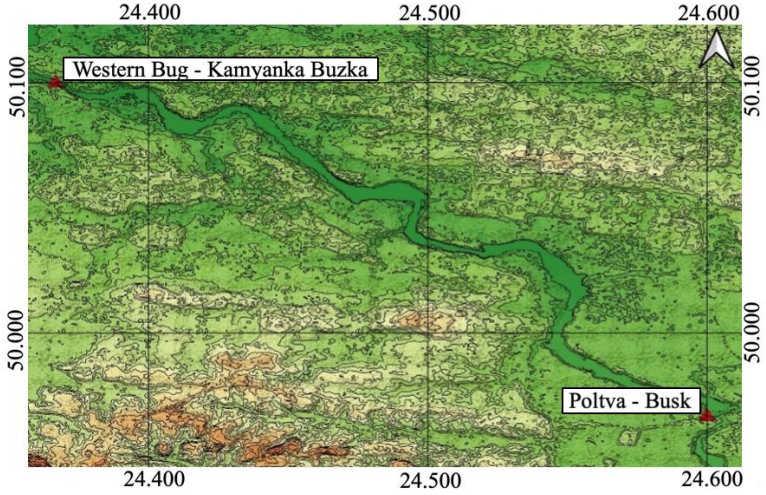

Fig. 4. DEM of the studied territory.

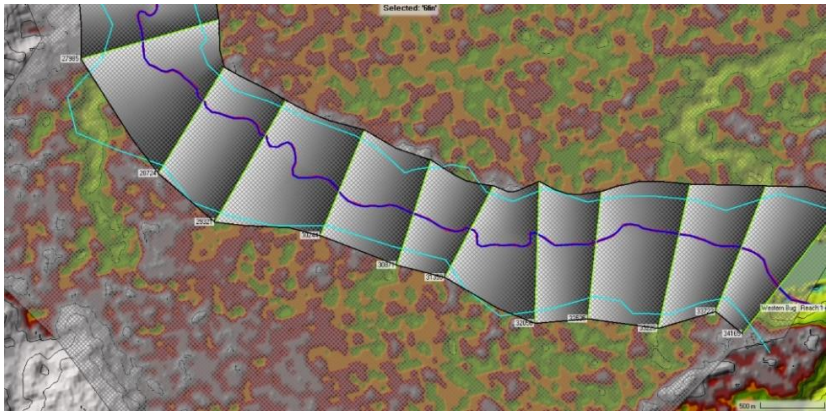

Fig. 5. One-dimensional flow model (HEC-RAS) Poltva river – WGS Busk

The next step is to build a two-dimensional (2D) flow model. At this stage, the territory for further analysis is determined by the polygonal layer, that is, in our case, the territory of the river's floodplain at the highest points of the terrain. In the constructed layer, it is necessary to specify the distance between the calculation points, which are the centers of the calculation cells. Choosing the smallest possible size is more expedient for greater calculation accuracy. For the study area, the distance between the plotted points is 5 m, respectively the number of calculated cells is about 500,000. It is also necessary to indicate the Manning roughness coefficients for individual sections, depending on the description of the watercourse and floodplain.

For the studied area, the Manning coefficients of the flow ranged from 0.06 for the channel to 0.10 for the floodplain. After entering all the necessary characteristics, the formation of the table of hydraulic characteristics of the calculation cells is started. Also, at this stage, the lines of limiting flow parameters are plotted on the map (Fig. 7)

To simulate flooding, enter the abscissa and ordinate values of the hydrograph and the river's slope in the "Unsteady flow data" tab.

After entering the input information, it is necessary to configure the parameters of the Unsteady Flow Analysis, namely, the calculation interval and the mapping interval. The calculation interval was chosen to be 1s, which corresponds to greater accuracy but is also more resource-intensive. The mapping interval has been adjusted to reflect the maximum runoff rate.

After processing the input information and checking for errors, a raster layer is created, showing the depth of flooding of the territory. For better display and the possibility of further processing, the flooding layer was imported into Quantum GIS (Fig. 8).

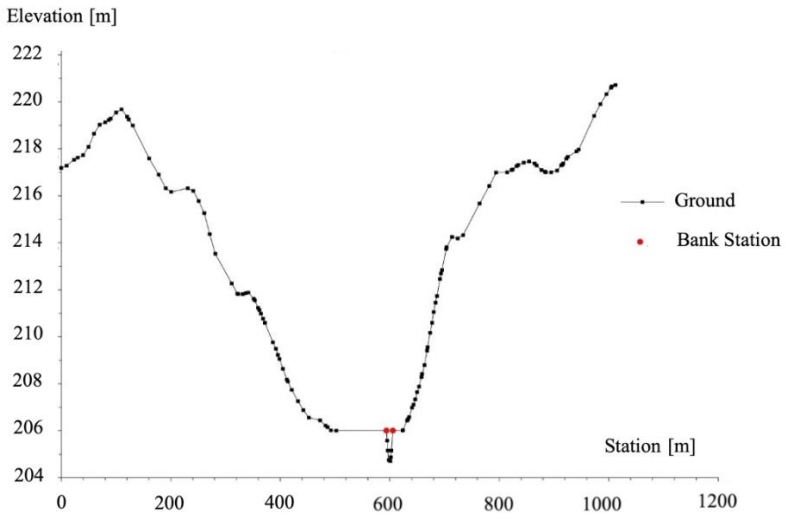

Fig. 6. Cross section of the Poltva river – WGS Busk.

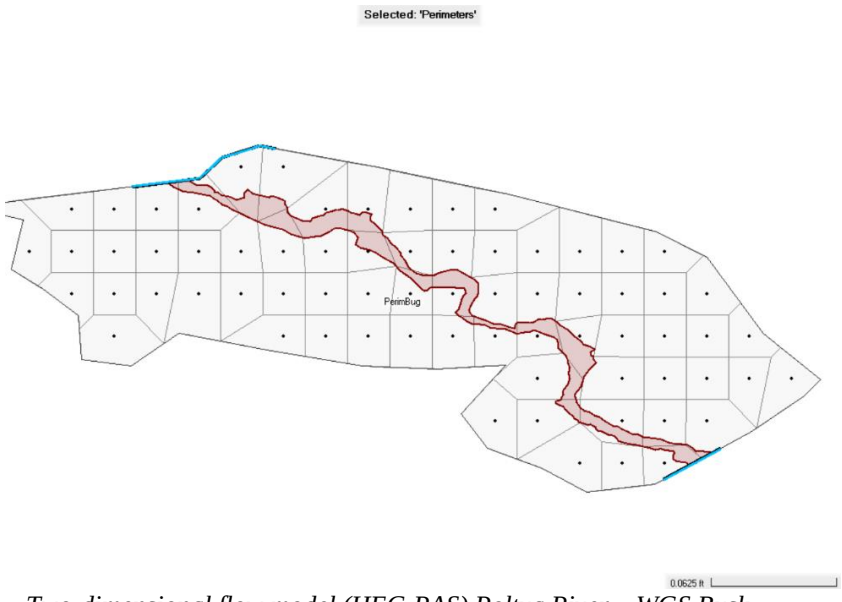

Fig. 7. Two-dimensional flow model (HEC-RAS) Poltva River – WGS Busk.

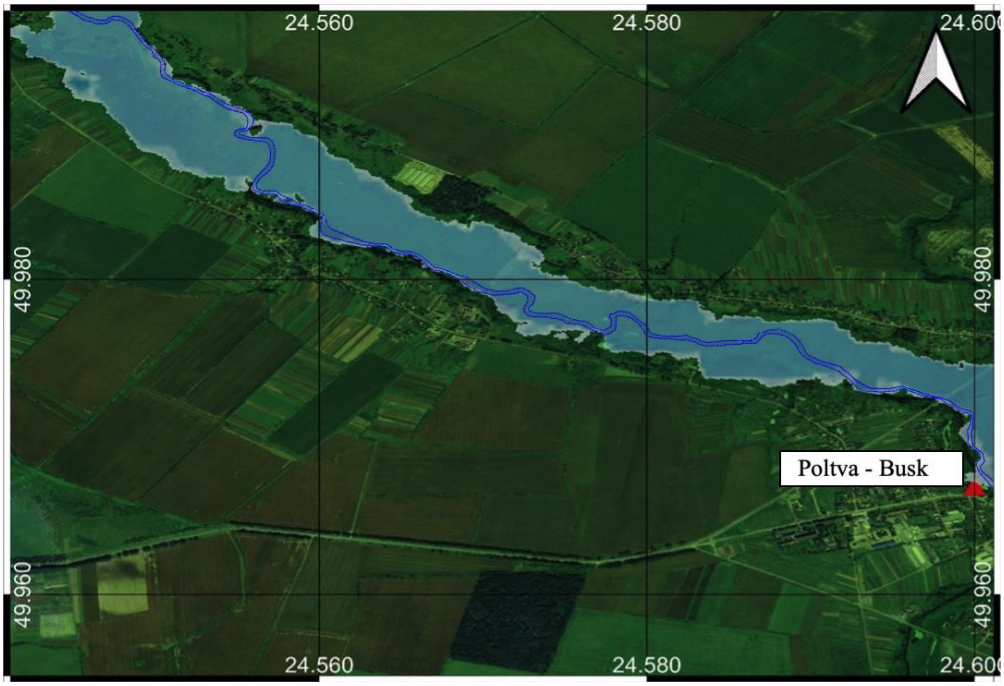

Fig. 8. Flood Hazard and Risk Map of Poltva river – WGS Busk.

Thus, flood zones were modeled in the study area. To further assess the threat of flooding and determine the possible damage, it is necessary to use cartographic data containing the coordinates and exact dimensions, including heights, of all infrastructure facilities (roads, bridges, power lines, dams), as well as agricultural land. To reduce the consequences of natural disasters, it is necessary to identify in advance many characteristics that affect the level of damage and determine the most effective and adequate measures to reduce it.

Conclusion

- Floods in the Vistula river basin are a dangerous hydrological phenomenon in all its sections, including the upper Vistula in Ukraine.
- Development and adaptation of modern methods for determining flood zones are part of the Integrated Flood Management and Vistula river basin management plans.
- As a result of the study, a method for determining inundation zones during spring floods using the example of the Poltva river within Vistula basin was justified.
- This methodology gives good results for a preliminary assessment of APSFR and can be used throughout the Vistula river basin within Ukraine. The constructed map allows identifying areas with potentially significant risks of flooding.
- In the future, such areas need to be carefully studied and the flood zones refined, taking into account field research data, particularly more accurate DEMs obtained from LiDAR images and actual sections of the stream.

References

Alekseev, H. (1955): Calculations of the flood runoff of rivers in the USSR. Leningrad: Gidrometeoizdat. 200 p. (in Russian).

Bildirici, I. O, Ustun, A., Ulugtekin, N., Selvi, H. Z., Abbak, R. A., Bugdayci, I., Dogru, A. O. (2007): SRTM Data In Turkey: Void Filling Strategy And Accuracy Assessment. In: The 4th Middle East Spatial Technology (MEST) Conference & Exhibition, 10–12 December, Bahrain.

Cyberski, J., Grześ, M., Gutry-Korycka, M., Nachlik, E., W. Kundzewicz, Z. W. (2006): History of floods on the River Vistula, Hydrological Sciences Journal, 51:5, 799–817, DOI: 10.1623/hysj.51.5.799

Farooq, M., Shafique, M., Khattak, M. S. (2019): Correction to Flood hazard assessment and mapping of River Swat using HEC-RAS 2D model and high-resolution 12-m TanDEM-X DEM (WorldDEM). Nat Hazards 97, 493. https://doi.org/10.1007/s11069-019-03644-x

Karwel, A. K., Ewiak. I. (2008): Estimation of the accuracy of the SRTM terrain model on the area of Poland, The International Archives of the Photogrammetry, Remote Sensing and Spatial Information Sciences. Vol. XXXVII. Part B7. Beijing 2008, pp. 169–172.

Manual to Determining the Calculated Hydrological Characteristics (1984): edited by A. Rozhdestvensky and A. Lobanova. Leningrad: Gidrometeoizdat. 447 p. (in Russian).

Marko, K., Elfeki, A., Alamri, N., Chaabani, A. (2019): Two Dimensional Flood Inundation Modelling in Urban Areas Using WMS, HEC-RAS and GIS (Case Study in Jeddah City, Saudi Arabia). In: El-Askary, H., Lee, S., Heggy, E., Pradhan, B. (eds) Advances in Remote Sensing and Geo Informatics Applications. CAJG 2018. Advances in Science, Technology & Innovation. Springer, Cham. https://doi.org/10.1007/978-3-030-01440-7_62

Martyniuk, M., Ovcharuk, V. (2020a): Determining the characteristics of the maximum runoff of the rare

probability of exceeding the Vistula River basin within Ukraine. Ecology, neo-ecology, environmental protection and sustainable use of nature: proceedings VIII international. Science. Conf. young scientists (Kharkiv, Ukraine, 229–231). (In Ukrainian).

Martyniuk, M., Ovcharuk, V. (2020b): Study the influence of zonal and azonal factors on the maximum flood runoff in the Vistula basin (within Ukraine). International Baltic Earth Secretariat Publication, 18, 209.

Nagaveni, C., Kumar, K. P., Ravibabu, M. V. (2019): Evaluation of TanDEMx and SRTM DEM on watershed simulated runoff estimation. J Earth Syst Sci 128, 2 (2019). https://doi.org/10.1007/s12040-018-1035-z

Parhi, P. K. (2018): Flood Management in Mahanadi Basin using HEC-RAS and Gumbel's Extreme Value Distribution. J. Inst. Eng. India Ser. A 99, 751–755. https://doi.org/10.1007/s40030-018-0317-4

Resolution of the Cabinet of Ministers of Ukraine on April 4, 2018 No. 247 On approval of the Procedure for developing a flood risk management plan / Official Gazette of Ukraine on April 24, 2018 – 2018, No. 32, p. 29, article 1116, act code 89821/2018

Sathya, A., Thampi, S. G. (2021): Flood InundationMappingof Cauvery River Using HEC-RASandGIS. In: Singh, R. M., Sudheer, K. P., Kurian, B. (eds) Advances in Civil Engineering. Lecture Notes in Civil Engineering, vol 83. Springer, Singapore. https://doi.org/10.1007/978-981-15-5644-9_2

Starodub, Y. P., Havrys, A. P. (2015): Use of HEC-GEORAS and HEC-RAS assistant software in territorial security projects. Project management and development of production, 1(53), 30–35. Luhansk. [In Ukrainian].

Šugareková, M., Zeleňáková, M. (2021): Flood risk assessment and flood damage evaluation–The review of the case studies, Acta Hydrologica Slovaca, vol. 22, no. 1, 156–163 DOI: https://doi.org/10.31577/ahs-2021-0022.01.0019

Wang, H., Zhou, J., Tang, Y., Liu, Z., Kang, A., Chen, B. (2021): Flood economic assessment of structural measure based on integrated flood risk management: A case study in Beijing. Journal of Environmental Management, 280, 111701

Maksym Martyniuk, Ph.D.-student of the Department of Land Hydrology
(*corresponding author, e-mail: martyniuk0904@gmail.com)
Valeriya Ovcharuk, Doctor of Geographical Sciences, Professor
Odessa State Environmental University
15 Lvovskaya Str.
Odessa, 65016
Ukraine

DOI: 10.31577/ahs-2023-0024.01.0012

ACTA HYDROLOGICA SLOVACA

Volume 24, No. 1, 2023, 101 – 112

Water erosion mapping using several erosivity factors in the Macta Basin (North-West of Algeria)

Khadidja SEMARI, Khaled KORICHI*

The quantification of the water erosion using empirical models has been applied for several regions around the world. Indeed, the model proposed by Wischmeier and Smith also called RUSLE model remains the most used approach. The main purpose of this work is to produce a soil losses vulnerability map of the Macta Basin and to determine its water erosivity potential, taking into account four rainfall erosivity indices that have been widely applied in the Mediterranean regions namely: Arnoldus index, MFI Modified Fournier Index, Roose index and Rango-Arnoldus index. The calculation of soil losses with the RUSLE model gives respectively the values: 7.94, 13.98, 12.5 and 20.6 t ha^{-1} $year^{-1}$. By comparing with other basins of the same characteristics, we note a good correlation.

KEY WORDS: Macta Basin, Water erosion, Rainfall erosivity, RUSLE, Soil loss

Introduction

The water erosion process at the catchment scale is characterized by three phases, namely: the tearing phase, the transport phase and the deposit or sedimentation phase. Downstream of the watershed, the storage capacity of the dams is reduced under the siltation effect, this is the case of the Fergoug dam in the wilaya of Mascara (North West of Algeria). Upstream of the watershed, there will be land losses, which causes a drop in agricultural production. The and losses vary from country to other but many work show that erosion is accelerated in the Maghreb countries.

In Algeria, and like most semi-arid zones, the consequences of water erosion are disastrous, offering a naked landscape and crisscrossed by an intense ravine, particularly in mountainous regions with a dense hydrographic network. The operational dams are therefore threatened, especially in the west of Algeria, given that 47% of all of its land is affected (Kouri, 1993; Gomer, 1992; Touaïbia, 2000). In Morocco, cumulative annual land losses are estimated at 100 million tons (Heusch, 1970). In Tunisia, water erosion totals 8.5 million hectares which represents 52% of the total country area (Cormary and Masson, 1964).

The intensity of water erosion depends on the climatic conditions, hence the rains erosivity, the slope which acts directly on the kinetic energy of the runoff, the cover land which absorbs the energy kinetics of the raindrops and increases the soil resistance against erosion, and finally soil erodibility which is closely related to the texture and soil structure.

To estimate and quantify water erosion, several scientific approaches are proposed in the literature. The simplest empirical models are applied only for sufficiently large spatiotemporal scales. More elaborate mechanistic models that estimate the spatial distribution of solid fluxes for each meteorological event. However, the availability and the quality of data required to estimate the risk of water erosion remains a real challenge especially in large ungauged catchments, but with the rapid development of GIS tools, empirical models have become more effective approaches and thus constitute a better decision-making tool.

Empirical models are hydrological models based on mathematical laws applied and validated in the laboratory or on experimental fields. The simplest and most widely used model, which relates soil loss to rainfall or runoff is governed by the Universal Soil Loss Equation (USLE) and carried out by (Wischmeier and Smith 1965; 1978). The modified version of the model, proposed by (Williams, 1975), estimates the solid transport of each storm by taking into account the volume of runoff instead of the rain erosivity (Djoukbala et al, 2018).

In this work we are interested in the mapping of the vulnerability to water erosion expressed in soil losses in the Macta Basin. A parametric investigation of the erosivity is thus carried out using four empirical formulas dedicated to Mediterranean semiarid catchments with ephemeral streams called also Wadis, to estimate their effects. The Macta Basin is characterized

by a long period of drought, over the period 1930–2002, from which annual rainfall recorded a drop of around 40% on average (Meddi et al, 2009), adding the predominance of silt and clayey-sandy textures. The consequences of water erosion are manifested by the siltation of the Fergoug dam located downstream of the Macta Basin. The mapping of areas with high water erosion requiring development has become essential to minimize the rate of siltation.

Materials and Methods

Study area

Located in the North-West of Algeria, the Macta Basin extends over an area close to 14400 km^2. It is limited to the North by the Mediterranean Sea, to the South by the Oran highlands, to the East by the Cheliff Zahrez region and to the West by the Tafna catchment and the Oran coast (Fig. 1).

The Macta Basin encompasses two representative sub-basins: Mekerra and Wadi El Hammam over which two main streams flow:

1. The Wadi Mekerra covers a distance of 115 km and takes its source from Ras El-Ma, precisely, in the heights of Djebel El-Beguira at an altitude of 1402 m, 86 kilometers from the center of Sidi Bel Abbes city. The Wadi Mekerra crosses obliquely, from the South-West to the North-East, dozens of rural and urban perimeters before flowing into the Macta marshes and then into the Mediterranean Sea (Semari and Benayada, 2019).
2. The Wadi El Hammam rises 16 km south-west of Ras El Ma at an altitude of 1100 m and travels 172 km in the south-east direction. It is formed by the confluence of three Wadis: Melrir, Hounet and Sahouet which join at the point named Trois Rivières (Fig. 1).

The Macta Basin is subject to the semiarid climate characterized by a cold winter and hot summer, it undergoes the Mediterranean influence in the North and the continental conditions in the South from where the precipitations are irregular in space and in time.

The northern borders where the marshes are located and the southern limits of the Macta Basin are characterized by low slopes which vary between 0 and 9%. Upstream of the marshes, most of the areas have steep slopes between 40 to 58%. To the east, the slopes range between 18 and 47%, while in the West the slopes are moderate and do not exceed 27% (Fig. 2).

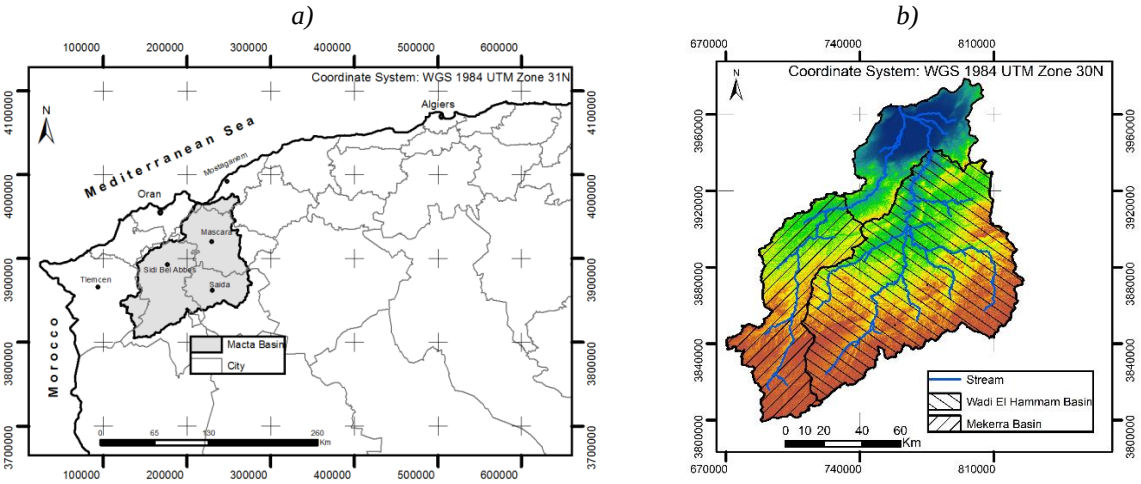

Fig. 1. a) Geographic location of the Macta Basin, b) sub-basins and hydrographic network.

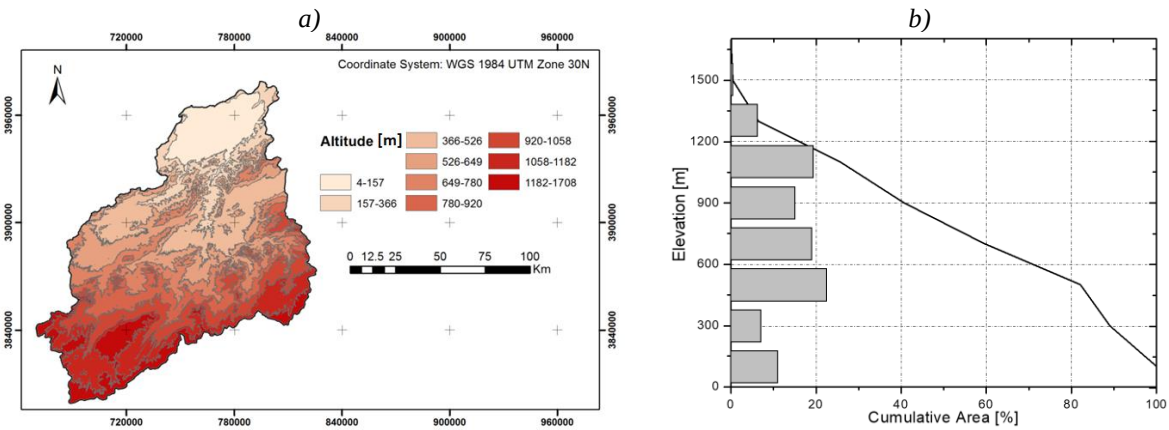

Fig. 2. a) Level curves map of the Macta Basin, b) Hypsometric curve.

The relief of the Macta Basin is characterized by the existence of plains interspersed with massifs:

- *Low coastal plain:* It is separated from the sea by a band of dune and has altitudes below 9 m. We notice the presence of water bodies, marshes and more or less humid steppes. Upstream, the plain extends to the southeast through the valleys of the Wadis of Sig and Habra.
- *Plain of Ghriss*: is located in the sub-basin of Wadi El Hammam and drained by Wadi Fekane. It is limited to the north by the mountains of Beni-Chougrane, to the south by the mountains of Saïda, to the west by the valley of Wadi Melrir. The average altitude is 500 m. It has no outlet to the sea; which has favored the frequent presence of floodplains.
- *Plain of Sidi Bel Abbes:* Located in the sub-basin of Wadi Mekerra. It is bordered to the north by the Tessala Mountains, to the south by the Tlemcen and Saïda mountains, to the west by the Wadi Isser valley and to the east by the Beni-Chougrane Mountain chain. The plain of Sidi Bel Abbes is classified as flood prone.
- *Beni-Chougrane's mountains:* They separate both plains of the Mascara province; the peak can reach 910 m. These massifs are covered by forests and scrubland or maquis which are subject to degradation linked to soil erosion and the intensity of human activity.
- *Mountains of Tessala*: constitute a complex massif of an average altitude of 800 m, where the highest point reaches 1061 m. They are crossed by the Mebtouh Wadi before it joins the lower low plain. They limit the Macta Basin to the West and North-West. In the South-West, the Tessala Mountains are relayed by the eastern part of the Tlemcen Mountains.

According to Strahler (1952), the hypsometric curve can give indications on the dynamic equilibrium state of the watershed. The shape of the hypsometric curve (Fig. 2) shows that the Macta Basin is an erosive basin which presents non-equilibrium (young) stage.

Data collection

Fig. 3 schematizes the flowchart of the followed operations to estimate the soil losses in the Macta Basin. The used data are from different sources (Fig 3.) and have been projected in the WGS 84 system, UTM zone 30. One cites:

1. Climate data provided by the National Agency of Hydraulic Resources (NAHR) from forty-two (42) gauge stations distributed throughout the Basin, for a study period which extends from 1967 to 2011 (Fig. 4).
2. Soil data was provided from Harminised World Soil Database HWSD.
3. Topographic data with (30m x 30 m) resolution from SRTM (Shuttle Radar Topography Mission).
4. Satellite images from Landsat 8 (2007) to see the evolution of the density of the vegetation cover.

All the collated data were used to estimate the parameters defied below of the Revised Universal Soil Loss Equation. Data processing was carried out with the ArcGis V.10.4 geographic information system.

RUSLE model factors

The model proposed by Wischmeier and Smith (1965; 1978) is the most commonly used for the quantification of soil losses. This model requires available data on the watershed such as topography, soils, rainfall, landcover, cropping systems and erosion control practices. The Universal Soil Loss Equation (USLE) is written as follows:

$$A = R \times K \times LS \times C \times P \quad (1)$$

where

A is the annual soil loss rate (t ha^{-1} $year^{-1}$);
R is the rainfall erosivity factor expressed in Mega-Joule mm ha^{-1} $hour^{-1}$$year^{-1}$;
K is the soil erodibility factor (t ha $hour^{-1}$$ha^{-1}$$MJ^{-1}$$mm^{-1}$);
LS is a dimensionless factor that represents the slope (S in %) and the length of the slope (L in m);
C is dimensionless factor of plant cover and cropping practices;
P is a dimensionless factor related to land use and the conservation practices.

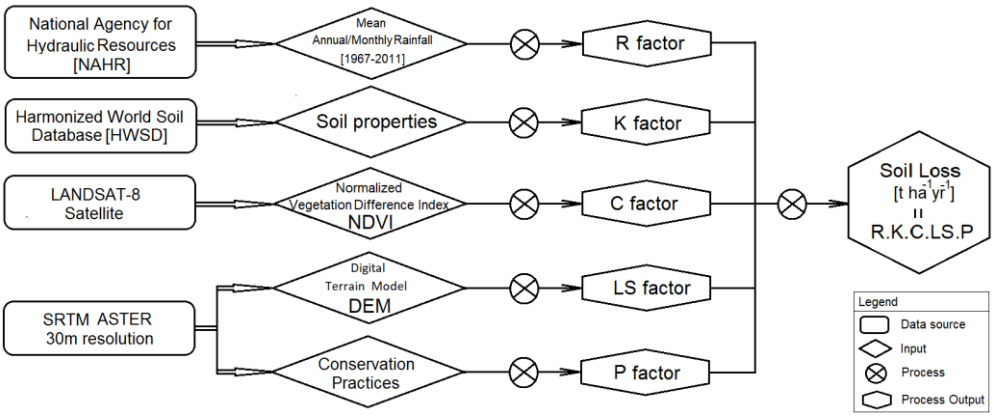

Fig. 3. Methodological flowchart of water erosion mapping.

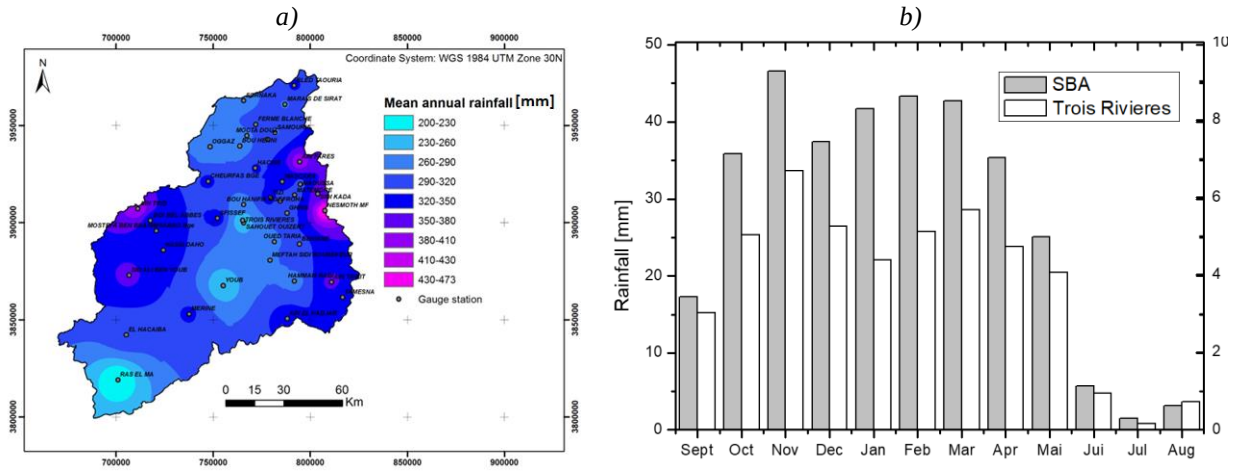

Fig. 4. a) Spatial distribution of average annual precipitation, b) Histogram of monthly precipitation at the stations of Sidi Bel Abbes and the Trois Rivieres.

Rainfall erosivity indices

In the literature, several authors have proposed a variety of rainfall erosivity indices. In this study we are mainly interested in four indices such as: 1) Erosivity index of Arnoldus, 2) Modified Fournier Index, 3) Roose's erosivity index and Rango-Arnoldus index:

Arnoldus Index

The Arnoldus formula (Arnoldus, 1980) translates a linear regression with the Modified Fournier Index according to equation (2).
This combination has been tested and applied in the regions of West Africa.

$$\mathrm{R1} = 0.66\mathrm{MFI} - 3 \tag{2}$$

Modified Fournier Index (MFI)

The (MFI) index proposed by Arnoldus (1980), consists of using the sum of the Fournier indices for the twelve months of the year, it is the sum of the ratio of the squares of the average monthly rainfall and the average annual rainfall.

$$R2 = MFI = \sum_{i=1}^{12} \left(\frac{P_i^2}{P}\right) \tag{3}$$

Roose erosivity index

Roose's work (Roose, 1981), for over than 20 years of measurements, led to the proposal of simple empirical relationships, linking the erosivity index to the average annual rainfall P_{an} for the same period such as:

$$R3 = a\, P_{an} \tag{4}$$

The value of (a) is around 0.1 to 0.12 in northwestern Algeria (Morsli et al, 2004).

Rango-Arnoldus index

An alternative formula, that involves monthly and annual precipitation to determine the R factor, are proposed by Arnoldus (Rango and Arnoldus, 1987). It has been applied by several authors for the quantification of erosion in the Maghreb regions is presented in the form:

$$\mathrm{Log\ R4} = 1.74.\mathrm{Log} \sum \left(\mathrm{Pi}^2/\mathrm{P}\right) + 1.29 \tag{5}$$

where
R4 – is in [MJ mm ha^{-1} hour^{-1} year^{-1}]
Pi and *P* – represents respectively the monthly and mean annual rainfall in [mm]

Soil erodibility factor (K)

This factor reflects the resistance of a soil to water erosion. The *K* factor depends on several properties of the soil in particular; the percentage of sand, silt and clay and also the content of organic matter and permeability. Based on Global Harmonized Soil data version 1.2, one can establish the map of soil properties in the study area. The value of the soil erodibility is calculated using the formula proposed by (Neitsch et al, 2011).

$$K = f_{csand} \cdot f_{cl-si} \cdot f_{orgc} \cdot f_{hisand} \tag{6}$$

where
f_{csand} – decreases the value of *K* in case of high coarse sand content and increases it in case of fine sand soil;
f_{cl-si} – decreases the value of *K* for soils with a high ratio of clay to silt;
f_{orgc} – decreases the value of *K* for soils with high organic matter content;
f_{hisand} – decreases the value of *K* for soils with a very high sand content.

Each parameter is given as:

$$f_{csand} = 0.2 + 0.3.exp\left[-0.256.m_s.\left(1-\frac{m_{silt}}{100}\right)\right] \quad (7)$$

$$f_{cl-si} = \frac{m_{silt}}{m_{silt}+m_c} \quad (8)$$

$$f_{orgc} = 1 - \frac{0.25.orgC}{orgC+exp(3.72-2.95.orgC)} \quad (9)$$

$$f_{hisand} = 1 - \frac{0.7.\left(1-\frac{m_S}{100}\right)}{1-\frac{m_S}{100}+exp\left[-5.51+22.9.\left(1-\frac{m_S}{100}\right)\right]} \quad (10)$$

where

m_s – is the percentage of sand content in where the particle diameter is between 0.05 and 2 mm;

m_{silt} – is the percentage of silt content with particle diameters between 0.002 and 0.05 mm;

m_c – is the percentage of the clay content whose particle diameters are less than 0.002 mm;

$orgC$ – is the percentage of organic carbon content.

Land cover factor (C)

The land cover plays an important role in soil protection, land losses decrease with the increase in the landcover rate. Many studies have been proposed to estimate the *C* factor using the Normalized Vegetation Difference Index (NDVI) (Lin et al., 2002; Wang et al., 2002). Knowing that the vegetation absorbs a significant part of the solar radiation in the red band and it reflects it to the maximum in the near infrared band, this index is determined as follows:

$$NDVI = \frac{PIR-R}{PIR+R} \quad (11)$$

where:

PIR – Numerical value of the same pixel in the near infrared band (between 0.55 and 0.68μm);

R – Numerical value of the same pixel in the red band (between 0.73 and 1.1 μm).

The NDVI value varies between -1 and +1; negative values correspond to surfaces other than plant cover, such as snow, water or clouds for which the reflectance in the red band is greater than that of the near infrared. For bare soils, the reflectance being roughly of the same order of magnitude in the red and the near infrared where the NDVI is close to zero. On the other hand, the plant formations, have positive NDVI values, generally between 0.4 and 0.7. The highest values correspond to very dense plant cover.

NDVI data are obtained from the Landsat-8 satellite. To estimate the C factor, several authors have developed regressions with NDVI (Karaburun, 2010; Ouallali et al, 2016). Since our study area is located in the North-West of Algeria, it is more convenient to select the regression proposed by (Toumi et al, 2013) given as:

$$C = 0.9167 - 1.1667NDVI \quad (12)$$

Topographic factor (LS)

The slope plays a crucial role in the process of uprooting, transport and sediments deposition. Runoff increases with the slope increasing. Several formulas allow the evaluation of the LS factor from the DEM, such as that of Kalman (1967), David (1987) and Mitasova et al. (1996). In our case, we use the formula of (Wischmeier and Smith, 1978) given by:

$$LS = \left(\frac{L}{22.13}^{m}\right)(0.065 + 0.045S + 0.0065S^2) \quad (13)$$

where:

L – is the length of the slope in [m];

S – the inclination of the slope in [%];

m – is a classification parameter such:

m=0.5 if the S >5%,

m=0.4 if 3.5% < S < 4.5%;

m=0.3 if 1< S < 3%,

m=0.3 if S < 1%.

Soil conservation practices factor (P)

The *P*-factor takes into account anti-erosion practices and cultivation techniques used to reduce the runoff effect and erosion. Among these techniques, we find contour farming, the laying of grassy strips between two cultivation areas, natural or artificial mulching, and the laying of cover crops. Based on the work of (Roose, 1994), the P value is determined from the following Table 1.

Table 1. *P*-factor classes (Roose, 1994)

Land-use type	*P*-factor
Degraded bare ground	1
Fallow	1
Big cultures	0.7
Low density forest plantation	0.5
Vegetable crops	0.5
Arboriculture	0.5
Contour ploughing	0.2
Planting on terraces	0.14
Water body	0

Results and discussion:

R-erosivity factor

The erosivity maps generated from the rainfall data of the 42 stations, and using the four empirical formulas give the same erosivity distribution. They thus show that the values of the R1, R2, R3 and R4 factors in the Macta Basin vary from 9.54 (Arnoldus) to 73 (Rango-Arnoldus) MJ mmha^{-1}hour^{-1}year^{-1} (Table 2). The high values are recorded at the eastern and western of the basin borders, while the southern areas indicate lower values (Fig. 5). It can thus be seen that erosivity is directly related to

the precipitation (Fig. 3a), both distribution are well correlated.

The erosivity indices Rare distributed in the Macta Basin into four classes, R1, R2, R3 and R4. With the exception of the Roose index, the other approaches show that the high erosivity class has a low percentage (Table 2), (R1 6.01%, R2 6.49%, R3 18.36%, R4 6.92%). The low erosivity classes also occupy small areas (R1 8.52%, R2 8.45%, R3 8.51%, R4 8.55%). The average erosivity class dominates the surface of the Macta Basin with values from R1 (15.17) to R4 (57.09) MJ mm ha^{-1} $hour^{-1}$ $year^{-1}$. Given the large surface area of the Macta Basin, the range of precipitation values (200–473 mm) is wide enough that the variance is also high and the extrema values (min and max) occupy a small part of the basin.

Table 2. Distribution of R-erosivity factors in the Macta Basin

R1 Arnoldus Classes	Area [ha]	Area [%]	R2 MFI Classes	Area [ha]	Area [%]
9.54–15.17	122640.61	8.52	19–27.53	121721.89	8.45
15.17–18.96	620097.61	43.06	27.53–33.27	600931.66	41.73
18.96–22.39	610638.53	42.41	33.27–38.47	623844.48	43.33
22.39–31.98	86593.27	6.01	38.47–53	93471.97	6.49
Total	1439970	100	Total	1439970	100
R3 Roose Classes	Area [ha]	Area [%]	R4 Rango-Arnoldus Classes	Area [ha]	Area [%]
20–26.35	122497.22	8.51	34–44.45	123063.24	8.55
26.35–30.16	495484.63	34.41	44.45–51.28	597000.94	41.46
30.16–33.45	557624.12	38.72	51.28–57.09	620248.24	43.07
33.45–47	264364.03	18.36	57.09–73	99657.58	6.92
Total	1439970	100	Total	1439970	100

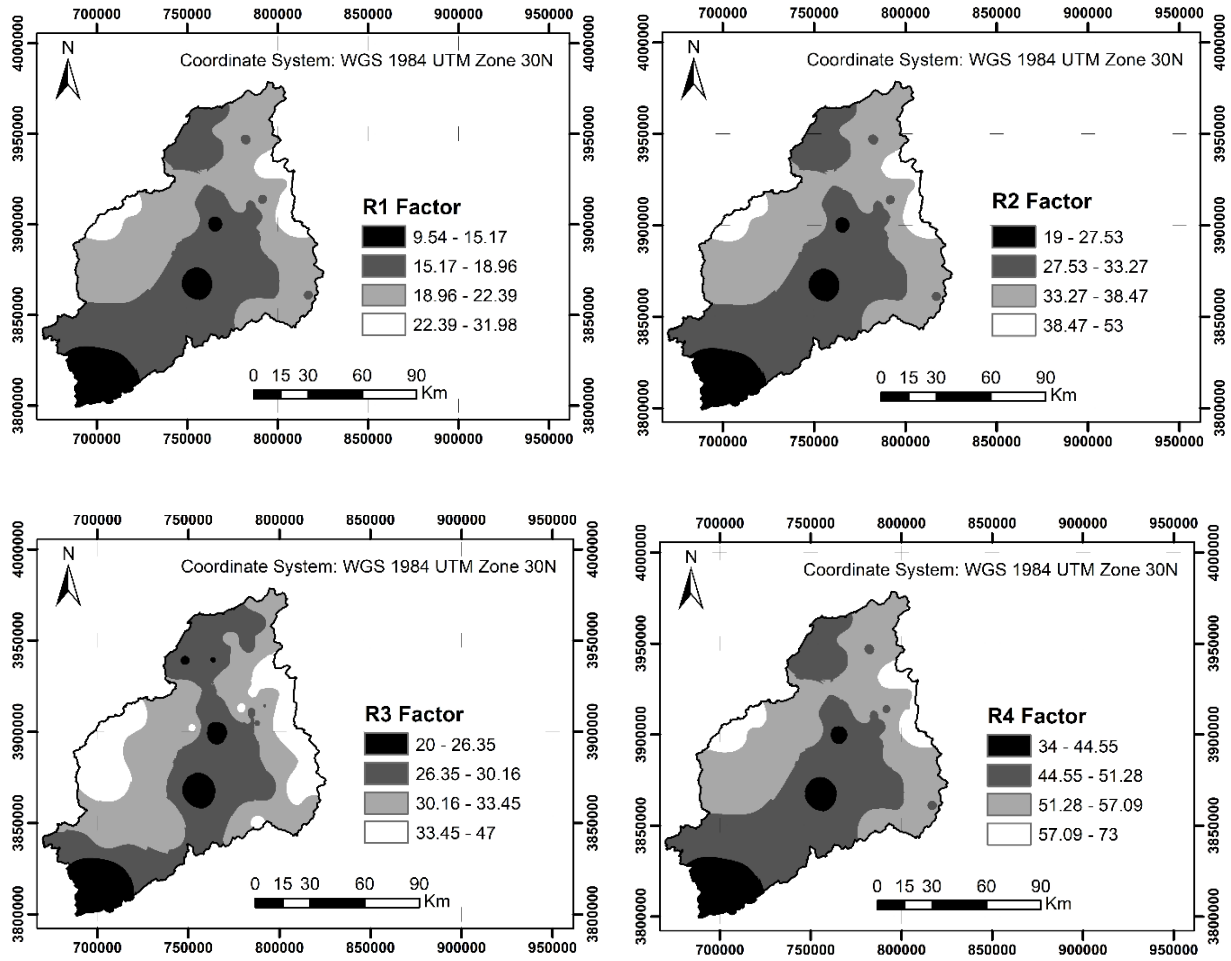

Fig. 5. Spatial distribution of R-erosivity factors in the Macta Basin.

K-erodibilityfactor

Fig. 6a indicates the classification of soils in the Macta Basin, one can see that grazing areas dominate the surface of the basin. The spatial distribution of the erodibility classified into four groups (Fig. 6b) indicates that the soil *K*-erodibility factor in the Macta Basin ranges from 0.0138 to 0.0227 t ha hour MJ^{-1} ha^{-1} mm^{-1}. Almost half of the basin surface (58.35%) has a low *K* index (0.013) Table 3.

C-landcover factor

Using the NDVI map (Fig. 7a), the spatial distribution of the *C*-landcover factor of the Macta Basin is generated using ArcGIS software. The values of C factor observed over the entire study area vary from 0.09 to 1.8. More than 60% of the area of the basin has very low vegetation cover, 8% of the area has a *C* index less than 0.5. Values below 0.5 refer to dense forests, dense scrubland or matorral and arboriculture. Values between 0.5 and 0.9 are assigned to areas covered with sparse forests. Values tending to 1 are related to bare soil and harvested cropland (Table 4).

LS-slope factor

Erosion has been shown to increase exponentially with the degree and length of slope inclination represented by the *LS* factor. The length *L* and the slope *S* are very decisive parameters in the erosion process. Thus, the transport accelerates downward due to the increase in the kinetic energy of the runoff. In the Macta Basin, the distribution of the LS factor has been classified into five groups (Table 5). The highest values of *LS* are noticed from upstream to downstream and show a southwest-northeast orientation; they are mainly concentrated in the eastern side of the Macta Basin (Fig. 8). The *LS* low values are observed in the plain, this corresponds to 1) low altitude areas, concentrated mainly in the western part of the basin, 2) plain areas such as the plains of Ghris, Sidi Bel Abbes and of Mohammadia and 3) to the floodplains of Wadi Mekerra and Wadi El Hammam.

Table 3. Distribution of the *K*-erodibility factor in the Macta Basin

K factor classes	Area [ha]	Area [%]
0.013885	840231.70	58.35
0.01594	433841.30	30.13
0.018043	15355.20	1.07
0.02276	150541.80	10.45
Total	1439970	100

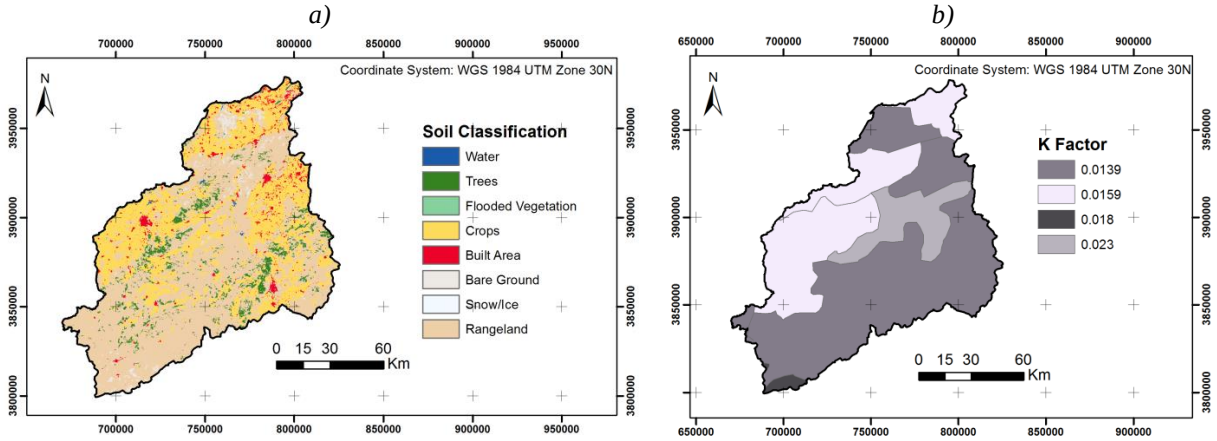

Fig. 6. a) Spatial distribution of soils and b) erodibility factor K in the Macta Basin.

Table 4. Distribution of the *C*-landcover factor in the Macta Basin

Classes *C* factor	Area [ha]	Area [%]
0.09–0.57	121753.27	8.46
0.57–0.66	342287.45	23.76
0.66–0.75	521277.37	36.20
0.75–0.88	450792.44	31.31
0.88–1.18	3859.47	0.27
Total	1439970	100

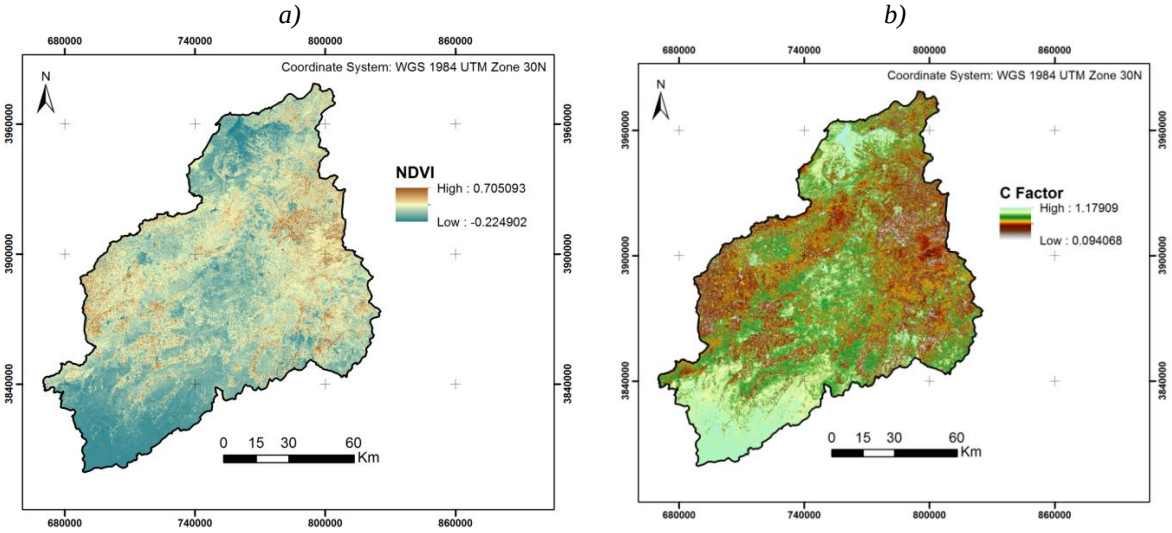

Fig. 7. a) Spatial distribution of NDVI and b) Landcover in the Macta Basin.

Table 5. Distribution of *LS*-factor in the Macta Basin

Classes *LS* factor	Area [ha]	Area [%]
0–0.59	1182214.91	82.10
0.59–2.95	197462.31	13.71
2.95–7.37	45151.38	3.14
7.37–15.33	12823.29	0.89
15.33–75.17	2318.11	0.16
Total	1439970	100

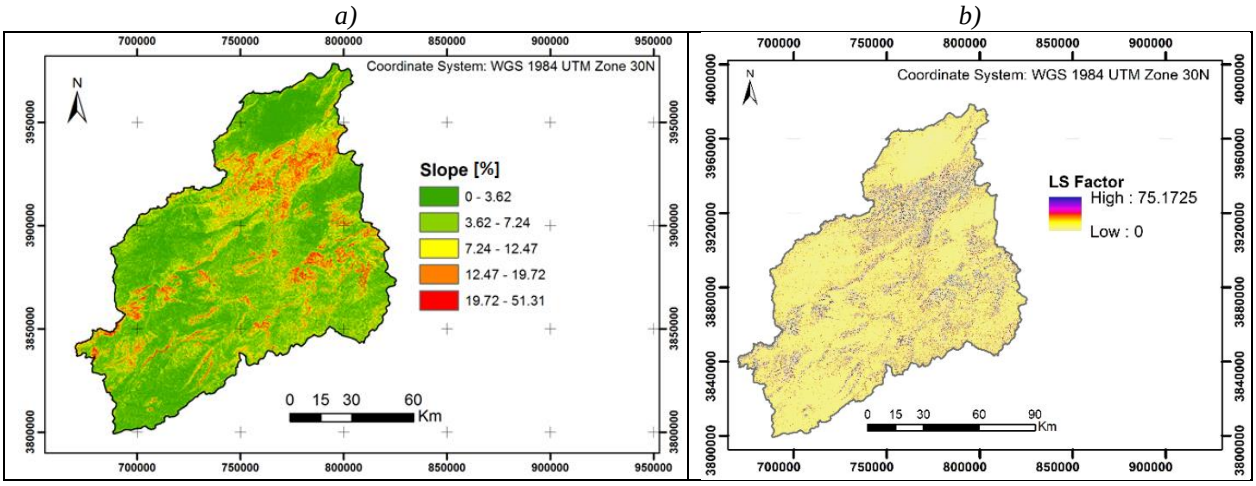

Fig. 8. a) Spatial distribution of the slope [%] and b) LS-slope factor in the Macta Basin.

P-Occupation factor

The *P*-factor takes into account control practices that reduce the erosion potential of runoff in terms of its concentration, velocity and hydraulic forces applied on the soil surface. Support practices include contour tillage, strip-cropping on the contour, and terrace systems. Table 6 summarizes the *P* values in hectares and in [%]. It can be seen that the maximum values coincide with those of the steep slopes following the southwest-northeast orientation (Fig. 9).

RUSLE Soil loss

The average annual soil losses in the Macta Basin have been calculated with the RUSLE model using the four

empirical erosivity formulas discussed above. The erosivity factors are calculated from rainfall data from 42 stations over 45 years (1967–2011). The vector product of the five factors is produced using ArcGIS software and gives a spatial resolution matrix of 30 m x 30 m. These are the four maps showing average soil losses in [t $ha^{-1}year^{-1}$] (Fig. 10). The soil loss classes are summarized in Table 7, from which the mean values are respectively; 7.94, 13.98, 12.5 and 20.6 t ha^{-1} $year^{-1}$. We notice that the model calculated based on R1 Arnoldus indices, underestimates the value of RUSLE, on the other hand the RUSLE obtained by R4 Rango-Arnoldus indices overestimates the soil losses. The results obtained with the R2 (MFI-indices) and R3 (Roose index) show a good correlation with other Algerian basins with similar climatic and environmental characteristics and extracted from the literature, such as 1) the Wadi Mina 11.2 t $ha^{-1}year^{-1}$ (Benchettouh et al., 2017); 2) Wadi Boumahdane basin of 11.18 t ha^{-1} $year^{-1}$ (Bouguerra et al., 2017); 3) basin of the Wadi Sahouat between 12 and 16 t ha^{-1} $year^{-1}$ (Toubal et al., 2018) and 4) Wadi Gazouana between 9.65 and 11.33 t ha^{-1} $year^{-1}$ (Djoukbala et al., 2018).

Table 6. Distribution of *P*-occupation factor in the Macta Basin

Classes *P* factor	Area [ha]	Area [%]
0–0.55	1045732.62	72.62
0.55–0.78	215552.53	14.97
0.78–1	178684.85	12.41
Total	1439970	100.00

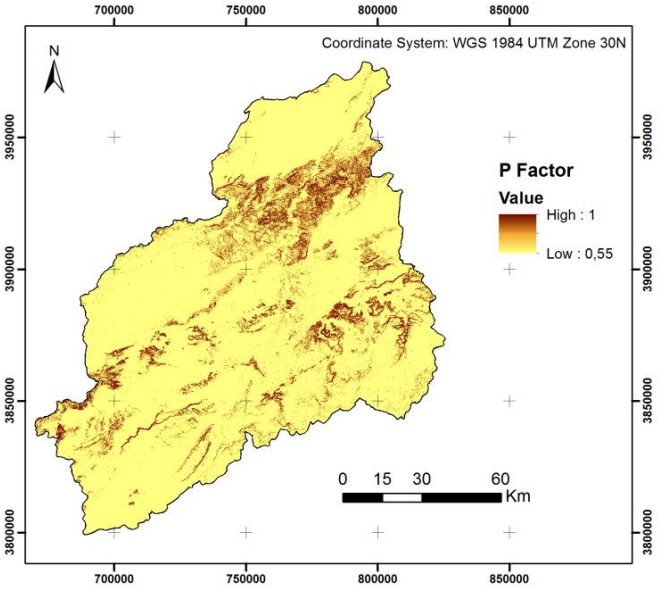

Fig. 9. Spatial distribution of the P-factor in the Macta Basin.

Table 7. Distribution of the soil losses in Macta Basin

RUSLE 1 Classes	Mean [t $ha^{-1}year^{-1}$]	Area [ha]	Area [%]	RUSLE 2 Classes	Mean [t ha^{-1} $year^{-1}$]	Area [ha]	Area [%]
0–0.17		1384676.68	96.16	0–0.65		1384892.62	96.18
0.17–1.35		41548.26	2.89	0.65–2.38		41359.33	2.87
1.35–3.32	7.94	10670.31	0.74	2.38–5.84	13.98	10656.94	0.74
3.32–15.69		3074.75	0.21	5.84–27.59		3061.11	0.21
Total		1439970	100	Total		1439970	100
RUSLE 3 Classes	Mean [t ha^{-1} $year^{-1}$]	Area [ha]	Area [%]	RUSLE 4 Classes	Mean [t ha^{-1} $year^{-1}$]	Area [ha]	Area [%]
0–0.60		1384897.75	96.18	0–1.01		1385826.75	96.24
0.60–2.19		41377.58	2.87	1.01–3.72		40656.30	2.82
2.19–5.39	12.5	10630.94	0.74	3.72–8.96	20.6	10411.98	0.72
5.39–25.44		3063.73	0.21	8.96–43.14		3074.97	0.21
Total		1439970	100	Total		1439970	100

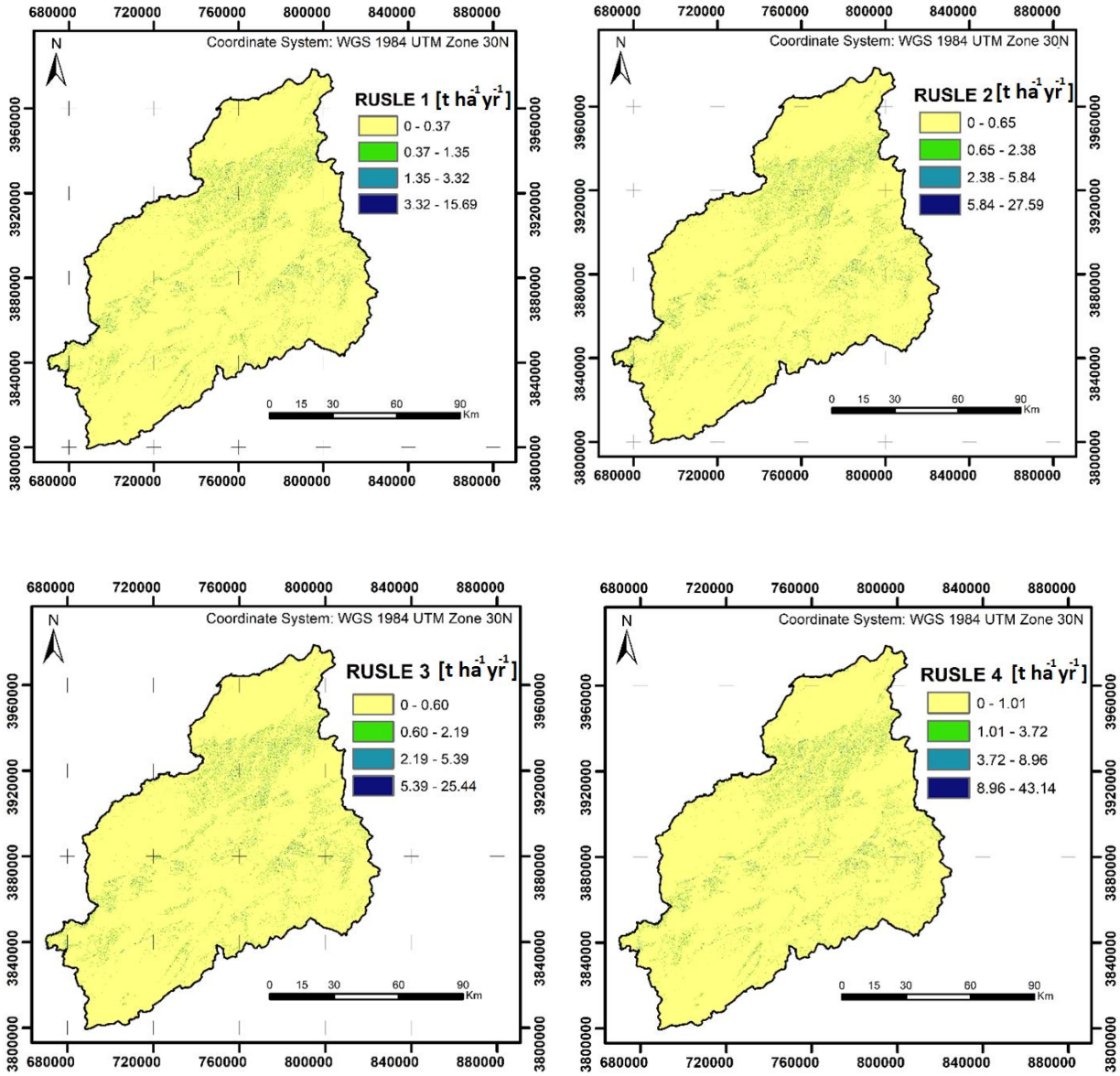

Fig. 10. Spatial distribution of different soil loss in the Macta Basin.

Conclusion

This study focuses on the estimation of soil losses by water erosion in the Macta Basin located in northwest Algeria using the Revised Universal Soil Loss RUSLE model proposed by Wischmeier and Smith. The spatial distribution of the soil losses is thus parameterized using four empirical erosivity factors; (Arnoldus, MFI, Roose and Rango-Arnoldus) and indicates an average values of 7.94, 13.98, 12.5 and 20.6 t ha^{-1} $year^{-1}$ respectively. With the exception of the value calculated using Rango-Arnoldus indices (20.6 t ha^{-1} year-1) and by comparing with other similar Algerian basins, the calculated results are in good agreement. These results also show that about 0.21% of the surface of the watershed has a higher erosion rate, greater than 5 (t ha^{-1} $year^{-1}$), observed on the hills and lands characterized by steep slopes of the catchment. This explains the severity of the soil degradation especially upstream of the Macta Basin due to the lithology, aggressive climate but also unfavourable land use.

Erosion maps, obtained from the four erosivity approaches, provide useful information for selecting suitable areas for planning conservation and preservation works. The modeling of soil loss remains an investigation subject given the complexity of natural phenomena and the non-linearity of the relationships between the intervening variables. However, the use of empirical models is still part of the decision-making tools. It thus has several advantages in terms of mitigating risk with perimeters protection and also to predict soil protection

scenarios by planning intervention works to fight against the phenomenon of water erosion.

References

Arnoldus, H. M. J. (1980): An Approximation of the Rainfall Factor in the Universal Soil Loss Equation. In: De Boodt, M. and Gabriels, D., Eds., Assessment of Erosion, John Wiley and Sons, New York, 127–132.

Benchettouh, A., Kouri, L., Jebari, S. (2017): Spatial estimation of soil erosion risk using RUSLE/GIS techniques and practices conservation suggested for reducing soil erosion in Wadi Mina watershed (northwest, Algeria). Arab J Geosci. https://doi.org/10.1007/s12517-017-2875-6

Bouguerra, H., Bouanani, A., Khanchoul, K. Derdous, O., Tachi, S. (2017): Mapping erosion prone areas in the Bouhamdane watershed (Algeria) using the Revised Universal Soil Loss Equation through GIS. J Water LandDev 32:13–23. https://doi.org/10.1515/jwld-2017-0002

Cormary, Y., Masson, J. (1964): Etude de conservation des eaux et du sol au Centre de Recherches du Génie Rural de Tunisie: application à un projet-type de la formule de perte de sols de Wischmeier. Cahiers ORSTOM, série pédologie 2.3:3–26. ISSN 0029-7259 (in french).

David, W. P. (1987): Soil and water conservation planning. Policies, Issues and recommendations. DENR Quezon City. Journal of Philippine Development, N26, Volume 15, 47–84.

Djoukbala, O., Hasbaia, M., Benselama, O., Mazour, M. (2018): Comparison of the erosion prediction models from USLE, MUSLE and RUSLE in a Mediterranean watershed, case of Wadi Gazouana (N-W of Algeria). Model. Earth Syst.Environ. https://doi.org/10.1007/s40808-018-0562-6

Gomer D. (1992): Ecoulement et érosion dans des bassins versants à sols marneux sous climat semi-aride méditerranéen. GTZ - ANRH 1992; 207 p (in french).

Heusch, B. (1970): L'érosion dans le Prérif: Une étude quantitative de l'érosion hydraulique dans les collines marneuses du Prérif occidental. Annales des recherches forestières, 12, 9–176 (in french). https://doi.org/10.1080/01431160110114538

Kalman, R. (1967): Essai d'évaluation pour le pré-Rif du facteur couverture végétale de la formule de Wischmeier de calcul de l'érosion. Rapport pour l'administration de la forêt et d'eau, Rabat, 1–12 (in french).

Karaburun, A. (2010): Estimation of C factor for soil erosion modeling using NDVI in Buyukcekmece watershed. Ozean Journal of Applied Sciences 3(1) (in french).

Kouri, L. (1993): L'érosion hydrique des sols dans le bassin versant de l'oued Mina. Etudedes processus et type de fonctionnement des ravins dans la zone des marnes tertiaires (in french). PhD Theisis,University of Louis Pasteur, Strasbourg, France.

Landsat 8 (2007): https://earthexplorer.usgs.gov/

Lin C.-Y., Lin W. T., Chou W. C. (2002): Soil erosion prediction and sediment yield estimation: the Taiwan experience. Soil Tillage Res68:143–152. https://doi.org/10.1016/S0167-1987(02)00114-9

Meddi, M., Talia, A., Martin, C. (2009): Evolution récente des conditions climatiques et des écoulements sur le basin versant de la Macta (Nord-ouest de l'Algérie). Physio-Géo – Géographie Physique et Environnement, vol III (in french).

Mitasova, H., Hofierka, J., Zlocha, M. (1996): Modeling topographic potential for erosion and deposition using GIS. International Journal of Geographical Information Science. 10, 629–641.

Morsli, B., Halitim, A. Roose, E. (2004): Effet des systèmes de gestion sur le ruissellement,l'érosion et le stock de Carbone ; du sol dans les monts de Beni-Chougrane (Algérie). Bull RéseauErosion, IRD France, 23: 416–430 (in french).

Neitsch, S., Arnold, J., Kiniry, J., Williams, J. (2011): Soil & water assessment tool theoretical documentation version 2009. Texas Water Resources Institute, 1–647

Ouallali, A., Moukhchane, M., Aassoumi, H., Berrad, F., Dakir, I. (2016): Evaluation and mapping of water erosion rates in the watershed of the Arbaa Ayacha River (Western Rif, Northern Morocco). Bulletin de l'Institut Scientifique, Rabat, Section Sciences de la Terre, 38, 65–79 (in french).

Rango, A., Arnoldus, H. M. J. (1987): Aménagement des bassins versants. Cahiers techniquesdela FAO.

Roose, E. (1981): Dynamique actuelle de sols ferralitiques et ferrugineux tropicaux d'Afrique Occidentale. Étude expérimentale des transferts hydrologiques et biologiques de matièressous végétation naturelles ou cultivées. ORSTOM, Paris (France). Collection travaux et docu-ments, no 130, Thèse d'État Orléans. 569 p (in french).

Roose, E. (1994): Introduction à la gestion conservatoire de l'eau, de la biomasse et de la fertilité dessols (GCES) Bull. Pédol. FAO, 70, 420 p (in french).

Semari, K., Benayada, L. (2019): Situation des ressources en eau du bassin versant de la Macta (nord-ouest Algérien), Techniques – Sciences – Méthodes (in french). https://doi.org/10.1051/tsm/201909065

SRTM (Shuttle Radar Topography Mission), https://lpdaac.usgs.gov/products/astgtmv003/

Touaibia, B. (2000): Erosion transport solide -envasement de barrages. Cas du bassin versant del'oued Mina. Thèse de Doctorat d'Etat, INA, El-Harrach, Algérie (in french).

Toubal, A. K., Achite, M., Ouillon, S., Dehni, A. (2018): Soil erodibility mapping using the RUSLE model to prioritize erosion control in the Wadi Sahouat basin, North-West of Algeria. Environ MonitAssess. https://doi.org/10.1007/s10661-018-6580-z

Toumi, S., Meddi, M., Mahé, G., Brou, Y. T. (2013): Cartographie de l'érosion dans le bassin versant de l'Oued Mina en Algérie partélédétection et SIG. Hydrol Sci J 58:1542–1558 (in french). https://doi.org/10.1080/02626667.2013.824088

Wang, G., Wente, S., Gertner, G. Z., Anderson, A. (2002): Improvement in mapping vegetation cover factor for the universal soil loss equation by geostatistical methods with Landsat Thematic Mapper images. Int J Remote Sens 23:3649–3667.

Williams, J. R. (1975): Sediment routing for agricultural watersheds. JAWRA J Am Water Resour Assoc 11: 965–974.

Wischmeier, W. H., Smith, D. D. (1965): Predicting rainfall erosion losses from cropland east of the Rocky Mountains [online]. In: Agricultural Handbook, No. 282. US Department of Agriculture – Agricultural Research Service, Brooksville, 47 p.

Wischmeier, W. H., Smith, D. D. (1978): Predicting rainfall erosion losses- a guide to conservation planning. In: Agriculture Handbook No537. U.S. Department of Agriculture, Washington, DC.

Khadidja Semari, PhD.
Laboratory of Water Sciences and Techniques
University of Mustapha Stambouli Mascara
BP 305 Mamounia Street
Mascara
Algeria

Khaled Korichi, PhD. (*corresponding author, e-mail: kh.korichi@gmail.com)
Laboratory of Civil Engineering and Environment
Djillali Liabes University of Sidi Bel Abbes
BP 89 Sidi Bel Abbes 22000
Algeria

DOI: 10.31577/ahs-2023-0024.01.0013

ACTA HYDROLOGICA SLOVACA

Volume 24, No. 1, 2023, 113 – 121

Changes in water balance components of river basins in the Slovak Republic and Ukraine

Pavla PEKÁROVÁ*, Viktor VYSHNEVSKYI, Ján PEKÁR, Pavol MIKLÁNEK

This study examined the long-term changes in water balance in five river basins located in Slovakia and Ukraine. Despite small increase in precipitation between 1961–1990 and 1991–2020, the study found a clear trend of decreasing water discharge, accompanied by an increase in evaporation and a significant decrease in the runoff coefficient. Data from two Slovak rivers and three Ukrainian rivers were used, chosen based on three criteria: the presence of at least two meteorological stations within the river basin, a long-term observation period, and minimal human impact on river runoff. The results of statistical analysis indicate that the Belá river basin in the Tatra Mountains had the smallest decrease in the runoff coefficient (–1.28%). The largest decrease in the runoff coefficient (–34%) was observed in the Sula River catchment area with the smallest altitude and the most eastern location. On average, the runoff coefficient decreased by 14% in studied basins. The study highlights the importance of monitoring water balance changes, particularly in regions where water resources are limited.

KEY WORDS: water balance, discharge, precipitation, evaporation, runoff coefficient

Introduction

One of the most pressing scientific issues in modern hydrology is the impact of climate change on the water regime. Climate change has become one of the most significant global environmental challenges of our time, leading to changes in the water cycle and water balance of many regions around the world. Changes in temperature, precipitation patterns, and extreme weather events all contribute to the transformation of the hydrological cycle, which has implications for freshwater resources, ecosystems, and human societies.

The observed and expected changes in water resources vary across different regions and models. For instance, Mahmood et al. (2020) predicted changes in water resources of the Chari river basin (contributing to Lake Chad in Africa) using the harmonic regression model for the periods 2021–2050, 2051–2080, and 2081–2100 with respect to the baseline period (1971–2001). According to their results, flows are expected to decrease under the HRM and RCP2.6 scenarios but to increase under RCP4.5 and RCP8.5. In the period 1941–2002, statistically significant increasing runoff trends were found in Finland, probably because the first year of the period (1941) was the driest ever observed in many sites (Hyvärinen, 2003). In Hanel et al. (2012), the climate change impact on mean runoff in the Czech Republic was assessed. The hydrological balance was modelled using the BILAN conceptual hydrological model at 250 catchments with varying sizes and climatic conditions. Climate change scenarios were derived using a simple delta approach, where observed data for precipitation, temperature, and relative air humidity were perturbed to reflect the changes seen in 15 regional climate model (RCM) simulations between the control and scenario periods. The parameters of the hydrological model were estimated for each catchment using observed data, and these parameters were then used to calculate discharge under climate change conditions for each RCM simulation. Although there were considerable differences in the absolute values of the runoff changes, consistent patterns of change were identified. The majority of scenarios projected an increase in winter runoff in the northern part of the Czech Republic, particularly in catchments with high elevation. Furthermore, the scenarios were in agreement regarding a decrease in spring and summer runoff in most of the catchments.

Interesting results as to water balance with regard to agricultural products was published by Vanham (2013). Author focuses on quantifying the net virtual water import (net VWi, agr) amounts for agricultural products in river basins larger than 1000 km^2 within the EU28. The study reveals the highest positive net VWi, agr values along a densely populated and industrialized axis stretching from Northwest England to Milan. Specifically, the Rhine, Po, Thames, Scheldt, Elbe, and Seine river basins exhibit the highest positive values. The WFcons, agr (water footprint of consumption) for these basins is significantly higher than the WFprod, agr (water footprint of production). Conversely, the basins

with the most negative net VWi, agr are located on the Iberian Peninsula (Guadiana, Ebro, and Duero), in Western France (Loire and Garonne), and in the eastern Baltic Region (Nemunas). These exporting basins have lower population densities and extensive agricultural areas.

Senf et al (2020) address the issue of tree mortality caused by drought, with a particular focus on Europe. Through the analysis of high-resolution annual satellite-based canopy mortality maps from 1987 to 2016, the study reveals a significant relationship between excess forest mortality (mortality exceeding the long-term trend) and drought across continental Europe. The authors estimate that drought caused approximately 500 000 hectares of excess forest mortality between 1987 and 2016. The research utilizes generalized additive mixed modeling to examine the statistical relationship between the fractional deviation in forest canopy mortality and the climatic water balance (CWB). The findings support the hypothesis that decreasing water availability, reflected in CWB, is associated with increased excess mortality. The study also identifies regions and years as hotspots of drought-related excess forest canopy mortality, highlighting the potential for widespread tree mortality in Europe with future increases in drought.

Previous findings suggest that lowland areas used for agricultural purposes are particularly vulnerable to decreased runoff in the region of Central Europe. Moreover, in recent years, changes in water balance have also been observed in high-altitude catchment areas, leading to forest decline due to draught.

Mammoliti et al. (2021) presented an alternative WebApp for monthly water balance calculation, based on the original Thornthwaite–Mather method. The developed solution relies on a serverless approach, exploiting a large set of cloud-based micro-services. This type of approach enables asynchronous processing (from request to result) using a queue manager that integrates and decouples distributed software components. To provide an example of its application, the basic water balance components were calculated on two small watersheds located in the Northern Apennines (Central Italy) and in Northwestern Slovenia. In similar areas in Europe, many authors demonstrated that the error associated to the use of this method is smaller than the one due to the rainfall measurements. In many of these cases, researchers focused on relatively small catchment areas located in the central part of Europe.

In the region of Slovakia, a number of scientific papers have been dedicated to the study of changes in water runoff and water balance resulting from climate change. These papers include research conducted by Garaj et al. (2019), Halmová et al. (2022), Holko et al. (2001), Parajka et al. (2023), Pekárová et al. (2005; 2009a; 2009b; 2010a; 2010b), Petrovič et al. (2010), and Sleziak et al. (2021). For instance, Garaj et al. (2019) examined the Topľa river basin situated in eastern Slovakia and discovered a significant decrease in the runoff coefficient from 0.34 to 0.29 during the period of 1961–2017.

Longer datasets were utilized to analyze changes in water balance in the Krupinica River, located in the southern part of Slovakia (Halmová et al., 2022). The runoff coefficient of the Krupinica River obtained the following values for different periods: 1931–1960: 0.32, 1961–1990: 0.27, and 1991–2020: 0.21.

The impact of climate change on evaporation, as well as long-term changes in the water regime of rivers in Ukraine, were investigated by Vyshnevskyi and Donich (2021) and Graf and Vyshnevskyi (2022).

In this study, we built upon our previous work. The primary objective of this article is to determine changes in water balance in small forested catchments, as well as large agricultural basins, located in regions with varying elevations and climate conditions in Slovakia and Ukraine. The changes in the runoff components and runoff coefficient of the analyzed river basins were identified during two periods: 1) 1961–1990, and 2) 1991–2020.

Material

This study utilized data from five small to medium-sized river basins located across two countries: two in the Slovak Republic and three in Ukraine. Among the two Slovak rivers, the Belá River is situated in the mountains, while the Litava River is located in a highland area. One Ukrainian river, the Prut River, is situated in the Carpathian Mountains, while the other two rivers (the Styr and Sula rivers) are located on the plains. The selection of these river basins was based on three main criteria: the presence of at least two meteorological stations within the catchment area, a long-term observation period, and minimal human activity that could affect river runoff. The last criterion was particularly important in the southern part of Ukraine, where water is frequently used for irrigation (Fig. 1).

To study the meteorological and hydrological conditions of the river basins, data from various meteorological and hydrological stations were used.

The Belá river basin is situated in the Tatra Mountains. Hydrological data for this study were collected at a gauging station located in Podbanske (catchment area: 93.49 km^2, stream gauge elevation: 922.72 m above sea level). The upper part of the Belá river basin, up to the Podbanské gauge, is located within the TANAP reserve, which is a protected area unaffected by human activity. The most significant anthropogenic modifications occurred primarily in the 19th century when forests were cleared for pastures. However, after the establishment of the Tatra National Park (TANAP) in 1948, grazing was prohibited, and forests were recognized for their flood protection benefits (Pekárová et al., 2009b). The vegetation within the Belá basin, up to the Podbanské water gauge, consists of 40% coniferous forests, 4.5% deciduous forests, 21% dwarf pine, 18% meadows and pastures, 15.8% rocks, and the rest consists of water bodies and built-up areas (in year 2015). Two meteorological stations situated on the edges of the Belá river catchment area provided data for this study (Fig. 2). The Polish observatory Kasprowy Wierch has an elevation of 1987 m above sea level, while the Podbanské station is at 972 m above sea level. Additionally, data from the Štrbské Pleso meteorological

station were utilized (Table 1). The main hydrological characteristics of the selected basins are presented in Table 2.

The catchment area of the Litava River is situated in a region that combines highland and lowland characteristics. It originates in the Krupinska Planina mountain range, with its source located at an altitude of approximately 650 m above sea level. The Litava

Fig. 1. The location of the studied river basins: 1 – Belá: Podbanské, 2 – Litava: Plášťovce, 3 – Prut: Yaremche, 4 – Styr: Lutsk, 5 – Sula: Lubny.

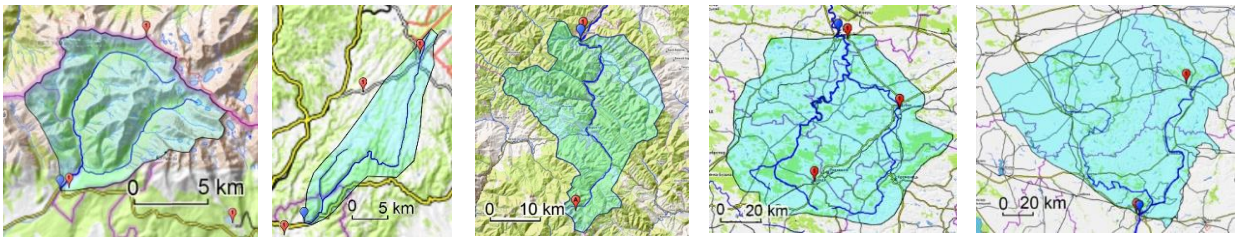

1 2 3 4 5

Fig. 2. The studied river basins and the location of meteorological (in red) and hydrological (in blue) stations: 1 – Belá: Podbanské, 2 – Litava: Plášťovce, 3 – Prut: Yaremche, 4 – Styr: Lutsk, 5 – Sula: Lubny.

Table 1. The main climatic characteristics at meteorological stations located near the studied catchment areas

River	Station	Elevation [m a.s.l.]	Temperature		Precipitation	
			1961–1990	1991–2020	1961–1990	1991–2020
Belá	Kasprowy Wierch	1987	-0.77	0.16	1825	1760
	Podbanské	972	4.68	5.63	921	996
	Štrbské Pleso	1322	3.76	3.98	960	1107
Litava	Senohrad	586	–	–	681	736
	Bzovík	355	8.20	9.52	578	644
	Horné Semerovce	131	–	–	563	585
Prut	Pozhezhevska	1451	2.7	3.5	1424	1544
	Yaremche	531	6.9	7.9	930	1013
Styr	Brodu	228	7.5	8.7	689	699
	Dubno	202	7.4	8.6	612	649
	Lutsk	197	7.3	8.4	558	580
Sula	Romny	169	6.7	8.0	604	618
	Lubny	158	7.4	8.6	625	608

Table 2. The characteristics of the studied river basins, *Qa* – long term discharge; *R* – runoff depth; period 1961–2020

Station No.	The name of rivers and gauging stations	Area [km^2]	Mean elevation [m]	*Qa* [m^3 s^{-1}]	*R* [mm]
1	Belá: Podbanské	93.49	1572	3.52	1181
2	Litava: Plášťovce	214.3	450	0.94	138
3	Prut: Yaremche	597	990	12.7	669
4	Styr: Lutsk	7200	230	31.2	136
5	Sula: Lubny	14200	120	26.4	59

catchment area, extending up to the Plášťovce gauging station, covers an area of 214.3 km^2. The river system within the basin follows a mostly parallel course due to the relatively gentle terrain, with an average altitude of 450 m above sea level.

The Prut River upstream of the Yaremche hydrological station is a typical mountain river. Moreover, the source of the river is located near Hoverla Mountain, which is the highest mountain in Ukraine, with an elevation of 2061 m. The main part of the catchment area is covered by forest, mainly spruce. There are two meteorological stations located on the river's catchment area: Pozhezhevska and Yaremche.

The Styr River is located in the north-western part of Ukraine and it is a tributary of the Prypiat River, which in turn is the largest tributary of the Dnipro River. The upper and southern part of the catchment area, upstream of Lutsk city, is mainly located on the Volyno-Podilska highland, while the lower part is on the Poliska lowland. There are three meteorological stations (Brodu, Dubno, and Lutsk) the data of which were utilized in the study. The climate of the catchment area is moderate with cool winters and warm summers.

The Sula River is located in the north-eastern part of Ukraine, not far from the centre of Ukraine. The characteristic feature of this river is its location on the Dniprovska lowland with a flat relief. The entire catchment area is located in the Forest-Steppe zone, which has few forests. On the catchment area of the Sula River are located two meteorological stations data of which were used: Romny and Lubny. The Romny meteorological station is located in the northeast part of the river basin, and the Lubny meteorological station is located in the south. The climate of the catchment area is moderate with cool winters and warm, sometimes hot summers (Vyshnevskyi and Kutsiy, 2022).

Methods

The study utilized data from the period 1961–2020. In order to calculate the total areal precipitation and the mean basin temperature in the mountainous Belá River basin and the highland-lowland Litava River basin, precipitation and temperature gradients were employed. To determine the average monthly areal precipitation totals, monthly precipitation data from the Podbanské and Štrbské Pleso meteorological stations, as well as data from the Polish observatory Kasprowy Wierch, were used (Fig. 2). For the Ukrainian river basins, precipitation was calculated as the average value of data from meteorological stations situated within those basins.

The hydrological balance quantifies the circulation of water in a closed system with a concentrated runoff in the final profile of the catchment. The atmospheric precipitation over the basin serves as the only input to the basin balance. For a sufficiently long period, the difference in soil water content at the beginning and end of the time period can be neglected. In such cases, we can identify the total annual evapotranspiration with the difference between precipitation and runoff.

The water balance equation used is as follows:

$$P = R + ET + \Delta S \quad (1)$$

where:

P – annual precipitation depth [mm];
R – annual average runoff [mm];
ET – annual evapotranspiration depth [mm];
ΔS – average total losses that have a higher significance in shorter time intervals Δt. For the long-term water balance, this element can be neglected and replaced by $\Delta S = 0$.

For the long-term monthly balance, if we determine the monthly total evapotranspiration independently, we can calculate the change in water storage in the basin in the monthly step during the year according to the water balance equation.

Results and discussion

Precipitation

Among the river basins studied, the highest precipitation is observed at the Kasprowy Wierch climatic station, located in the High Tatra Mountains. The average annual precipitation at this station was 1825 mm during the period from 1961 to 1990 and 1760 mm during the period from 1991 to 2020. Fig. 3 illustrates the annual precipitation totals averaged over the Belá Basin. Precipitation data were calculated using the Podbanské, Kasprowy Wierch, and Štrbské Pleso stations, based on the precipitation gradient relative to the average elevation of the Belá river basin. The lowest long-term mean precipitation totals at a Slovakian station were recorded at the Bzovík station, with 578 mm during the period

from 1961 to 1990 and 644 mm during the period from 1991 to 2020. Annual mean areal precipitation totals in the Litava river basin showed a slight increase over time. The largest long-term mean precipitation totals among the river basins located in Ukraine is observed at the Pozhezhevska meteorological station, with a mean annual precipitation total of 1548 mm during 1991–2020. The Yaremche meteorological station, located at a lower altitude, recorded significantly less precipitation, with a mean of 1013 mm. In the Prut river basin, precipitation increased by 100 mm during the second period. In the Sula river basin, changes in precipitation were very small during the period of 1961–2020, with no clear tendency to increase or decrease, as shown in Fig. 3.

Annual runoff

For a visual comparison of long-term variability and trends in water discharge, we have plotted the annual runoff R [mm] on Fig. 3 (right). Long-term averages of the runoff exhibit significant differences between the watersheds and are generally influenced by annual precipitation and the mean elevation (temperature) within the watershed. In the high mountain river basin of Belá, there have been no changes in the discharge observed thus far. In the Prut basin, we can observe how multi-year fluctuations in precipitation, spanning approximately 28 years, correspond to fluctuations in annual water runoff. Similar variability in discharge can also be observed in the Styr river basin.

Furthermore, a decrease in water discharge has been detected in recent years in the lowland watersheds. This decrease is particularly noticeable in the watershed of the Sula river. The decline in water discharge in lowland watersheds is caused by rising air temperatures (see Fig. 4 on the left).

Water balance and evaporation

With data on precipitation and water runoff, it is possible to calculate evaporation from river basins using equation (1). As shown in Fig. 4 on the right, there is an observed tendency of increased evaporation (with the exception of the Belá river basin), which is caused by a significant increase in air temperature after 1987. The results of comparing two 30-year periods are summarized in Table 3. As shown in Table 3, the runoff coefficient decreased significantly in all basins.

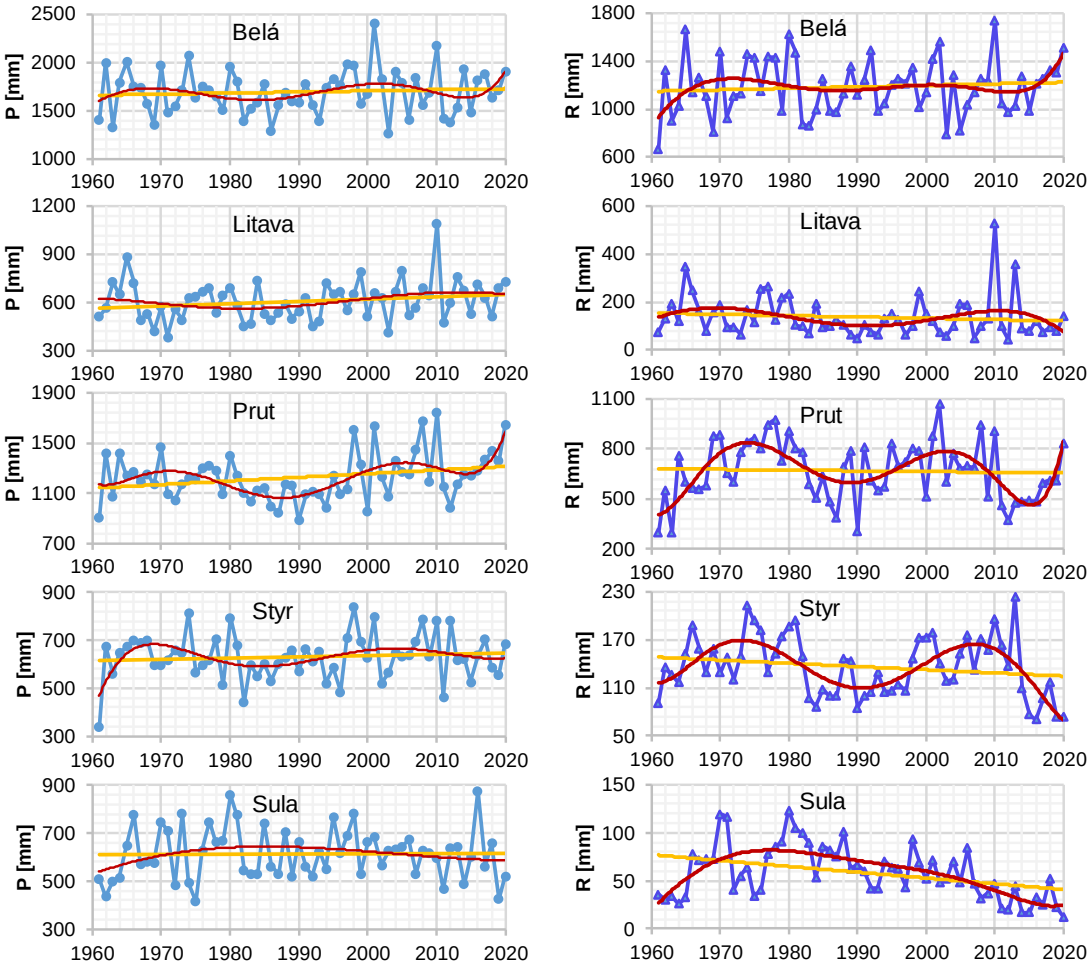

Fig. 3. Long-term changes and log-term variability of mean areal annual precipitation P (left); runoff R (right) of the studied river basins: Belá: Podbanské, Litava: Plášťovce, Prut: Yaremche, Styr: Lutsk, Sula: Lubny.

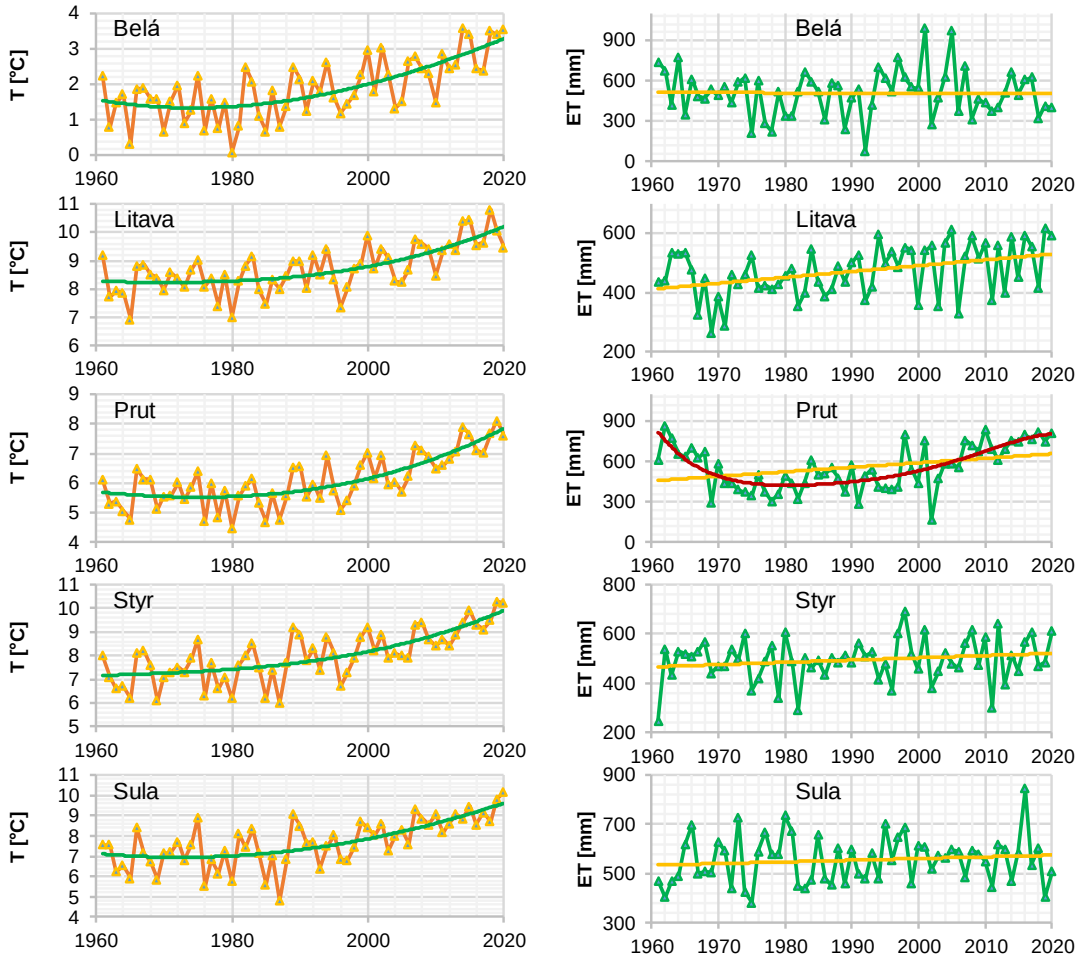

Fig. 4. Long-term changes and log-term variability of mean areal air temperatur T (left); balance evapotranspiration ET (right) of the studied river basins: Belá: Podbanské, Litava: Plášťovce, Prut: Yaremche, Styr: Lutsk, Sula: Lubny.

Table 3. The changes in the runoff components and runoff coefficient of the analysed river basins during two periods: 1) 1961–1990, and 2) 1991–2020. *P* represents precipitation, *R* represents runoff depth, *ET* represents the balance evapotranspiration, *k* represents the runoff coefficient, and *dP, dR, dET, and dk* represents the percentage change of the *P, R, ET* and *k* compared to the first period

River	*P*		*dP*	*R*		*dR*	*ET*		*dET*	*k*		*dk*
	1961–1990	1991–2020	[%]	1961–1990	1991–2020	[%]	1961–1990	1991–2020	[%]	1961–1990	1991–2020	[%]
Belá	1662	1732	**4.21**	1170	1204	**2.91**	492	528	**7.32**	0.704	0.695	**-1.28**
Litava	582	638	**9.62**	145	131	**-9.66**	438	507	**15.8**	0.248	0.205	**-17.4**
Prut	1177	1278	**8.58**	668	669	**0.15**	509	609	**19.6**	0.568	0.523	**-7.82**
Styr	620	643	**3.71**	141	131	**-7.09**	478	511	**6.90**	0.228	0.205	**-10.4**
Sula	614	613	**-0.16**	71	47	**-33.8**	544	566	**4.04**	0.115	0.076	**-33.7**

To illustrate the differences in series of precipitation, runoff, air temperature, and balance evapotranspiration of two periods (1. 1961–1990, and 2. 1991–2020), we used a box-and-whisker diagram (see Fig. 5). A boxplot is a standardized method of displaying the dataset based on the five-number summary: the minimum, maximum, sample median, and first and third quartiles. Outliers that significantly differ from the rest of the dataset are plotted

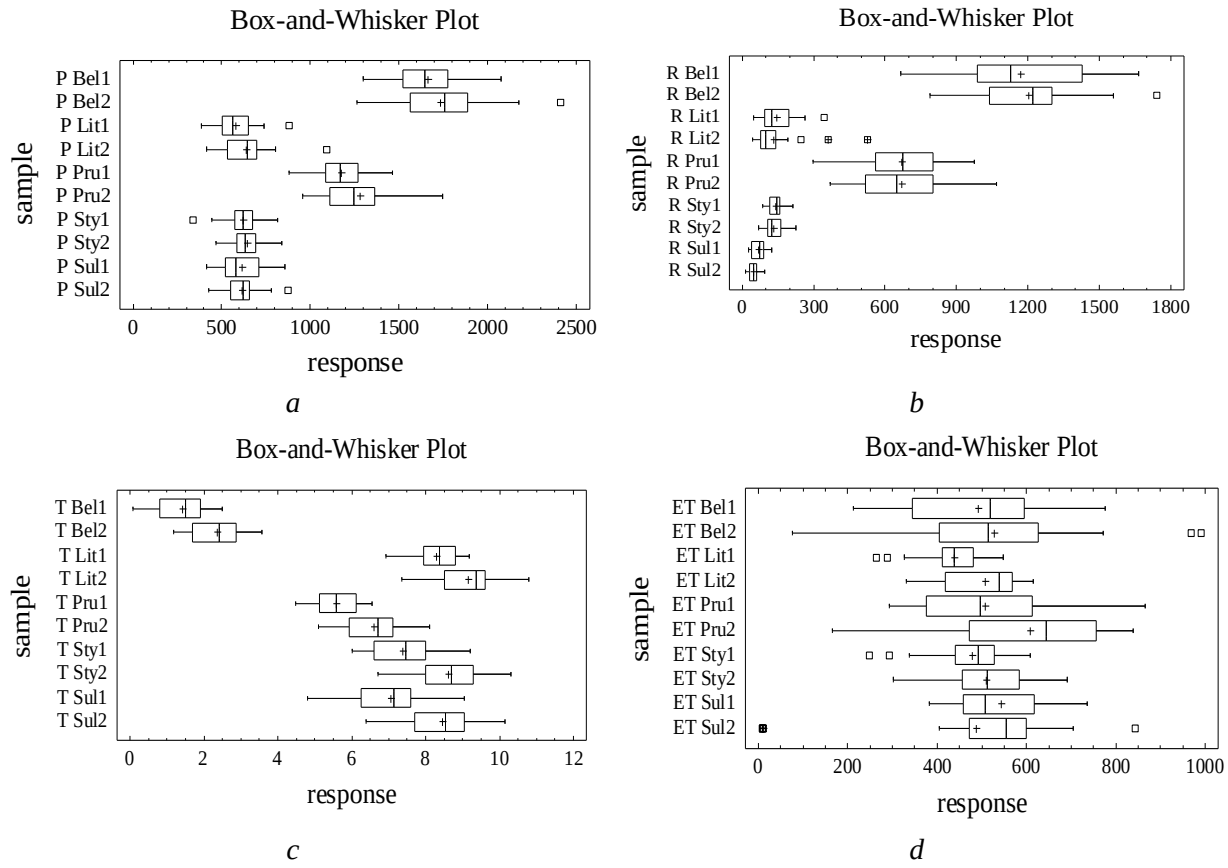

Fig. 5. Changes in basic precipitation (a), runoff (b), air temperature (c), and evapotranspiration (d) characteristics from selected five basins using box-and-whisker diagrams for the 1st period (1961–1990) and the 2nd period (1991–2020)

as individual points. According to the box-and-whisker diagrams, the most significant changes in statistical characteristics were observed in air temperature for all basins – all characteristics (the minimum, maximum, sample median, and first and third quartiles) increased. An increase in precipitation was also recorded at all basins. A decrease in runoff depths and balance evapotranspiration was observed in four watersheds. However, the runoff coefficient decreased in all basins, including the high-mountain Belá river basin (Table 2). Table 2 presents the average values of all hydrological components during the comparison of two 30-year periods. On average, the runoff coefficient has decreased by 14% in these basins.

Discussion

The data presented in Table 2 indicate that the largest decrease in the runoff coefficient (33.7%) is observed in the Sula river catchment area. This can be partially explained by significant evaporation from wetlands, reservoirs, and ponds located within the catchment area. As identified in the study by Vyshnevskyi (2022), the relationship between air temperature and evaporation from water surfaces is nonlinear. This implies that even a small increase in air temperature can result in a significant increase in evapotranspiration, particularly during the high-temperature summer months in Ukraine.

The smallest decrease in the runoff coefficient (1.28%) was observed in the mountainous Belá river basin. The absence of large changes for the Belá mountain river can be explained by the low temperature. Other possible reason could be the fact that higher air temperatures are causing spruce forests to dry out in Slovakia as well (Senf et al., 2020). In the High Tatra Mountains, there was an intensive bark beetle outbreak during the period 1993–1998. The outbreak resulted in tree mortality, affecting Norway spruce stands on both the Polish and Slovak sides of the territory. The forest mortality likely led to reduced evapotranspiration, thus resulting in a less significant decrease in the runoff coefficient in the Belá basin. Additionally, on November 19, 2004, a catastrophic windstorm occurred in the Tatra National Park and damaged an area of roughly 12 600 ha, which represented about 50% of the local spruce forests. The windthrow area in the Belá river basin was left uncleared for natural development (Pekárová et al., 2011). As a result, many trees dried up (Fig. 6a–b). In the following years, the old dry spruce forest in the Tichá and Kôprová valleys is gradually being replaced by a mixed forest (Fig. 7a–b).

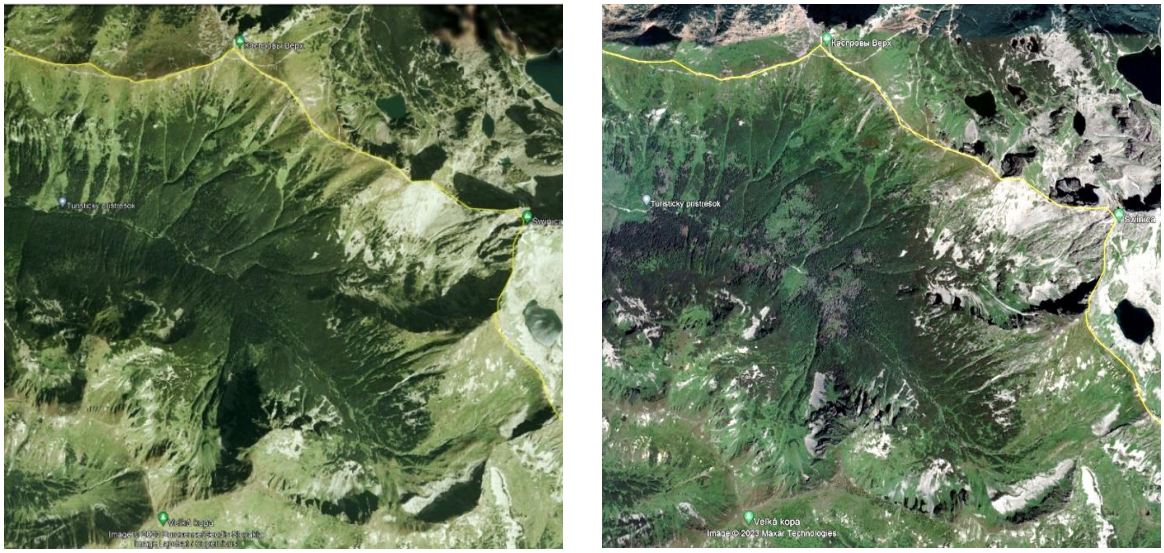

a) Tichá valley, 2006 *b) Tichá valley, 2021*

Fig. 6. Tichá valley, Belá river basin (Image 2006, Eurosense/Geodis Slovakia; Image 2021, Maxar Technologies).

a) 21. 10. 2008, dead spruce forest *b) 11. 05. 2023, new mixed forest*

Fig. 7. Kôprovský stream above the confluence with Tichý stream; 977 m a.s.l., Belá river basin, Kriváň peak, 2495 m a.s.l. (photo: P. Pekárová).

Conclusions

The available data from numerous meteorological stations located in the five river basins on the territories of Slovakia and Ukraine show a clear tendency of changes in water balance. Despite the fact that the amount of precipitation was slightly higher, there is a trend towards a decrease in water discharge. Simultaneously, an increase in evaporation and a significant decrease in the runoff coefficient were observed. These changes are more pronounced in flat rivers than in those located in mountainous areas.

Although projecting water resources is important for longer-term (50–100 years) water resource planning, predicting water resources in the near future (10–20 years) is even more crucial for policymakers and planners to minimize the impacts of climate change on water resources by adopting some proper mitigative and adaptive actions.

Acknowledgement

This work was supported by the project APVV-20-0374 DETECTIVES and by the project VEGA No. 2/0015/23.

References

Garaj, M., Pekárová, P., Pekár, J., Miklánek, P. (2019): The Changes of Water Balance in the Eastern Slovakia. IOP Conf. Ser.: Earth Environ. Sci. 362 012014. ISSN 1755–1307. https://iopscience.iop.org/article/10.1088/1755-1315/362/1/012014

Graf, R., Vyshnevskyi, V. (2022): Forecasting Monthly River Flows in Ukraine under Different Climatic Conditions. Resources 2022, 11, 111. https://doi.org/10.3390/resources11120111

Halmová, D., Pekárová, P., Podolinská, J., Jeneiová, K. (2022): The assessment of changes in the long-term water balance in the Krupinica River basin for the period 1931–2020. Acta Hydrologica Slovaca, 23, 1, 21–31,

https://doi.org/10.31577/ahs-2022-0023.01.0003
Hanel, M., Vizina, A., Máca, P., Pavlásek, J. (2012): A multi-model assessment of climate change impact on hydrological regime in the Czech Republic. J. Hydrol. Hydromech., 60, 3, 152–161. https://doi.org/10.2478/v10098-012-0013-4
Holko, L., Parajka, J., Majerčáková, O., Faško, P. (2001): Hydrological balance of selected catchments in the Tatra Mountains region in hydrological years 1989–1998. J. Hydrol. Hydromech., 49, 3–4, 200–222
Hyvärinen, V. (2003): Trends and characteristics of hydrological time series in Finland. Nord. Hydrol. 34 (1/2), 71–90.
Mahmood, R., Jia, S., Mahmood, T., Mehmood, A. (2020): Predicted and projected water resources changes in the Chari catchment, the lake Chad basin, Africa. Journal of Hydrometeorology. 21, 1, 73–91. https://doi.org/10.1175/JHM-D-19-0105.1
Mammoliti, E., Fronzi, D., Mancini, A., Valigi, D., Tazioli, A. (2021): WaterbalANce, a WebApp for Thornthwaite–Mather Water Balance Computation: comparison of applications in two European watersheds. Hydrology, 8(1), 34. https://doi.org/10.3390/hydrology8010034
Parajka, J., Vizina, A., Komma, J., Valent, P., Štepánek, P., Haslinger, K., Schellander-Gorgas, T., Viskot, M., Fischer, M., Froschauer, W., Trnka, M., and Blöschl, G. (2023): Impact of climate change on the water balance of the Thaya basin, EGU General Assembly 2023, Vienna, Austria, 24–28 Apr 2023, EGU23-14941, https://doi.org/10.5194/egusphere-egu23-14941
Pekárová, P., Miklánek, P., Halmová, D., Onderka, M., Pekár, J. (2011): Long-term trend and multi-annual variability of water temperature in the pristine Belá River basin (Slovakia). J. Hydrol., ISSN 0022-1694 400, p. 333–340.
Pekárová, P., Martincová, M., Miklánek, P. (2010a): Water balance of the Belá River basin in 1940/41–2004/05 period (Part I.: Basin water storage change in two 30-years periods). Acta Hydrologica Slovaca, 11, 1, 3–11.
Pekárová, P., Miklanek, P., Skoda, P., Pekár, J., Pacl, J. (2010b): Multiannual discharge variability and trend analyses of the Belá River (Slovakia) in 1895–2006. IAHS Publication 336, Wallingford, 59–64.
Pekárová, P., Halmova, D., Miklanek, P., Pekár, J., Skoda, P., Liova, S., Kucarova, K. (2009a): Homogeneity analysis of the water temperature measurements, Belá River at Podbanske. Acta Hydrologica Slovaca, 10, 1, 140–150.
Pekárová, P., Pacl, J., Liova, S., Miklanek, P., Skoda, P., Pekár, J. (2009b): Analysis of the maximum annual discharge regime in the high mountain basin of Belá River in Podbanske. Acta Hydrologica Slovaca, 10, 2, 300–311.
Pekárová, P., Pekár, J., Pacl, J. (2005): Temporal variability of annual discharges of Belá River basin for the period 1901–2000. Proc. Hydrologic days 2005, CD, SHMI, Bratislava.
Petrovič, P., Mravcová, K., Holko, L., Kostka, Z., Miklánek, P. (2010): Basin-Wide Water Balance in the Danube River Basin. In: Brilly, M. (eds) Hydrological Processes of the Danube River Basin. Springer, Dordrecht. https://doi.org/10.1007/978-90-481-3423-6_7
Senf, C., Buras, A., Zang, C. S., Rammig, A., Seidl, R. (2020): Excess forest mortality is consistently linked to drought across Europe. Nature communications, 11(1), 6200. https://doi.org/10.1038/s41467-020-19924-1
Sleziak, P., Výleta, R., Hlavčová, K., Danáčová, M., Aleksić, M., Szolgay, J., Kohnová, S. (2021): A Hydrological Modeling Approach for Assessing the Impacts of Climate Change on Runoff Regimes in Slovakia. Water, 13, 23, 3358. ISSN 2073–4441, https://doi.org/10.3390/w13233358
Vanham, D. (2013): An assessment of the virtual water balance for agricultural products in EU river basins. Water Resources and Industry, 1, 49–59. https://doi.org/10.1016/j.wri.2013.03.002
Vyshnevskyi, V. I. (2022): The impact of climate change on evaporation from the water surface in Ukraine. Journal of Geology, Geography and Geoecology. Vol. 31. N 1. P. 163–170. https://doi.org/10.15421/112216
Vyshnevskyi, V. I., Donich, O. A. (2021): Climate change in the Ukrainian Carpathians and its possible impact on river runoff. Acta Hydrologica Slovaca. Vol. 22, № 1, 3–14. https://doi.org/10.31577/ahs-2021-0022.01.0001
Vyshnevskyi, V. I., Kutsiy, A. V. (2022): Long-term changes in the water regime of rivers in Ukraine. Kyiv, 252 p. (in Ukrainian). Available online: https://er.nau.edu.ua/handle/NAU/56293

RNDr. Pavla Pekárová, DrSc. (*corresponding author, e-mail: pekarova@uh.savba.sk)
RNDr. Pavol Miklánek, CSc.
Institute of Hydrology SAS
Dúbravská cesta 9, 841 04 Bratislava
Slovak Republic

Prof. Viktor Vyshnevskyi, DrSc.
National Aviation University
Liubomyra Huzara Av.1
030 58 Kyiv
Ukraine

Assoc. Prof. RNDr. Ján Pekár, PhD.
Comenius University in Bratislava
Faculty of Mathematics, Physics, and Informatics
Department of Applied Mathematics and Statistics
Mlynská dolina, 842 48 Bratislava
Slovak Republic

DOI: 10.31577/ahs-2023-0024.01.0014

ACTA HYDROLOGICA SLOVACA

Volume 24, No. 1, 2023, 122 – 133

Development and validation of an Approximate Redistributive Balance model to estimate the distribution of water resources using the WEAP: The lower Hron river basin, Slovakia

Miroslav KANDERA*, Roman VÝLETA

The Approximate Redistributive Balance (ARB) model integrated within the Water Evaluation And Planning (WEAP) software environment aims to retrospectively simulate the flows measured by water gauging stations with sufficient accuracy according to objectives of study. It does so by initially approximating the runoff distribution with a rainfall-runoff model along the modeled streams and then redistributing the difference between the sum of the total simulated runoff to the water gauging station and the flow in the water gauging station (cleaned of any anthropogenic influences). Due to its different approach to the modeling method and the user-friendly environment of the WEAP software, this model, with a relatively small scale of input data, retrospectively simulates flows along the modeled streams with a high degree of accuracy (NSE = 0.89 for similar hydrological regime of validation and calibration basins). This paper describes its development and basic characteristics and provides partial insights into the degree of accuracy with which it can simulate monthly streamflow at water gauging stations and along modeled rivers. It can therefore be a precise foundation for analyses of water management balance scenarios.

KEY WORDS: water balance, hydrological components, water evaluation and planning, water resources, model development

Introduction

To be able to create and analyze scenarios showing the impact of the water management on surface flows in the form of a balance, it is first necessary to specify what flow data representing the available source of water will be entered the balance equation. If it would be necessary to evaluate the flow regime along streams used for water management, rainfall-runoff modeling appears to be the only possibility. Within the modeling, the individual components of the hydrological cycle, such as runoff, infiltration, evapotranspiration, etc., whose interrelationships are not constant over time and in space, are defined. Therefore, almost all hydrological modeling is a cycle of the calibration, validation, and optimization of the model to refine these relationships and model the results to the required level (Sleziak et al., 2021). To use modeling in a quantitative water management balance, the evaluation of which is ongoing retrospectively in Slovakia by the Slovak Hydrometeorological Institute (2021), we started to develop a different approach based on redistributing runoff.

In previous papers (Kandera and Výleta, 2020; Kandera et al., 2021), we proposed an approach framework where, from a spatial point of view, the basin modeled was divided into two levels. The first level consisted of sub-basins, i.e., drainage areas bounded by stable water gauging stations with long and uninterrupted rows of observed flows. Each sub-basin thus had one outlet (closing) profile and could have several inlet profiles, from which runoff from higher sub-basins flowed into the given sub-basin. From a hydrological point of view, a sub-basin without any inlet profiles is, so to speak, the roof of the entire modeled basin. Both streams with water gauging stations and tributaries without them were modeled within the model. Since the WEAP software is a nodal model (Sieber and Purkey, 2015), a second basin subdivision level, namely, the level of the micro-basins, was used to partially simulate longitudinal runoff along streams. The modeled streams were divided into individual sections at regular lengths, and each section had its own drainage area, which was its micro-basin. Runoff from the individual micro-basins was calculated by distribution from the sub-basin under which the individual micro-basins fell. This procedure was based on the following equation:

$$Q_{c,i} = Q_{r,i} - X_i \quad (1)$$

where

$Q_{c,i}$ – the cleansed outflow from a sub-basin in time step i [m^3 s^{-1}];

$Q_{r,i}$ – the calculated outflow from the sub-basin in time step *i* [$m^3 s^{-1}$];
X_i – the anthropogenic impact in time step *i* [$m^3 s^{-1}$].

The equation to calculate the outflow from the sub-basin is given in the form:

$$Q_{r,i} = Q_{out,i} - \sum Q_{in,i} \quad (2)$$

where
$Q_{out,i}$ – the streamflow measured in the water gauging station outlet of a sub-basin in time step *i* [$m^3 s^{-1}$];
$\sum Q_{in,i}$ – a summary of the streamflow measured in the inlet water gauging stations of the sub-basin in time step *i* [$m^3 s^{-1}$].

The cleansed outflow was subsequently distributed as runoff to selected reaches on the river network modeled based on the defined share of the individual micro-basins of the corresponding reaches. While this procedure made it possible to simulate the flow simply and accurately in the water gauging station, the distribution of the runoff along the modeled tributaries was relatively imprecise, as it was only based on the share of the micro-basins in the area, the total rainfall, and the difference from the average slope of the sub-basin. In the modeled basin, the unevenness of the variables affecting the basin's outflow regime over time and in space is fully manifested.
The main objective of this paper is to describe and evaluate the newly created ARB model and to underline its specific characteristics along with possible issues and how to handle them. The methodology developed was tested on the lower Hron river basin in Slovakia.

Methods and material

In this paper, we have developed a new methodology where the one-step distribution model is extended to a multi-step Approximate Redistributive Balance (ARB) model. In the WEAP software, it is possible to apply changes in the data structure of the model and thereby create a deeper structure of the model using the branching form of scenarios. From this point of view, it is possible to break down the structure of the model into the individual scenarios according to Fig 1.
The structure of the ARB model consists of several sub-models (i.e., a snow sub-model, runoff approximation sub-model, and redistribution sub-model). The task of this article is not to specify all the sub-models in detail but to outline a methodical procedure for solving the problem of the redistribution of the runoff from the basin. For this reason, we will mainly focus on a description of the approximation and redistributive sub-models.

Snow sub-model

The setup scenario represents an input scenario in which the individual variables, references to input data, and mutual relations of the individual variables are defined. The snow sub-model calibration scenario is a separate scenario from which only the calibrated parameters are subsequently taken. The snow sub-model was created out of the need for a compatible tool that, when using data from the precipitation, air temperature, and altitude, will provide sufficiently accurate data for the necessary approximation. In general, the snow sub-model can be described as a non-linear, deterministic, dynamic snow sub-model with (5) distributed parameters calibrated to the data of the snow water equivalent. The output of the sub-model is the calculated value of the snow water equivalent, which is then entered into the equation:

$$SWB_i = SWE_{i-1} - SWE_i \quad (3)$$

where
SWB_i – the change in the snow water balance in time step *i* [mm];
SWE_i – the snow water equivalent in time step *i* [mm];
SWE_{i-1} – the snow water equivalent in time step *i-1* [mm].

This relationship assumes that information on how much snow cover remains during the transition from one time step to another is essential in defining the impact of the snow cover formation and its subsequent melting

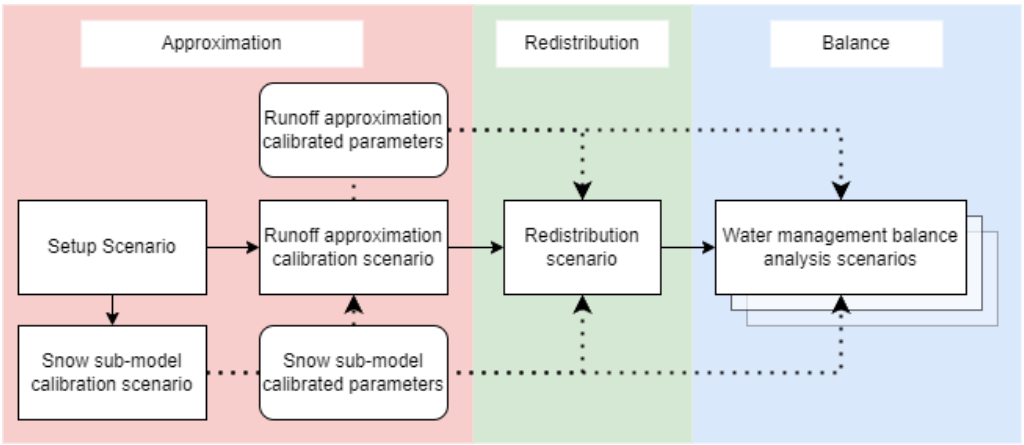

Fig. 1. Approximate Redistributive Balance model scenario branching.

over time. For example, with a monthly time step, the average monthly value is not important, but the value at the end of the month is. It follows from equation (3), that if the value of *SWB* is a negative value, it equals the accumulation of snow cover, while a positive value equals snowmelt.

Runoff approximation sub-model

Since the runoff approximation sub-model fulfills only an approximate role in the ARB model, it was possible to build it on simplified deterministic relationships. The individual variables were defined according to the simplified assumption that, except for the atmospheric components, the individual components of the hydrological cycle are interconnected and operate on the water balance principle in such a way that they decline/increase in order to maintain the water balance. The runoff approximation sub-model has five calibration parameters, with each sub-basin having its own set of parameters calibratable to the flow in the water gauge profile. Each variable in the model is affected by at least two other variables or calibration parameters.
In Healy (2010), the recharge, or, by Healy's definition, the drainage as well was defined by the general equation:

$$R = P - EA \tag{4}$$

where
R – the recharge [mm];
P – the precipitation [mm];
EA – the actual evapotranspiration [mm].

From equation (4), two representations of the potential recharge, i.e., RE_{pot} and C_{REpot} , were derived:

$$RE_{pot,i} = P_i + SWB_i - PET_i \tag{5}$$

and

$$C_{REpot,i} = \min\left(1, \max\left(0, \frac{(P_i + SWB_{,i} - PET_i)}{100}\right)\right) \tag{6}$$

where
$RE_{pot,i}$ – the potential recharge in time step i [mm];
$C_{REpot,i}$ – the coefficient of the potential recharge in time step i [-];
P_i – the precipitation in time step i [mm];
SWB_i – the change in snow water balance in time step i [mm];
PET – the potential evapotranspiration in time step i [mm].

The potential recharge quantifies the ratio between the atmospheric resources and demands in the form of an impact on the hydrological cycle, while the coefficient of the potential recharge serves as an indicator.
Fig. 2 shows a simplified form (without any input data) of the calculation cycle of the variables influencing the calculation of the total runoff. Each variable apart from the direct runoff is successively calculated with respect to the soil water capacity remaining from the previous time step and is then added to the calculation of the following variable. The calculation of the variables affecting the soil water capacity is therefore based on maintaining the water balance of the soil water capacity. The potential recharge serves as a counterweight that disturbs this balance, either towards a decrease or an increase in the soil water capacity.
The total runoff was divided into three parts: R_d as the direct runoff, R_s as the surface runoff, and R_{ss} as the sub-surface runoff. The variables themselves do not aim to precisely divide the parts of the runoff into separate components of the runoff but serve in a gradual sequence to approximate the amount of water that is available for the runoff from available sources. The calculation of the direct runoff is defined as:

$$\begin{aligned} &if\ RE_{pot,i} > 0 \qquad then \\ &R_{d,i} = RE_{pot,i}\left(\frac{(C_{REpot,i}\, C_{Rd} + C_r)}{(1 + C_{Rd})}\right) C_{Rd} \\ &elseif\ RE_{pot,i} \leq 0 \qquad then \qquad R_{d,i} = 0 \end{aligned} \tag{7}$$

where
$R_{d,i}$ – the direct runoff in time step i [mm];
C_r – the coefficient of the runoff [–];
C_{Rd} – the coefficient of the direct runoff (calibration range of the parameter used: $1 > C_{Rs} > 0$ [–]).

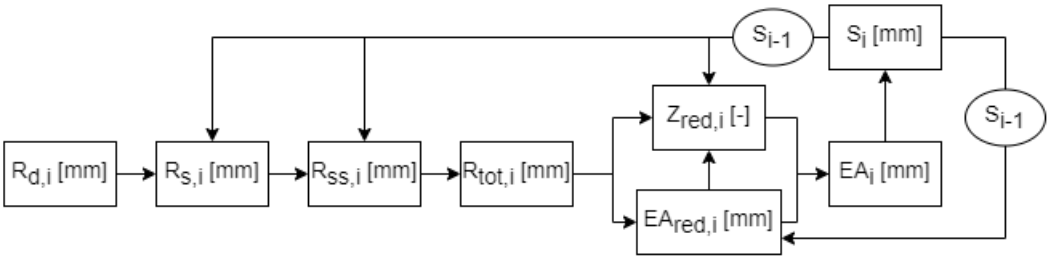

Fig. 2. Simplified order of the calculation of the runoff approximation sub-model variables ($R_{d,i}$ – direct runoff, $R_{s,i}$ – surface runoff, $R_{ss,i}$ – sub-surface runoff, $R_{tot,i}$ – total runoff, $EA_{red,i}$ – evapotranspiration reduction, $Z_{red,i}$ – relative value of the reduced soil water capacity, EA_i – actual evapotranspiration, S_i – soil water capacity in time step i, S_{i-1} – soil water capacity from time step i-1).

Direct runoff only occurs if the atmospheric sources (*P*, *SWB*) overweigh the requirements (*PET*). A calibratable parameter C_{Rd} was included in equation (7) so that the effect of the runoff coefficient on the direct runoff calculations was not reduced by changes in C_{Rd} as significantly as C_{REpot} was. The second part of the runoff could be described as surface runoff. The water supply in the soil is included in the calculation of this variable, while it no longer includes the runoff coefficient. The surface runoff is defined as:

$$if\ R_s < 0 \cap R_{pot} < 0 \qquad then \qquad R_{s,i} = 0$$

$$elseif\ RE_{pot,i} - R_{d,i} \leq 0 \quad then$$
$$R_{s,i} = \left(S_{i-1} - \left(C_{REpot,i} + C_{Rs}\right)/2\, S_{max,i}\right) C_{REpot,i} \qquad (8)$$

$$elseif\ RE_{pot,i} - R_{d,i} > 0 \quad then$$
$$R_{s,i} = \Big(\left(RE_{pot,i} - R_{d,i} + S_{i-1}\right) - \left(C_{REpot,i} + C_{Rs}\right)/2\, S_{max,i}\Big)\, C_{REpot,i}$$

where

$R_{s,i}$ – the surface runoff in time step *i* [mm];
S_{i-1} – the soil water capacity from time step *i*-1 [mm];
$S_{max,i}$ – the maximum capacity of the soil water storage in time step *i* [mm];
C_{Rs} – the coefficient of the surface runoff (range of the calibration of the parameter used: $1 > C_{Rs} > 0.75$ [-]).

The sum of the potential recharge $RE_{pot,i}$ and the soil water capacity S_{i-1} from the time step *i*-1 and the subsequent subtraction of the direct runoff $R_{d,i}$ defines the water supply after the calculation of the direct runoff. By multiplying the maximum capacity of the soil water storage $S_{max,i}$ with the arithmetic mean between the coefficient of the potential recharge $C_{Repot,i}$ and the calibration parameter of the surface runoff C_{Rs}, it defines the amount of water that is, with respect to them, theoretically available from the water supply in the soil. The coefficient of the potential recharge $C_{REpot,i}$ serves here as a natural indicator of the need for availability of atmospheric water. The difference between these two sides multiplied by the coefficient of the potential recharge defines the amount of water that is available after calculating the direct runoff, but due to the high soil water capacity, it does not have enough space in the soil and must therefore also be part of the runoff.

Sub-surface runoff serves as the transition between a positive and negative potential recharge. As it is the only part of the runoff that is active when the potential recharge goes below zero, determining its boundaries is currently subject to change, as it is a decisive element in determining when a stream reaches the point of drying up. Currently, sub-surface runoff is defined as:

$$if\ RE_{pot,i} - R_{d,i} \leq 0_{pot,i} \quad then$$
$$R_{ss,i} = \left(S_{i-1} - R_{s,i}\right) C_{Rss} \left(1 - \left|C_{REpot,i}\right|\right) \qquad (9)$$

$$elseif\ RE_{pot,i} - R_{d,i} > 0 \quad then$$
$$R_{ss,i} = \left(S_{i-1} + RE_{pot,i} - R_{d,i} - R_{s,i}\right) C_{Rss} \left(1 - \left|C_{REpot,i}\right|\right)$$

where

C_{Rss} – the coefficient of the sub-surface runoff (range of the calibration of the parameter used: $0.3 > C_{Rss} > 0$ [–]).

According to equation (9), the values of the sub-surface runoff will be at their maximum if the potential recharge is zero, and the soil water capacity from time step *i*-1, together with the potential recharge after subtracting the direct runoff and surface runoff, is reaching the maximum soil water capacity. The absolute value of C_{REpot} ensures a linear decrease until RE_{pot} reaches values of less than -100 mm or a value greater than 100 mm, at which point the sub-surface runoff reaches zero value. The calibratable parameter C_{Rss} defines how much of the water supply is available for the sub-surface runoff. The total runoff is calculated according to:

$$R_{tot,i} = R_{d,i} + R_{s,i} + R_{ss,i} \qquad (10)$$

where

$R_{tot,i}$ – the total runoff in time step *i* [mm].

The quantitative estimation of *EA* is, as in many general numerical codes, based on a comparison between the amount of available water and *PET*. If *PET* can be satisfied by the amount of available water, then *EA* is taken as *PET*; otherwise, *EA* is lower than *PET* and limited by the water available (Vázquez, 2003). Therefore, the amount of preserved water, by which the amount of water available from the soil water capacity will be reduced, is called the evapotranspiration reduction, and is calculated as:

$$EA_{red,i} = \min\Big(P + R_{sw}, \max\Big(0, C_{EA} S_{max} - \big(S_{i-1} + \max\left(0, R_{pot} - R_d\right) - R_s - R_{ss}\big)\Big)\Big) \qquad (11)$$

where

$EA_{red,i}$ – the evapotranspiration reduction in time step *i* [mm];
C_{EA} – the coefficient of the evapotranspiration (range of the calibration of the parameter used: $0.5 > C_{EA} > 0$ [-]).

The calibration parameter serves as a relative value of the water preserved. Subsequently, in the form of a relative value of the reduced soil water capacity, the water content in the soil, that is available for evapotranspiration is calculated. The reduced soil water capacity is defined as:

$$if\ RE_{pot,i} - R_{d,i} > 0 \qquad then$$
$$z_{red,i} = \frac{s_{i-1} + RE_{pot,i} - R_{d,i} - R_{s,i} - R_{ss,i} + EA_{red,i}}{S_{max,i}}$$

$$elseif\ RE_{pot,i} - R_{d,i} \leq 0 \qquad then \qquad (12)$$
$$z_{red,i} = \frac{S_{i-1} - R_{s,i} - R_{ss,i} + EA_{red,i}}{S_{max,i}}$$

where
$Z_{red,i}$ –the reduced soil water capacity in time step *i* [mm].

The method used by (Delworth and Manabe, 1988) was integrated into the calculation of actual evapotranspiration, while the relative soil water capacity as variable *z* was replaced in this calculation by the reduced relative soil water capacity as z_{red}. The function "max(0, min(*PET*, *P* + *SWB*) -EA_{red})", which is subsequently added, ensures that at low values of z_{red}, the simultaneous exceedance of the *PET* value by the sum of *P* and *SWB* does not cause a sharp increase in *EA*:

$$EA_i = \min\Big(PET_i, \max\big(0, \min\big(PET_i, P_i + SWB_{,i}\big) - EA_{red,i}\big) + \ if\ \Big(z_{red,i} < 0.75, \frac{z_{red}{}^2 S_{max}}{0.75}, z_{red}{}^2 S_{max}\Big)\Big) \qquad (13)$$

The equation to calculate the value of the soil water capacity at the end of the time step is:

$$S_i = S_{i-1} + P_i + SWB_i - R_{tot,i} - EA_i \qquad (14)$$

Thanks to the calculation method used, the variables R_{tot} and *EA* maintain the value of S_i in the range (0, S_{max}) without using the min/max functions in the equation of S_i. By observing the behavior of the variables during modeling, they show an asymptotic bound to the range (0, S_{max}) while the S_i values balance within this range, which provides a more realistic approach to the data range (de Figueiredo et al., 2021).
In order to calculate the cycle, it is necessary to determine the definition of the maximum capacity of the soil water storage S_{max}, whose effect on the relationship with the soil moisture is barely described in the literature (Demirel et al., 2019; Zhuo and Han, 2016). The soil water storage capacity may present a wide range of spatial variations, depending on the soil and crop characteristics (Hillel, 2003); they are also important to include in the calculation of S_{max}, since it is possible to smooth out the different proportions of the individual micro-basins. Regarding the current variables, the number of which was not intended to be expanded, the best variable, considering both the soil and the crop characteristics to some degree, was the runoff coefficient. For the purpose of evaluating how capable a micro-basin is in absorbing and maintaining water in the soil, instead of the runoff coefficient, it was more appropriate to use the infiltration coefficient, which, according to Suryoputro et al. (2017) is:

$$C_i = 1 - C_r \qquad (15)$$

where
C_i – the coefficient of infiltration in time step *i* [–].

Incorporating temporal variability into the calculation of S_{max} was a matter of rough estimation due to the limitations of the input data, while the averaged values of the vegetation coefficient K_v were used based on the table of monthly K_v (for Grass Reference Evapotranspiration) from the monthly vegetation evapotranspiration observed for different types of vegetation and site conditions (Howes et al., 2015), see Table 1.
When combining the infiltration coefficient with the vegetation coefficient, the maximum capacity of the soil water storage is defined as:

$$S_{max,i} = K_{v,i}(t) C_i C_{Smax} \qquad (16)$$

where
$S_{max,i}$ – the maximum capacity of the soil water storage in time step *i* [mm];
$K_{v,i}(t)$ – the vegetation coefficient in time step *i*; when the month t = 1, 2 … 12) [mm];
C_{Smax} – the coefficient of the maximum capacity of soil water storage (range of the calibration of the parameter used: $100 < C_{Smax} < 1000$ [mm]).

Because the runoff approximation sub-model ignores the effect of the interaction with the groundwater, the values of S_{max} tend to be higher than in models that do take the groundwater into account.

Redistribution sub-model

The redistribution sub-model is represented as a scenario following the runoff approximation scenario. It does not require any calibration, but the precalculated variables in the data structure, which are required for the redistribution sub-model, are calculated for every micro-basin, and each micro-basin is dependent on the summarized variables of all the micro-basins in the sub-basin to which they belong. The enforced recalculation of one of those variables in one micro-basin by the user requires all the dependent variables of the micro-basins subordinated to the sub-basin to be automatically recalculated, thereby significantly increasing the computational time required to recalculate these variables in the data structure of the WEAP model, thus making it difficult to analyze them effectively in real-time. On the other hand, the recalculation of the results is not affected because all the variables in the scenario are recalculated during the process anyway. The outflow volume from the micro-basin equation is in the form:

$$V_{MB,i\,(j)} = R_{tot,i}\, \mathrm{A}_{MB(j)}\, 10^3 \qquad (17)$$

where
$V_{MB,i(j)}$ – the outflow volume from micro-basin *j* in time step *i* [m^3];
$A_{MB(j)}$ – the micro-basin area [km^2].

In WEAP, the variable with which it is possible to define the outflow from the node on the modeled stream is called the Surface Water Inflow (SWI). To calculate it from the outflow volume of the micro-basin, the form of the equation is:

$$SWI_i = V_{MB,i(j)}/(86400\ nDays_i) \quad (18)$$

where
SWI_i – the surface water inflow in time step *i* [$m^3\ s^{-1}$];
86 400 – the number of seconds in a day [–];
$nDays_i$ – the number of days in time step *i* [–].

The *nDays* variable is represented via the "Days" function in WEAP. To be able to calculate the difference between the cleansed outflow from the sub-basin from equation (1) and the volume of runoff from the micro-basins subordinated to the sub-basin, it is necessary to summarize them with the equation:

$$V_{SB,i} = \sum_{j=1}^{n} V_{MB,i(j)} \quad (19)$$

where
$V_{SB,i}$ – the outflow volume from the sub-basin in time step *i* [m^3];
n – the number of micro-basins in the sub-basin [–];
$V_{MB,i(j)}$ – the outflow volume from micro-basin *j* in time step *i* [m^3].

Subsequently, the difference in the outflow volume is defined by the equation:

$$V_{d,i} = Q_{c,i}\ 86400\ nDays_i - V_{SB,i} \quad (20)$$

where
$V_{d,i}$ – the difference in the outflow volume [m^3];
$Q_{c,i}$ – the cleansed outflow from the sub-basin in time step *i* [$m^3\ s^{-1}$].

The positive value of the difference in the outflow volume means that the runoff approximation sub-model in the current time step produces less water than it should according to the cleansed outflow, while the negative value means the opposite. Therefore, the positive value of V_d needs to be additionally distributed into the nodes of the micro-basins, while in the case of a negative value, the outflow from the nodes of the micro-basins should be reduced by the absolute value of negative V_d, with respect to the same redistribution pattern as for a positive V_d. For the spatial variability between the micro-basins, the infiltration coefficient calculated according to equation (15) was used at the initial point of defining the model. According to this equation, the calculation based on the runoff coefficient define the distribution of water sources only between the runoff and infiltration, while in fact the calculated coefficient also includes the evapotranspiration coefficient. Therefore, using the trial-and-error method, an equation defining the approximate value of the infiltration (and therefore also the evapotranspiration) coefficient based on the runoff coefficient was created. The equation fits the ratio between the runoff, infiltration, and evapotranspiration in the annual water balance for humid and sub-tropical regions (Keszeliová et al., 2021; Olofintoye et al., 2022), but it is a struggle to adapt it to semi-arid regions (Yaykiran et al., 2019), as the relationship between *PET* and *P* is not yet incorporated into the equation:

$$C_{inf} = \max(0, (C_r + \log((1 - C_r)/C_r))/2) \quad (21)$$

The redistributive share of the micro-basin is calculated from C_{inf} and the area of the micro-basin as:

$$C_{red} = C_{inf}\ A \quad (22)$$

where
C_{red} – the redistribution share of the micro-basin [km^2];
A – the area of the micro-basin [km^2].

Subsequently, C_{red} is then summarized for all the micro-basins in the sub-basin as:

$$C_{red,SB} = \sum_{j=1}^{n} C_{red,MB(j)} \quad (23)$$

where
$C_{red,SB}$ – the summarized redistribution coefficients of the micro-basins in sub-basin [m^3];
n – the number of micro-basins in the sub-basin [-];
$C_{red,MB(j)}$ – the redistribution coefficient of the micro-basin *j* [m^3].

For redistribution purposes, predefined WEAP variables, the Groundwater Inflow Volume (GIV) and the Groundwater Outflow Volume (GOV) are used to equalize the simulated and measured outflows from the sub-basin. To function correctly, these variables need to be connected to the groundwater node; therefore, for each sub-basin, a groundwater node is created with a sufficient volume of water. In this stage of the development of the model, the use of these features of the model has nothing to do with modeling groundwater, although it is part of the plan for possible future integration.

$$if \quad V_{d,i} > 0 \quad then \ GIV_i = V_{d,i} \frac{C_{red,MB(j)}}{C_{red,SB}} \quad (24)$$
$$elseif\ V_{d,i} < 0 \quad then \ GIV_i = 0$$

$$if \quad V_{d,i} < 0 \quad then \ GOV_i = \left| V_{d,i} \frac{C_{red,MB(j)}}{C_{red,SB}} \right| \quad (25)$$
$$elseif\ V_{d,i} > 0 \quad then \ GOV_i = 0$$

where
GIV_i – the groundwater inflow volume in time step *i* [m^3];
GOV_i – the groundwater outflow volume in time step *i* [m^3].

Data

The WEAP software calculates the change in the flowrate in the nodes created in the scheme; therefore, the nodes were created in the streams at each kilometer of their length, for which the outflow areas called micro-basins were delineated. The areas of the individual micro-basins of the basin modeled range from 48 km^2 to 0.01 km^2 with a median value of 1.447 km^2; and the altitude ranges from 103 m a.s.l. up to 822 m a.s.l. Fig. 3 shows the location of the lower Hron river basin. The variables defining both the snow sub-model and runoff approximation sub-model are calculated for every micro-basin in the basin modeled. Each sub-basin has a set of the same calibration parameters for its corresponding micro-basins.

As to validating the ARB model, two sub-basins of the water gauging station (WGS), were separately modeled. As seen in Fig. 3, the WGS 7310 sub-basin served as the first calibration sub-basin, while WGS 7308 was the validation station within it. The second sub-basin of WGS 7335 was used, as it has WGS 7318 within its area. Because the second's sub-basin's boundaries were delineated by the water gauging stations selected for the purpose of the whole model of the lower Hron River, the runoff from the WGS 7335 sub-basin was calculated according to equation (2) by subtracting the inflow into the sub-basin. In the case of the first sub-basin, the outflow from the sub-catchment was equal to the flow in WGS 7310.

WGS 7335 is located on the main Hron River catchment, while the validation WGS 7318 is situated on its tributary the Lužianka. WGS 7310 is located on a tributary of the Hron River called the Sikenica; and its validation WGS 7308 is similarly located on

Table 1. The averaged values of the vegetation coefficient for incorporating an estimation of the temporal variability into S_{max} calculations

Month	Jan.	Feb.	Mar.	Apr.	May	Jun	Jul.	Aug.	Sep.	Oct.	Nov.	Dec.
K_v [–]	0.62	0.62	0.66	0.72	0.85	0.92	0.98	0.95	0.86	0.84	0.78	0.70

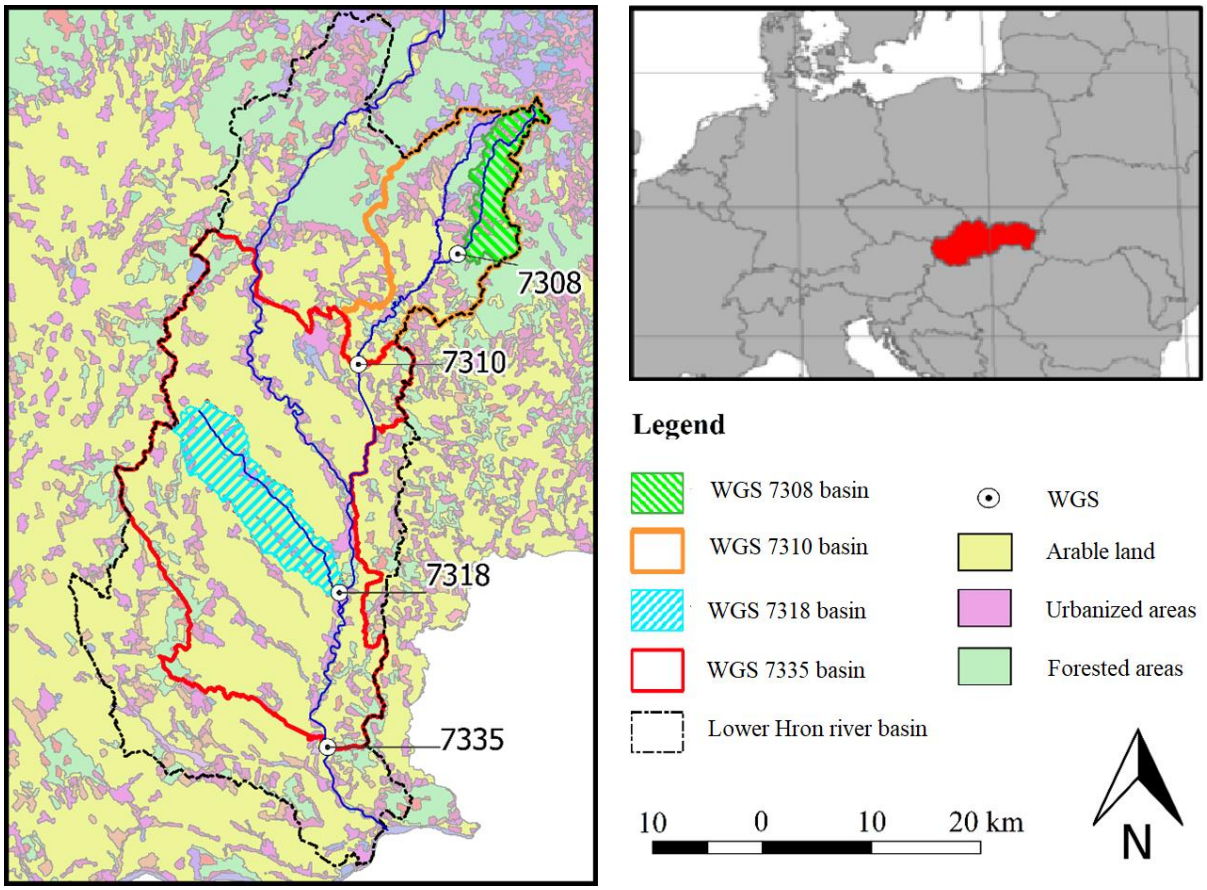

Fig. 3. Sub-basins of the calibration and validation water gauging stations (WGS) in the basin of the lower Hron River.

a tributary of the Sikenica called the Jablonovka. Both the first and second sub-basins therefore have their validation WGS located beside the main river of the sub-basin, thereby adding strength to the validation of the accuracy of the model.

The input data, as described in Tables 2 and 3, can be divided between the sub-basins and micro-basins. The time series of the hydrometeorological data in the period 2007–2019 was selected for the approximate redistributive balance modelling to estimate the distribution of the water resources. Point data from measuring stations for the temperature (14 stations) and precipitation (45 stations) were input for IDW and conventional kriging methods, used to create the raster data, from which a time series of the average values was subsequently created using zonal statistics for the individual micro-basins. All the hydrological variables calculated within the micro-basins, such as runoff or evapotranspiration, were represented as a water column in millimeters. In the case of the runoff coefficient and average altitude, the raster input data was also processed using zonal statistics. The calculation of the runoff coefficient was based on the tabular processing of the linear dependence on the slope, land use, and soil types (Mahmoud and Alazba, 2015). The total potential monthly evapotranspiration was aggregated from the total daily potential evapotranspiration, which was estimated according to the Blaney-Criddle empirical method (Schrödter, 1985).

Table 2. Input data used for calculation of the sub-basin variables: Slovak Hydrometeorological Institute (SHMÚ), Slovak Water Management Enterprise (SVP)

Input data	Precalculated from	Source	Measurement	Data application
Streamflow [m^3 s^{-1}]		SHMÚ	Stations	Redist. sub-model
The abundance of springs [m^3 s^{-1}]		SHMÚ	Stations	Redist. sub-model
Surface water withdrawals [m^3]		SHMÚ	Reporting	Redist. sub-model
Wastewater discharges [m^3]		SHMÚ	Reporting	Redist. sub-model
Water diversions [m^3 s^{-1}]		SHMÚ	Reporting	Redist. sub-model
Manipulation of the volume of reservoirs [m^3 s^{-1}]	Water level elevation [m a.s.l.] Volume-elevation curve [–]	SVP	Monitoring Documentation	Redist. sub-model

Table 3. Input data used for calculation of the micro-basin variables: Slovak Hydrometeorological Institute (SHMÚ), Geodetic and Cartographic Institute Bratislava (GKÚ), State Geological Institute of Dionýz Štúr (GÚDŠ), digital elevation model (DEM), airborne laser scanning (ALS), S_d - the potential length of sunlight during the day [h], S_y – the length of the average annual amount of potential sunlight during the day [h]

Input data	Precalculated from	Source	Measurement	Data application
Monthly average temperature [°C]	Daily average temperature	SHMÚ	Stations	Snow sub-model
Average temperature in the last week of the month [°C]	Daily average temperature	SHMÚ	Stations	Snow sub-model
Total monthly precipitation [mm]	Total daily precipitation	SHMÚ	Stations	Snow sub-model
Average altitude [m a.s.l.]	DEM 1x1 [m]	GKÚ	ALS	Snow sub-model/Runoff approx. sub-model
Monthly total potential evapotranspiration [mm]	Daily average temperature	SHMÚ	Stations	Snow sub-model
	S_d (DEM 1x1 [m])	GKÚ	ALS	Runoff approx. sub-model
	S_y (DEM 1x1 [m])	GKÚ	ALS	Runoff approx. sub-model
Coefficient of runoff [–]	Slope (DEM 1x1 [m])	GKÚ	ALS	Runoff approx. sub-model/Redist. sub-model
	Soil type	GÚDŠ	GIS	
	Land use	Author	Delineation	

Results

The performance of the ARB model was visually assessed using the correlations between the observed and simulated outflows (see Fig. 4–5). The left side of Fig. 4 shows the ability of the redistributive model to equalize the inequalities between the approximated and observed outflows. The right side of Fig. 4 shows how with a sufficiently good approximation, the redistributive sub-model can simulate runoff even on tributaries above the standard, if the sub-basin is homogeneous to some extent, which can also be evaluated according to the similarity of the flows modeled in the sub-basin.

On the right side of Fig. 5, the blue dots representing the runoff approximation sub-model outflow values show a general overestimation, while the red dots in the redistribution process lead to a more precise, yet opposing underestimation of the outflows.

To evaluate the performance of the model, the Nash-Sutcliffe Efficiency (NSE), Mean Absolute Error (MAE), and Pearson's correlation coefficient (*r*) between observed and simulated outflows were also calculated (see Table 4). The performance of the runoff approximation sub-model was significantly better in the first sub-basin, while the second sub-basin could not simulate the trends in the flow regime at either the validation or the calibration station.

From October to March, the mostly higher approximated long-term average monthly outflows compared to the observed data can be seen in Table 5, especially for the second sub-basin. The opposing trend can be observed from April to September, which can be identified as the result of calibration of the parameters during the approximation of the runoff i.e., the effort to even out inaccuracies during the winter months.

First sub-basin tested: Calibration – WGS 7310; Validation – WGS 7308

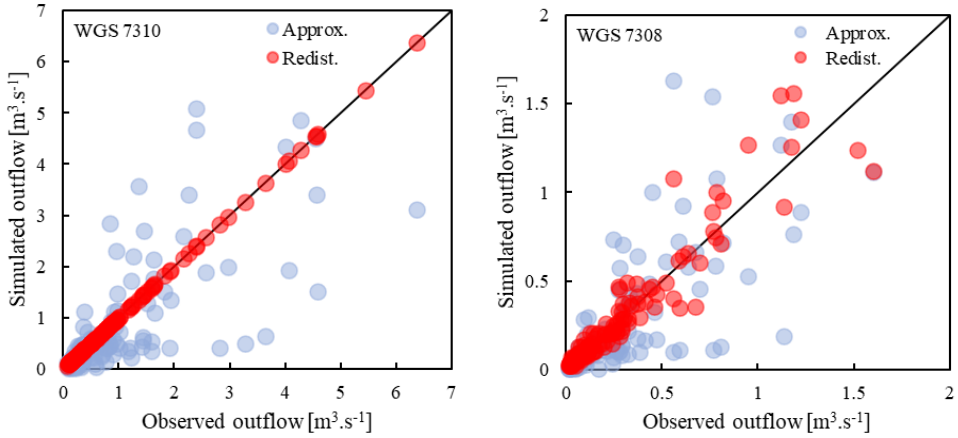

Fig. 4. The correlation between the observed and simulated outflows for the first sub-basin tested: Approximation (Approx. – blue dots) and redistribution (Redist. – red dots) scenarios.

Second sub-basin tested: Calibration – WGS 7335; Validation – WGS 7318

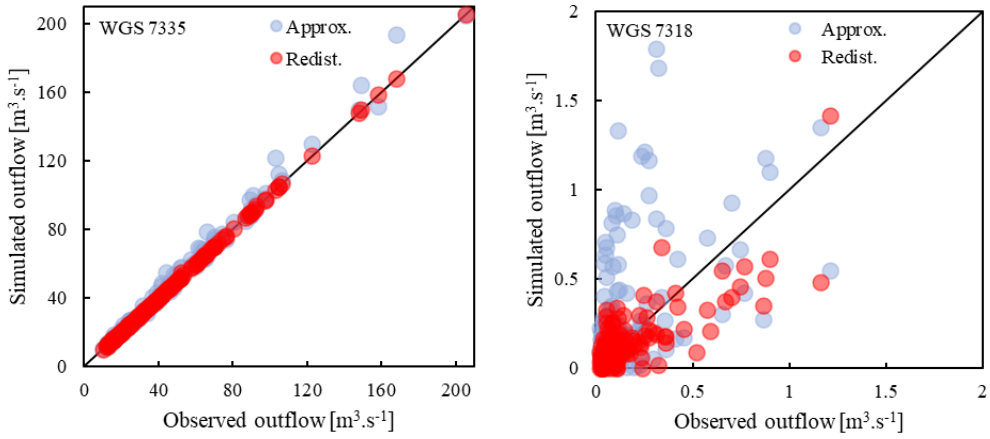

Fig. 5. The correlation between the observed and simulated outflows for the second sub-basin tested: Approximation (Approx. – blue dots) and redistribution (Redist. – red dots) scenarios.

Table 4. The ARB model performance statistics in time period 2007–2019 (time steps – 156 months) for the first and second sub-basins tested

Characteristics	Sub-basins							
	1st sub-basins tested				2nd sub-basins tested			
No. WGS	7308		7310		7318		7335	
Area [km^2]	50.1		164.1		92.2		651.8	
Scenario	Approx.	Redist.	Approx.	Redist.	Approx.	Redist.	Approx.	Redist.
NSE [–]	0.48	0.89	0.42	1	-3	0.59	-9.1	1
MAE [m^3 s^{-1}]	0.12	0.052	0.45	0.00081	0.24	0.09	2	0.079
r [–]	0.78	0.95	0.75	1	0.49	0.77	0.24	1

Table 5. Long-term average monthly outflows for first and second tested sub-basins

Tested	No. WGS	Scenario	Long-term average monthly outflows											
			Jan.	Feb.	Mar.	Apr.	May	Jun	Jul.	Aug.	Sep.	Oct.	Nov.	Dec.
1st sub-basins	7308	Observ.	0.275	0.487	0.560	0.369	0.246	0.164	0.059	0.087	0.094	0.100	0.206	0.335
		Approx.	0.326	0.546	0.645	0.226	0.103	0.093	0.053	0.042	0.172	0.113	0.204	0.219
		Redistr.	0.286	0.572	0.513	0.394	0.210	0.194	0.067	0.096	0.156	0.107	0.202	0.286
	7310	Observ.	0.975	2.006	1.731	1.274	0.778	0.712	0.249	0.371	0.478	0.390	0.798	1.122
		Approx.	1.144	1.899	2.276	0.593	0.343	0.299	0.189	0.152	0.541	0.409	0.804	0.845
		Redistr.	0.977	2.007	1.731	1.274	0.778	0.712	0.249	0.371	0.478	0.386	0.797	1.122
2nd sub-basins	7318	Observ.	0.174	0.241	0.239	0.217	0.166	0.197	0.093	0.104	0.114	0.127	0.135	0.171
		Approx.	0.656	1.000	0.739	0.194	0.139	0.088	0.106	0.076	0.171	0.190	0.263	0.443
		Redistr.	0.155	0.163	0.229	0.179	0.153	0.218	0.085	0.104	0.091	0.129	0.155	0.148
	7335	Observ.	1.616	1.576	1.819	1.455	1.288	1.766	0.644	0.770	0.614	0.912	1.173	1.390
		Approx.	5.631	8.366	5.909	1.528	1.147	0.710	0.803	0.578	1.287	1.526	2.026	3.732
		Redistr.	1.571	1.596	1.790	1.402	1.243	1.758	0.667	0.782	0.647	1.112	1.238	1.383

Discussion

The right side of Fig. 6 interprets how much water had to be distributed via the redistribution model to equalize the simulated and measured streamflow. The increasing value indicates that the runoff approximation sub-model overestimated, while the decreasing value indicates the opposite; the graph thus serves as an indicator of the accuracy of the runoff approximating the sub-model. Therefore, a prerequisite for satisfaction with the simulation of the runoff approximation sub-model could be the condition that the variable ΔVd fluctuates around its initial value. The low degree of precision in the second sub-basin approximation has several causes (as set out in the results). They all come from the difference between the sub-basin conditions of the validation and calibration stations. The difference between their sub-basins lies not only in the significant difference in the area and runoff (compared to the first sub-basin), but the Hron River, on which WGS 7335 is located, also crosses the gravely alluvium of the lower Hron along the entire length of the sub-basin of WGS 7335, and thus is significantly more affected by the interaction with groundwater than the other streams that flow into the Hron River in this area.

Since the conceptual snow sub-model used can also be responsible for significant deviations in the runoff approximating sub-model during the winter season, the statistical parameters of the simulation in Table 6 are evaluated in the range of the month May – October (summer season without the influence of snow). While the evaluation of only the summer months showed a significant improvement in the second sub-basin, thereby indicating the significant effect of the inaccuracy of the snow sub-model, in the case of the first sub-basin, the statistical parameters show a slight deterioration, which can be represented in this case as the slightly better results of the snow sub-model rather than the runoff approximation sub-model.

The issue which, at this spatial scale in a monthly time step that any modeling of snow water equivalent would face, is the fact that precipitation is not equally distributed during a month. Another explanation could be that the snow water equivalent data observed in the weekly time step, which were used in the snow sub-model calibrations, are not efficient for this sub-basin scale. Therefore, the snow sub-model's degree of inaccuracy would be better solved via evaluating it on a weekly or even daily time step, either externally or in a separate model created in WEAP using a more detailed time step. When trying to use the ARB model in any analysis of the future scenarios, it would be necessary to transform time-invariant inputs such as land use into the variables in the form of scenarios (see Kohnová et al., 2019).

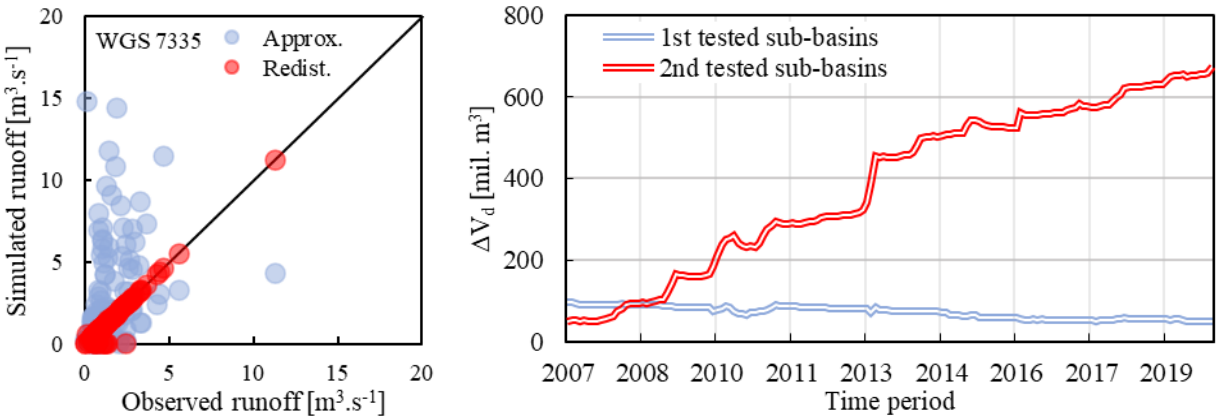

Fig. 6. The correlation between the observed and simulated runoff for WGS 7335: Approximation (Approx. – blue dots), redistribution (Redist. – red dots) scenario (left), and cumulative outflow volume difference of redistribution sub-model for the first and second sub-basins tested (right).

Table 6. The ARB model performance statistics in time period 2007–2019 (time steps – 156 months) for the first and second sub-basins tested

Sub-basin	1st tested sub-basins				2nd tested sub-basins			
Scenario	WGS 7308		WGS 7310		WGS 7318		WGS 7335	
	Approx.	Redist.	Approx.	Redist.	Approx.	Redist.	Approx.	Redist.
NSE [–]	-0.02	0.79	0.25	1	0.53	0.8	0.32	1
MAE [m^3 s^{-1}]	0.077	0.037	0.29	0.00074	0.094	0.062	0.79	0.066
r [–]	0.52	0.92	0.58	1	0.74	0.89	0.58	1

Conclusion

The ARB model was created as the gradual result of a vision of accurate modeling in the field of retrospective analysis of the quantitative water management balance of flows, which in Slovakia focuses more on the evaluation of the quantity of the outflow from smaller tributaries, which lack continual measurement equipment.

The results indicate that the validation water gauging stations show a relatively high degree of precision of the simulation in the redistribution scenario; however, the simulation of sub-basins affected more by groundwater will also require more attention to detail, as will the conceptual snow sub-model. Although the ARB model uses an unconventional method, it provides the expected and satisfactory results. The research on the model will be followed by testing the model on a weekly time step and creating the concept of scenarios for an analysis of the impact of water management on the water balance to fulfill the balance part of the ARB model.

Acknowledgement

This work was supported by the Slovak Research and Development Agency under Contract Nos. APVV 19-0340 and APVV 20-0374 and the VEGA Grant Agency No. VEGA 1/0782/21.

References

Demirel, M. C., Özen, A., Orta, S., Toker, E., Demir, H. K., Ekmekcioğlu, Ö., Booij, M. J. (2019): Additional value of using satellite-based soil moisture and two sources of groundwater data for hydrological model calibration. Water, 11(10), 2083. Available at: https://doi.org/10.3390/w11102083

de Figueiredo, T., Royer, A. C., Fonseca, F., de Araújo Schütz, F. C., Hernández, Z. (2021): Regression Models for Soil Water Storage Estimation Using the ESA CCI Satellite Soil Moisture Product: A Case Study in Northeast Portugal. Water, 13(1), 37. Available at: https://doi.org/10.3390/w13010037

Delworth, T. L., Manabe, S. (1988): The influence of potential evaporation on the variabilities of simulated soil wetness and climate. Journal of Climate, 1(5), 523–547. Available at: https://doi.org/10.1175/1520-0442(1988)001< 0523: TIOPEO>2.0.CO;2

Healy, R. W. (2010): Estimating groundwater recharge. Cambridge University Press. p. 245.

Hillel, D. (2003): Introduction to environmental soil physics. Elsevier.

Howes, D. J., Fox, P., Hutton, P. H. (2015): Evapotranspiration from natural vegetation in the Central Valley of California: Monthly grass reference-based vegetation coefficients and the dual crop coefficient approach. Journal of Hydrologic Engineering, 20(10), 04015004. Available at: https://doi.org/10.1061/(ASCE)HE.1943-5584.0001162

Kandera, M., Výleta, R. (2020): Application of the Water

Evaluation and Planning (WEAP) model to quantitative water balance modeling in the Upper Hron River basin (Slovakia). In IOP Conference Series: Earth and Environmental Science (Vol. 609, No. 1, p. 012055). IOP Publishing. Available at: https://doi.org/10.1088/1755-1315/609/1/012055

Kandera, M., Výleta, R., Liová, A., Danáčová, Z., Lovasová, Ľ. (2021): Testing of water evaluation and planning (Weap) model for water resources management in the Hron river basin. Acta Hydrologica Slovaca, 22(1), 30–39. Available at: https://doi.org/10.31577/ahs-2021-0022.01.0004

Keszeliová, A., Hlávčová, K., Danáčová, M., Danáčová, Z., Szolgay, J. (2021): Detection of Changes in the Hydrological Balance in Seven River Basins Along the Western Carpathians in Slovakia. Slovak Journal of Civil Engineering, 29(4), 49–60. Available at: https://doi.org/10.2478/sjce-2021-0027

Kohnová, S., Rončák, P., Hlavčová, K., Szolgay, J., Rutkowska, A. (2019): Future impacts of land use and climate change on extreme runoff values in selected catchments of Slovakia. Meteorology Hydrology and Water Management. Research and Operational Applications, 7. Available at: https://doi.org/ 10.26491/mhwm/97254

Mahmoud, S. H., Alazba, A. A. (2015): Hydrological Response to Land Cover Changes and Human Activities in Arid Regions Using a Geographic Information System and Remote Sensing. PLoS ONE 10(4): e0125805. Available at: Available at: https://doi.org/10.1371/ journal.pone.0125805

Olofintoye, O. O., Ayanshola, A. M., Salami, A. W., Idrissiou, A., Iji, J. O., Adeleke, O. O. (2022): A study on the applicability of a Swat model in predicting the water yield and water balance of the Upper Ouémé catchment in the Republic of Benin. Slovak Journal of Civil Engineering, 30(1), 57-66. Available at: https://doi.org/10.2478/sjce-2022-0007

Schrödter, H. (1985): Verdunstung – Anwendungsorientierte Meßverfahren und Bestimmungsmethoden, Springer Verlag. p. 187.

Sieber, J., Purkey, D., (2015): Water Evaluation And Planning (WEAP) System user guide, Stockholm Environment Institute, Somerville, MA, USA.

Sleziak, P., Výleta, R., Hlavčová, K., Danáčová, M., Aleksić, M., Szolgay, J., Kohnová, S. (2021): A Hydrological Modeling Approach for Assessing the Impacts of Climate Change on Runoff Regimes in Slovakia. Water, 13, 3358. Available at: https://doi.org/10.3390/w13233358

Slovak Hydrometeorological Institute (2021): Water resource balance of surface water quantity for 2020, SHMÚ Bratislava, 399.

Suryoputro, N., Suhardjono, Soetopo, W., Suhartanto, E. (2017): Calibration of infiltration parameters on hydrological tank model using runoff coefficient of rational method. In AIP Conference Proceedings (Vol. 1887, No. 1, p. 020056). AIP Publishing LLC. Available at: https://doi.org/10.1063/1.5003539

Vázquez, R. F. (2003): Effect of potential evapotranspiration estimates on effective parameters and performance of the MIKE SHE-code applied to a medium-size catchment. Journal of Hydrology, 270(3–4), 309–327. Available at: https://doi.org/10.1016/S0022-1694(02)00308-6

Yaykiran, S., Cuceloglu, G., Ekdal, A. (2019): Estimation of water budget components of the Sakarya River Basin by using the WEAP-PGM model. Water, 11(2), 271. Available at: https://doi.org/10.3390/w11020271

Zhuo, L., Han, D. (2016): Could operational hydrological models be made compatible with satellite soil moisture observations? Hydrological Processes, 30(10), 1637–1648. Available at: https://doi.org/10.1002/ hyp.10804

Ing. Miroslav Kandera (*corresponding author, e-mail: miroslav.kandera@stuba.sk)
Assoc. Prof. Ing. Roman Výleta, PhD.
Department of Land and Water Resources Management
Faculty of Civil Engineering
Slovak University of Technology in Bratislava
Radlinského 11
810 05 Bratislava
Slovak Republic

DOI: 10.31577/ahs-2023-0024.01.0015

ACTA HYDROLOGICA SLOVACA

Volume 24, No. 1, 2023, 134 – 140

Change of the Manning´s coefficient in small stream influenced by vegetation

Radoslav SCHÜGERL*, Yvetta VELÍSKOVÁ

Aquatic vegetation in natural streams impedes the flow of water and may increase flood risks. This paper analyses impact of aquatic vegetation density on the dynamics of flow process by evaluation of the Manning´s coefficient value obtained from field measurements. Measurements performed during two years (2020 and 2021) along the part of the Malina stream were used for determination of the Manning´s roughness coefficient value for different extents of river bed overgrowth during the year. This stream, located at the Zahorská Lowland, is a stream with a low longitudinal slope (0.00037–0.00039) and aquatic vegetation occurrence. Value of the Manning´s coefficient is varying during the growing season in the range from 0.025 to 0.157 for the year 2021 and from 0.038 to 0.266 for the year 2021.

KEY WORDS: Manning coefficient, aquatic vegetation, growing season, discharge and flow conditions

Introduction

The process of morphology development of streams is affected by many factors: flow, slope, bed material, its grain size, vegetation distribution, obstacles (constructions, woods), etc. Aquatic vegetation (type of plant, age, size), in particular, plays a significant role in this process and considerably influences discharge and flow conditions. Aquatic vegetation increases the flow resistance and effectively reduces the flow velocity (Thorne, 1990), sediment carrying capacity, and thus affecting the sediment transport - deposition process and final river bed morphology (Demich, 2008; Li et al., 2016; Oorschot et al., 2016). Many geomorphologists and engineers have recognized that aquatic vegetation impacts river channel hydrodynamic characteristics and morphology: vegetation roots alter morphological conditions and riparian stability, reduce riparian erosion, which in turn affects the channel lateral migration characteristics (Yang et al., 2018). The effects of different vegetation types and densities on these river parameters vary significantly. Channel with dense vegetation generally have lower river-widening rates than those without vegetation (Beeson and Doyle, 1995; Huang and Nanson, 1997), because aquatic vegetation can change the river pattern by changing its width and depth ratio (Van de Lageweg et al., 2010).

Although flow resistance can be reduced by a complete or partial removal of the in-stream vegetation, this is an expensive procedure and also can have ecological implications. A complete removal of the plants in a river can lead to erosion of the bed and banks and turbidity of water. The roots of the vegetation bind the soil mass, the aquatic vegetation protects the channel from the erosive action of flowing water and hinders moving soil particles on the bed of the channel (Kováčová, 2022). This protective action varies with the species of vegetation and with uniformity of coverage. For any individual type of vegetation, it varies depending on the age and condition of the plants and on the season of the year. On the other hand, an unrestricted growth of vegetation can lead to a total loss of capacity to convey water (Boscolo, 2014).

The role of aquatic vegetation in morphodynamic behavior of rivers was largely investigated through field studies, which study the importance of vegetation for river process (stability/erosion), hydraulic efficiency of river channels or channel narrowing and sediment retention. For example, Dan and Wittenberg (2007) highlighted the importance of shrubs in reducing flow velocities, studied the effect of vegetation density on the river channel. Other results showed that when the vegetation coverage was high, the channel was narrow and deep; when the vegetation coverage was low, the channel was wide and shallow (Allmendinger et al., 2005; Huang and Nanson, 1997).

In this study, we try to evaluate the changes of the Manning´s roughness coefficient value for flow conditions in the lowland stream with low longitudinal slope during growing seasons. Value of this coefficient was determined from sets of field measurements performed along the part of the Malina stream located at Záhorská lowland during the years 2020–2021.

Theoretical background

Aquatic vegetation affects fluvial environment and flow, so it is one of the important objectives in river management and river hydraulics. In hydraulic analysis, non-submerged and submerged plant conditions is usually distinguished because the flow phenomenon becomes more complicated when the flow depth exceeds the plant height (Stone and Shen, 2002). Several authors, including Maione et al. (2000) and Sellin and van Beesten (2002) have reported considerable seasonal variation caused by the growth of vegetation. Any progress in understanding the behavior of flow over vegetation allow us to improve both the knowledge of flow-velocity profiles and flow resistance and the design of vegetated channels, eventually (Carollo et al., 2002). Understanding or determining of aquatic vegetation impact on flow in streams is not an easy task. Aquatic vegetation during growing season changes its properties – it can have various density, amount, flexibility, tallness, etc. – so the rate of impact on the hydraulic roughness also changes. This process is dynamic because of temporal changes in roughness due to natural vegetative growth, management practices, and dynamic response of vegetation to the flow (Franklin et al., 2008). Many studies have tried to solve this problem by different ways (Stephan and Gutknecht, 2002; Okhravi and Gohari, 2020; Čubanová et al., 2022).
In this study, our approach is based on commonly and widely applied empirical derived Manning´s formula.
The Chézy´s equation (also empirically derived) was initially identified as a method for finding flow velocity in form (Kolář et al., 1983):

$$v = C\sqrt{R.i_e} \tag{1}$$

where
v – is a mean flow velocity [m s^{-1}],
C – is the Chézy´s coefficient,
R – is a hydraulic radius [m],
i_e – is a slope of energy line [–].

Consequently, if Manning's empirical formula is introduced into the Chezy's equation, then we get formula for flow velocity in form:

$$v = \frac{1}{n}R^{2/3}i_e^{1/2} \tag{2}$$

where
n – is the Manning´s roughness coefficient.

Both equations look simple, but in practical applications in the conditions of natural streams, the determination of flow resistance is not quite simple. Most difficulties connect with determination of channel roughness, which should mirror existed conditions along investigated or designed reach of a stream. There are various approaches how the roughness can be expressed, for example description with constant roughness coefficient through the Chézy formula, the Darcy-Weisbach equation, the Manning´s equation or roughness coefficient dependent on flow characteristics, for example the Strickler and Keulegan approach (Carlier d´Odeigne and Soares Frazao, 2016).
Factors affecting flow resistance in open channels include granular composition of the channel bottom, flow depth, cross-sectional shape, vegetation, sinuosity, bed forms, sediment transport, etc. Vegetation can be a major source of temporal variation in flow resistance. Dense vegetation can also alter the effective area of a cross section that conveys the discharge (Järvelä, 2004). Most of the factors impact affecting the value of the roughness coefficient can be quantified in laboratory conditions, but its complex value can be, and more correctly, obtained from field measurements. Evaluation of the impact of aquatic vegetation on flow conditions in a lowland stream is complicated. Influence of vegetation on the coefficient n can be described, for example as a function of the flow depth, density, velocity distribution and type of vegetation (Tuozzolo et al., 2019). Nevertheless, it is possible to determine the value of the roughness coefficient n for a stream reach by using the Manning´s formula (Eq. 2) along the part of a stream with steady uniform flow conditions, on which can be considered that the slope of energy line equals the water level slope i as follows:

$$n_m = \frac{A_m R_m^{2/3} i_m^{1/2}}{Q_m} \tag{3}$$

where
A_m – is a measured discharge area [m^2],
Q – is a discharge [m^3 s^{-1}],
index m – means a measured value.

This equation (Eq. 3) is used also in this study.
Since the vegetation is strongly dependent on the season, the roughness coefficient can be significantly different for summer or winter conditions. Thus, the effects of vegetation on the roughness or on the flow field in this method are not taken into account arbitrarily, but are calculated from the actual velocity profile and represent the equivalent roughness of the bed.

Material and methods

Field measurements, related to the investigation of aquatic vegetation impact on Mannning´s coefficient in a lowland stream, were performed along the Malina stream at the Záhorská lowland. The Malina stream is a small stream flows through the territory of the Malacky district. It is a left tributary of the Morava River, its length is 47.75 km. Catchment area is 516.6 km² and its discharge is from 0.828 m^3 s^{-1} in the first monitoring cross-section profile at the Jakubov village to 2.234 m^3 s^{-1} in the estuary. Two observation cross-sectional profiles were selected along the Malina stream (river kilometer 7–8), their location is shown in Fig. 1.
Measurements were performed in the channel segments with steady uniform flow conditions. In general, field measurements were done from April to September to detect what changes occur in different periods of the growing season. The measurement were carried out

in a part of the stream with a length of 1140 meters (from profile A to profile B), along which the width varied from 5 to 8 meters. Average depth in the study stream reach ranged from 0.4 m to 1.2 m (depending on flow and biomass of aquatic vegetation). Cross-section profiles parameters (channel width, water depth distribution along the cross-section profile width), water levels (by levelling device), discharges and velocity profile (by ADV – Acoustic Doppler Velocimeter – device Flow Tracker) were measured (Fig. 2). Each cross-section profile was measured at least three times and the average value from these measurements was used in the calculation. The ADV Flow Tracker device determines the discharge value immediately after the finishing of the measurement (SonTek, 2009). If this value differed by about 5%, the measurement was excluded from further processing and repeated once more. This ADV device uses three methods for calculations of discharge in the open channels in accordance with the applicable standard (mid-section, mean-section and Japanese method). In our case, we used the mid-section method.

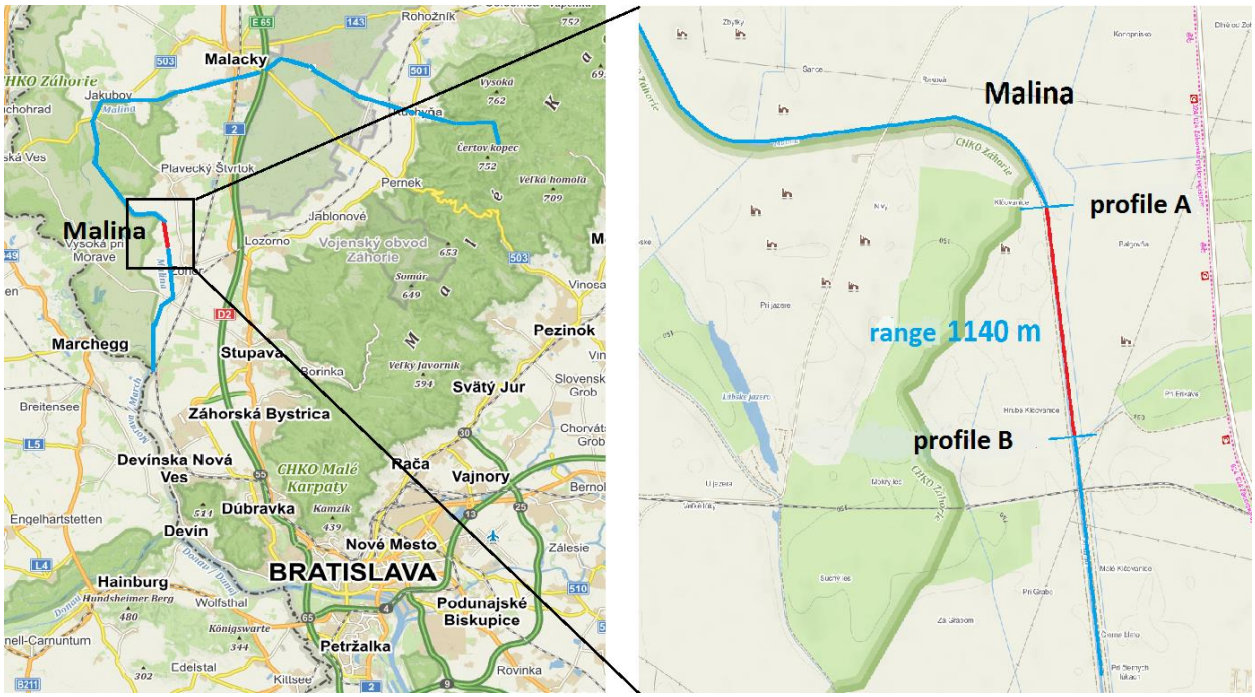

Fig. 1. Map and location of the Malina stream and observation cross-sectional profiles - profile A and profile B.

Fig. 2. Acoustic Doppler Velocimeter – Flow Tracker device for measurement of velocity profile and discharge (left) and photo of the overgrowth of the Malina stream during summer season (right).

Results and discussion

As it was mentioned, aquatic vegetation has significant impact on change of Manning´s coefficient. Measurements on the Malina stream were carried out during two growing seasons (years 2020 and 2021). Table 1 shows the measured data from individual months (from April to September) for defined reach. Table contains discharge (*Q*), cross section profile area (*A*), average flow velocity (*v*), average flow depth (*h*), water level slope (*i*) and Manning´s coefficient (*n*).

The roughness coefficient value *n* in the overgrown streambed is changing during the growing season depending on aquatic vegetation growth. In consequence of raised roughness, the velocity profile is changing and thereafter the discharge capacities are also changed. The rate of the vegetations impact on flow regime during the vegetation season differed. The reason is that each month had different climatic conditions, which stimulated aquatic vegetation growth to a different extent.

Higher roughness coefficient values (from 0.038 to 0.266) were recorded in each month in 2021 than in 2020 (from 0.025 to 0.157). For example, the value of the Manning´s roughness coefficient by Chow (1959) for channels not maintained (dense uncut weeds, high equals the flow depth) is from 0.050 to 0.120 or for channels with dense brush is from 0.080 to 0.140. The difference between minimum and maximum in roughness coefficient values was 0.132 (for 2020) and 0.228 (for 2021). Values of Manning´s coefficient continuously increase during the growing season, with the highest values recorded in August and September. The lowest value of the flow velocity was recorded in the spring, in April or May. After these months, the aquatic vegetation starts to grow and influences the value of roughness coefficient evidently. The relationship between the discharge values and the Manning´s coefficient values is shown in the Fig. 3. The highest values of the discharge were in the months without dense vegetation (until June; in June 2021, the highest discharge value was recorded due to excessive precipitation). On the other hand, discharges around 0.4 $m^3 s^{-1}$ were measured in wide range of the Manning´s coefficient values. It is interesting, that in 2020 value of Manning´s coefficient increased with value of the discharge. In contrast, year 2021 shows opposite results – the increasing value of the coefficient shows lower value of the discharge. Relation between values of flow velocity and Manning´s coefficient, in the Fig. 4, more evidently shows indirect dependence of flow velocity and the Manning´s coefficient values. Comparable result published also O´Hare et al. (2010). The highest values of the flow velocity were measured in April (without dense vegetation) in both measured profiles, the lowest values in August (when vegetation is fully-grown).

Regarding the measured water depth, results indicate increasing value of the Manning´s coefficient with increasing water depth (Fig. 5) during the growing season. The greatest depth was reached in August in both measured years and in both profiles, when the flow velocity had its minimal value the observed data. On the other side, the smallest depth was measured in April, respectively in May, with the highest values of the flow velocity. Our measurement results confirmed the fact that with aquatic vegetation growing/occurrence the water depth in the channel increases together with the decrease of the flow velocity during the growing season.

Table 1. Summary of measured and calculated data for studied reach (from cross section profile A to cross section profile B)

date of measurement	Profile A				Profile B					
	h **[m]**	***A*** **[m^2]**	***v*** **[m s^{-1}]**	***Q*** **[$m^3 s^{-1}$]**	***h*** **[m]**	***A*** **[m^2]**	***v*** **[m s^{-1}]**	***Q*** **[$m^3 s^{-1}$]**	***i***	***n***
04/2020	0.25	2.10	0.23	0.33	0.42	1.27	0.28	0.35	0.000328	0.025
05/2020	0.24	1.40	0.12	0.31	0.46	1.47	0.27	0.33	0.000395	0.027
06/2020	0.56	2.90	0.13	0.38	0.59	3.57	0.14	0.37	0.000248	0.067
07/2020	0.73	4.02	0.09	0.39	0.55	3.88	0.17	0.40	0.000409	0.086
08/2020	0.90	4.09	0.09	0.36	0.84	4.24	0.07	0.34	0.000451	0.157
09/2020	0.84	4.39	0.09	0.42	0.78	4.44	0.09	0.40	0.000411	0.150
average	**0.58**	**3.15**	**0.13**	**0.36**	**0.60**	**3.14**	**0.17**	**0.37**	**0.000374**	**0.085**
04/2021	0.36	2.92	0.28	0.82	0.41	2.55	0.30	0.86	0.000357	0.038
05/2021	0.38	2.52	0.27	0.71	0.39	2.37	0.29	0.74	0.000416	0.039
06/2021	0.71	4.25	0.24	1.05	0.61	5.56	0.26	1.08	0.000375	0.054
07/2021	0.79	4.08	0.09	0.50	0.57	3.95	0.09	0.49	0.000378	0.139
08/2021	0.88	4.03	0.05	0.35	0.74	4.32	0.04	0.34	0.000407	0.265
09/2021	0.85	4.85	0.05	0.20	0.55	4.09	0.04	0.19	0.000392	0.266
average	**0.66**	**3.77**	**0.16**	**0.60**	**0.54**	**3.80**	**0.17**	**0.62**	**0.000387**	**0.133**

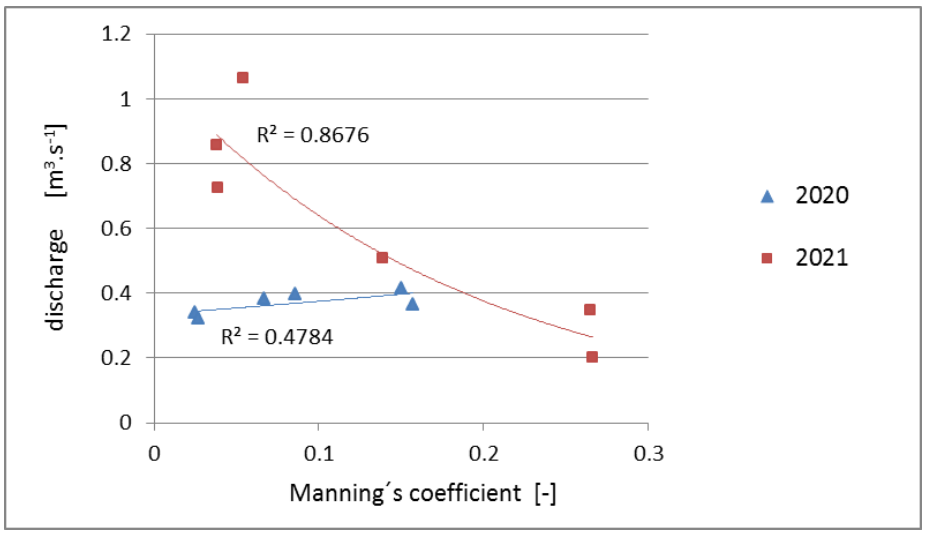

Fig. 3. Dependence between values of discharge and Manning´s coefficient.

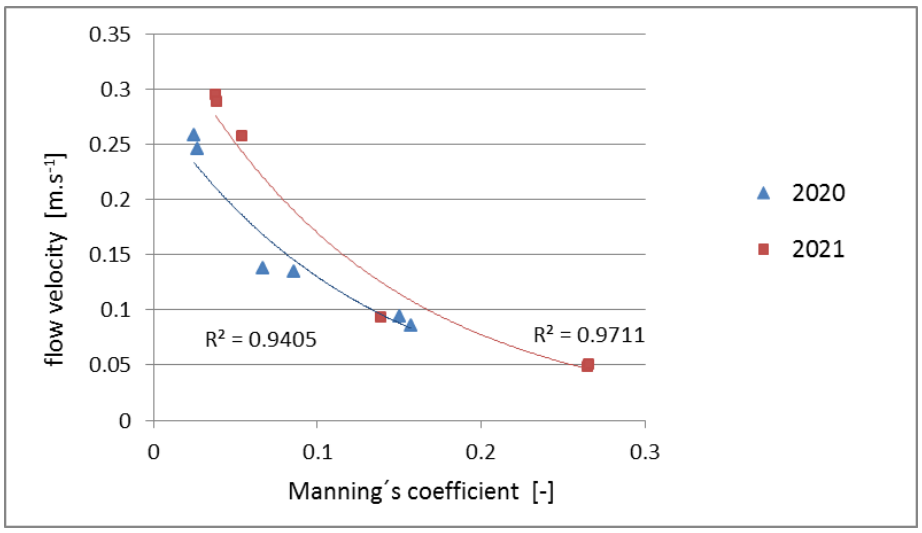

Fig. 4. Dependence between values of flow velocity and Manning´s coefficient.

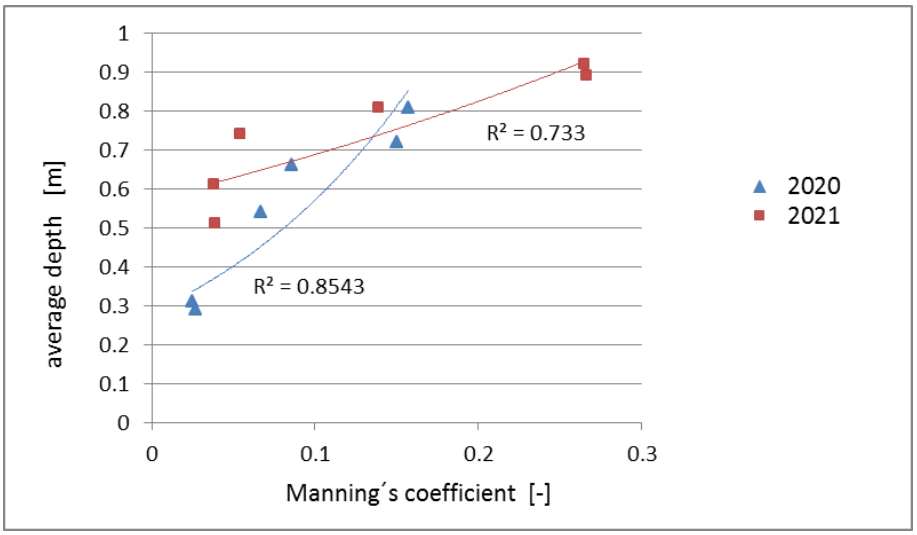

Fig. 5. Dependence between values of average depth and Manning´s coefficient.

Conclusion

Vegetation in natural streams influences the flow and related characteristics and phenomena, such as discharge capacity, velocity profile, roughness, but also erosion and sedimentation, pollutant transport and water biota. The aim of this paper was to investigate and determine the impact rate of aquatic vegetation on change of the Manning´s coefficient, based on field measurements along the Malina stream.

The analysis of the obtained data shows increase values of the roughness coefficient during the vegetation period to a significant degree. More influence is manifested not exactly in the summer, but more in the end of this season or in the beginning of autumn. Value of flow velocity significantly decreases with increasing roughness coefficient value in growing season (when *n* increases 6–7 times, the velocity decreases 3–7 times, depending on other conditions that need to be analyzed in the future). In contrast, but logically, the water depth value and the discharge area increase with the roughness coefficient value, but not in such steep way. In general, the discharge value is also related to the value of Manning´s roughness coefficient, but this dependence is not unambiguous.

Our measurements were carried out from April to September, but results show the necessity to extend this period, because evident weakening of vegetation influence was not observed. Anyway, analyses of measured data showed and confirmed the complexity of the impact of lowland river vegetation on flow condition, and the necessity to continue investigation of this problem.

Acknowledgement

This paper was prepared with the support of the project No. VEGA 2/0028/23.

References

Allmendinger, N. E., Pizzuto, J. E., Potter, N., Johnson, T., Hession, W. C. (2005): The influence of riparian vegetation on stream wisth, Eastern Pennsylvania, USA. Geol. Soc. Am. Bull. 2005, 117, 229–243.

Beeson, C. E., Doyle, P. F. (1995): Comparison of bank erosion at vegetated and non-vegetated channel bends. Water Resour. Bull. 1995, 31, 983–990.

Boscolo, V. (2014): Effect of in-stream vegetation on hydraulic resistance in regulated rivers. Master thesis, Padova, Aberdeen, 2014, 117 p.

Carlier d´Odeigne, O., Soares Frazao, S. (2016): Determination of bed roughness parameters from field survey: application to the Cavaillon River, Haiti. In: International Conference on Fluvial Hydraulics, 2016, 2262–2268. http://hdl.handle.net/2078.1/183207

Carollo F. G., Ferro V., Termini D. (2002): Flow velocity measurements in vegetated channels. In: Journal of Hydraulic Engineering, vol. 128, no. 7, 2002, 664–673. ISSN 0733-9429

Chow, V. T. (1959): Open channel hydraulics. McGraw-Hill, 1959.

Čubanová, L., Šoltész, A., Mydla, J. (2022): Analysis of droughts due to the operation of water structures: Gidra river case study. Pollack Periodica. vol. 17, no.1, 2022, 111–116. ISSN: 1788-1994

Dan, M., Wittenberg, L. (2007): Scaling the effects of riparian vegetation on cross-sectional characteristics of ephemeral mountain streams - A case study of Nahal Oren, Mt. Carmel, Israel. CATENA 2007, 69, 103–110.

Demich, R. L. (2008): The effect of submerged aquatic vegetation on flow in irrigation canals. Disertation thesis, Texas A&M University, 2008, 165 p.

Franklin, P., Dunbar, M., Whitehead, P. (2008): Flow controls on lowland river macrophytes: A review. In: Science of the Total Environment, 2008, vol. 400, no. 1–3, 369–378. https://doi.org/10.1016/j.scitotenv.2008.06.018

Huang, H. Q., Nanson, G. C. (1997): Vegetation and channel variation; a case study of four small streams in Southeastern Australia. Geomorphology 1997, 18, 237–249.

Järvelä, J. (2004): Flow resistance in environmental channels: Focus on vegetation. Helsinki University of Technology, Espoo, 2004, 54 p. ISBN 951-22-7073-0.

Kolář, V., Patočka, C., Bém, J. (1983): Hydraulics, Alfa, Prague, 474 p. (in Czech)

Kováčová, V. (2022): Impacts of excessive nutrients load in aquatic ecosystems. In: Acta Hydrologica Slovaca, vol. 23, no. 1, 2022, 99–108. DOI: 10.31577/ahs-2022-0023.01.0011

Li, Z. W., Yu, G. A., Brierley, G., Wang, Z. Y. (2016): Vegetative impacts upon bedload transport capacity and channel stability for differing alluvial planforms in the Yellow River source zone. Hydrol. Earth Syst. Sci. 2016, 20, 3013–3025.

Maione, U., Monti, R., Romiti, R. (2000): Hydraulic drag in vegetated channels – A campaign investigation. In: Maione, U., Lehto, M. and Monti, R. (eds.). Proceedings of an international conference New Trends in Water and Environmental Engineering for Safety and Life. Balkema, Rotterdam.

O´Hare, T. M., McGahey, C., Bisset, N., Cailes, C., Henville, P., Scarlett, P. (2010): Variability in roughness measurements for vegetated rivers near base flow, in England and Scotland. In: Journal of Hydrology, 2010, vol. 385, no. 1–4, 361–370. https://doi.org/10.1016/j.jhydrol.2010.02.036

Okhravi, S., Gohari, S. (2020). Form friction factor of armored river beds. Canadian Journal of Civil Engineering, 47(11): 1238–1248.

Oorschot, M. V., Kleinhans, M., Geerling, G., Middelkoop, H. (2016): Distinct patterns of interaction between vegetation and morphodynamics. Earth Surf. Process. Landf. 2016, 41, 791–808.

Sellin, R. H. J., van Beesten, D. (2002): Berm vegetation and its effects on flow resistance in a two-stage river channel: an analysis of field data. In: Bousmar, D. and Zech, Y. (eds.). River Flow 2002. 319–327.

SonTek, (2009): FlowTracker Handheld ADV Technical Manual, Firmware Version 3.7, Software Version 2.30 – SonTek/YSI, San Diego, p. 126, 2009.

Stephan, U., Gutknecht, D. (2002): Hydraulic resistance of submerged flexible vegetation. In: Journal of Hydrology, vol. 269, no. 1–2, 27–43. https://doi.org/10.1016/S0022-1694(02)00192-0

Stone, M. B., Shen, H. T. (2002): Hydraulic resistance of flow in channels with cylindrical roughness. In: Journal of Hydraulic Engineering, vol. 128, no. 5, 2002, 500–506.

Thorne, C. R., (1990): Effects of vegetation on riverbank erosion and stability. In: Vegetation and Erosion; Thornes, J. B., Ed.; John Wiley: Chichester, UK, 1990; 125–143.

Tuozzolo, S., Langhorst, T., de Moraes Frasson, R. P., Pavelsky, T., Durand, M., Schobelock, J. J. (2019): The impact of reach averaging Manning´s equation for an in-situ dataset of water surface elevation, width and slope. In: Journal of Hydrology, vol. 578, 2019. https://doi.org/10.1016/j.jhydrol.2019.06.038

Van de Lageweg, W. I., Van Dijk, W. M., Hoendervoogt, R., Kleinhans, M. G. (2010): Effects of riparian vegetation on experimental channel dynamics. In: Proceedings of the International Conference on Fluvial Hydraulics River Flow, Braunschweig, Germany, 8–10 September 2010; p. 2.

Yang, S., Bai, Y., Xu, H. (2018): Experimental analysis of river evolution with riparian vegetation. In: Water, 2018, vol. 10, no. 11. https://doi.org/10.3390/w10111500.

Mgr. Radoslav Schügerl, PhD. (*corresponding author, e-mail: schugerl@uh.savba.sk)
Ing. Yvetta Velísková, PhD.
Institute of Hydrology SAS
Dúbravská cesta 9
841 04 Bratislava
Slovak Republic

DOI: 10.31577/ahs-2023-0024.01.0016

ACTA HYDROLOGICA SLOVACA

Volume 24, No. 1, 2023, 141 – 150

Deterioration of water quality in aquatic system

Viera KOVÁČOVÁ*

The need to reduce anthropogenic pollutants inputs to aquatic ecosystems in order to protect drinking-water supplies and to reduce eutrophication, including the proliferation of harmful algal blooms. Nitrogen (N), needed for protein synthesis, and phosphorus (P), needed for DNA, RNA, and energy transfer, are both required to support aquatic plant growth and are the key limiting nutrients in most aquatic and terrestrial ecosystems. Most researchers have concluded that no single factor is responsible, but rather interactions between two or more factors control the rates.
River aquatic systems that have been heavily loaded with nutrients can display P limitation, N limitation, and colimitation, and what nutrient is most limiting can change both seasonally and spatial. At the transition between fresh and saline water, P can often be the limiting nutrient. P and dissolved silicate are also often limiting during the spring, with N limitation commonly occurring during summer months. Algal production during summer is supported by rapidly recycled P within the water column or released from sediments.

KEY WORDS: surface water, pollution, eutrophication, nutrients

Introduction

Water quality assessment is important for environmental protection. Mechanisms and assessment of water pollution investigated (Rathore et al., 2016; Yang et al., 2008; Hem, 1985; Harper, 1992; David and Gentri, 2000; Gali et al., 2012). Water deterioration has become an environmental problem in recent years, and understanding the mechanisms of water pollutation will help for prevention, remediation of water pollution (Singht and Karla, 1975; Marandi et al., 2013). Recent advances in current status and major mechanisms of water pollution, assessment, evaluation criteria, and the influencing factors were reviewed. The need to reduce anthropogenic nutrient inputs to aquatic systems in order to protect drinking-water supplies and to reduce pollution. Developing the appropriate nutrien management strategy is very important. Nitrogen and phosphorus are the main pollutants and affect the deterioration of the water status (Carpenter et al., 1998; Conley et al., 2009) due to agricultural activities in this region. In small amounts they are necessary. Nitrogen (N), needed for protein synthesis, and phosphorus (P), needed for DNA, RNA and energy transfer, are both required to support aquatic plant growth and are the key limiting nutrients in most aquatic ecosystems.
The inputs included from row crop agriculture, animal production, human consumption of food, and sewage production related net anthropogenic addition. The external supplies of N and P to aquatic systems are derived from a wide variety of sources, including groundwater, fluvial, and atmospheric inputs. The sum of these three sources is the external load. As can be seen the external supplies of nutrients to a water body can originate both as point sources, which are localized and more easily monitored and controlled, and as nonpoint sources, which are diffuse and much more difficult to monitor and regulate (Sokáč and Velísková, 2022; McCleskey et al., 2011; Khan and Ansari, 2005).
Monitoring of surface water quality in Žitný ostrov channel network (Fig. 1) has been provided in terms of requirements Supplement No.1 Directive of Government SR No. 269/2010, Part A (general indicators) and Part E (hydrogiological and micro-biological indicators) in the period of 2000–2022 (Schügerl at al., 2018; Koczka Bara et al., 2014; Makovinská et al., 2015).
Losses of nitrogen (N) and phosphorus (P in land run-off and drainage from agricultural land can impair river water quality and may pose a potential health hazard. Losses of P are up to an order of magnitude smaller than those of N, but may be more significant with respect to freshwater pollution (Withers and Lord, 2002; Jickells, 2005).
Management of the environment requires integrated approaches which include both N and P taking account of differences in their source areas and delivery mechanisms, the vulnerability of land use of safe management options in relation to landscape. For P, the identification of vulnerable zones represents a step

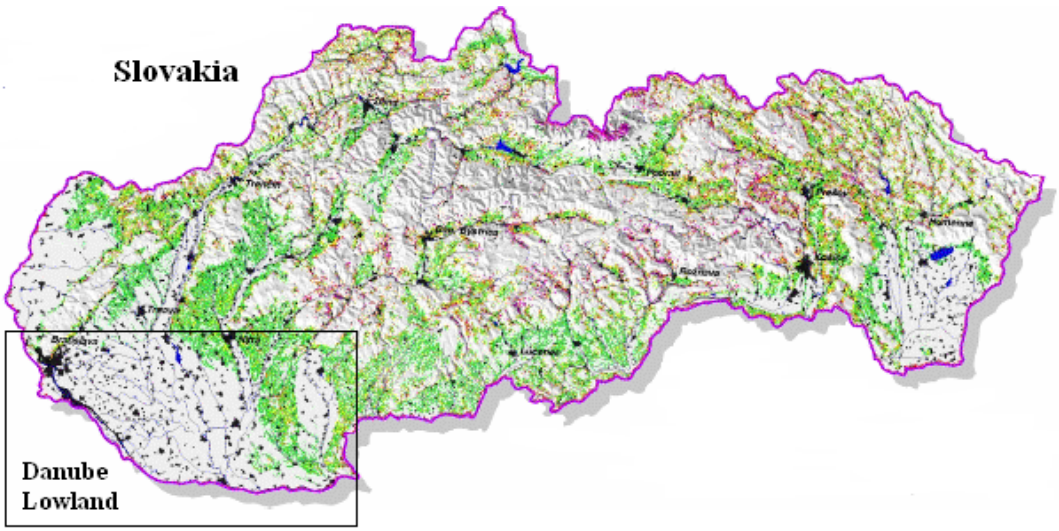

Fig. 1. Žitný ostrov (Danube Lowland) channel network.

forward to the management of the river basin in smaller definable units, which can provide a focus for safe management practices (van Niekerk, 2014).

Nutrient emissions from agricultural land are a major cause of elevated nutrient concentrations in ground and surface waters (Smith et al., 1999; Samuel, 2022). The nutrients of main concern are P and N, and an oversupply of either nutrient can cause highly undesirable changes in the structure and function of aquatic systems, although P is probably the more important in rivers impacted by agriculture. (Velísková et al., 2017; Conley et al., 2009).

Reductions in point P loads from sewage treatment works now being implemented to reduce fluvial P inputs in sensitive catchments has focused attention on the role of diffuse P inputs from agriculture. Many surface waters in lowland regions now exceed the EC drinking water limit of 50 mg l^{-1} and nitrate (11.3 mg l^{-1} NO_3-N). for at least a part of the winter. There are a range of situations which might lead to increased rates of nutrient transfer from agricultural land to water.

Whilst landscape characteristics such as climate, topography and soil type govern the inherent risk of nutrient loss within a given locality, current nutrient inputs and land management practices can exacerbate N and P losses from different agricultural land uses. The significance of these factors varies appreciably between the two nutrients, and between different geographic regions and farming systems This paper our knowledge of diffuse nutrient transfer to surface waters and how N and P emissions from agricultural land might be managed to meet future demands.

Estimations of total dissolved solids (TDS) content are commonly based on electrical conductivity (EC) measurements, using a conversion factor f retrieved from in situ monitoring. Chemical and biological processes taking place in the water can significantly affect the pH and conductivity of the water. We found a general upward trend. We observed regularity in the seasonal dynamics. Improvements in the water quality of many freshwater requires reductions in both nitrogen and phosphorus inputs. Although the TDS-EC method is capable of providing very accurate TDS concentrations, the use of a universal conversion factor can result in over- or underestimates. Users of EC meters need to follow certain basic procedures to ensure good representative TDS values, namely, proper calibration and maintenance, correct instrument use and application of the correct TDS-EC conversion factor (van Niekerk et al., 2014; Conley et al., 1999; Devlin et al, 2011; Thirumaliny and Kurian, 2009; Rusydi, 2019).

Additions N and P to the biosphere, largely through the production of fertilizers and increases in fossil fuel emissions. P levels have also significantly increased because of fertilizer use, as well as from municipal and industrial wastewater. The question of whether one or both nutrients should be controlled to reverse the detrimental effects of eutrophication. If N limitation were the only factor governing blooms of N_2-fixing cyanobacteria, then their blooms would be widespread in estuarine.

Estuaries ecosystems, that have been heavily loaded with nutrients can display P limitation, N limitation, and colimitation and what nutrient is most limiting can change both seasonally and spatially. At the transition between fresh and saline water, P can often be the limiting nutrients P and dissolved silicate are also often limiting during the spring, with N limitation commonly, occurring during summer months. Algal production during summer is supported by rapidly recycled P. Nitrogen has clearly been established as the nutrient limiting spring phytoplankton production; it is the sinking spring bloom that sends organic matter to bottom waters, which partly sustains hypoxia. The excess P in the water column leads to summer blooms of cyanobacteria. Controlling only P inputs to freshwaters and ignoring the large anthropogenic inputs of N can reduce algal uptake of N and thus allow more N to be transported downstream where it can exacerbate eutrophication problems in ecosystems.

The external supplies of N and P to aquatic systems are derived from a wide variety of sources, including

groundwater, fluvial, and atmospheric inputs. The environmental consequences of excessive nutrient enrichment are the degradation of water resources by eutrophication and worsening of water quality (David and Gentri, 2000; Hessen, 1999).
Excess of nutrients (mainly nitrogen and phosphorus) in water or soil from sewage outfalls and fertilized farmland. In water, eutrophication accelerates the growth of algae and other vegetation in water (Maistone and Parr, 2002). The degradation of organic material consumes oxygen resulting in oxygen deficiency and, in some cases, fish death. Eutrophication translates the quantity of substances emitted into a common measure expressed as the oxygen required for the degradation of dead biomass (James et al., 2004). In soil, eutrophication favours nitrophilous plant species and modifies the composition of the plant communities (Conley et al., 1999; Devlin et al., 2011; Siosemard et al., 2010).

Material and methods

Factors influencing water pollution

For the evaluation the water quality we went out from the data obtained on Institute of Hydrology SAS.
One of the most important tools for evaluating water quality and character in a catchment is a detailed knowledge of the ranges and trends in salinity pollution of natural water. Žitný ostrov is one of the most productive agricultural areas of Slovakia, situated on the Danube Lowland. Under its surface is the richest water reservoir of Slovakia. For this reason, it is very important to deal with quantity and quality of water resources in this region. The channel network at the Žitný Ostrov area was built up for drainage and also to provide irrigation water (Dulovičová et al., 2022; Velísková et al., 2017; Wang et al., 2001).
There are three main channels of this network: Chotárny channel – is the P1M water body type (partial river-basin Váh, code SKW0029), Gabčíkovo-Topoľníky channel – is the P1M water body type (partial river-basin Váh, code SKW0023), Komárňanský channel – is the P1M water body type (partial river-basin Váh, code SKV0226). We carrying out the measurements in the period 2020–2022. Monitoring and assessment of following indicators were performed-total nitrogen (N_{TOT}), nitrate nitrogen ($N\text{-}NO_3^-$), nitrite nitrogen ($N\text{-}NO_2^-$), ammonia nitrogen ($N\text{-}NH_4^+$), total phosphorus (P_{TOT}), phosphate phosphorus ($P\text{-}PO_4^{3-}$) according the Supplement No.1 Directive of Government SR No. 269/2010, Part A biomas of phytoplankton (CHL_a) according Part E (Makovinská et al., 2015) (Table 1, 2).
Electrical conductivity (EC) and total dissolved solids (TDS) are water quality parameters, which are used to describe salinity level. These two parameters are correlated and usually expressed by a simple equation: TDS = f .EC (in 25°C) by finding the correlation value. TDS concentration can be determined from EC value, which are measured easily and inexpensively in situ by a portable water quality checker (YSI Multiparametric probe). The analysis of TDS is more difficult and expensive as it needs more equipment and time. The relationship between total dissolved solids (TDS) and electrical conductivity (EC) is established in 648 samples collected from Žitný ostrov channels. These data are extremely variable in content, reliability and periodicity of sampling.
Electrical conductivity (EC) and total dissolved solids (TDS) are water quality parameters, which are used previous research (Smith et al. 1999; Schneider and Menzel, 2003) results have found that the correlation between TDS and EC are not always linear. For more precision, TDS concentrations need to be analyzed using the gravimetric method in the laboratory.

Sampling

We take samples once per month in the same day as samples for chosen indicators of water quality assessment from the same sampling sites. By the evaluation of the obtained results we used statistical methods. Water quality was evaluated by the comparison of the characteristic values for individual indicators in all sampling sites calculated and the recommended value for these indicators (Rainwater and Thatcher, 1960; Makovinská et al., 2015).
Three locations were monitored in each main channel, i.e. total of 9 measurements each month in time period 2020–2022. A total of 648 samples were investigated.
Profiles with an assumed higher pollution value were selected by previous observation. For each locality, the quality in selected indicators was separately evaluated through YSI multiparametric probe. In-situ measurements were carried out to evaluate the quality of surface water on Žitný ostrov territory. The samples provide a wide range of EC, TDS and conversion factors. The dry and warm summer climate, evaporation soil, water regime and mineralized groundwater create here convenient conditions for development and spreading of pollutants. These conditions, in addition to the use of high to medium salt-content irrigation water and bad drainage lead to an increased pollutantion in agricultural area (Climate Atlas of Slovakia, 2015).
In-situ measurements were carried out to evaluate the quality of surface water on Žitný ostrov. Profiles with an assumed higher pollution value were selected by previous observation. For each locality, the quality in selected indicators was separately evaluated using the YSI multiparametric probe.
The Okoličná profile on the island was selected as the most polluted. The limit values in it were exceeded in 4 parameters and in the other 2 profiles Komárňanský channel, therefore it was evaluated as the most polluted.
This contribution analysed pollution problem, factors affecting this process, its consequences and possibilities of prevention. Important was to evaluate pollution state of surface water in Žitný ostrov channel network following the assessment physical-chemical and microbiological indicators in monitored period 2020–2022. The sets out the ecological consequences of increased nutrient loading to freshwaters in the context of providing information on the effects of implementing international and national legislative for the ecological

Table 1. Evaluation of surface water status in various polluted waters

Indicator	Symbol	Unit	Value
Ammonia nitrogen	$N\text{-}NH_4^+$	[mg l^{-1}]	1
Nitrite nitrogen	$N\text{-}NO_2^-$	[mg l^{-1}]	0.02
Nitrate nitrogen	$N\text{-}NO_3^-$	[mg l^{-1}]	5
Nitrogen total	N_{TOT}	[mg l^{-1}]	9
Phosphorus total	P_{TOT}	[mg l^{-1}]	0.4
Phytoplankton biomass (chlorophyll-a)	CHL_a	[μg l^{-1}]	50

Table 2. Limited values of surface water according to Supplement No.1 Directive of Government SR No. 269/2010

Place of sampling point: Komárňanský channel	Typ VÚ: P1M	Partial watershed Váh
Profile : Okoličná na Ostrove	Code VÚ: SKV0226	Monitoring: 2020

Part A – general water quality indicator

Term of indikator	Symbol	Unit	Number statements	Min.	Max.	Average	P90	Value according to NV 269/2010	Meet/Does not meet
Dissolved oxygen	O_2	[mg l^{-1}]	12	8.4	14.0	10.8	9.5	> 6.0	M
Temperature	t	[°C]	12	3	21.6	11.4	20.3	< 27	M
Chemical consump. oxyg	CHSKCr	[mg l^{-1}]	12	5.0	18.0	7.7	10.8	< 25	M
Reaction	pH	–	12	6.39	8.19	7.93	8.16	8.5	M
Conductivity	EC	[μS cm^{-1}]	12	349	543	420	536.1	≤ 700	M
Specific conductivity	SPC	[μS cm^{-1}]	12	370	933	548	857.0	700	N
Total dissolved solids	TDS	[mg l^{-1}]	12	284	630	405	621.0	800	M
Ammonia nitrogen	N-NH4	[mg l^{-1}]	12	0.05	0.9	0.34	0.16	1	M
Nitrate nitrogen	N-NO3	[mg l^{-1}]	12	2.7	5.2	3.68	3.61	5	N
Total nitrogen	Ntot	[mg l^{-1}]	12	2.2	9.4	7.23	3.17	9	N
Phosphate phosphorus	P-PO4	[mg l^{-1}]	12	0.17	0.42	0.30	0.32	0.35	N
Total phosphorus	Ptot	[mg l^{-1}]	12	0.18	0.43	0.35	0.38	0.4	N
Turbidity	T	NTU	12	14	64	42	38	100	M
Phytoplankton biomass (chlorophyll-a	CHLa	[μg l^{-1}]	12	20	46	33.3	16	50	M

status assessment (WHO).

Water eutrophication is mainly caused by excessive loading of nutrients into water bodies like N and P. Excessive nutrients come from both point pollution such as waste water from industry, municipal sewage, and non-point pollution like irrigation water, surface run water containing fertilizer from farmland, etc. Increased nutrient load to water body is now recognized as a major threat of water quality degradation.

At present, excessive total nitrogen (TN) and total phosphorus (TP) in water are considered as the only factors inducing water eutrophication, but nutrient enrichment is only the necessary but not the sufficient condition for algal boom. Eutrophication is not likely to occur if both TN and TP in water are low, but eutrophication may not occur in water high in TN and TP if other conditions such as temperature and current speed are not favorable. The influencing factors of water pollution include: a) nutrient enrichment – excessive TN and TP; b) hydromechanics - slow current velocity; c) adequate temperature and favorable other environmental factors; d) light and Ph; e) microbial activity and biodiversity.

Results and discussion

a) The relationship of nutrient enrichment to water eutrophication and algal bloom: When P concentration in water is low, it may be the limiting factor for inducing water eutrophication and algal bloom. When P concentration in water increases rapidly, other may become a new limiting factor, such as pH, water depth, temperature, light, wave, wind or other biological factors. N and P input and enrichment in water are the most primary factors to induce water pollution. Electrical conductivity (EC) and total dissolved solids (TDS) are frequently used as water quality parameters (Hubert and Wolkersdorfer, 2015; McNeal et al., 1970).

b) Hydrodynamics is not related to disturbing water itself but is influenced indirectly by changing light and nutrient status. In shallow water, increased frequency of disturbance could increased the P release from the sediment, especially at high temperature. Electrical conductivity strongly depends on the sample's temperature because the movement of ions is directly proportional to the temperature.

c) Temperature and salinity are the two important factors to induce alga bloom, which always occurs at temperature between 23°C and 28°C, salinity between 25% and 30%. The variation of temperature and salinity also affect algal bloom, and an important condition for algal bloom is that temperature increases and salinity decreases faster than ever in short time (Smith 1962; McNeil and Cox, 2000; Gali, et al., 2012). Statistical analysis shows that the influence of temperature on algal growth rate is the largest, followed by salinity and their interaction. Change of salinity is also influenced by the concentration of nutrition. Research shows that salinity is negatively related with $N\text{-}NO_3^-$ and $P\text{-}PO_4^3$, but positively related with $N\text{-}NH_4^+$ and however, it is not very related with $N\text{-}NO_2^-$. The change in pH is directly related to the availability and absorption of nutrients from solution. Ionization of electrolytes or the valence numbers of different ion species are influenced by changes in pH. High pH values promote the growth of phytoplankton and result in bloom (Mainstore and Parr, 2002; Velísková et al., 2017; Western, 2001).

d) Light and pH plays an important role in the growth. The direct relationship between phytoplankton and dissolved oxygen content has been observed by a number of researchers. pH is a plant growth limiting factor. The change in pH is directly related to the availability and absorption of nutrients from solution. Ionization of electrolytes or the valence numbers of different ion species are influenced by changes in pH. High pH values promote the growth of phytoplankton and result in bloom. It must be pointed out that many factors influencing pollution are relative and affect each other.

e) Microbial activity is the inducement factor to alga bloom. It can enhance abundant breeding of alga bloom. Nutrient-enhanced microbial production of organic matter, or eutrophication, is frequently accompanied by altered microbial community structure and function. The amount of microbial biomass is positively related to the content of organic matter and the amount of plankton in eutrophicated water. There exists certain intrinsic relationship between the amount of bacteria and the occurrence of eutrophication. The decomposition of organic matter by bacteria activities can produce nutrients and organic substances, which may promote algal bloom breaking out (Mainstore and Parr, 2002; Walton, 1989; Newman et al., 2005). Chemical and biological processes taking place in the water can significantly affect the pH and conductivity of the water. We found a general upward trend. We observed regularity in the seasonal dynamics, too (Pärn et al., 2012).

Monitoring and assessment of following indicators were performed: total nitrogen (N_{TOT}), nitrate nitrogen ($N\text{-}NO_3^-$), nitrite nitrogen ($N\text{-}NO_2^-$), ammonia nitrogen ($N\text{-}NH_4^+$), total phosphorus (P_{TOT}), phosphate phosphorus ($P\text{-}PO_4^{3-}$) according the Supplement No.1 Directive of Government SR No. 269/2010, Part A, biomas of phytoplankton (CHL_a) according Part E and with regards to WHO recommendations (Eq. 1).

Generally, the physical and chemical evaluation parameters were used to assess water eutrophication, mainly nutrient concentration (N and P), algal chlorophyll, water transparency and dissolved oxygen. Although there are many different assessment parameters, the concentrations of total nitrogen and total phosphorus are the two basic ones. (Cheng and Li, 2006) used total nutrient status (TNS) to assess eutrophication status of surface water. The calculation of total nutrient status is as follows (Eq. 1).

$$TNS = \sum W_j TNS_j, W_j = r_{ij}^2 / \sum r_{ij}^2 \quad (1)$$

where
TNS – the sum of indexes of all nutrient parameters;
TNS_j – the TNS of j parameter;
W_j – the proportion of j parameter in the TNS;
r_{ij} – the relation of chlorophyll a (Chla) to other parameters.

The available parameters concerned include total nitrogen (TN), total phosphorus (TP), Chla, dissolved oxygen (DO), chemical oxygen demand by K_2MnO_4 oxidation method (CODMn), biological oxygen demand (BOD5), etc., and TN, TP and Chla are selected for calculating the TNS (Cheng et al., 2006; Yang et al., 2008).
The results of TNS will be part of the project.
Statistical processing was performed for the entire monitoring period. Water samples were taken along the main Žitný ostrov channels. The dry and warm summer climate, evaporation soil water regime and mineralized groundwater create here convenient conditions for development polluted water. These conditions, in addition to the use of high to medium salt-content irrigation water and bad drainage, lead to an increased risk of pollution in agricultural area (Climate Atlas of Slovakia, 2015).
The need to reduce anthropogenic nutrient inputs to aquatic systems in order to protect drinking-water supplies and to reduce eutrophication. Developing the appropriate nutrient management strategy is very important. Nitrogen (N), needed for protein synthesis and phosphorus (P), needed for DNA, RNA, and energy transfer, are both required to support aquatic plant growth and are the key limiting nutrients in most aquatic ecosystems. (Nedwell et al., 2001).
Mechanisms and assessment of water pollution investigated (Appelo, 2015; Rathore et al., 2016; Yang et al., 2008). Understanding the mechanisms of water pollution will help for prevention and remediation of water pollution. Recent advances in current status and major mechanisms of water pollution, assessment and evaluation criteria, and the influencing factors were reviewed. The need to reduce anthropogenic nutrient inputs to aquatic systems in order to protect drinking-water supplies and to reduce eutrophication. Nitrogen (N), needed for protein synthesis and phosphorus (P), needed for DNA, RNA, and energy transfer, are both required to support aquatic plant growth and are the key limiting nutrients in most aquatic ecosystems. (Conley et al., 2009).
The study was focused on identification of the long-term trends in the surface water quality in channel network at Žitný ostrov region. The paper shows changes in measured values in years 2000–2022. It was shown the channel water quality has been changed significantly during this period, after 1990 is slightly decreased. The nutrient level in surface water has decreased after 1990th in response to decreased discharge of domestic wastes and non-point pollution from agricultural practices and urban development. We observe slight increasing in some profiles of Komárňanský channel, mainly Okoličná na Ostrove and Čalovec (Fig. 2, 3, 4, 5) with major agricultural activities during last few years (2020–2022).
Investigation of surface water and determination surface

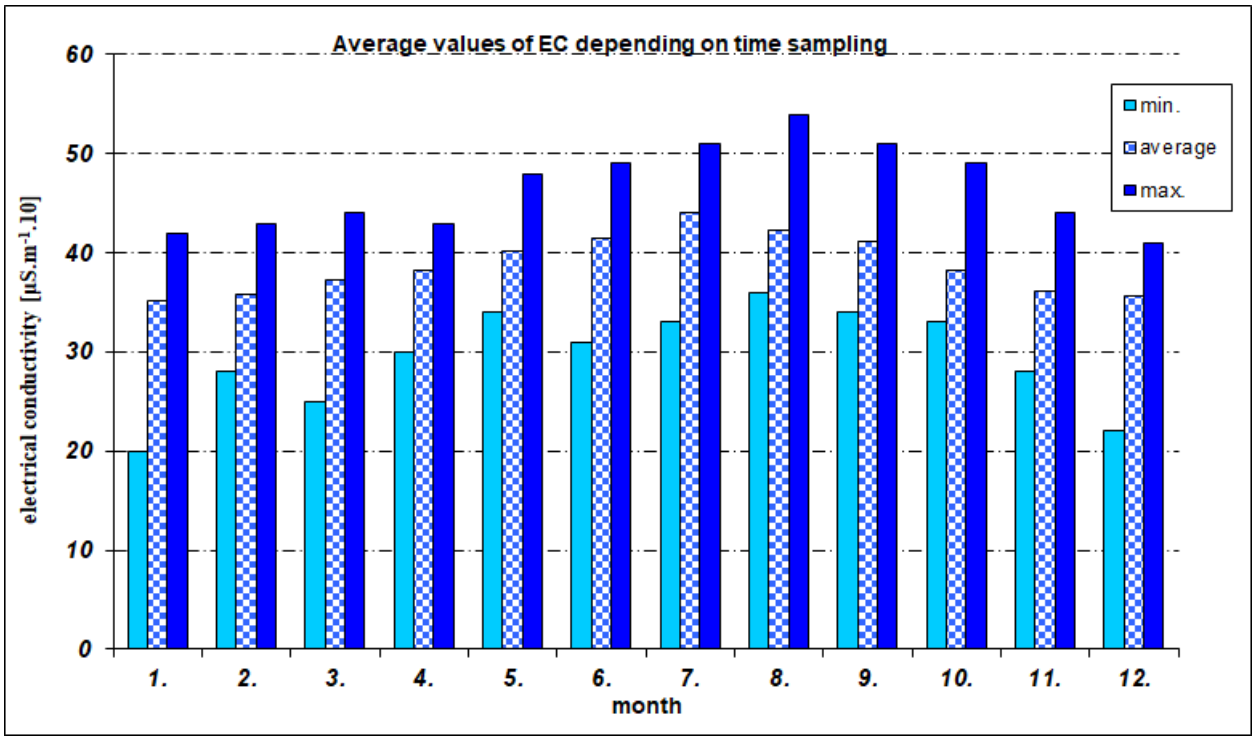

Fig. 2. Average EC values depending on the time sampling (1–12 months in year 2020–2022) Komárňanský channel.

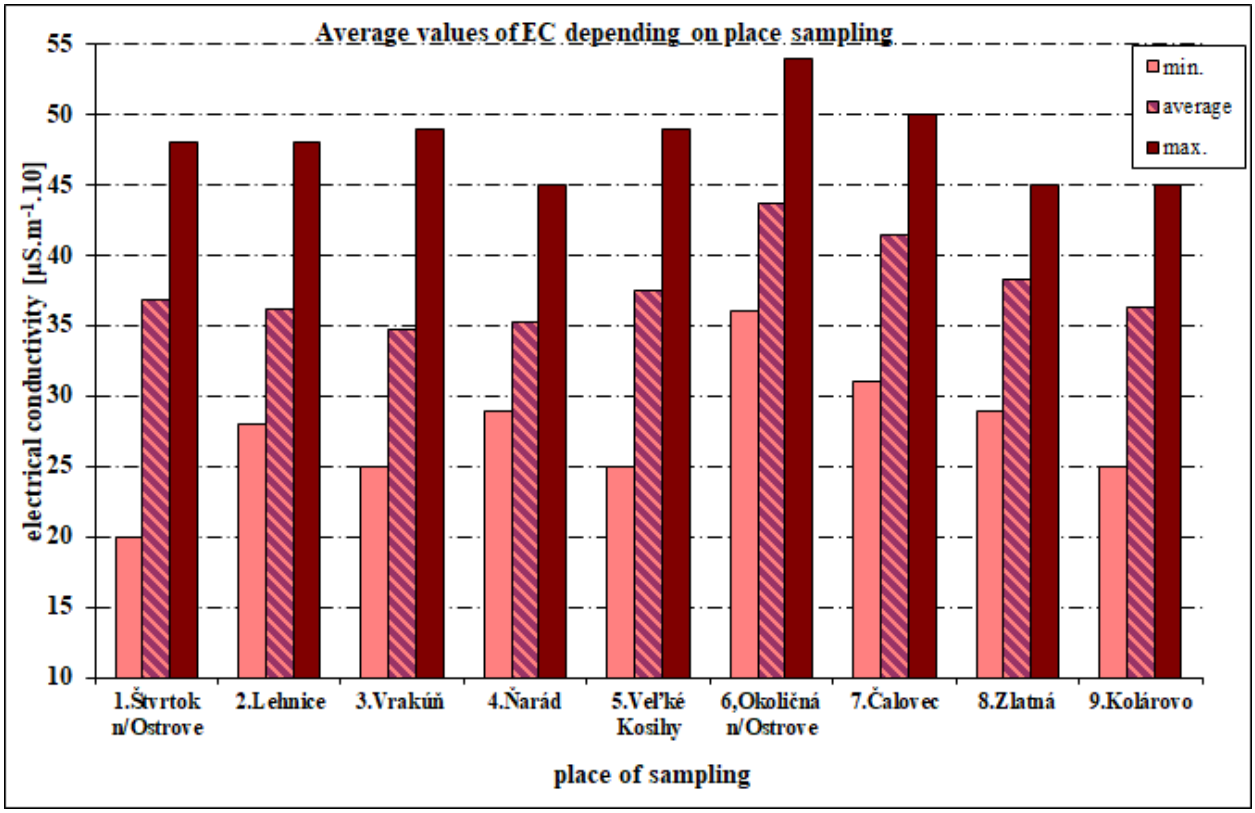

Fig. 3. Average EC values depending on the place sampling (9 places) in year 2020–2022) Komárňanský channel.

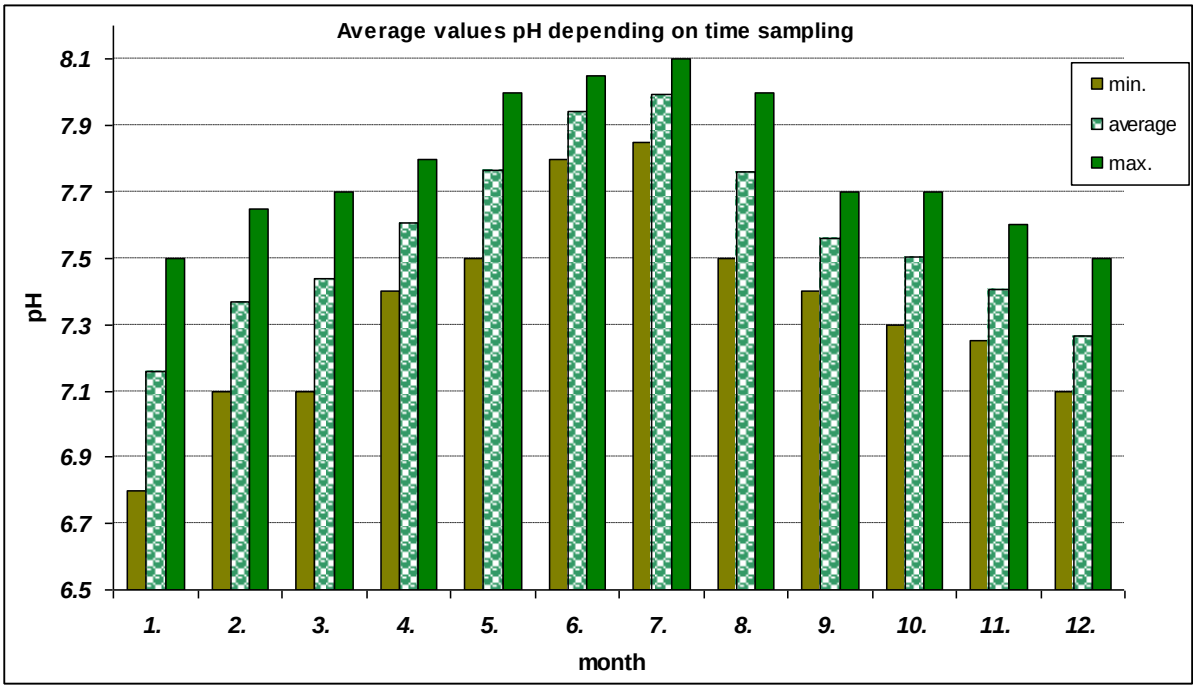

Fig. 4. Average pH values depending on time sampling (1–12 month, 2020–2022), Komárňanský channel.

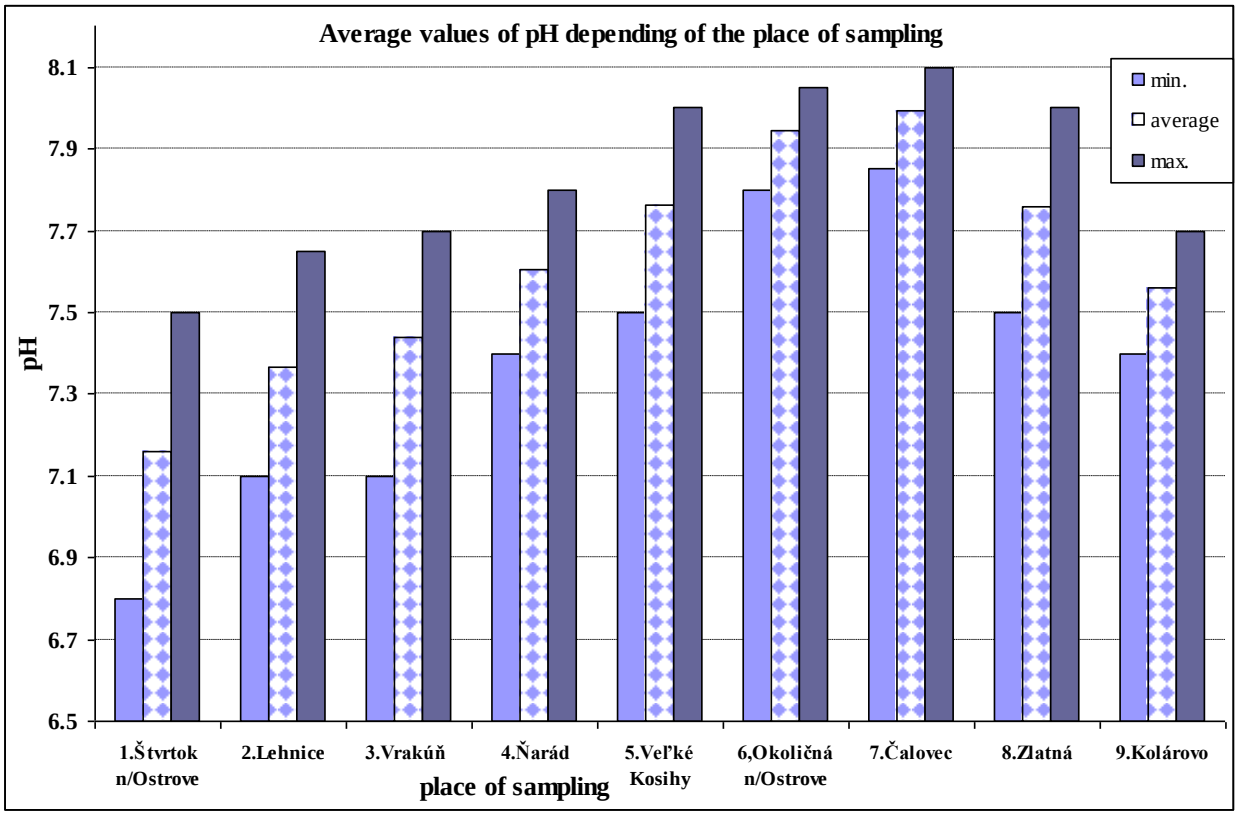

Fig. 5. Average pH values depending on the place sampling (1–12 month, 2020–2022), Komárňanský channel.

water status, measured by water chemistry, biological indicators and briefly review the process, the impacts of pollution in freshwater systems. The present article evaluated the ecological consequences of increased nutrient loading to freshwaters in the context of providing information on the effects of implementing international and national legislative for the ecological status assessment. The limiting factors – namely concentrations of nitrogen (N) and phosphorus (P), temperature, pH, light, dissolved oxygen and CO_2 level are known to affect polluted water bodies.

Conclusion

The present review deals with the studies conducted on the impact of pollutants amount in surface water on the Žitný ostrov channel network. The review covers the definition and concept of indicators for the adverse effects on quality and ecosystem functioning. The contaminations of several water bodies leads to significant changes in the structure and function of the aquatic system. Some profiles in this region have recently been found to be highly polluted. Some of indicators and methods access to biodiversity
Mechanisms and assessment of water pollution investigated many authors. Water pollution has become a environmental problem in recent years. Understanding the mechanisms of water deterioration will help for prevention and remediation of water pollution. The need to reduce anthropogenic nutrient inputs to aquatic systems in order to protect drinking-water supplies and to reduce eutrophication. Developing the appropriate nutrien management strategy is very important. Nitrogen (N), needed for protein synthesis and phosphorus (P), needed for DNA, RNA, and energy transfer, are both required to support aquatic plant growth and are the key limiting nutrients in most aquatic ecosystems.
Electrical conductivity (EC) and total dissolved solids (TDS) are frequently used as water quality parameters. These two parameters are indicators of pollution level, which make them very useful. The value of EC and TDS are correlated. Its ability depends mainly on dissolved ion concentrations, ionic strength, and temperature of measurements. The analysis of TDS concentration from EC value can be used to give an overview of water quality. For more precision, TDS concentrations need to be analyzed using the gravimetric method in the laboratory. EC can be measured easily and inexpensively in situ by a portable water quality checker. This paper provides establishing a conversion factor for EC and TDS parameters using dataset of measurements in Žitný ostrov region (Danube Lowland, Slovakia). Monitored localities was chosen so that they be the most representative area-covering. Measurements shows that just one simple linear conversion factor cannot be suitable throughout the range of waters.
The conversion factors were determined using field and laboratory measurements. The site-specific validation are sed. The limit value in Okoličná na Ostrove has been exceeded (Table 2) for ions nitrate nitrogen $N\text{-}NO_3$,

ammonia nitrogen N-NH4, total nitrogen N tot, phosphate phosphorus P-PO4, total phosphorus Ptot. Some profiles in this region have recently been found to be highly polluted. The degradation of water resources by pollution can result in worsening of water quality.

The present review deals with the studies conducted on the impact of pollutants amount on eutrophication in surface water on the Žitný ostrov channel network. Were compared 648 samples, whether it meets the limit values, covers the definition and concept of pollution and the adverse effects on quality ecosystem functioning. The pollution of several water bodies leads to significant changes in the structure and function of the aquatic ecosystem. Some profiles in this region have recently been found to be highly eutrophic. Most of the surface water bodies are surrounded with densely populated human settlement areas and agricultural fields. Frequent sampling is needed to capture intra-event and seasonal fluctuations of pollutants concentrations for accurate load estimations to surface waters; however, processing water samples for multiple nutrients can be expensive and time consuming.

The goal of this study was to investigate electrical conductivity as an inexpensive surrogate for traditional water quality sampling and analysis. This study is being conducted in a heavily tile-drained-agricultural watershed typical of the Žitný ostrov region. This watershed has a unique setup where drained water from flows into a single location, where both surface runoff and drained water from the drainage district can be monitored.

Acknowledgement

This contribution was supported by project VEGA 2/0028/23 Seasonal variations of hydrodynamic and morphological parameters in lowland vegetated rivers.

References

Appelo, C. A. J. (2015): Specific Conductance: how to calculate, to use, and the pitfalls 2015 http://www.hydrochemistry.eu/exmpls/sc.html

Carpenter, S. R. N., Caraco, N. F. D., Correll, L. R. W., Howarth, A. N., Sharpley, V., Smith, H. (1998): Nonpoint Pollution of Surface waters whit Phosphorus and Nitrogen, Ecological Applications, 559–568.

Climate Atlas of Slovakia, (2015): Slovak Hydrometeorological Institute, Bratislava, ISBN 978-80-88907-90-9.

Conley, D. J., Paerl, H. M., Howarth, R. V., Boesch, D. F., Seitzinger, S. P., Havens, K. E., Lancelot, Ch. (2009): Controlling Eutrophication: Nitrogen and Phosphorus, Science, Vol. 323,1014–1017.

Conley, D. J., Schelske, C. L., Stoermer, E. F. (1999): Hydrobiologia 410, 87–96 https://doi.org/10.1023/A:1003784504005

David, M. B., Gentry, L. E. (2000): Anthropogenic Inputs of Nitrogen and Phosphorus and Riverine Export. J. of Environmental Quality, Vol. 29, no. 2, 494–508

Devlin, M., Bricker, S., Painting, S. (2011): Comparison of five methods for assessing impacts of nutrient enrichment using estuarine case studies. Biogeochemistry 106, 177–205.

Directive of Government SR No. 269/2010 for accomplish suitable state of water.

Dulovičová, R. Schűgerl, R., Velísková, Y. (2022): Hydraulic conductivity of saturated bed silts in Chotárny channel, Žitný ostrov area, Slovakia. Acta Hydrologica Slovaca, vol. 23, no. 2, 180–189.

Gali, R. K. Soupir, M. L. Helmers, M. J. (2012): Electrical Conductivity as a tool to estimate chemical properties of drainage water quality in the Des Moines Lobe, Iowa. An ASABE Conference, Dallas, Paper Number: 12–1338083. DOI:10.13031/2013.42270.

Harper, D. (1992): Eutrophication of Freshwaters: Principles, problems and restoration. Chapman and Hall 1992, ISBN 978-94-011-3082-0, https://doi.org/10.1007/978-94-011-3082-0

Hem, D. (1985): Study and interpretation of the chemical characteristics of natural water" U.S. Geol. Surv. Water Suppl. Pap. 2254 1–263.

Hessen, D. O. (1999): Catchment properties and the transport of major elements. In: Nedwell, D.B., Raffaelli, D.G. (Eds.), Estuaries. Adv. Ecol. Res. vol. 29, 1–41.

Hubert, E., Wolkersdorfer, Ch. (2015): Establishing a conversion factor between electrical conductivity and total dissolved solids in waters Water SA Vol.41, No.4.

Cheng, X. Y., Li, S. J. (2006): An analysis on the evolvement processes of lake eutrophication and their characteristics of the typical lakes in the middle and lower reaches of Yangtze River. Chinese Science Bulletin, 51(13): 1603-1613. [doi:10.1007/s11434-006-2005-4]

James, C. S., Birkhead, A. L., Jordanova, A. A., O'Sullivan J. J. (2004): Flow resistance of emergent vegetation. J. Hydraul. Biologia 72/8, 840-846.

Jickells, T. (2005): External inputs as a contributor to eutrophication problems. J. Sea Res. 54, 58–69.

Khan, F. A., Ansari, A. A. (2005): Eutrophication: An ecological vision. The Botanical Review, 71(4): 449–482.

Koczka Bara, M., Velísková, Y., Dulovičová, R., Schügerl, R. (2014): Influence of surface water level fluctuation and riverbed sediment deposits on groundwater regime. Journal of Hydrology and Hydromechanics, vol. 62, no. 3, 177–185. DOI:http://dx.doi.org/10.2478/johh-2014-0030.

Mainstone, C. P., Parr, W. (2002): Phosphorus in rivers-ecology and management. The Science of the Total Environ., 282–283.

Marandi, A., Polikarpus, M., Jõeleht, A. (2013): A new approach for describing the relationship between electrical conductivity and major anion concentration in natural waters" Appl. Geochemistry 38, 103–109.

McCleskey, R. B., Nordstrom, D. K., Ryan, J. N. (2011): Electrical conductivity method for natural waters Applied Geochemistry 26, S227–S229.

McNeal, B. L., Oster, J. D., Hatcher, J. T. (1970): Calculation of electrical conductivity from solution composition data as and aid to in-situ estimation of soil salinity Soil Sci. 110. 405– 414.

McNeil, V. H., Cox, M. E. (2000): Relationship between conductivity and analyze composition in a large set of natural surface water samples. Environ. Geol. 39 (12) 1325–1333.

Meisinger, J. J., Delgado. J. A. (2002): Principles for managing nitrogen leaching. Journal of Soil and Water Conservation, vol. 57, no. 6, p. 485

Makovinská, J., Mišíková Elexová, E., Rajczyková, E., Baláži, P., Plachá, M., Kováč, V., Fidlerová, D., Ščerbáková, S., Lešťáková, M., Očadlík, M., Velická, Z., Horváthová, G., Velegová, V. (2015): Methodology of monitoring and assessment of Slovak surface water bodies. Water

Research Institute, Bratislava, 64 p (without annexes), ISBN 978–80-89740–02–4.

Nedwell, D. B., Dong, L. F., Sage, A., Underwood, G. J. C. (2001): Variations of the nutrient loads to the mainland UK estuaries: correlations with catchment areas, urbanisation and coastal eutrophication. Est. Coast. Shelf Sci. 56, 951– 970.

Newman, J. R., Anderson, N. J., Bennion H., Bowes, M. J., Luckes, S., Winder, J. (2005): Eutrophication in rivers: an ecological perspective. Centre for Ecology and Hydrology, 37 p., DOI: 10.13140/2.1.3711.5208

Pärn, J., Pinay, G., Mander, Ű. (2012): Indicators of nutrients transport from agricultural catchments under temperature climate: A review. Ecological Indicators, 22 (2012), 4–15.

Rainwater, F. H., Thatcher, L. L. (1960): Methods for Collection and Analysis of Water Samples. Geol. Surv. Water Suppl. Pap. 1454 1–301.

Rathore, S. S., Chandravanshi, P., Jaiswal, K. (2016): Eutrophication: Impacts of Excess Nutrients Inputs on Aquatic Ecosystem, Journal of Agriculture and Veterinary Science, Vol. 9, 89–96.

Rusydi, A, F. (2019): Correlation between electrical conductivity and total dissolved solid in various type of water: (A review) IOP Conf. Ser.: Earth Environ. Sci. 118 01.

Samuel, R. (2022): Disolved solids (TDS) less than 1000 ppm in drinking water did not impact nursery pig performance. Vet. Sci. 2022, 9(11),622;

Schneider, S., Melzer, A. (2003): The Trophic Index of Macrophytes (TIM) – a new tool for indicating the trophic state of running waters. Hydrobiology, vol. 88, 1 , 49–67, doi.org/10.1002/iroh.200390005

Singht, T., Karla, Y. (1975): Specific conductance method for in-situ estimation of total dissolved solids. J. Am. Water Works Assoc. 67(2) 99–100.

Siosemard, M., Kave, F., Pazira, E., Sedghi, H., Ghaderi, S. (2010): Determine of constant coefficients to relate total dissolved solids to electrical conductivity Int. J. Environ. Chem. Ecol. Geol. Geophys. 4, 457–459.

Schügerl, R., Velísková, Y., Dulovičová, R. (2018): Identifikácia zmien prietokových pomerov a rýchlostného profilu pri prúdení s voľnou hladinou. Hydrologický výskum v podmienkach prebiehajúcej klimatickej zmeny. Monografia ÚH SAV. Veda, Bratislava, 391 s. (in Slovak)

Sokáč, M. Velísková, Y. (2022): YDispersion process in conditions of real sewer systems – in situ experiments. In Acta Hydrologica Slovaca, vol. 23, no. 2, 288–295, 2022. (https://doi.org/10.31577/ahs-2022-0023.02.0033).

Smith, S. H. (1962): Temperature correction in conductivity measurements. Limnology and oceanography methods, Vol. 7, Issue 3, 330–334.

Smith, V. H., Tilman, G. D., Nekola, J. C. (1999): Eutrophication: impacts of excess nutrient inputs on freshwater, marine, and terrestrial ecosystems. Environmental Pollution, 100, 179–196.

Thirumaliny, S., Kurian, J. (2009): Correlation between electrical conductivity and total dissolved solids in natural waters Malaysian J. Sci. 28 56–61.

van Niekerk, H., Silberbauver, M. J., Maluleke, M. (2014): Geographical differences in the relationship between total dissolved solids and electrical conductivity in South African rivers. Water SA 40 (1) 133–137.

Velísková, Y., Dulovičová R., Schügerl, R. (2017): Impact of vegetation on flow in a lowland stream during the growing season. Biologia 72/8, 840–846, DOI: 10.1515/biolog-2017-0095.

Walton, N. R. G. (1989): Electrical Conductivity and total dissolved solids – What is their precise relationship Desalination 72 275–292.

Wang, J., Fu, B., Qiu, Y., Chen, L. (2001): Soil nutrients in relation to land use and landscape position in the semi-arid small catchment on the loess plateau in China. Journal of Arid Environments, 48, 537–550.

Western, D. (2001): Human-modified ecosystems and future evolution. Proceedings of the National Academy of Sciences of the United States of America, 98(10):5458-5465. doi:10.1073/pnas.101093598

WHO guidelines for drinking water quality: (1996) Total dissolveds solids in drinking water. 2nd ed. Vol. 2. Health criteria and other supporting information. World Health Organization, Geneva, 1996.

Withers, P. J. A., Lord, E. I. (2002): Agricurtural nutrien inputs to rivers and groundwaters in the UK: policy, environmental management and research needs. The Science of the Total Environment 282 – 283.

Yang, X., Wu, X., Hao, H., He, Z. (2008): Mechanisms and assessment of water eutrophication. J. of Zhejjang Univ. Sci., 9 (3), 197–209.

Ing. Viera Kováčová (*corresponding author, e-mail: kovacova@uh.savba.sk)
Institute of Hydrology SAS
Dúbravská cesta 9
841 04 Bratislava
Slovak Republic

DOI: 10.31577/ahs-2023-0024.01.0017

ACTA HYDROLOGICA SLOVACA

Volume 24, No. 1, 2023, 151 – 158

Fire induced water repellency in the forest soil covered with different types of forest floor biomass

Slavomír HOLOŠ, Anton ZVALA, Peter ŠURDA*, Ľubomír LICHNER

The intensity and severity of a wildfire can influence the persistence of soil water repellency (SWR) in the affected area. The effects of fire on the SWR of forest soils depend on the type of forest vegetation, the quantity of the organic component of the forest soil, the characteristics of the organic matter, the soil type, and its properties.

Three study sites were located in the Borská nížina lowland (southwestern Slovakia). The first site IL1 represents a 100-years-old stand of Scots pine (*Pinus sylvestris*), the second site IL2 is a 30-years-old stand of Scots pine (*Pinus sylvestris*), and the third site LL is a deciduous stand with a predominance of alder (*Alnus glutinosa*). The article aimed to determine the influence of forest floor biomass (FFB) in IL1, IL2 and LL on SWR induced by different heating temperatures. WDPT test was measured on the surface of burned mineral soil samples without FFB, and two series of measurements were carried out in samples covered with FFB. First were carried on the surface of burned FFB and second, under burned FFB on the exposed mineral soil. Our first hypothesis was that heating temperatures would induce higher SWR persistence on soil covered with forest floor biomass compared to bare soil; the second hypothesis was that different forest floor biomass would induce different post-fire SWR persistence.

The differences between the samples covered with FFB and samples without FFB in mean values of SWR induced by different temperatures were not statistically significant for either research site. On the other hand, the highest individual SWR values were measured at or below the forest floor biomass in both deciduous and coniferous forests.

The second hypothesis was not confirmed. We found similar fire-induced SWR in the different types of forest floor biomass and the soil under forest floor biomass.

KEY WORDS: soil water repellency, soil heating, water drop penetration time, forest floor biomass

Introduction

Fire-induced water repellency is a phenomenon that occurs when a wildfire burns through an area, leaving behind a layer of ash and charred debris on the soil surface. This layer can alter the physical and chemical properties of the soil, resulting in increased soil water repellency (SWR) (Zvala et al., 2022).

The intensity and severity of a wildfire can influence the extent, persistence and severity of SWR in the affected area. Higher-intensity fires tend to cause more severe SWR, which can profoundly impact the ecosystem. The water-repellent layer can cause soil erosion, reduce infiltration rates, increase runoff, and alter soil chemistry. The waxy substances produced during combustion can alter the soil's chemistry, making it more acidic (Hološ et al., 2022).

The hydrophobicity induced by wildfires is caused by the combustion of organic matter, such as plant debris and soil organic matter, which produces waxy substances that coat soil particles. Waxes, resins and other organic matter are converted by fire into charred organic residues that release large amounts of hydrophobic organic matter while covering soil particles (DeBano, 2000). The effects of fire on the SWR of forest soils depend on the type of forest vegetation and its density, the content and quantity of the organic component of the forest soil, the characteristics of the organic matter, the soil type, and its properties (Arcenegui et al., 2007; Mataix-Solera et al., 2008; Negri et al., 2021). A forest fire can increase or decrease pre-existing SWR depending on the amount and type of organic matter consumed and the temperature reached (DeBano et al., 1998; Doerr et al., 2004; Certini, 2005; Robichaud and Hungerford, 2000). The composition of organic matter and its interactions with the soil mineral component of the forest soil play an important role in the change in SWR (Lichner et al., 2006). In addition to the redistribution and concentration of hydrophobic substances in the soil, the heat generated by fire is also thought to improve the binding of these substances to soil particles (Savage et al., 1972). Studies of burned stands conducted on forest soils under *Pinus pinaster* and *Pinus halepensis* have found that they are capable of causing extreme SWR (Arcenegui et al.,

2008). Burning non-woody leaves in forest soil organic matter layers can cause SWR in deciduous forests, indicating that this condition is not exclusive to coniferous and dry forests (Chen et al., 2020). The strength of post-fire SWR depends on the severity of the fire. Laboratory experiments have found that heating the soil below 175°C causes slight changes in SWR. Significant increases in SWR were found at temperatures between 175 and 270°C. Micromorphological investigations indicated that high temperatures increased the formation of organic carbon coatings responsible for SWR (Dekker et al., 1998). Temperatures between 270°C and 400°C destroy hydrophobic substances in the soil and suppress SWR (Doerr et al., 2004; Varela et al., 2005; Wu et al., 2020).

Management strategies to reduce the impacts of fire-induced SWR are critical for maintaining ecosystem health and function. One approach is to use fire-retardant materials or chemicals to prevent or reduce the intensity of wildfires. Another method is to use mechanical treatments, such as thinning and prescribed burning, to reduce the fuel load and intensity of fires. In some cases, post-fire rehabilitation, such as the application of mulch and seed, may be necessary to promote vegetation growth and prevent further erosion.

The principal aim of the article was to determine the influence of different types of forest floor biomass on SWR induced by the simulated fire. Our first hypothesis was that heating temperatures would induce higher SWR persistence on soil covered with forest floor biomass compared to bare soil; the second hypothesis was that different forest floor biomass would induce different post-fire SWR persistence.

Material and methods

Research site

Soil samples were taken from the experimental sites IL1, IL2, and LL located at Studienka village with an altitude of 203 m a. s. l. in the Borská nížina lowland (southwestern Slovakia). The region has a temperate climate (Cfb) (Kottek et al., 2006) with a mean annual temperature of 9°C and mean annual precipitation of 600 mm, mainly during the summer months. The soils of the Studienka sites are classified as Arenosol and have a sandy texture (WRB, 2014) (Table 1).

Experimental sites were selected to include different stand ages and types of forest floor biomass (organic surface horizon) under the relatively same site conditions (climate, soil and relief conditions).

The IL1 site is a stand older than 100 years (Fig. 1a); its purpose is to stabilize the sand dune. The herbaceous undergrowth is dominated by grass, especially sheep fescue (*Festuca ovina* agg), and often covered with bushgrass (*Calamagrostis epigejos* (L.) Roth). Other species are rare, such as the wall hawkweed (*Hieracium murorum* L.), the weed species of the black nightshade (*Solanum nigrum* L.) and allochthon species with invasive behaviour, such as the pokeweed (*Phytolacca americana* L.), the black cherry (*Prunus serotina* Ehrh.) and horseweed (*Conyza canadensis* (L.) Cronq.). Rare species here are also red-stemmed feathermoss (*Pleurozium schreberi* (Bird.) Mitt.) and neat feathermoss (*Pseudoscleropodium purum* (Hedw.) M. Fleisch).

The IL2 site represents 30-year-old Scots pine (*Pinus sylvestris*) stand (Fig. 1b). The tree layer is very dense without undergrowth. The soil surface is covered with a few centimetres of coniferous litter. The mechanical site preparation was used for forest restoration, while the surface layer of soil with humus was removed, so the pine trees were planted in the bare sand.

The LL research site represents a younger stand of alder (*Alnus glutinosa*) (30–40 years) in an indistinct terrain depression situated under a sand dune overgrown with monocultures of Scots pine (Pinus sylvestris) in an undergrowth dominated by tall sedges (*Carex elata*) and the presence of other more moisture-loving species (Fig. 1c).

Table 1. Soil parameters of the topsoil horizon (0–10 cm) of study plots IL1, IL2 and LL (Cox = organic carbon content; WDPT = SWR measured before heating). The results are presented in the form of arithmetic mean ± standard deviation. Properties denoted with different letters are significantly different on significance level 0.05.

Parameter	IL1	IL2	LL
Sand [%]	91.82±0.03	92.31±0.02	92.96±0.48
Silt [%]	5.81±0.12	4.96±0.07	3.36±0.33
Clay [%]	2.37±0.09	2.72±0.03	3.68±0.12
$CaCO_3$ [%]	<0.05	<0.05	<0.05
Cox [%]	0.64^{a}±0.13	0.55^{a}±0.08	1.43^{b}±0.37
pH (H_2O)	4.96^{a} ±0.01	5.33^{b} ±0.01	4.20^{c} ±0.01
pH (KCl)	3.99^{a} ±0.01	4.39^{b} ±0.01	3.65^{c} ±0.01
WDPT [s]	16040^{a}±5828.30	958^{b}±495.70	146^{b}±92.15

Soil sampling and heating experiment

The mineral part of the soil from the 2.5 cm depth was sampled into the prepared containers after the organic horizon (0–2.5 cm) was gently removed from the soil surface and sampled separately. After returning to the laboratory, the mineral soil samples were sieved through a 2 mm sieve and dried at 40°C. After reaching equilibrium, the samples were weighed into ceramic dishes. We weighed five ceramic dishes for each temperature. The forest floor biomass (FFB) was air-dried in the laboratory to a constant weight. The dried FFB was processed into 1 to 10 mm material and mixed. For the analysis of the mineral component of the forest soil, we weighed 60 grams of sieved soil sample into ceramic dishes of 70 mm diameter and 35 mm height. To analyze the samples covered with FFB, we first weighed 60 g of the laboratory-prepared mineral component and then weighed 5 g of the FFB (Arcenegui et al., 2007). The samples were heated in a muffle furnace LE 15/11 (Fig. 2) at temperatures of 50, 100, 150, 200, 250, 300, 350, 400, 450, 500, 550, 600, 650, 700, 750, 800, 850 and 900 ° C for 20 min (a new sample for each temperature). After a given time, we pulled the samples out of the furnace and allowed them to cool to room temperature.

Measurement of soil water repellency

The persistence of SWR was assessed by the WDPT test. It involves placing 50 ± 5 µl of a drop of water from a standard dropper or pipette on the soil surface and recording the time of its complete penetration (infiltration) into the soil. A standard drop release height of approximately 10 mm above the soil surface was used to minimize the crater effect on the soil surface (Doerr, 1998; Tinebra et al., 2019). WDPT test was measured on the surface of burned mineral soil samples without FFB (treatment MN). We made two series of measurements for samples covered with FFB; the first was carried on the surface of burned FFB (treatment FFB), and the second under burned FFB on the exposed mineral soil (treatment MNE).

Our experiment's natural background water repellency is represented by the mean value of the persistence of SWR, measured before heating (SWRn). The induced SWR was estimated as the mean of WDPT values measured after heating soil samples at temperatures of 50–900°C (SWRi). SWRmax is the highest value of induced SWR, determined as the highest group average of WDPT measured after heating at a specific temperature. Tmax is the heating temperature that induced SWRmax.

List of abbreviations

Cox	organic carbon content
WDPT	water drop penetration time
SWR	soil water repellency
SWRn	natural background water repellency, measured before heating
SWRi	induced SWR, measured after heating of soil samples at temperatures of 50–900°C
SWRmax	highest value of induced SWR, measured after heating at a specific temperature
Tmax	the heating temperature that induced SWRmax
IL1	100-year-old pine stand
IL2	30-year-old pine stand
LL	30-year-old alder stand
MN	surface of burned mineral soil without FFB (treatment)
MNE	the exposed mineral soil under burned FFB (treatment)
FFB	forest floor biomass

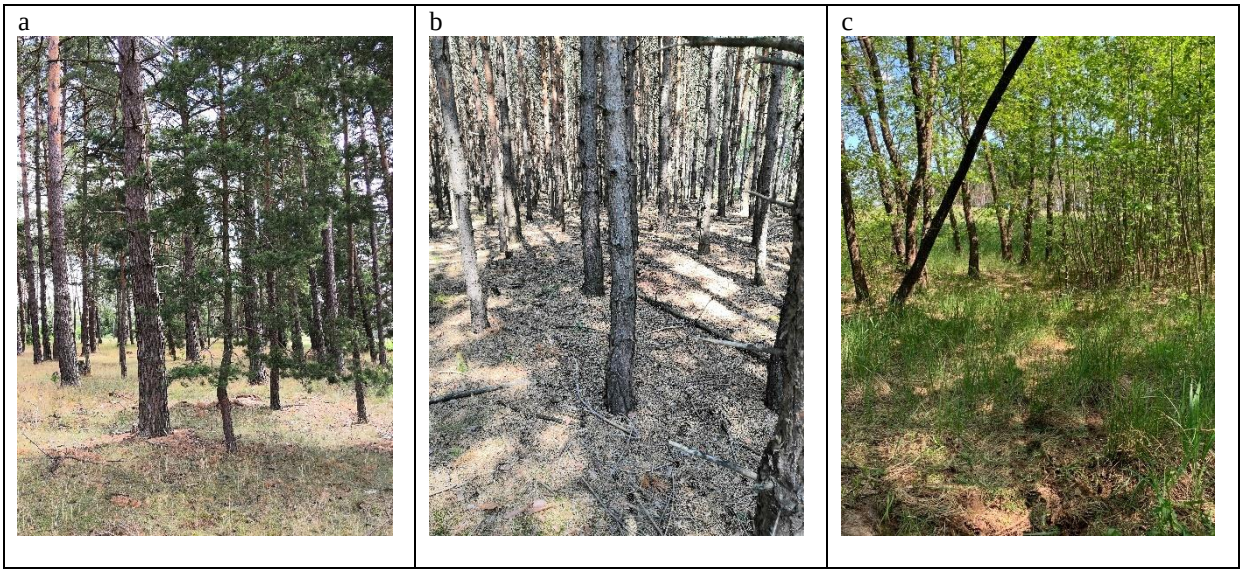

Fig. 1. Research sites: a) IL1 – over 100-year-old Scots pine (Pinus sylvestris L.) plantation; b) IL2 – 30-year-old Scots pine plantation; c) LL – approx. 30-year-old deciduous tree stand.

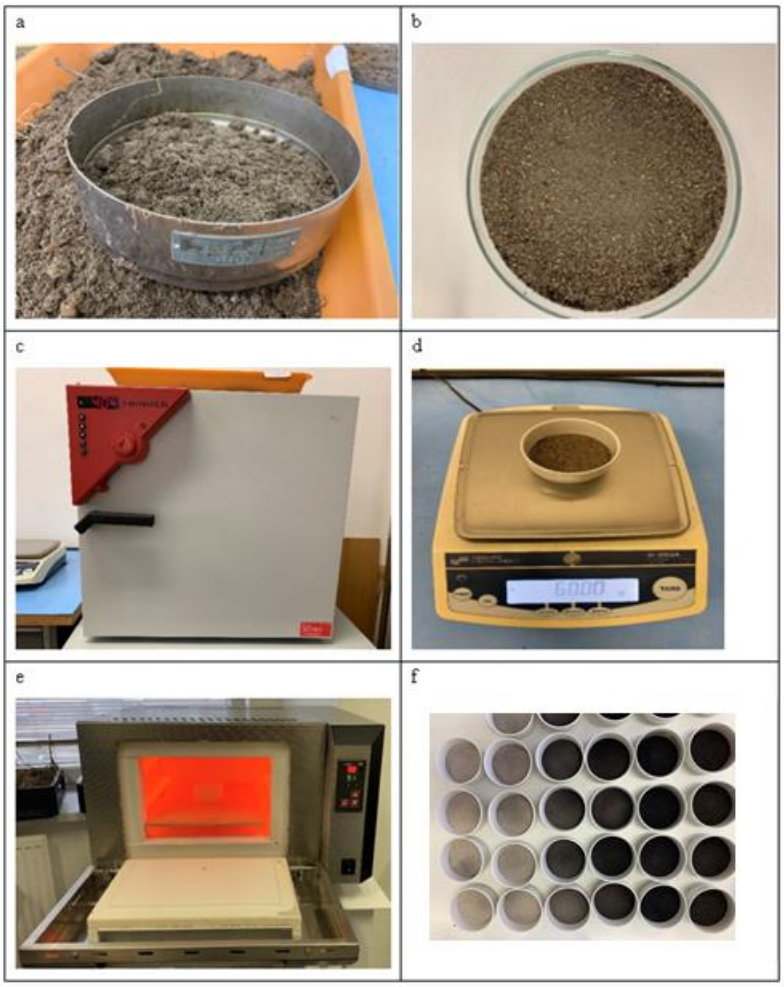

Fig. 2. Sample preparation and heating procedure in the muffle furnace a) sieving through a 2 mm sieve; b) Petri dish; c) BINDER drying oven for drying the samples; d) weighing the samples on a DENVER INSTRUMENT SI-2002A balance; e) burning of the samples in the muffle furnace (LE 15/11); f) soil samples after different temperature heating treatments.

Statistical analysis

The data were first analyzed by the omnibus normality test, which combines the skewness and kurtosis tests into a single measure. After the data had passed the omnibus normality test, differences between the parameters were evaluated using single-factor ANOVA with Tukey's Honest Significant Difference (HSD) post-hoc test. When the assumption of normality was not valid, the nonparametric Kruskal-Wallis test with multiple comparison Kruskal-Wallis Z test was used. It is a distribution-free multiple comparison, meaning that the assumption of normality is unnecessary. It is to be used for testing pairs of medians following the Kruskal-Wallis test. The statistical significance of the analysis was defined at $P < 0.05$. All statistical analyses were performed using the NCSS statistical software (NCSS 12 Statistical Software, 2018).

Results and discussion

The highest mean value of fire-induced SWR (SWRi) in a 100-year-old pine forest was measured in the soil without FFB (MN), followed by exposed soil under FFB (MNE), and the lowest value was measured in the FFB. We did not find statistically significant differences between the mean values of MN and MNE treatment. SWRmax, the highest value of induced SWR, declined in the order MNE>FFB>MN. Based on Fig. 3, it is possible to observe differences in the shape of the line showing the WDPT vs temperature relation. We observed a slight increase in the MN treatment, a relatively long steady state with high SWR, and a subsequent decrease. In the FFB treatment, we observed a steep increase followed by a subsequent decline; interestingly, the steep increase in the MNE treatment occurred only after the SWR decrease in the FFB treatment.

In the 30-year-old pine stand, we measured the highest mean SWRi value in the MNE treatment and a decrease in other treatments in the order FFB > MN (Fig. 4). We found no statistically significant differences between treatments. The highest SWRmax value was measured on the MNE treatment (26 676 s) and decreased in the order of FFB>MN. The shape of the WDPT vs temperature relation in all treatments is similar; the MNE treatment has a higher SWR at low heating temperatures as MN,

while the FFB treatment has a steep rise and fall in SWR. The highest mean value of SWRi in the alder stand was measured in the FFB, followed by MNE, and the lowest value was measured in the MN (which means exactly the opposite of a 100-year-old pine forest). However, this trend has not been statistically confirmed (Fig. 5). SWRmax declined in the order MNE>FFB>MN. The shape of the WDPT vs temperature relation in all alder stand treatments is similar; the MNE treatment has a similar SWR at 100–250°C as MN, while the FFB treatment has a higher SWR.

We did not find a statistically significant difference between the research sites (IL1, IL2, LL) in the SWRi measured below FFB. The shape of the WDPT vs temperature relation in research sites IL1 and IL2 is very similar. The difference is in the lower SWR measured in

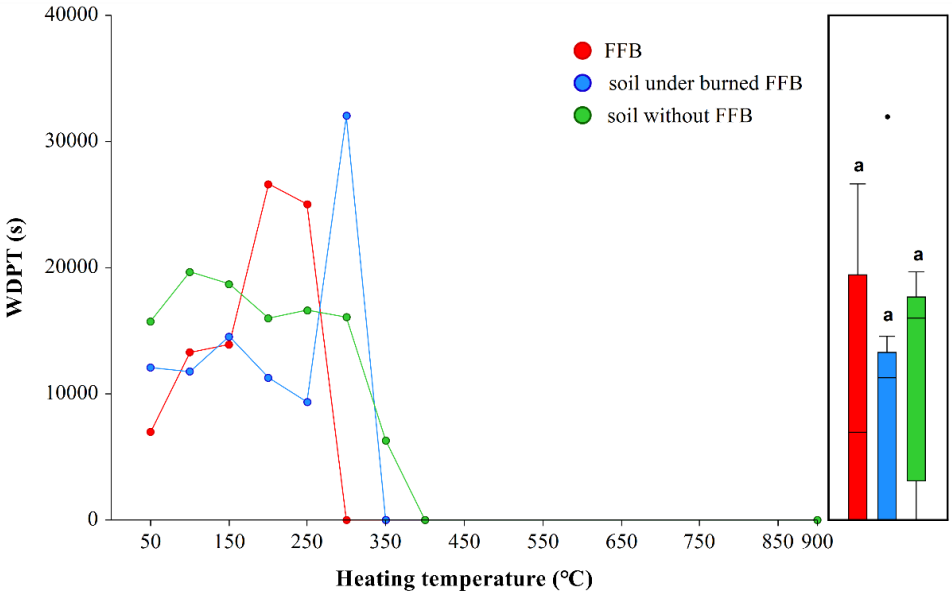

Fig. 3. Persistence of SWR induced by increasing temperature in soil from research site IL1, measured in forest floor biomass (FFB), in soil under FFB and soil without FFB. Box plots denoted with different letters are significantly different on significance level 0.05. The whiskers in the border plot show minima and maxima, and points represent outliers.

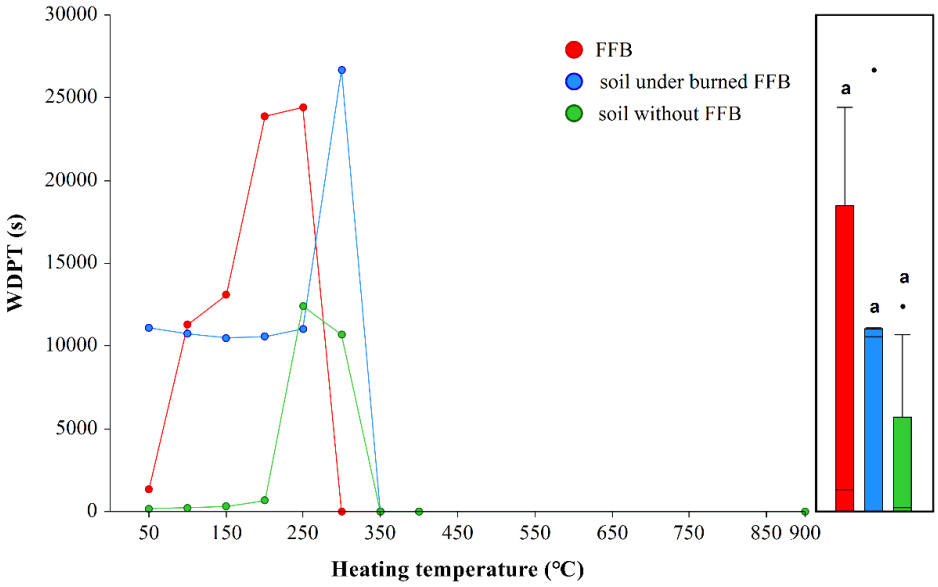

Fig. 4. Persistence of SWR induced by increasing temperature in soil from research site IL2, measured in forest floor biomass (FFB), in soil under FFB and soil without FFB. Box plots denoted with different letters are significantly different on significance level 0.05. The whiskers in the border plot show minima and maxima, and points represent outliers.

the LL site (Fig. 6). The highest mean for SWRi was measured on research site IL1, followed by IL2 with a minimal difference and the lowest value was measured on LL. SWRmax was very similar, 32 040 s, 26 676 s resp. 27 888 s, for sites IL1, IL2 resp. LL measured at 300°C.

The highest mean SWRi of FFB was measured on research site IL1, followed by LL with a very small difference and the lowest value was measured in IL2 (Fig. 7). However, this trend has not been statistically confirmed. SWRmax was very similar in all research sites, with the highest value measured in IL1 at 200°C, followed by LL and IL2 at 250°C. The shape of the WDPT vs temperature relation in all research sites is very similar. Differences are in the SWR measured at 50°C (for all sites) and shift in SWRmax in IL1 (Fig. 7).

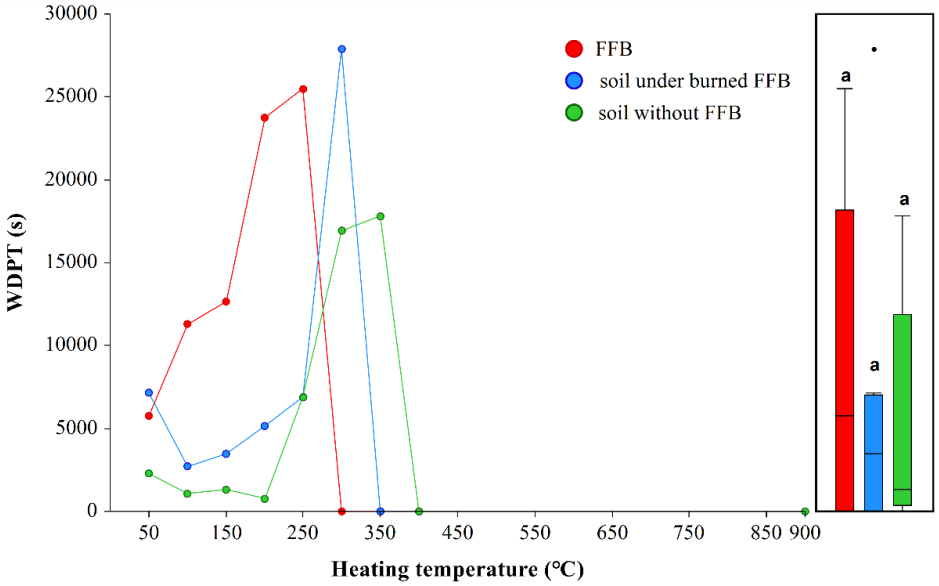

Fig. 5. Persistence of SWR induced by increasing temperature in soil from research site LL, measured in forest floor biomass (FFB), in soil under FFB and soil without FFB. Box plots denoted with different letters are significantly different on significance level 0.05. The whiskers in the border plot show minima and maxima, and points represent outliers.

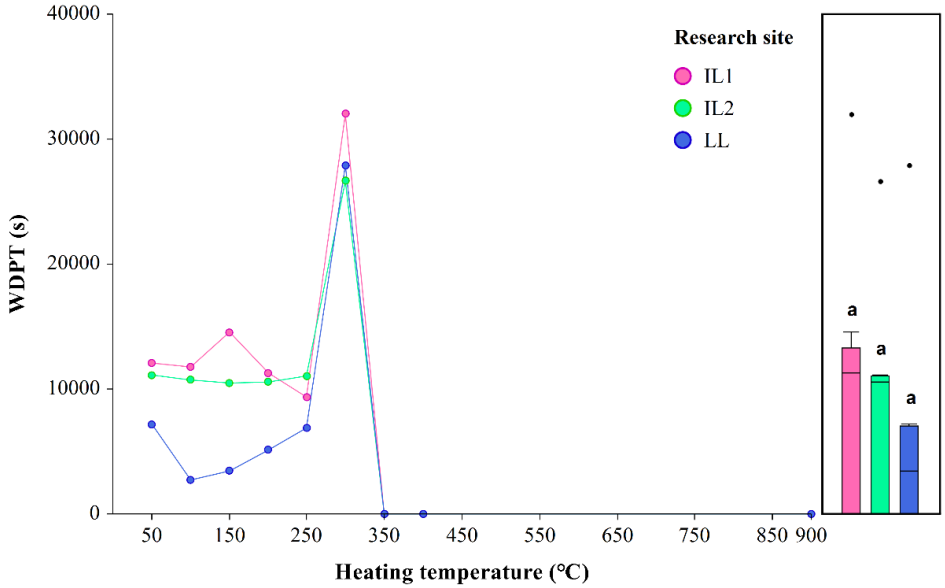

Fig. 6. Persistence of SWR induced by increasing temperature in soil under FFB for all research sites. Box plots denoted with different letters are significantly different on significance level 0.05. The whiskers in the border plot show minima and maxima, and points represent outliers.

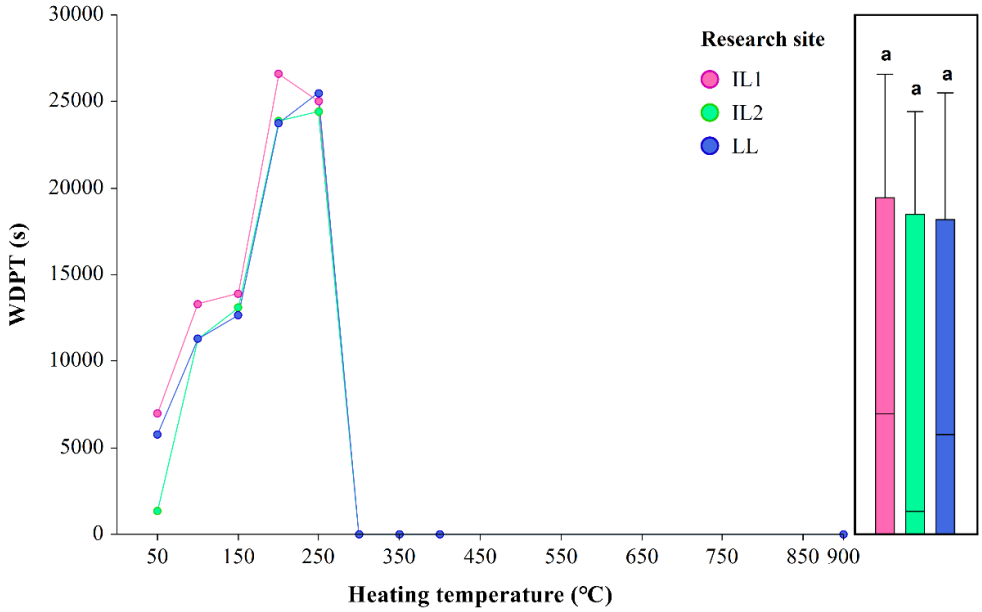

Fig. 7. Persistence of SWR induced by increasing temperature in the FFB for all research sites. Box plots denoted with different letters are significantly different on significance level 0.05. The whiskers in the border plot show minima and maxima, and points represent outliers.

Conclusion

In our study, we found the changes in fire-induced SWR that may be attributed to the different types of forest floor biomass (FFB); however, none of the observed differences was statistically confirmed.

Our first hypothesis that heating temperatures would induce higher SWR in soil covered with FFB compared to bare soil was partially confirmed. The highest SWRmax values were measured at or below the FFB in deciduous and coniferous forests. Higher SWR can cause reduced infiltration, increased runoff and erosion, greater soil moisture variability and alter nutrient cycling. Removing dead biomass reduces the fuel load and can help mitigate SWR and fire risk in forest plantations. It's important to note that deadwood and biomass play significant ecological roles in forest ecosystems, providing habitat for numerous organisms, contributing to nutrient cycling, and promoting biodiversity. Therefore, deadwood removal should be carefully considered, and sustainable management practices should aim to balance the removal of dead biomass with the conservation of ecosystem functions and biodiversity.

The second hypothesis that different forest floor biomass would induce different post-fire SWR persistence was not confirmed. We found similar fire-induced SWR in the different types of forest floor biomass and the soil under forest floor biomass.

Acknowledgement

This work was supported by Scientific Grant Agency No. VEGA 2/0020/20, VEGA 2/0150/20 and EIG CONCERT-Japan No. EIG JC2019-074.

References

Arcenegui, V., Mataix-Solera, J., Guerrero, C., Zornoza, R., Mayoral, A. M., Morales, J. (2007): Factors Controlling the Water Repellency Induced by Fire in Calcareous Mediterranean Forest Soils. European Journal of Soil Science, vol. 58, 1254–1259.

Arcenegui, V., Mataix-Solera, J., Guerrero, C. Zornoza, R., Mataix-Beneyto, J., García-Orenes, F. (2008): Immediate Effects of Wildfires on Water Repellency and Aggregate Stability in Mediterranean Calcareous Soils. Catena, vol. 74, no. 3, 219–226.

Certini, G. (2005): Effects of Fire on Properties of Forest Soils: A Review. Ecologia, vol. 143, no. 1, 1–10.

Chen, J., Pangle, L. A., Gannon, J. P., Stewart, R. D. (2020): Soil Water Repellency after Wildfires in the Blue Ridge Mountains, United States. International Journal of Wildland Fire, vol. 29, 1009–1020.

DeBano, L. F., Neary, D. G., Folliott, P. F. (1998): Fire's Effects on Ecosystems. Wiley, New York, 333 p.

DeBano, L. F. (2000): The Role of Fire and Soil Heating on Water Repellency in Wildland Environments: A Review. Journal of Hydrology, vol. 231–232, 195–206.

Dekker, L. W., Ritsema, C. J., Oostindie, K., Boersma, O. H. (1998): Effect of Drying Temperature on the Severity of Soil Water Repellency. Soil Science, vol. 163, no. 10, 780–796.

Doerr, S. H. (1998): On Standardizing the "Water Drop Penetration Time" and the "Molarity of an Ethanol Droplet" Techniques to Classify Soil Hydrophobicity: A Case Study using Medium Textured Soils. Earth Surface Processes and Landforms, vol. 23, 663–668.

Doerr, S. H., Blake, W. H., Shakesby, R. A., Stagnitti, F., Vuurens, S. H., Humphreys, G. S., Wallbrink, P. (2004): Heating Effects on Water Repellency in Australian Eucalypt Forest Soils and their Value in Estimating Wildfire Soil Temperatures. International Journal of Wildland Fire, vol. 13, no. 2, 157–163.

Hološ, S., Šurda, P., Lichner, Ľ., Zvala, A., Píš, V. (2022): Fire-induced Changes in Soil Properties Depend on Age and Type of Forests. Journal of Hydrology and Hydromechanics, vol. 70, no. 4, 442–449.

Kottek, M., Grieser, J., Beck, C., Rudolf, B., Rubel, F. (2006): World Map of the Köppen-Geiger Climate Classification Updated. Meteorologische Zeitschrift, vol. 15, 259–263.

Lichner, L., Dlapa, P., Doerr, S. H., Mataix-Solera, J. (2006): Evaluation of Different Clay Minerals as Additives for Soil Water Repellency Alleviation. Applied Clay Science, vol. 31, 238–248.

Mataix-Solera, J., Arcenegui, V., Guerrero, C., Jordán, M. M., Dlapa, P., Tessler, N., Wittenberg, L. (2008): Can Terra Rossa Become Water Repellent by Burning? A Laboratory Approach. Geoderma, vol. 147, 178–184.

NCSS 12 Statistical Software (2018): NCSS, LLC. Kaysville, Utah, USA, ncss.com/software/ncss.

Negri, S., Stanchi, S., Celi, L., Bonifacio, E. (2021): Simulating Wildfires with Lab-heating Experiments: Drivers and Mechanisms of Water Repellency in Alpine Soils. Geoderma, vol. 402, 115357.

Robichaud, P. R., Hungerford, R. D. (2000): Water Repellency by Laboratory Burning of Four Northern Rocky Mountain Forest Soils. Journal of Hydrology, vol. 231–232, 207–219.

Savage, S. M., Osborn, J., Letey, J., Heaton, C. (1972): Substances Contributing to Fire-induced Water Repellency in Soils. Proceedings of the Soil Science Society of America, vol. 36, 674–678.

Tinebra, I., Alagna, V., Iovino, M., Bagarello, V. (2019): Comparing Different Application Procedures of the Water Drop Penetration Time Test to Assess Soil Water Repellency in a Fire Affected Sicilian Area. Catena, vol. 177, 41–48.

Varela, M. E., Benito, E., de Blas, E. (2005): Impact of Wildfires on Surface Water Repellency in Soils of Northwest Spain, Hydrological Processes, vol. 19, no. 18, 3649–3657.

WRB (2014): World Reference Base for Soil Resources 2014. World Soil Resources Reports No. 106. Rome, 192 p.

Wu, Y., Zhang, N., Slater, G., Waddington, J. M., de Lannoy, Ch.-F. (2020): Hydrophobicity of Peat Soils: Characterization of Organic Compound Changes Associated with Heat-induced Water Repellency. Science of The Total Environment, vol. 714, 136444.

Zvala, A., Šurda, P., Hološ, S. (2022): The effect of different fire temperatures on the water repellency parameters of forest sandy soil under different types of vegetation. Acta Hydrologica Slovaca, vol. 23, no.1, 140–146. 2644-6290.

Ing. Slavomír Hološ
Mgr. Anton Zvala, PhD.
Ing. Peter Šurda, PhD. (*corresponding author, e-mail: surda@uh.savba.sk)
Ing. Ľubomír Lichner, DrSc.
Institute of Hydrology SAS
Dúbravská cesta 9
841 04 Bratislava
Slovak Republic

Ing. Slavomír Hološ
Institute of Landscape Engineering
Faculty of Horticulture and Landscape Engineering
Slovak University of Agriculture
Hospodárska 7
949 76 Nitra
Slovak Republic